

eman ta zabal zazu



Universidad  
del País Vasco

Euskal Herriko  
Unibertsitatea

---

# **Studies on UAF1-regulated deubiquitinase complexes: USP1/UAF1, USP12/UAF1 and USP46/UAF1**

PhD Thesis

Ane Olazabal Herrero

2017

Supervisor: Jose Antonio Rodríguez Pérez



Ane Olazabal Herrero is the recipient of a predoctoral fellowship from the University of the Basque Country. She also received financial support for training courses by the COST action (Proteostasis BM1307).

This work was supported by the Department of Industry of the Basque Country Government (ETORTEK BioGUNE2010), the Spanish Government MICINN (BFU2009-13,245), and the UPV/EHU (UFI11/20).



# Table of contents

<b>Abbreviations</b> .....	1
<b>Abstract</b> .....	5
<b>1. Introduction</b> .....	6
1.1. PROTEIN UBIQUITINATION/DEUBIQUITINATION.....	6
1.2. HUMAN DEUBIQUITINATING ENZYMES (DUBs).....	10
1.2.1. Cellular functions of DUBs.....	10
1.2.2. Domain architecture and classification of DUBs.....	11
1.3. THE USP SUBFAMILY OF DUBs .....	12
1.3.1. General structural features and ubiquitin chain specificity of USPs.....	12
1.3.2. Regulation of USP catalytic activity.....	14
1.4. WDR48/UAF1, AN ACTIVATING COFACTOR OF USP1, USP12 AND USP46 .....	15
1.4.1. UAF1 domain structure .....	15
1.4.2. UAF1 function.....	16
1.5. THE USP1/UAF1 DEUBIQUITINASE COMPLEX .....	17
1.5.1. Domain structure and functional motifs in USP1.....	17
1.5.2. The role of the USP1/UAF1 complex in the response to DNA damage .....	18
1.5.3. Regulation of the USP1/UAF1 complex.....	22
1.5.4. USP1 alterations in cancer .....	25
1.5.5. The USP1/UAF1 complex as a therapeutic target in cancer .....	26
1.6. THE USP12/UAF1 AND USP46/UAF1 DEUBIQUITINASE COMPLEXES .....	27
1.6.1. Domain structure and functional motifs of USP12 and USP46.....	27
1.6.2. Cellular functions of the USP12 and USP46 .....	28
1.6.3. Regulation of USP12 and USP46 by UAF1 and WDR20.....	29
<b>2. Hypotheses and aims</b> .....	32
<b>3. Materials and Methods</b> .....	34
3.1. BIOINFORMATICS TOOLS .....	34
3.1.1. Sequence alignment and 3D structure modeling.....	34
3.1.2. COSMIC mutation database .....	34
3.2. CLONING AND MUTAGENESIS.....	34
3.2.1. “Classical”-restriction enzyme-based cloning .....	35
3.2.2. Gibson assembly cloning.....	37
3.2.3. Site-directed mutagenesis.....	39

3.2.4.	Plasmid isolation and DNA sequencing.....	40
3.3.	CELL CULTURE .....	41
3.3.1.	Cell lines and cell culture conditions.....	41
3.3.2.	Cell seeding .....	41
3.3.3.	Transfection.....	42
3.3.4.	Drug treatments .....	44
3.3.5.	Sulforhodamine B (SRB) cell viability assay.....	44
3.4.	FLUORESCENCE MICROSCOPY TECHNIQUES.....	46
3.4.1.	Immunofluorescence .....	46
3.4.2.	Live cell microscopy.....	47
3.4.3.	Microscopes .....	47
3.4.4.	Image analysis for quantification of FK2 fluorescence and 53BP1 foci .....	48
3.5.	TECHNIQUES FOR RNA ANALYSIS.....	48
3.5.1.	RNA isolation.....	48
3.5.2.	cDNA synthesis.....	49
3.5.3.	qRT-PCR.....	49
3.5.4.	Analysis of DNA adducts using quantitative extra-long PCR (XL-PCR) and Taqman assays.....	49
3.6.	TECHNIQUES FOR PROTEIN ANALYSIS .....	50
3.6.1.	Protein extraction.....	50
3.6.2.	Protein quantification .....	51
3.6.3.	Immunoprecipitation using GFP-trap magnetic beads .....	52
3.6.4.	Immunoblot.....	52
3.7.	PULLDOWN OF ENDOGENOUS UBIQUITINATED PROTEINS USING <sup>bio</sup> Ub .....	54
3.7.1.	The bioUb strategy .....	54
3.7.2.	<sup>bio</sup> Ub protocol: preparation of cell extracts and purification of biotinylated proteins.....	56
3.7.3.	Silver staining .....	58
3.8.	IDENTIFICATION OF <sup>bio</sup> Ub-ENRICHED ENDOGENOUS UBIQUITINATED PROTEINS USING MASS SPECTROMETRY .....	58
3.8.1.	General aspects of mass spectrometry.....	58
3.8.2.	In-gel trypsin digestion and peptide extraction .....	59
3.8.3.	Liquid chromatography (LC)-MS/MS analysis .....	60
3.8.4.	Data processing and bioinformatics analysis .....	61
3.9.	SUPPLEMENTARY MATERIALS AND METHODS.....	62

3.9.1.	PCR reactions and programs .....	62
3.9.2.	Solutions.....	64
<b>4.</b>	<b>Results.....</b>	<b>67</b>
4.1.	INSIGHTS INTO THE REGULATION OF USP1 BY PHOSPHORYLATION AND AUTOCLEAVAGE .....	67
4.1.1.	Phosphorylation of USP1 at serine 313 is dispensable for the formation and activity of USP1/UAF1 complex.....	67
4.1.2.	USP1 autocleavage at the G670/G671 diglycine motif occurs most likely in <i>cis</i> .....	71
4.2.	CONFIRMATION AND FINE MAPPING OF THE USP1/UAF1 INTERACTION INTERFACE .....	74
4.2.1.	Side-by-side comparison of the two reported UAF1-binding sites in USP1.....	74
4.2.2.	The "Fingers" subdomain is the UAF1-binding site in USP1 .....	78
4.2.3.	Fine-mapping of the UAF1/USP1 interaction.....	81
4.2.4.	Assesing the functional effect of the mutations that disrupt USP1/UAF1 interaction .....	88
4.3.	USP1/UAF1 IN CANCER .....	92
4.3.1.	Novel functional readouts to study USP1 activity in cells: general ubiquitin deconjugation and blockade of 53BP1 foci formation.....	92
4.3.2.	Functional effects of cancer-related USP1 mutations .....	99
4.3.3.	Activity of the USP1/UAF1 inhibitor ML323 in pancreatic cancer cells .....	104
4.4.	SEARCHING FOR NEW USP1 SUBSTRATES USING <sup>bio</sup> Ub .....	117
4.4.1.	The <sup>bio</sup> Ub system and mass spectrometry.....	117
4.4.2.	Validation of MS-detected potential novel USP1 substrates by immunoblot ..	124
4.5.	SEARCHING FOR MOLECULAR MECHANISMS THAT MAY UNDERLIE THE FUNCTIONAL DIFFERENCES BETWEEN USP12 AND USP46 .....	127
4.5.1.	Analysis of USP12 and USP46 binding to UAF1 and WDR20 using relocation assays.....	128
4.5.2.	Analysis of the binding of DMWD, a WDR20 paralog, to USP12 and USP46 complexes.....	129
4.5.3.	The amino terminal motif "MEIL" in USP12 contributes to binding to WDR20 and DMWD.....	133
<b>5.</b>	<b>Discussion.....</b>	<b>135</b>
5.1.	DEEPENING INTO USP1 REGULATION: SERINE 313 PHOSPHORYLATION, AUTOCLEAVAGE AND UAF1-INTERACTION.....	136
5.2.	FINE-MAPPING THE USP1/UAF1 INTERACTION .....	138
5.3.	FUNCTIONAL CONSEQUENCES OF CANCER-RELATED USP1 MUTATIONS .....	141

5.4.	EFFECT OF THE USP1 INHIBITOR ML323 IN PANCREATIC CANCER CELLS.....	143
5.5.	NOVEL USP1 SUBSTRATES RELATED TO DNA DAMAGE.....	146
5.6.	USP12/USP46: SIMILAR PROTEINS, DIFFERENT FUNCTIONS .....	147
<b>6.</b>	<b>Conclusions</b> .....	<b>150</b>
<b>7.</b>	<b>References</b> .....	<b>152</b>
<b>8.</b>	<b>Supplementary tables</b> .....	<b>164</b>



---

# ABBREVIATIONS

**AMPAR:**  $\alpha$ -amino-3-hydroxy-5-methyl isoxazole-4-propionic acid receptor

**AP:** Alkaline phosphatase

**APC/C<sup>Cdh1</sup>:** Anaphase Promoting Complex/Cyclosome<sup>Cdh1</sup>

**AR:** Androgen receptor

**bHLH:** basic-helix-loop-helix

**BirA:** Biotin holoenzyme synthetase

**<sup>bio</sup>Ub:** Biotinylated ubiquitin

**BRCA1:** Breast cancer 1

**BSA:** Bovine serum albumin

**CAA:** Chloroacetamide

**CDK:** Cyclin-dependent kinase

**cDNA:** Complementary DNA

**CI:** Combination index

**Co-IP:** Co-immunoprecipitation

**COSMIC:** Catalogue Of Somatic Mutations in Cancer

**CRM1:** Chromosomal region maintenance 1

**DAPI:** 4',6-diamidino-2-phenylindole

**DDR:** DNA damage response

**DM:** Dystrophia myotonica

**DMEM:** Dubelcco's modified eagle medium

**DMSO:** Dimethyl sulfoxide

**DMWD:** Dystrophia myotonica WD repeat containing protein

**DNA:** Deoxyribonucleic acid

**DSB:** Double-strand break

**DTT:** Dithiothreitol

**DUB:** Deubiquitinating enzyme / Deubiquitinase

**EBV:** Epstein-Barr virus

**ECL:** Enhanced chemiluminescence

**EDTA:** Ethylenediaminetetraacetic acid

**Fa:** Fraction affected

**FA:** Fanconi anemia

**FANC:** Fanconi anemia complementation

**FANCD2:** Fanconi anemia complementation group D2  
**FANCI:** Fanconi anemia complementation group I  
**FBS:** Fetal bovine serum  
**FDR:** False discovery rate  
**FL:** Full-length  
**FT:** Flow through  
**GBP:** GFP-binding protein  
**GFP:** Green fluorescent protein  
**GluR:** Glutamate receptor  
**HCD:** Higher energy C-trap dissociation  
**HPV:** Human papillomavirus  
**HR:** Homologous recombination  
**HRP:** Horseradish peroxidase  
**HTS:** High throughput screening  
**HU:** Hydroxyurea  
**ICL:** Interstrand crosslink  
**ID:** Inhibitors of DNA binding  
**IF:** Immunofluorescence  
**IGS15:** Interferon-stimulated gene 15  
**Imp:** Importin  
**IP:** Immunoprecipitation  
**JAMM:** JAB1/MPN/Mov34 metalloprotease  
**LB:** Lysogeny Broth  
**LC-MS/MS:** Liquid chromatography- tandem mass spectrometry  
**LFQ:** Label free quantification  
**MGV:** Mean grey value  
**MJD:** Machado-Joseph domain disease protease  
**MMC:** Mytomicin C  
**mRFP:** Monomeric red fluorescent protein  
**mRNA:** Messenger RNA  
**MS:** Mass spectrometry  
**MW:** Molecular weight  
**m/z:** Mass-to-charge ratio  
**NCS:** Neocarzinostatin  
**NEDD8:** Neural precursor cell expressed developmentally down-regulated 8

**NEDP1:** NEDD8-specific protease 1

**NEM:** N-ethylmaleimide

**NES:** Nuclear export signal

**NHEJ:** Non-homologous end joining

**NLS:** Nuclear localization signal

**Notch R:** Notch receptor

**NSCLC:** Non-small cell lung cancer

**OTU:** Ovarian-tumor protease

**PAF15:** PCNA-associated factor

**PBS:** Phosphate buffered saline

**PBS-T:** Phosphate buffered saline-tween 20

**PCNA:** Proliferating cell nuclear antigen

**PCR:** Polymerase chain reaction

**PHLPP:** Pleckstrin homology domain leucine rich repeat protein phosphatases

**PIC:** Protease inhibitor cocktail

**PMSF:** Phenylmethanesulfonyl fluoride

**PTM:** Posttranslational modification

**PVDF:** Polyvinylidene difluoride

**P/S:** Penicillin/Streptomycin

**qRT-PCR:** Quantitative real-time PCR

**RAD51AP1:** RAD51-associated protein 1

**RIPA:** Radioimmunoprecipitation assay buffer

**RNA:** Ribonucleic acid

**RPMI:** Roswell park memorial institute

**SDS:** Sodium dodecyl sulfate

**SDS-PAGE:** Sodium dodecyl sulfate-polyacrylamide gel electrophoresis

**SENP:** SUMO-specific protease

**siRNA:** Small interfering ribonucleic acid

**SLD:** SUMO-like domain

**SRB:** Sulforhodamine B

**SUMO:** Small ubiquitin-like modifier

**SV40:** Simian virus 40

**TAE:** Tris/Acetic acid/EDTA

**TBS-T:** Tris buffered saline-tween 20

**TCA:** Trichloroacetic acid

**TCR:** T-cell receptor  
**TLS:** Translesion synthesis  
**Tm:** Melting temperature  
**TX-100:** Triton X-100  
**UAF1:** USP1-associated factor 1  
**Ub:** Ubiquitin  
**UBA:** Ubiquitin-associated motif  
**UBD:** Ubiquitin-binding domain  
**UBL:** Ubiquitin-like protein  
**UBP43:** Ubiquitin protease 43  
**UCH:** Ubiquitin C-terminal hydrolase  
**UIM:** Ubiquitin-interacting motif  
**ULD:** Ubiquitin-like domain  
**USP:** Ubiquitin-specific protease  
**UT:** Untreated  
**UTR:** Untranslated region  
**UV:** Ultraviolet  
**WB:** Washing buffer  
**WCE:** Whole cell extract  
**WDR:** WD repeat  
**WDR20:** WD-repeat containing protein 20  
**WDR48:** WDR-repeat containing protein 48  
**WT:** Wild type  
**YFP:** Yellow fluorescent protein  
**53BP1:** p53-binding protein 1  
 **$\gamma$ -H2AX:** phosphorylated histone H2AX

# Abstract

Deubiquitinases (DUBs), the enzymes that catalyze the removal of ubiquitin moieties from target proteins, regulate a wide range of cellular processes and are potential targets for cancer therapy. Our knowledge on the basic biology of these important enzymes is still very limited. In this Thesis we have focused on three human DUBs (USP1, USP12 and USP46) that share a common regulatory mechanism: they are activated by the cofactor UAF1. We have explored several aspects of the function and regulation of these three DUBs to clarify standing controversies and to uncover novel details.

Our results show that phosphorylation of USP1 at serine 313 is not necessary for UAF1 binding, neither for its catalytic activity. We also provide evidence that USP1 autocleavage occurs most likely in *cis*. Importantly, we map the UAF1-binding site of USP1, USP12 and USP46 to their so-called “Fingers” subdomain, and contribute to identify single residues that are critical for the interaction between these DUBs and their cofactor. Using a panel of functional tests, we show for the first time that cancer-related mutations in USP1 can alter its function and regulation. Regarding the potential role of the USP1/UAF1 complex as a target in cancer, we observed overexpression of USP1 and UAF1 in pancreatic tumors and derived cell lines, and our data suggest that the USP1 inhibitor ML323 can increase oxaliplatin sensitivity in relatively resistant pancreatic cancer cell lines.

In this Thesis we also significantly expand the repertoire of potential USP1 substrates. By applying a novel approach, termed <sup>bio</sup>Ub, and label-free quantification (LFQ)-based proteomics, we have identified 10 proteins whose ubiquitination level increases when USP1 is silenced.

Finally, regarding USP12 and USP46, our data suggest that these enzymes may differently bind to their common cofactor WDR20, and to at least another interactor (DMWD). This differential binding appears to be mediated by the presence/absence of a 4 amino acid motif (MEIL) at their N-terminus, and may contribute to explain the previously observed functional differences between these two highly similar enzymes.



# **Introduction**

**1**





# 1. Introduction

Posttranslational modifications (PTM) are important regulatory events that influence the properties of most cellular proteins including their activity, their interactions with other proteins and their subcellular localization. Proteins can be modified, for example, by methylation, acetylation, hydroxylation, phosphorylation or conjugation to ubiquitin (Ub) and ubiquitin-like (UBL) proteins. Ubiquitin conjugation has emerged as a crucial regulator of practically all aspects of cell biology.

## 1.1. PROTEIN UBIQUITINATION/DEUBIQUITINATION

For a long time, most intracellular proteins were thought to be long-lived. This view remained virtually unchallenged until ubiquitin and the process of ubiquitination linked to the degradation of proteins in the proteasome were discovered (Goldstein et al., 1975; Hershko, 1983).

The conjugation of ubiquitin is one of the most common posttranslational modifications of proteins, and it is implicated in modulating many aspects of protein stability and function. Ubiquitin, a highly conserved 76 amino acid polypeptide, is covalently attached by its C-terminal dyglycine motif to either the N-terminal methionine or, most frequently, to a lysine of the target substrates (**Figure 1**).

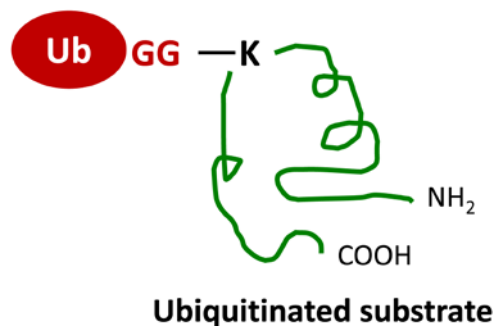


**Figure 1: Ubiquitin linkage.** The ubiquitin molecule can be conjugated by its C-terminal dyglycine motif (GG, red) to a specific lysine (K) residue on the target substrate.

The attachment of ubiquitin to a substrate is a multi-step enzymatic cascade involving three enzymes (Hershko et al., 1983) (**Figure 2**). In the first step, ubiquitin is activated by an E1 ubiquitin-activating enzyme in an ATP-dependent reaction. In the second step,

the activated ubiquitin is transferred to the active site of an E2 ubiquitin-conjugating enzyme. Finally, an E3 ubiquitin ligase catalyzes the ligation of ubiquitin to the target protein.

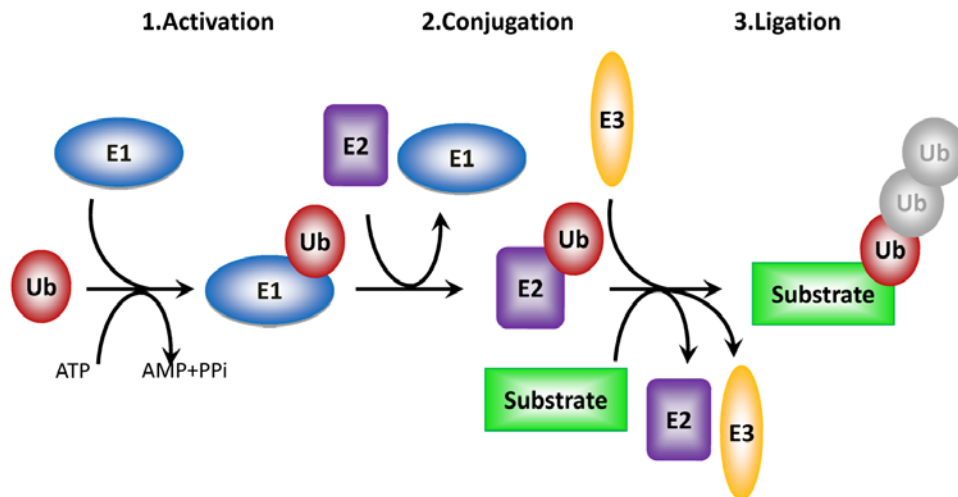


**Figure 2: The ubiquitination pathway.** Ubiquitination is mediated by the sequential action of three enzymes: E1 (ubiquitin-activating enzyme), E2 (ubiquitin-conjugating enzyme) and E3 (ubiquitin ligase).

In humans, two E1s, around 35 E2s and several hundred E3 enzymes exist, thus, reflecting the wide variety of cellular functions that are modulated by ubiquitination. It must be noted that in addition to ubiquitin, mammalian cells encode approximately 20 ubiquitin-like proteins (UBLs) that may be conjugated to target proteins via enzymatic cascades comparable to that of ubiquitination (Veen and Ploegh, 2012). These UBLs include, among others, small ubiquitin-like modifier (SUMO), neuronal-precursor-cell-expressed developmentally downregulated protein 8 (NEDD8) and interferon-stimulated gene 15 (ISG15). UBLs have variable sequences, but display three-dimensional structure similar to ubiquitin.

Protein ubiquitination is a highly versatile process due to the possibility of generating different types of ubiquitin chains (**Figure 3**). Thus, ubiquitination may occur on a single one or on several lysine/s of the target protein, resulting in monoubiquitination or multiubiquitination, respectively (**Figure 3A**) (Petroski and Deshaies, 2003, 2005). In addition, in the process of homotypic polyubiquitination (**Figure 3B**), further ubiquitin moieties can be sequentially attached to one of the seven internal lysine residues of ubiquitin (K6, K11, K27, K29, K33, K48 or K63) (Pickart and Fushman, 2004), or

ubiquitin chains can be assembled in linear configuration through the amino group at the N-terminus (Kirisako et al., 2006). Finally, several studies have described the existence of the so-called heterotypic polyubiquitination (Ikeda and Dikic, 2008) (**Figure 3C**), which involves the formation of mixed or branched ubiquitin chains, and could also include combinations of different UBLs, such as ubiquitin-SUMO hybrid chains (Guzzo and Matunis, 2013).

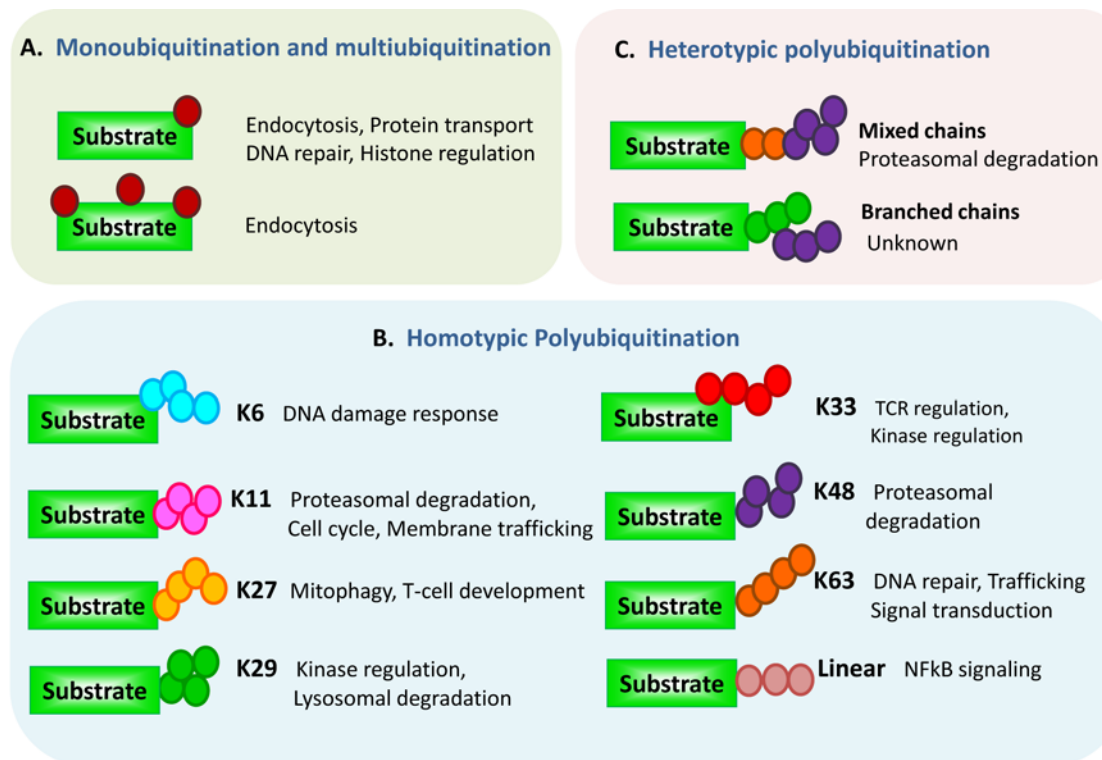


**Figure 3: Schematic representation of the different types of ubiquitin modifications and their functional role.** The diversity of ubiquitin linkage and chain types regulates the fate of the protein substrates. *Adapted from* (Wong and Cuervo, 2010).

The diversity of ubiquitin linkages is essential for determining the fate of cellular proteins. Monoubiquitination can regulate endocytosis, protein transport and DNA repair among other functions (Hicke, 2001). Multiubiquitination is important for receptor endocytosis (Haglund et al., 2003). K48-linked polyubiquitination targets proteins for degradation in the proteasome (Chau et al., 1989), whereas K63-linked polyubiquitination is required for proteasome-independent functions such as DNA damage tolerance, vesicle trafficking and signal transduction (Haglund and Dikic, 2005). Until recently, only K48- and K63-linked chains have been extensively studied

and the outcome of other linkage types, such as K29 or K33, is still poorly characterized. The functions so far assigned to these atypical ubiquitin linkages (summarized in **Figure 3B**) are very diverse (Kulathu and Komander, 2012).

Like other PTMs, such as phosphorylation or methylation, ubiquitination is a reversible process (**Figure 4**). Deubiquitinating enzymes or deubiquitinases (DUBs), oppose the activity of E3 ligases by removing ubiquitin moieties from protein substrates. DUBs catalyze the hydrolysis of the isopeptide bond between ubiquitin and the target protein or between ubiquitin moieties in a polyubiquitin chain. (Reyes-Turcu et al., 2009) (**Figure 4**).

Fulfilling an analogous role to DUBs, there are also deconjugating enzymes for other UBLs, such as SUMO-specific proteases (SENPs) (Mukhopadhyay and Dasso, 2007), NEDD8-specific proteases (NEDP1) (Mendoza et al., 2003) and ISG15-specific proteases (UBP43) (Malakhov et al., 2002).

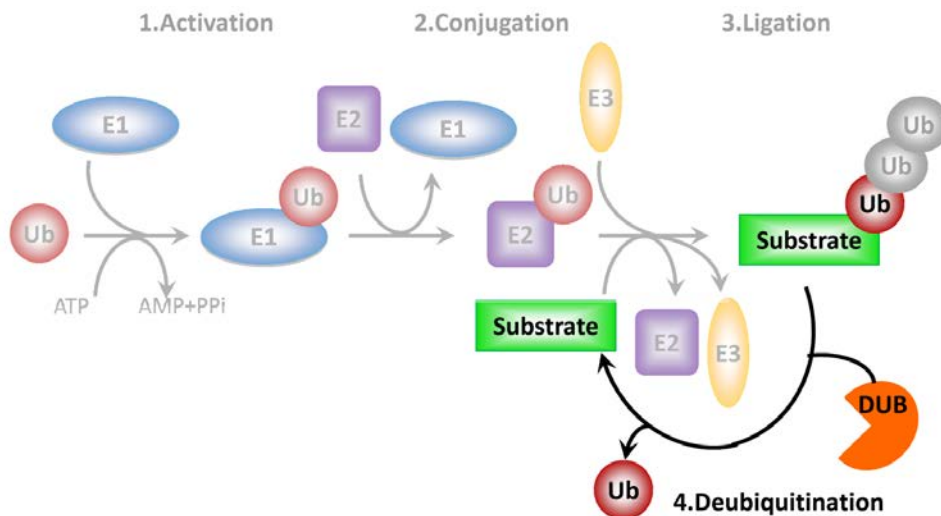


**Figure 4: Deubiquitination pathway.** Deubiquitinating enzymes (DUBs) catalyze the removal of ubiquitin moieties from ubiquitinated substrates.

The dynamic balance between the activity of ubiquitin E3 ligases and DUBs determines the final ubiquitination status of the substrate, and this balance must be carefully regulated to ensure cellular homeostasis. In this regard, the ubiquitination/deubiquitination processes play an essential role in critical cellular functions such as gene expression (Geng et al., 2012), cell cycle progression (Nakayama

and Nakayama, 2006), apoptosis (Vucic et al., 2011) and DNA repair (Ulrich and Walden, 2010). Dysregulations in protein ubiquitination/deubiquitination have been found to be involved in several human diseases, such as neurodegenerative disorders (Atkin and Paulson, 2014) and cancer (Satija et al., 2013). These findings provide opportunities for new therapeutic approaches. For example, targeting the ubiquitin-proteasome pathway using the proteasome inhibitor bortezomib, has proven to be an effective strategy in the treatment of multiple myeloma (Chen et al., 2011; Richardson et al., 2003). More recently, the enzymes that conform the ubiquitination/deubiquitination machinery have begun to be studied as potential targets in cancer therapy (Hoeller and Dikic, 2009). In this regard, E3 ligases were initially the focus of these studies, and E3 inhibitors are already undergoing clinical trials (Mattern et al., 2012). On the other hand, several small molecule DUB inhibitors have shown therapeutic potential in preclinical trials (Mattern et al., 2012).

The development of DUBs as therapeutic targets for cancer and other diseases requires a more detailed understanding of the function and regulation of these enzymes.

## **1.2. HUMAN DEUBIQUITINATING ENZYMES (DUBs)**

The human genome encodes nearly 100 putative DUBs, although only 79 of them are predicted to be active enzymes (Nijman et al., 2005a).

### **1.2.1. Cellular functions of DUBs**

The major cellular functions of DUBs are illustrated in **Figure 5**. A first function is the processing of ubiquitin precursors (**Figure 5 a**). Ubiquitin is expressed from several genes as a linear fusion of multiple ubiquitin moieties or fused with ribosomal proteins. The generation of a pool of free ubiquitin units in cells requires DUB activity. A second function consists on the removal of degradative or non-degradative ubiquitin tags from proteins. By removing the ubiquitin tags from modified substrates, DUBs may reverse ubiquitin signaling or rescue a substrate from degradation (**Figure 5 b,c**). A third function relates to the recycling of ubiquitin moieties from those ubiquitinated proteins that undergo proteasomal degradation. This activity of DUBs is critical to maintain the pool of free ubiquitin (**Figure 5 d,e**) (Swaminathan et al., 1999; Verma et al., 2002). Finally, by helping to exchange one type of ubiquitin modification for another, DUBs

contribute to edit the length and topology of ubiquitin tags, and can thereby alter the fate of the ubiquitinated substrate (**Figure 5 f**) (Heyninck and Beyaert, 2005; Komander et al., 2009).

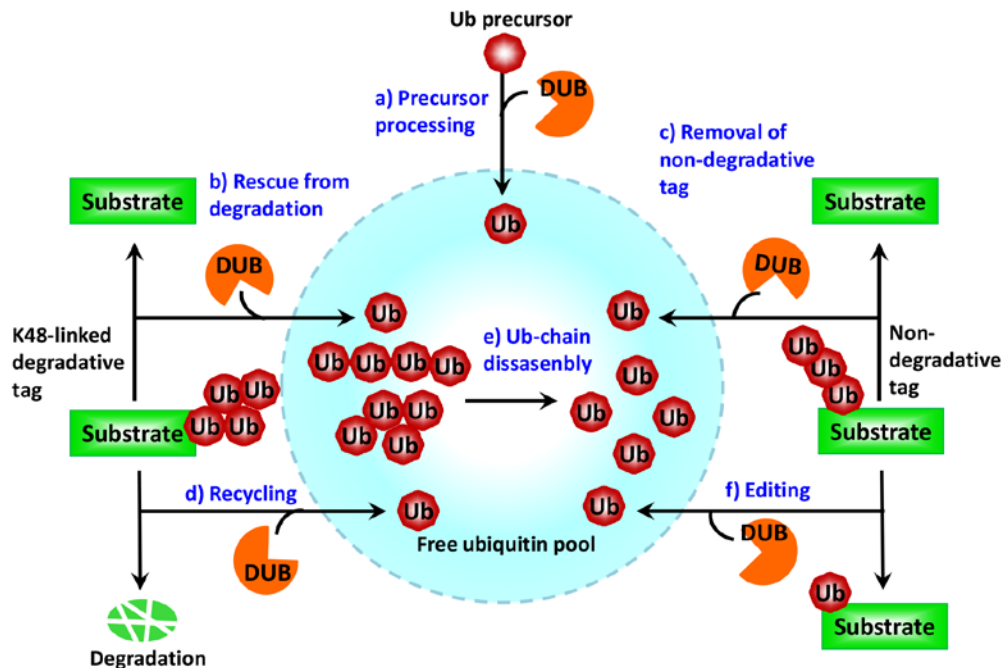


**Figure 5: Schematic diagram of DUBs functions.** Adapted from (Komander et al., 2009).

### 1.2.2. Domain architecture and classification of DUBs

DUBs are modular proteins. Besides their active site-containing core catalytic domain, they may contain additional inserted sequences as well as N- and/or C-terminal extensions. These additional amino acid sequences contribute to modulate the substrate specificity, protein-protein interactions, and subcellular localization of the enzymes, and may include, among others, motifs that recognize and non-covalently bind ubiquitin, such as the ubiquitin-binding domain (UBD), the ubiquitin-interacting motif (UIM) or the ubiquitin-associated motif (UBA) (Hurley et al., 2006), as well as ubiquitin-like domains (ULD) (Zhu et al., 2007).

Based on the structure of their catalytic domains, DUBs have been classified in five subfamilies: ubiquitin-specific proteases (USPs), ovarian-tumor proteases (OTUs), Machado-Joseph disease domain proteases (MJDs), ubiquitin C-terminal hydrolases (UCHs), and JAB1/MPN/Mov34 metalloproteases (JAMMs) (Nijman et al., 2005a)

(**Figure 6**). The first four families are cysteine proteases whose active site contains a so-called catalytic triad formed by cysteine, histidine and aspartate/asparagine residues. In contrast, JAMMs are zinc-dependent metalloproteases that contain histidine, aspartate and serine residues in their catalytic site (Komander, 2010; Nijman et al., 2005a).

The USP subfamily represents the largest and more diverse group of human DUBs, with more than sixty members (Komander et al., 2009; Nijman et al., 2005a; Quesada et al., 2004).

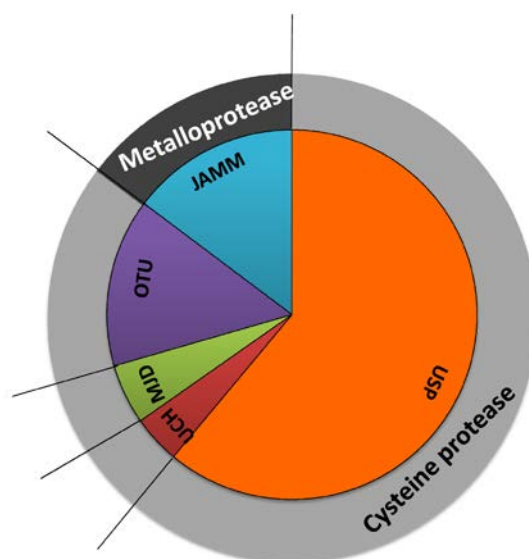


**Figure 6: DUB classification.** Human DUBs are classified in five subfamilies: USP, OTU, UCH, MJD and JAMMs.

### 1.3. THE USP SUBFAMILY OF DUBs

#### 1.3.1. General structural features and ubiquitin chain specificity of USPs

The DUBs belonging to the USP subfamily share a common structural fold of their catalytic domain, termed the USP fold (Dharadhar et al., 2016; Hu et al., 2002; Komander et al., 2009; Li et al., 2016; Reyes-Turcu et al., 2009).

The USP fold resembles an open right hand that contains three well-defined subdomains, referred to as the “Thumb” “Palm” and “Fingers” (**Figure 7**). The “Thumb” subdomain is principally composed of  $\alpha$ -helices and comprises the Cys Box, a region

that contains the active site cysteine. The “Palm” subdomain is formed by both  $\beta$ -strands and  $\alpha$ -helices and contains the other two catalytic amino acids: histidine and aspartate (or asparagine) residues. The catalytic core is located at the interface between the “Thumb” and “Palm” subdomains. This interface generates a cleft where the active site residues and the C-terminal tail of ubiquitin are accommodated (Hu et al., 2002, 2005; Komander et al., 2009; Renatus et al., 2006). The front side of the “Fingers” subdomain is the primary interaction site for ubiquitin. In several USPs, the “Fingers” subdomain contains a conserved Cys-X-X-Cys zinc-coordinating motif (Hu et al., 2002, 2005). Besides mediating ubiquitin binding, the “Fingers” subdomain may play an important role in the regulation of certain USPs, as described in detail in *section 4.2.2*.

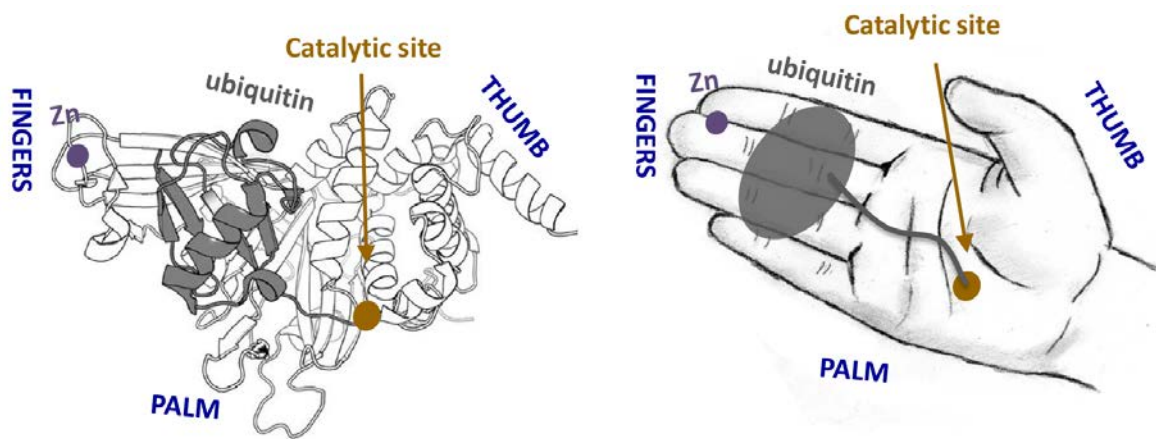


**Figure 7: Structural characteristics of the USP catalytic domain.** As a representative example, the structure of the catalytic domain of USP7 is shown on the left. The drawing on the right illustrates the “open right hand” shape that characterizes the USP domain. The “Thumb”, “Palm” and “Fingers” subdomains are indicated. The catalytic site is depicted in brown and the Zn binding site is represented in light purple. An ubiquitin molecule bound to “Fingers” subdomain is shown in grey. *Adapted from* (Faesen et al., 2012).

Despite their structural similarities, the catalytic domain of different USPs shows only limited amino acid sequence conservation. A detailed sequence alignment analysis (Ye et al., 2009) revealed that the USP core domain can be divided into six relatively-well conserved boxes (boxes 1–6) (**Figure 8**), but, several USPs, contain additional non-conserved domains of variable length inserted between the boxes. As a result of the presence of these insertions, the size of the catalytic domain may vary considerably between different USPs. It has been proposed that these so-called inserted domains play regulatory roles (Ye et al., 2009).



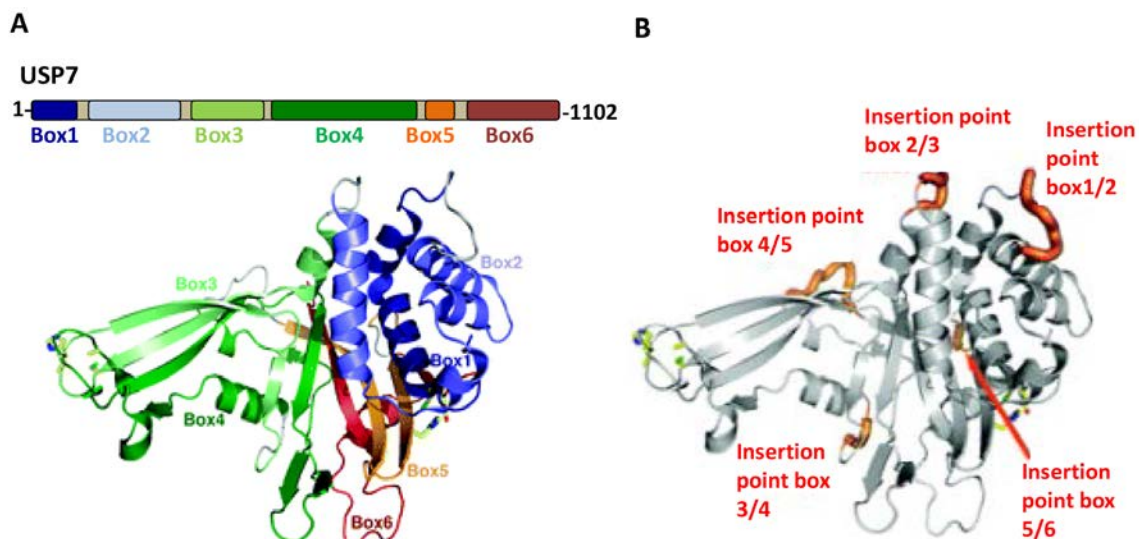


**Figure 8: Structure and box annotations of USP7, a representative example of the USP family.** **A.** Schematic illustration and ribbon representation of USP7 catalytic domain. The conserved boxes 1-6 are depicted in different colors **B.** Ribbon representation where the insertion points for non-conserved amino-acid segments are highlighted in red. *Adapted from* (Ye et al., 2009).

In comparison to DUBs belonging to other subfamilies, USPs are in general relatively promiscuous regarding the type of ubiquitin linkage they can cleave. Thus, whereas OTUs exhibit strong linkage preferences for specific di-ubiquitin topoisomers and many JAMMs are K63-specific (Bremm et al., 2010; Cooper et al., 2009; Faesen et al., 2011; Komander et al., 2009; Wang et al., 2009), some USPs, like USP4 and USP16, seem to be able to hydrolyze all ubiquitin topoisomers, including linear-linked ubiquitin chains (Faesen et al., 2011).

### 1.3.2. Regulation of USP catalytic activity

The catalytic activity of USPs is regulated by several mechanisms, including substrate-induced conformational rearrangement of the catalytic site, posttranslational modifications (PTMs) and binding to activating cofactors.

Upon binding to their ubiquitinated substrates, several USPs undergo different conformational changes that promote their catalytic activity. These changes may consist on the alignment of the catalytic triad in a productive conformation, as in USP7 (Hu et al., 2002), the displacement of a loop that blocks the catalytic site, as in USP14 (Hu et

al., 2002), or a movement of the “Fingers” subdomain to properly fit the globular body of the ubiquitin, as in USP8 (Avvakumov et al., 2006).

On the other hand, a variety of posttranslational modifications may regulate the catalytic activity of some USPs. A prominent example is the Akt-mediated phosphorylation of USP14, which activates its deubiquitinating activity (Xu et al., 2015).

Finally, a small subset of USPs requires binding to a cofactor to become catalytically active. The most prominent example of this regulatory mechanism is the activation of USP1, USP12 and USP46 by the WD-repeat containing protein WDR48/UAF1. These three USPs have a very low intrinsic deubiquitinating activity that is dramatically enhanced upon binding to the cofactor (Cohn et al., 2007, 2009). The work described in this Thesis focuses on different aspects of the function and regulation of the deubiquitinase complexes that USP1, USP12 and USP46 form with their cofactor WDR48/UAF1.

#### **1.4. WDR48/UAF1, AN ACTIVATING COFACTOR OF USP1, USP12 AND USP46**

The gene encoding WDR48/UAF1 is located on the 3p22.2 chromosomal region. A partial cDNA coding for a 607 amino acid protein (KIAA1449) was first identified in 2000 (Nagase et al., 2000). In 2002, Park and co-workers cloned the full-length cDNA encoding a 677 amino acid protein with a predicted molecular weight of 76.21 kDa, which they called p80 (Park et al., 2002). The officially recommended name for this protein is WDR48 (<http://www.uniprot.org/uniprot/Q8TAF3>). However, this protein is most commonly referred to as USP1-associated factor 1 (UAF1) in the scientific literature. For this reason, the name UAF1 will be hereafter used in this Thesis.

##### **1.4.1. UAF1 domain structure**

UAF1 belongs to the WD repeat (WDR) domain-containing protein family. This family is characterized by the presence of several copies of an approximately 40 residues-long sequence motif containing Trp-Asp repeats. UAF1 contains eight WD repeats. The structure of UAF1 reveals three different domains (**Figure 9**): repeats WD1-WD7 form the  $\beta$ -propeller domain, a domain shaped as a toroid with a narrow central pore, whereas

the WD8 repeat is included into the so-called ancillary-domain. On the other hand, the C-terminus of UAF1 contains a SUMO-like domain (SLD) with two subdomains (SLD1 and SLD2). The SLD adopts a coiled-coil conformation (Yin et al., 2015), although the structure of some regions of this domain remains unsolved in the currently available models. The SLD of UAF1 has been uncovered to be involved in the substrate recruitment (Yang et al., 2011).

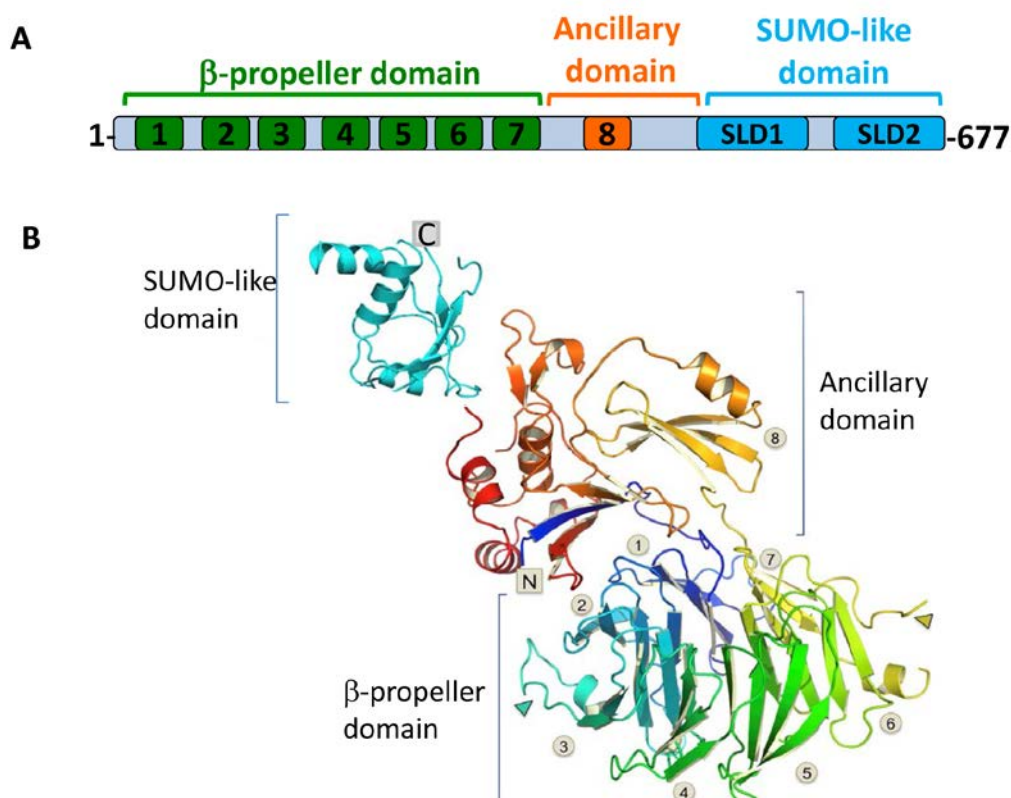


**Figure 9: Structure of UAF1.** **A.** Schematic representation of UAF1 domain structure: The  $\beta$ -propeller domain (green) with the WD repeats 1-7, the ancillary domain containing WD8 (orange) and the SUMO-like domain (blue) with the SLD1 and SLD2 subdomains are indicated. **B.** Three-dimensional structure of UAF1. The three domains, as well as the N- and C-termini are indicated, and the WD repeats are numbered. *Panel B is adapted from (Yin et al., 2015).*

### 1.4.2. UAF1 function

UAF1 was originally identified as a cellular protein targeted by the herpesvirus saimiri Tip protein during viral infection (Park et al., 2002). UAF1 has been subsequently found to bind other viral proteins, such as the E1 helicase of Human papillomavirus

(HPV) (Côté-Martin et al., 2008) or the EBNA3C protein of Epstein-Barr virus (EBV) (Ohashi et al., 2015) and to play a role in viral pathogenesis.

However, the best-characterized function of UAF1 is as a regulator of USP1, USP12 and USP46. UAF1 binding increases the stability of USP1, USP12 and USP46 (Cohn et al., 2007, 2009). In addition, UAF1 acts as a cofactor that stimulates the catalytic activity of these three enzymes (Cohn et al., 2007, 2009). The low intrinsic enzymatic activity of these DUBs is increased by up to 30 fold upon complex formation with UAF1 (Cohn et al., 2007; Faesen et al., 2011; Yin et al., 2015). By activating these DUBs, UAF1 contributes to regulate the ubiquitination level of several substrate proteins, and thus plays a role in a variety of cellular processes, which will be described in detail in *sections 1.5.2. and 1.6.2.*

Two different mechanisms have been proposed for UAF1-mediated stimulation of USPs. On one hand, UAF1 binding has been reported to induce a structural rearrangement of the DUB active site that allosterically increases catalytic turnover (Li et al., 2016; Villamil et al., 2012a). An alternative model proposes that activation relies mainly on UAF1-dependent stabilization of the DUBs, without significant rearrangements in their structure (Dharadhar et al., 2016; Yin et al., 2015). Of note, binding to UAF1 does not modify the affinity of the DUBs for their substrates (Yin et al., 2015).

## **1.5. THE USP1/UAF1 DEUBIQUITINASE COMPLEX**

The first deubiquitinase found to be activated by UAF1 was USP1 (Cohn et al., 2007). USP1 is a 785 amino acid protein with a predicted molecular weight of 88.2 KDa (Fujiwara et al., 1998), encoded by a gene located on chromosomal region 1p31.3. As detailed below, the USP1/UAF1 complex plays important roles in several aspects of the cellular response to DNA damage, and represents a potential target in cancer therapy.

### **1.5.1. Domain structure and functional motifs in USP1**

USP1 bears one of the largest catalytic domains within the USP subfamily due to the presence of inserted domains between boxes 2 and 3 and between boxes 5 and 6 (Ye et al., 2009). The catalytic domain of USP1 contains an N-terminal Cys box bearing the

catalytic residue C90 and a C-terminal His box bearing the catalytic residues H593 and D751. (Fujiwara et al., 1998; Villamil et al., 2012a) (**Figure 10**). Although the three-dimensional structure of USP1 has not yet been solved, a modeled structure suggests that these three amino acids, which constitute the catalytic triad, are close to each other forming the catalytic core of the enzyme (Villamil et al., 2012b). Mutation of any of these residues significantly decreases the catalytic activity of USP1 (Villamil et al., 2012a).

As indicated in **Figure 10**, several sequence motifs that contribute to modulate USP1 function have been identified in the inserted domains. The inserted domain between boxes 2 and 3 contains a degradation motif (degron) (Cotto-Rios et al., 2011a), a phosphorylation site (S313) (Cotto-Rios et al., 2011b; Villamil et al., 2012b) and two nuclear localization signals (NLSs) (Garcia-Santisteban et al., 2012). The inserted domain between boxes 5 and 6 includes an autocleavage site (G670-G671) (Huang et al., 2006). The relevance of these elements in the regulation of USP1 will be described in detail below.

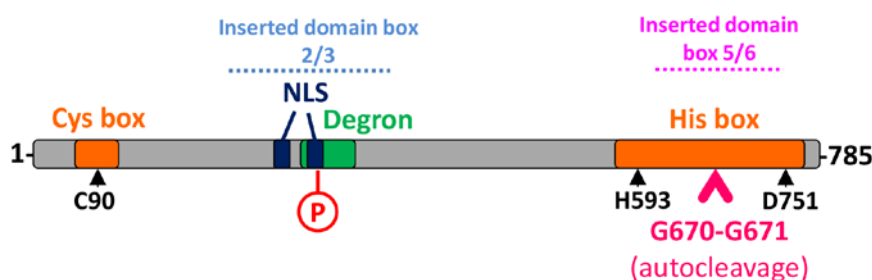


**Figure 10: Functional motifs in USP1** Schematic representation of USP1 protein showing the position of the amino acids that constitute the catalytic triad C90, H593 and D751 (black arrowheads). An inserted domain between boxes 2 and 3 contains a degron motif (green), the serine 313 phosphorylation site (red “P”) and two NLSs (dark blue). An inserted domain between boxes 5 and 6 contains a diglycine autocleavage site (pink).

### 1.5.2. The role of the USP1/UAF1 complex in the response to DNA damage

Living organisms can be exposed to a variety of endogenous and exogenous DNA-damaging agents that generate genomic lesions. To preserve genome integrity, cells

have evolved a complex array of mechanisms to detect, signal and repair these lesions, which collectively constitute the so-called DNA damage response (DDR) (Jackson and Bartek, 2009). During the DDR, multiple repair factors relocate into nuclear foci at the sites of damage (Lukas et al., 2004). Recruitment of these factors is regulated by a complex interplay of protein post-translational modifications (Zhao et al., 2014). In particular, ubiquitination has been shown to crucially regulate different DNA repair processes, such as translesion synthesis (TLS), the Fanconi anemia (FA) pathway and double-strand break (DSB) repair (Ulrich and Walden, 2010) (**Figure 11**).

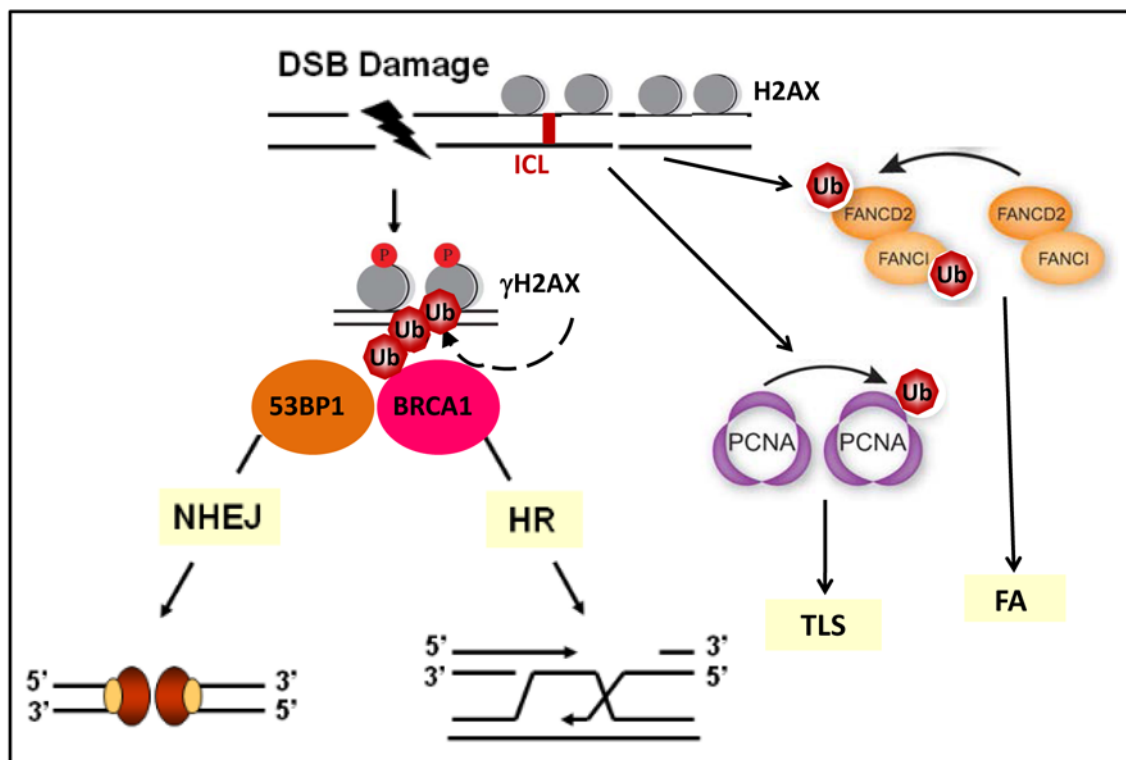


**Figure 11: Ubiquitination in the DNA damage response.** Following DNA double strand breaks (DSBs), histone H2AX is phosphorylated and recruited to the damage site. Next, downstream DNA repair factors, such as BRCA1 and 53BP1, are recruited in an ubiquitin-dependent manner to damage foci. In the response to interstrand DNA cross-link (ICL) lesions, Translesion Synthesis (TLS) and Fanconi Anemia (FA) pathways can be activated by ubiquitination of PCNA and FANCD2/FANCI, respectively.

DSBs are potentially hazardous chromosomal lesions. Two predominant pathways have evolved to repair DSBs: nonhomologous DNA end joining (NHEJ) and homologous recombination (HR). NHEJ operates by a direct ligation of the broken DNA ends, whereas HR involves repair of DSBs by duplicating the genetic information from the

---

sister chromatid. The balance between these pathways is essential for the successful maintenance of the genomic integrity. The first step following DNA damage, is the phosphorylation of histone H2AX ( $\gamma$ -H2AX) and its subsequent recruitment to damage foci. Then multiple repair factors, such as Breast cancer 1 (BRCA1) and p53-binding protein 1 (53BP1), relocalize into nuclear damage foci (Lukas et al., 2004). Recruitment of these factors is crucially regulated by ubiquitination (Ulrich and Walden, 2010). Genetic evidence suggests that BRCA1 and 53BP1 are the responsible for the choice between HR and NHEJ, respectively (Bouwman et al., 2010; Chapman et al., 2012).

The role of the ubiquitin conjugation machinery in the DNA damage response has been relatively well studied, but considerably less is known about the role of DUBs in these processes. In this regard, USP1 was one of the first DUBs identified as a DDR regulator. In particular, the USP1/UAF1 complex, regulates the Fanconi anemia (FA) pathway by deubiquitinating Fanconi anemia complementation group 2 (FANCD2) and Fanconi anemia complementation group I (FANCI) (Nijman et al., 2005b), as well as the process of translesion synthesis (TLS) by deubiquitinating Proliferating cell nuclear antigen (PCNA) (Huang et al., 2006). In addition USP1/UAF1 has been shown to promote HR-mediated DNA repair (Cukras et al., 2016; Liang et al., 2016; Murai et al., 2011).

Fanconi anemia (FA) is a rare genetic disease characterized by congenital malformations, progressive bone marrow failure, genomic instability, hypersensitivity to DNA cross-linking agents, such as mytomycin C (MMC) or cisplatin, and increased susceptibility to cancer (Kee and D'Andrea, 2012). To date, nineteen genes that encode Fanconi anemia complementation (FANC) group proteins have been identified. The products of these genes participate in a complex pathway that repairs interstrand DNA crosslinks (ICLs). Following DNA damage, eight FANC proteins (FANCA/B/C/E/F/G/L/M) form a multisubunit E3 ligase complex, termed the FA core complex. The FA core complex monoubiquitinates two other FA proteins, FANCD2 (at residue K561) and FANCI (at residue K523). Monoubiquitinated FANCD2 (UbFANCD2) and FANCI (UbFANCI) are subsequently translocated to DNA damage sites and recruit downstream DNA repair proteins (FANCD1J/N/O/P) (Kim and D'Andrea, 2012). USP1 regulates the FA pathway by deubiquitinating UbFANCD2 and UbFANCI, thus reversing the activation of the pathway (**Figure 12**; left panel). The

importance of a timely inactivation of FA pathway by USP1 is demonstrated by the observation that USP1 or UAF1 gene knockout in murine models or DT40 chicken cells results in a phenotype that resembles the phenotype of human patients with FA (Kim et al., 2009; Murai et al., 2011; Oestergaard et al., 2007; Park et al., 2013).

In addition to the FA pathway, USP1 also participates in translesion synthesis (TLS). TLS is a DNA damage tolerance mechanism that involves DNA replication by specialized DNA polymerases, called TLS polymerases (Waters et al., 2009). Following DNA damage that stalls the progression of the replication fork, PCNA is monoubiquitinated at K164 by RAD6 and RAD18 E3 ligases (Hoege et al., 2002). Monoubiquitinated PCNA (UbPCNA) promotes a switch between the classical replicative polymerases and the TLS polymerases, which can bypass the lesion and continue replication (Fox et al., 2011). However, TLS polymerases have a lower fidelity, and thus, TLS is a highly mutagenic process that needs to be tightly regulated. Central to this regulation, USP1 deubiquitinates UbPCNA, thus contributing to prevent unscheduled recruitment of error-prone TLS polymerases (Huang et al., 2006) (**Figure 12**; middle panel).

Finally, USP1/UAF1 promotes homologous recombination by an as yet unknown mechanism that appears to involve the suppression of the NHEJ pathway (Murai et al., 2011). This function has been reported to be, at least in part, mediated by interaction of UAF1 with RAD51-associated protein 1 (RAD51AP1) in a manner that could be independent from USP1 (Cukras et al., 2016; Liang et al., 2016) (**Figure 12**; right panel).



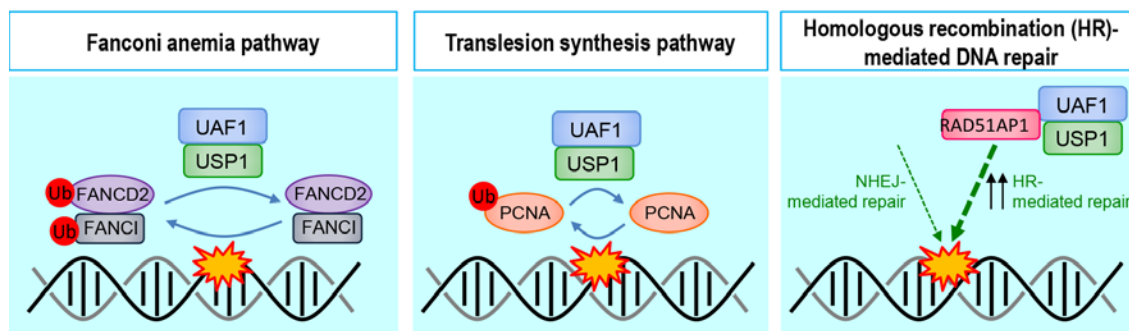


**Figure 12: Summary of the roles of the USP1/UAF1 complex in the DNA damage response.** USP1/UAF1 regulates DNA repair by reverting the monoubiquitination of FANCD2/FANCI in the Fanconi anaemia (FA) pathway and of PCNA in the translesion synthesis (TLS) pathway. In addition, the USP1/UAF1 complex promotes the repair of DNA damage via homologous recombination (HR) by the interaction of UAF1 with RAD51AP1.

To conclude, it is important to note that the function of USP1/UAF1 in the nucleus extends beyond its DDR-related roles, to include deubiquitination of inhibitors of DNA binding (ID) proteins (Williams et al., 2011). ID proteins, which are expressed in several undifferentiated and proliferative cells, negatively regulate basic-helix-loop-helix (bHLH) transcription factors and thus, inhibit cell differentiation. By deubiquitinating and stabilizing ID proteins, USP1/UAF1 contributes to maintain stem cell features in osteosarcoma (Williams et al., 2011). It can be reasonably assumed that the USP1/UAF1 complex may have still unknown substrates and carry out additional cellular functions that remain to be elucidated. To explore this possibility, we have used a novel proteomics-based strategy, termed <sup>bio</sup>Ub (Franco et al., 2011) to search for potential novel USP1/UAF1 targets, as described in *section 3.7.1*.

### 1.5.3. Regulation of the USP1/UAF1 complex

In addition to the catalytic activation of USP1 that results from binding to UAF1, several other regulatory mechanisms converge to determine the levels, localization and activity of USP1, ensuring that the function of the USP1/UAF1 complex is carried out in a properly controlled spatio-temporal manner. These mechanisms include cell cycle-regulated expression, autocleavage/degradation, phosphorylation, and subcellular localization.

Transcription of the USP1 gene is cell cycle-regulated: USP1 mRNA levels are low during G1 and reach a peak during S phase (Nijman et al., 2005b). The levels of USP1 protein are also regulated in a cell cycle-dependent manner by proteasomal degradation. In this respect, USP1 contains a degradation motif (degron) comprising amino acids 295-342 which is recognized by the Anaphase Promoting Complex/Cyclosome<sup>Cdh1</sup> (APC/C<sup>Cdh1</sup>) E3 ligase in G1, leading to USP1 degradation (Cotto-Rios et al., 2011a). APC/C<sup>Cdh1</sup>-induced degradation of USP1 can be further regulated by two different mechanisms. On the one hand, Cyclin-dependent kinase 1 (Cdk1)-mediated phosphorylation of USP1 at serine 313 could mask the degron motif and thus prevent USP1 degradation in M phase (Cotto-Rios et al., 2011b). On the other hand, calpains may indirectly prevent APC/C<sup>Cdh1</sup>-induced degradation of USP1 by activating Cdk5, a Cdh1 inhibitor (Cataldo et al., 2013).

Besides the cell cycle-related oscillations in USP1 levels, the activity of the USP1/UAF1 complex needs to be tightly regulated in response to genotoxic lesions. Thus, activation of FA and TLS pathways require the downregulation of USP1/UAF1 function in order to avoid FANCD2/FANCI and PCNA deubiquitination. In this regard, USP1 transcription is stopped upon DNA damage by a mechanism involving the p21 cyclin-dependent kinase inhibitor (Rego et al., 2012). In addition, exposure to genotoxic agents promotes autocleavage of the USP1 protein at the G670/G671 diglycine motif (Huang et al., 2006) (**Figure 10**). This cleavage event generates an N-terminal fragment (residues 1-671) and a shorter C-terminal fragment (672-785) of USP1, which are eventually degraded by the proteasome. USP1 autocleavage is thought to represent an important regulatory mechanism for USP1/UAF1 function. However, several aspects of this mechanism remain to be elucidated.

The function of the USP1/UAF1 complex can be also regulated by phosphorylation of USP1. The most relevant phosphorylation site in USP1 appears to be the serine residue at position 313. Besides the effect of this modification on APC/C<sup>Cdh1</sup>-induced USP1 degradation described above, S313 phosphorylation has been reported to regulate UAF1 binding. Using *in vitro* pull-down assays with purified recombinant proteins, Villamil et al, mapped the UAF1-binding region of USP1 to the non-conserved inserted domain between boxes 2 and 3 of USP1 (amino acid segment 235-408), which contains the S313 residue. They reported that this residue needed to be phosphorylated for the

USP1/UAF1 interaction to occur (Villamil et al., 2012b) (**Figure 13**). In contrast to these findings, our group had previously mapped the UAF1-binding region of USP1 to the amino acid segment 420–520 using cell-based assays (Garcia-Santisteban et al., 2012). This segment does not include the S313 phosphorylation site (**Figure 13**), and thus our findings raised questions about how modification of this residue could modulate USP1/UAF1 interaction. One of the aims of this Thesis has been to clarify these conflicting results, and to determine to what extent S313 phosphorylation contributes to USP1/UAF1 interaction.

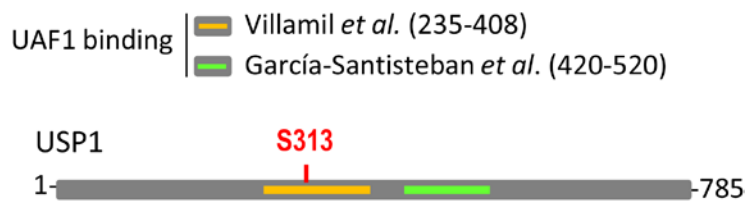


**Figure 13: Schematic representation of USP1 showing the two reported UAF1 binding sites.** The UAF1 binding site reported by Villamil et al. (including the serine 313 phosphorylation site) is highlighted in yellow. The UAF1 binding site reported by Garcia-Santisteban et al. is coloured in green.

Finally, the subcellular localization of the USP1/UAF1 complex is largely determined by two nuclear localization signals (NLSs) in USP1 (Garcia-Santisteban et al., 2012). In contrast to USP1, which is located in the nucleus, UAF1 is a cytoplasmic protein when expressed alone (**Figure 14A**). Our current data support a model in which USP1 and UAF1 form a complex in the cytoplasm that is subsequently relocated to the nucleus (Garcia-Santisteban et al., 2012) (**Figure 14B**). Thus, UAF1 enters the nucleus via a piggyback mechanism mediated by USP1 NLSs. Importantly, the nuclear relocation of UAF1 that results from USP1 co-expression provides a clear readout to analyze USP1/UAF1 complex formation in cells (**Figure 14C**) and can be easily applied to evaluate the ability of different USP1 or UAF1 mutants to interact with each other.

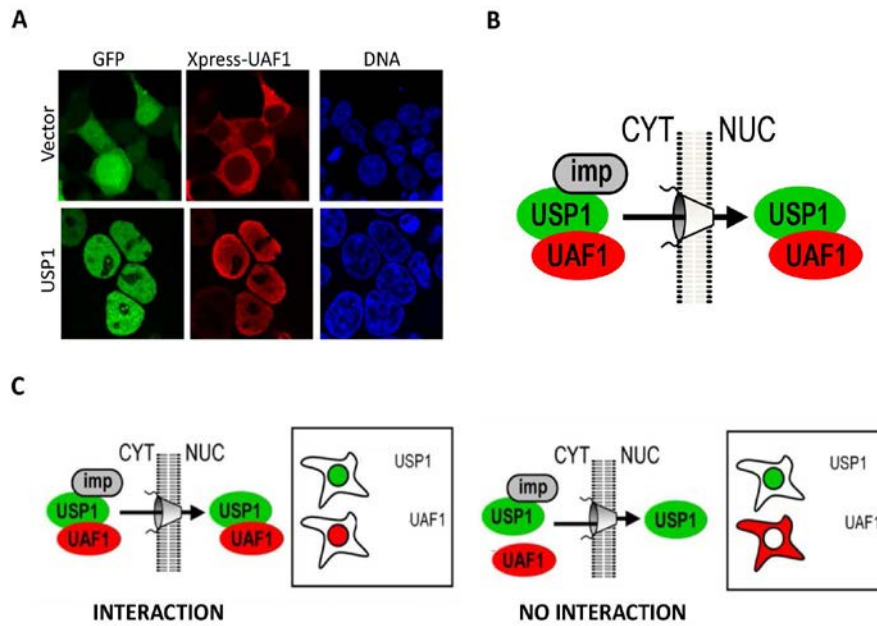


**Figure 14: Two NLSs in USP1 mediate the nuclear localization of USP1/UAF1. A.** Confocal images of 293T cells co-expressing Xpress-UAF1 with an empty GFP vector or with GFP-USP1. Xpress-UAF1 (red) relocates to the nucleus when co-expressed with GFP-USP1 (green), but remains in the cytoplasm when co-expressed with GFP. **B.** Model illustrating the import of the USP1/UAF1 complex to the cell nucleus. USP1 (green) and UAF1 (red) form a complex in the cytoplasm that is subsequently transported into the cell nucleus through active nuclear import mediated by the interaction between USP1 NLSs and importins (imp). **C.** UAF1 nuclear relocation assay. The interaction between USP1 and UAF1 complex can be observed in cells as a relocation of UAF1 to the nucleus. *Panels B and C are taken from (Garcia-Santisteban et al., 2012).*

#### 1.5.4. USP1 alterations in cancer

The DUBs that participate in the DNA damage response are increasingly gaining interest from the point of view of anticancer therapy. Given the crucial role of USP1 in this process, it is reasonable to assume that aberrant expression or mutational alteration of this DUB might contribute to cancer development.

USP1 mRNA levels are significantly altered in different human tumor types. In particular, USP1 is often overexpressed in cervical and gastric cancer, melanoma and sarcoma (García-Santisteban et al., 2013). On the other hand, although USP1 gene mutations are not a frequent event in human tumors, the Catalogue Of Somatic Mutations in Cancer (*COSMIC*) database (<http://cancer.sanger.ac.uk/cosmic>) includes

more than 100 USP1 gene mutations. Most of these mutations are missense substitutions (**Figure 15**), whose functional effect has not yet been tested (Forbes et al., 2011). We present a functional characterization of a subset of cancer-related USP1 mutants in *section 4.3.2*.

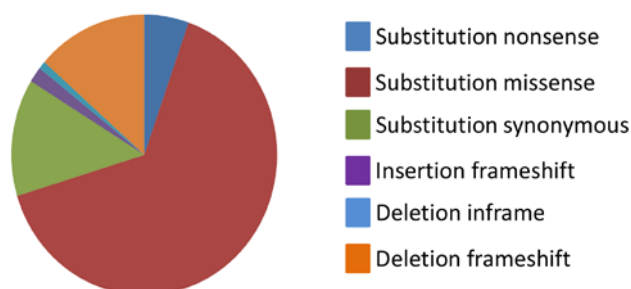


**Figure 15: Types of cancer-associated mutations in USP1.** Distribution of cancer-associated USP1 mutations reported in the *COSMIC* mutation database.

### 1.5.5. The USP1/UAF1 complex as a therapeutic target in cancer

A mainstay of conventional cancer therapy is the use of platinum-based genotoxic drugs, such as cisplatin or oxaliplatin. However, the DNA damage induced by these agents may lead to the activation of DNA repair pathways, which may act as escape routes resulting in resistance of cancer cells to the chemotherapy (Housman et al., 2014).

Importantly, interfering with USP1 function has been shown to increase sensitivity to a variety of chemotherapeutic agents in several model systems (Kim et al., 2009; Murai et al., 2011). These observations have led to propose that targeting the USP1/UAF1 complex might be a relevant approach to overcome resistance to commonly used chemotherapeutic drugs (Jackson and Durocher, 2013).

Several small molecule inhibitors that block the activity of USP1/UAF1 complex have been reported over the last years.

In 2011, a high throughput screening (HTS), lead to the identification of pimozone and GW7647 (Chen et al., 2011). In 2013, a similar screening identified SJB2-043, which inhibited the growth of leukemic cells (Mistry et al., 2013). In 2014, ML323, the most

selective USP1/UAF1 inhibitor reported to date was developed (Dexheimer et al., 2014). Finally, this year, a compound called SJB3-019A has been shown to inhibit USP1 and to decrease cell viability in myeloma cells (Das et al., 2017). Remarkably, pimozone, GW7647 and ML323 have been shown to reverse the resistance of non-small cell lung cancer (NSCLC) cells to cisplatin (Chen et al., 2011). These data suggest that combining USP1 inhibitors with platinum-based drugs can be a valid therapeutic strategy in cancer treatment. However, besides NSCLC, there is no information about the potential effects of this combination in other cancer types. In *section 4.3.3.3*, we present data on the effect of the combination of ML323 with oxaliplatin in cellular models of pancreatic cancer.

It is important to note that all the compounds described above are small-molecules that directly block the catalytic activity of USP1. Taking into account that USP1 enzymatic activity requires UAF1 binding, disruption of the USP1/UAF1 interaction could be an alternative strategy to inhibit USP1 for therapeutic purposes. As a first step to explore this possibility, a more detailed characterization of the USP1/UAF1 binding interface is necessary. In *section 4.2.3*, we describe our efforts to fine-map the amino acid residues that contribute to USP1/UAF1 interaction.

## **1.6. THE USP12/UAF1 AND USP46/UAF1 DEUBIQUITINASE COMPLEXES**

The USP12 gene is located in 13q12.13 and the USP46 gene is located in 4q12. These genes encode very similar proteins, USP12 (370 amino acids) and USP46 (366 amino acids), with 88% amino acid sequence identity. As described above for USP1, binding to UAF1 significantly enhances the catalytic activity of USP12 and USP46 (Cohn et al., 2009). However, full activation of these two enzymes, requires a second cofactor, termed WD-repeat containing protein 20 (WDR20) (Dahlberg and Juo, 2014; Kee et al., 2010).

### **1.6.1. Domain structure and functional motifs of USP12 and USP46**

USP12 and USP46 lack the inserted domains that are present in USP1, and are therefore shorter proteins. The three-dimensional structures of USP46 and USP12 have been recently solved (Dharadhar et al., 2016; Li et al., 2016; Yin et al., 2015). These DUBs

contain the catalytic triad that characterizes the USP family (**Figure 16A**), and the structure of their catalytic domains shows the distinctive open right hand conformation with the “Fingers”, “Thumb” and “Palm” subdomains (**Figure 16B**). There is still very limited information on the specific sequence motifs that contribute to their function, regulation or localization.

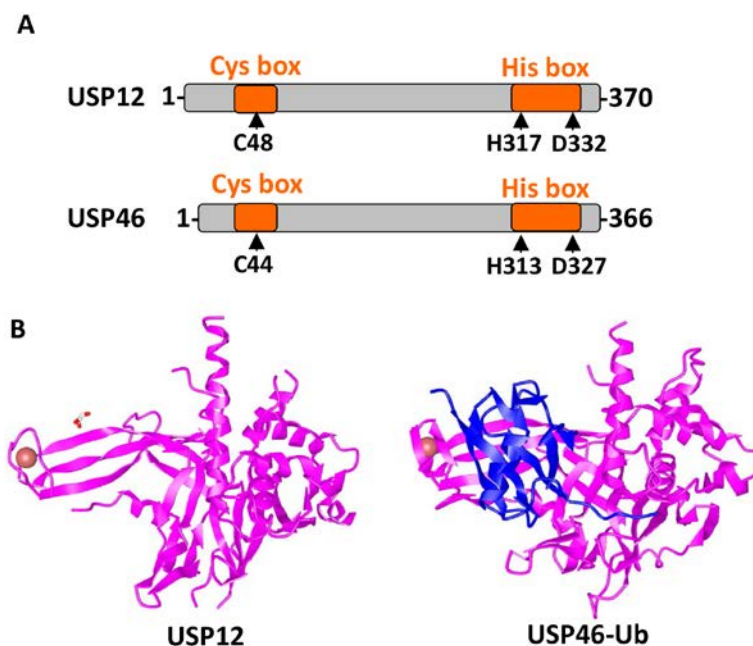


**Figure 16: USP12 and USP46 domains and structure.** **A.** Schematic representation of USP12 and USP46 showing the position of the residues that form the catalytic triad (USP12 C48/H317/D332 and USP46 C44/H313/D327). The N-terminal Cys box and the C-terminal His box domains are indicated in orange. **B.** Structural representation of free USP12 (left) and ubiquitin bound USP46 (right) showing the conserved open right hand conformation of the “USP fold”. The Zn atom is illustrated as a pink circle (*Taken from NCBI Structure*).

### 1.6.2. Cellular functions of the USP12 and USP46

As it might be expected from the high amino acid sequence similarity between USP12 and USP46, they share some substrates and participate in common cellular processes (summarized in **Figure 17**). For example, USP12 and USP46 regulate embryonic development in a *Xenopus* model by deubiquitinating histones H2A and H2B (Joo et al., 2011). In addition, both DUBs negatively regulate the Akt signaling pathway by stabilizing the Pleckstrin Homology domain Leucine rich repeat Protein Phosphatases

(PHLPPs) (Gangula and Maddika, 2013; Li et al., 2013), and thus play a crucial role in cell survival, proliferation, migration and cell death.

Remarkably, each of these DUBs has also specific substrates and regulates specific processes. On one hand, USP12 regulates Notch signaling by stabilizing the nonactivated form of the Notch receptor NotchR (Moretti et al., 2012), T-cell receptor (TCR) signaling by stabilizing the TCR signaling complex (Jahan et al., 2016), and androgen receptor (AR) signaling by stabilizing the AR protein (Burska et al., 2013; McClurg et al., 2014). On the other hand, USP46 may contribute to modulate synaptic transmission in the brain by deubiquitinating and regulating the turnover of neuronal glutamate receptors (GluR) and AMPA receptors (AMPA) (Dahlberg and Juo, 2014; Huo et al., 2015).

DUB	SUBSTRATES	CELLULAR PROCESSES
USP12	H2A H2B PHLPP Notch R AR TCR	Embryonic development (Xenopus) Signaling (Akt, Notch, Androgen receptor and T-cell receptor pathways)
USP46	H2A H2B PHLPP Glu R AMPA R	Embryonic development (Xenopus) Signaling (Akt pathway) Synaptic transmission ( <i>C. elegans</i> )

**Figure 17: Summary of the substrates and cellular roles of USP12 and USP46.** Common substrates are outlined in green and disparate substrates are outlined in red.

### 1.6.3. Regulation of USP12 and USP46 by UAF1 and WDR20

In the original report describing the USP12/UAF1 and USP46/UAF1 interactions, it was noted that these DUBs were activated by UAF1 to a lesser degree than USP1 (Cohn et al., 2009). It was later found that a second WD-repeat containing protein, WDR20, interacts with USP12 and USP46, but not with USP1, and further enhances the catalytic activity of these two enzymes (**Figure 18A**) (Dahlberg and Juo, 2014; Kee et al., 2010). WDR20 is a 569 amino acid protein containing a  $\beta$ -propeller domain architecture



formed by five WD repeats (**Figure 18B**). WDR20 has been proposed to regulate the activity of these enzymes through an allosteric mechanism, without altering their substrate affinity (Li et al., 2016).

The three-dimensional structure of a ternary USP12/UAF1/WDR20 complex (Li et al., 2016) has recently been solved, providing novel insights into its regulation. WDR20 is closely engaged with the USP12 “Palm” subdomain (**Figure 18C**). The proposed model for USP12 activation by UAF1 and WDR20 suggests that UAF1 helps adjusting the topology of the Ub tail to USP12 active site, whereas WDR20 regulates the conformation of the catalytic cleft (Li et al., 2016). The structure of a USP46/UAF1 complex has been reported (Yin et al., 2015), but the structure of a ternary USP46/UAF1/WDR20 complex remains to be solved.

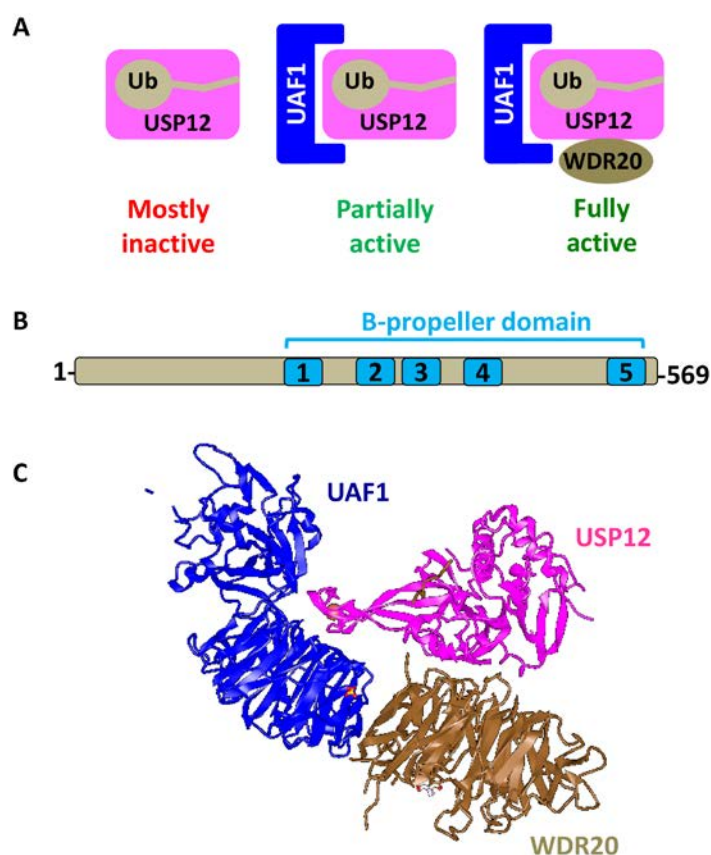


**Figure 18: USP12 forms a trimeric complex with UAF1 and WDR20 to achieve full catalytic activity.** **A.** Schematic representation of the level of enzymatic activity of free USP12, USP12/UAF1 complex and USP12/UAF1/WDR20 complex. **B** Schematic representation of the WDR20 protein showing the  $\beta$ -propeller domain with five WD repeats (blue). **C.** Three dimensional structure of the USP12/UAF1/WDR20 complex. Structures are taken from NCBI Structure.

In addition to UAF1 and WDR20, a global proteomics analysis identified several proteins that interact with both USP12 and USP46 (Sowa et al., 2009). Reported common interactors of these DUBs included PHLPP, PHLPP1 and DMWD. In our view, it is remarkable that USP12 and USP46, being very similar proteins and sharing many interactors, are nevertheless able to carry out disparate cellular functions, as described above. The molecular mechanisms that may underlie their functional differences are still unknown, but they could be related to a differential interaction of these DUBs with their regulatory cofactors or with other cellular proteins. A series of experiments carried out to test this possibility is described in *section 4.5*.

# **Hypotheses and aims**

**2**



## 2. Hypotheses and aims

The work presented in this Thesis deals with three human deubiquitinases USP1, USP12 and USP46, whose enzymatic activity is regulated by the cofactor UAF1. Most of the work focuses on USP1.

Over the last years, our knowledge about the role of USP1 as a crucial regulator of the DNA damage response has significantly increased. However, several aspects of the basic biology of this enzyme, including its regulation, remain to be fully characterized. We began this work (see **aim 1**) by trying to shed further light on three important regulatory mechanisms of USP1 (phosphorylation, autocleavage and UAF1 binding), and to clarify the controversies that have arisen regarding some of them.

USP1 is emerging as a potential therapeutic target in the treatment of cancer. However, there is no information about the functional effects of USP1 mutations detected in human tumors. We **hypothesized** that certain cancer-related missense mutations in USP1 could affect its binding to UAF1, autocleavage or function (see **aim 2**). On the other hand, USP1/UAF1 inhibitors, such as ML323, reverses resistance of cancer cells to chemotherapy, but ML323 has so far only been tested in NSCLC. We **hypothesized** that ML323 could show therapeutic potential in other tumor models, such as pancreatic cancer cells (see **aim 3**).

Finally, since only a limited number of bona-fide targets of USP1 (PCNA, FANCD2/FANCI and ID proteins) have been identified to date, we **hypothesized** that there would be USP1 substrates that remain to be identified (see **aim 4**).

On the other hand, USP12 and USP46 are two very similar proteins (88% amino acid sequence identity) whose enzymatic activity is regulated by UAF1 and WDR20. Remarkably, these enzymes participate in disparate cellular processes, but the mechanisms that may underlie these functional differences are unknown. We **hypothesized** that these mechanisms could be related to a differential interaction of USP12 and USP46 with their cofactors or with other cellular proteins (see **aim 5**).

Thus, the five aims of this Thesis are as follows:

**Aim 1.** To characterize in detail three aspects of the USP1 regulation that are controversial and/or not completely understood: phosphorylation, autocleavage and interaction with UAF1.

**Aim 2.** To investigate the functional consequences of several cancer-related missense mutations in USP1.

**Aim 3.** To evaluate the effect of the USP1 inhibitor ML323, in cellular models of pancreatic cancer, as a single agent and in combination with the chemotherapeutic drug oxaliplatin.

**Aim 4.** To identify novel USP1 substrates using the <sup>bio</sup>Ub system followed by mass spectrometry.

**Aim 5.** To investigate potential differences in the binding of USP12 and USP46 to their cofactors and other cellular proteins.

# **Materials and Methods**

3





## 3. Materials and Methods

### 3.1. BIOINFORMATICS TOOLS

#### 3.1.1. Sequence alignment and 3D structure modeling

Multiple sequence alignments were carried out using **ClustalW2** (<http://www.ebi.ac.uk/Tools/msa/clustalw2/>) (Larkin et al., 2007) or **Clustal Omega** (<http://www.ebi.ac.uk/Tools/msa/clustalo/>) (Sievers and Higgins, 2014).

The figures showing the modeled structure of USP1 and USP46 catalytic domains were prepared with **SWISS-MODEL** (<https://swissmodel.expasy.org/>) or **PyMOL** (<https://www.pymol.org/>) using the USP7 structure 1NB8 (Hu et al., 2002) as template. The figures showing the three-dimensional structure of USP12, USP46-ubiquitin and USP12-WDR20-UAF1 were taken from NCBI (Structure) (<https://www.ncbi.nlm.nih.gov/Structure>) and correspond to structures 5K16, 5CVM and 5K1C.

#### 3.1.2. COSMIC mutation database

In order to search for USP1 alterations in cancer, the publicly available **COSMIC** (Catalogue of Somatic Mutations in Cancer) database (<http://cancer.sanger.ac.uk/cosmic>) was used. This database describes over 136000 coding mutations in almost 542000 tumor samples (Forbes et al., 2011).

### 3.2. CLONING AND MUTAGENESIS

Several plasmids used in the Thesis were kindly provided by other researchers. A list of these plasmids and their original creators is provided as **Supplementary table 1**. On the other hand, the plasmids encoding GFP-USP1<sup>C90S</sup>, UAF1-mRFP, NLS-USP1(420-520)-GFP and YFP-USP1(del420-520) were previously generated by our group and have been described before (Garcia-Santisteban et al., 2012). Here we will describe the construction of the plasmids created for this Thesis, which are listed in **Supplementary table 2**.

### **3.2.1. “Classical”-restriction enzyme-based cloning**

Vector and insert were prepared separately, digested with the same restriction enzymes, ligated and used to transform chemically competent bacteria.

#### **3.2.1.1. Vector preparation**

1.5-2  $\mu\text{g}$  of the closed circular plasmid DNA were double digested with the desired restriction enzymes for 2 hours at 37°C. If a different reaction buffer was required for each enzyme, a sequential digestion was performed: first, DNA was digested with one enzyme, purified using the QIAquick PCR Purification Kit (Qiagen), and subsequently digested with the other enzyme.

For purification with the QIAquick PCR Purification Kit, 5 volumes of Buffer PB were mixed with 1 volume of DNA, placed in a QIAquick column and centrifuged for 1 minute at 13000 rpm. Flow-through was discarded, and the column was washed by adding 700  $\mu\text{l}$  Buffer PE and centrifuging twice for 1 minute at 13000 rpm. After placing the column in a clean microcentrifuge tube, H<sub>2</sub>O was added, incubated for 5 minutes, and centrifuged for 1 minute at 13000 rpm to elute the DNA. All centrifugations were carried out at room temperature.

To prevent vector self-ligation, digested vectors were dephosphorylated for 2 hours using alkaline phosphatase (AP, Roche), which removes the terminal 5'-phosphate residues from single- or double-stranded DNA. The dephosphorylation step was repeated two or three times. Finally, 2  $\mu\text{l}$  of 0.5 M EDTA were added to the dephosphorylation reaction and incubated for 10 minutes at 75°C to inactivate the AP.

Digested and dephosphorylated vectors were purified using the QIAquick PCR Purification Kit (Qiagen) as described above, and eluted in 30  $\mu\text{l}$  H<sub>2</sub>O.

### 3.2.1.2. Insert preparation

Three different methods were used to prepare the inserts:

#### 3.2.1.2.1. Insert preparation by restriction enzyme digestion (subcloning)

In those cases where the restriction enzyme sites were compatible, and the reading frame unaltered, the insert was excised from the original plasmid using restriction enzyme digestion. Briefly, the original plasmid was digested with the appropriate restriction enzymes for 2 hours at 37°C as described above. Next, digested DNA was separated in a 1.5% agarose gel made in 1XTAE with ethidium bromide. DNA was loaded onto the gel and run at 100 V for 15-25 minutes. The GeneRuler 1 kb DNA ladder plus (Thermo Fisher Scientific) was used as a marker. DNA was visualized using a UV transilluminator and the band corresponding to the insert was excised from the gel and purified using the QIAquick Gel Extraction Kit (Qiagen). The gel slice was dissolved in 3 volumes of Buffer QG by incubating at 50°C for 10 minutes. After adding 1 volume of isopropanol, the mixture was placed in a QIAquick column and centrifuged for 1 minute at 13000 rpm. The flow-through was discarded, 500 µl Buffer QG were added, and the column was centrifuged again for 1 minute at 13000 rpm. Flow-through was discarded, and washing and DNA elution steps were carried out as described in *section (3.2.1.1)*.

#### 3.2.1.2.2. Insert preparation by PCR

To prepare inserts by PCR, the template DNA was amplified with specific forward and reverse primers bearing the desired restriction sites. If needed, epitope tags or sequences required for the proper expression of the protein in eukaryotic cells were incorporated in the primers. These sequences include a Kozak sequence and a start codon (ATG) in the forward primer to ensure the initiation of the translation process, and a stop codon in the reverse primer to finish translation in those cases where a C-terminal tag was not present. The complete list of primers is provided in **Supplementary table 3**.

Forward and reverse primers were used to amplify the DNA template following the PCR reaction A and program A (*section 3.9.1*). The correct size of the PCR product was checked in an agarose gel. PCR products were purified using QIAquick PCR Purification Kit (Qiagen) as described above. Purified PCR products were digested for 2

hours at 37°C, purified again using the QIAquick PCR Purification Kit and eluted in 30 µl H<sub>2</sub>O.

#### 3.2.1.2.3. Insert preparation by using gBlocks

gBlocks (Integrated DNA Technologies) are custom double-stranded DNA fragments (up to 3 kb). Several inserts were purchased as gBlocks. Upon arrival, gBlocks were digested for 2h at 37°C, purified using the QIAquick PCR Purification Kit and eluted in 30 µl H<sub>2</sub>O.

#### 3.2.1.3. **Ligation of vector and insert and transformation of *E. coli* DH5α bacteria**

The digested vector and insert were run in an agarose gel to check their correct size and ratio. A ligation reaction was prepared maintaining a 3:1 insert:vector ratio. 10X reaction buffer (Fermentas), 10 mM ATP (Sigma), T4 DNA Ligase (Fermentas) and H<sub>2</sub>O up to a volume of 10 µl was added. The ligation mixture was incubated overnight at 4°C.

Chemically competent *Escherichia coli* DH5α bacteria were transformed with ligated DNA. Briefly, DH5α competent bacteria were thawed on ice. For a single transformation, 40 µl of bacterial suspension was mixed with 10 µl of ligation product in a thin-walled microtube, and incubated for 1 hour on ice. After heat-shock (37°C for 20 seconds), the tube was placed on ice for 5 minutes. Bacteria/DNA mix was added to a 15 ml tube containing 500 µl LB-medium and incubated at 37°C and 220 rpm in a shaker for 1 hour. Finally, all the suspension (~550 µl) was plated on an LB agar plate containing the appropriate antibiotic and incubated at 37°C overnight.

Next day, well-isolated colonies were picked from LB agar plates using a sterile toothpick, and grown overnight at 37°C and 220 rpm in 10 ml of LB medium containing the appropriate antibiotic.

### 3.2.2. **Gibson assembly cloning**

Gibson assembly is a cloning method that does not require the presence of compatible restriction enzyme ends in vector and insert. This method facilitates the joining of

multiple overlapping DNA fragments in a single-tube using a series of isothermal enzymatic reactions (Gibson et al., 2009). An overview of the Gibson Assembly Cloning Method is illustrated in **Figure 19**.

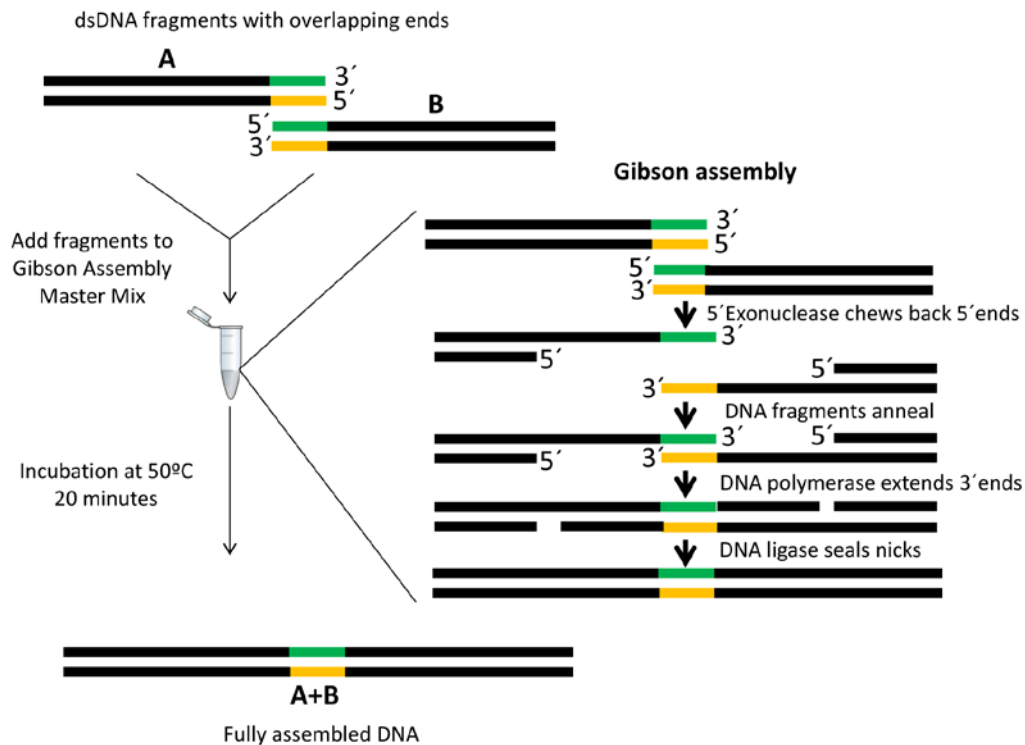


**Figure 19: Overview of the Gibson Assembly Cloning Method.** DNA fragments with overlapping ends are mixed with a Gibson Assembly master mix that includes three different enzymatic activities in a single buffer: the exonuclease that chews back 5' ends facilitating the annealing of fragments with overlapping region, the DNA polymerase that extends 3' ends and the DNA ligase that seals nicks in the assembled DNA.

Gibson assembly using the commercially available Gibson Assembly Cloning Kit (New England Biolabs) was carried out to clone the YFP-DMWD plasmid. Two separate, overlapping, DNA fragments that together encoded full-length DMWD cDNA were ordered as gBlocks (IDT). 160 ng of the two DNA fragments and 100ng of linearized pEYFP vector were mixed with 10  $\mu$ l of 2X Gibson Assembly Master Mix in a final volume of 20  $\mu$ l. The assembly reaction was incubated at 50°C for 20 minutes and then used to transform competent NEB5 $\alpha$  *E. coli* bacteria, essentially as described above for DH5 $\alpha$  bacteria.

Single colonies were picked from LB agar plates and grown overnight at 37°C and 220 rpm in 10 ml of LB medium containing the appropriate antibiotic.

### 3.2.3. Site-directed mutagenesis

The QuikChange Site-Directed Mutagenesis Kit (Stratagene) was used to generate point mutants. The list of mutants prepared using this strategy is provided in **Supplementary table 4**. The basic procedure, represented in **Figure 20**, uses a plasmid as DNA template and two synthetic primers containing the desired mutations (the complete list is provided in **Supplementary table 5**) These primers, each complementary to opposite strands of the plasmid, are extended by PCR, to generate a mutated plasmid. Next, the PCR product is treated with DpnI (a restriction endonuclease specific for methylated DNA) to digest the parental non-mutated DNA template and transformed into competent bacteria.

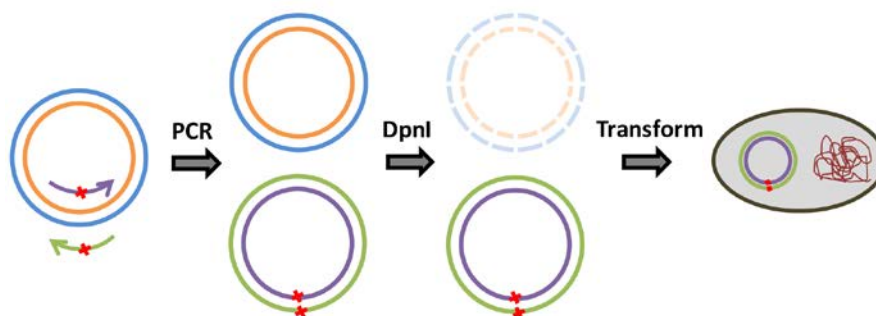


**Figure 20: Schematic representation of the site-directed mutagenesis strategy.** A pair of mutagenic primers (green and purple arrows) containing the desired point mutation(s) (red crosses) are used in a PCR reaction to generate mutated plasmids (green and purple). Parental non-mutated plasmids (blue and orange) are digested with DpnI. Finally, competent bacteria are transformed with the digestion product.

An optimized method (Zheng et al., 2004) was used for the design of mutagenic primers to minimize primer dimerization during PCR. The melting temperature ( $T_m$ ), which optimally should be higher than 81°C, was calculated with the following formula:

$$T_m = 81.5 + 0.41 \times (\%GC) - \frac{675}{N} - \% \text{ mismatch}$$

PCR reaction and program B (*section 3.9.1*) were used to amplify the template DNA with the pair of mutagenesis primers. Next, 2  $\mu$ l DpnI were added to the PCR reaction and incubated at 37°C for 5 minutes to digest parental non-mutated DNA. Finally, XL10-Gold ultracompetent bacteria were transformed with the digestion product. For a single transformation, 45  $\mu$ l of bacterial suspension were mixed with 2  $\mu$ l  $\beta$ -mercaptoethanol in a 15 ml tube, incubated for 2 minutes on ice, and 2  $\mu$ l of the PCR-digestion product were added and incubated for further 30 minutes on ice. After heat-shock (42°C for 30 seconds), the tube was placed on ice again for 2 minutes. Next, 500  $\mu$ l of pre-warmed LB-medium were added, and incubated at 37°C and 220 rpm for 1 hour in a shaker. Finally, all the suspension ( $\approx$ 550  $\mu$ l) was plated onto an agar plate containing the appropriate antibiotic and incubated at 37°C overnight. Picking of bacterial colonies and DNA isolation were carried out as described above.

If multiple mutations needed to be simultaneously introduced (e.g. to generate Xpress-UAF1<sup>2M</sup>, bearing K214E and W256A mutations), the QuikChange Multi Site-Directed Mutagenesis Kit (Stratagene) was used. The method is essentially as described above, but in this case, two different forward primers, one per mutation, are employed (PCR reaction and program C, *section 3.9.1*).

### **3.2.4. Plasmid isolation and DNA sequencing**

Bacterial suspensions were centrifuged at 3500 rpm for 10 minutes and QIAprep Spin Miniprep Kit (Qiagen) was used to isolate plasmid DNA. The pellet was resuspended in 250  $\mu$ l of Buffer P1 and transferred to a clean tube. The same volume of Buffer P2 was added and tubes were gently inverted 8-10 times to lyse bacteria. Next, 350  $\mu$ l of Buffer N3 were added and tubes were inverted again 8-10 times. After centrifuging for 10 minutes, the supernatant ( $\approx$ 700  $\mu$ l) was transferred to a QIAprep spin column and centrifuged for 1 minute. Flow-through was discarded and the column was washed adding 500  $\mu$ l Buffer PB and centrifuging again for 1 minute. The column was washed again with Buffer PE containing ethanol, and centrifuged twice for 1 minute to remove residual buffer. Finally, the column was placed in a clean microcentrifuge tube, 70  $\mu$ l H<sub>2</sub>O were added, incubated for 5 minutes, and centrifuged for 1 minute to elute DNA. All centrifugations, except the first one, were performed at 13000 rpm using a standard table-top microcentrifuge at room temperature.

All the new plasmids generated were confirmed by DNA sequencing at StabVida. The primers used for sequencing are listed in **Supplementary table 6**.

### **3.3. CELL CULTURE**

#### **3.3.1. Cell lines and cell culture conditions**

Cell lines were maintained as monolayer cultures in Dulbecco's modified Eagle's medium (DMEM) or Roswell Park Memorial Institute (RPMI) 1640 medium supplemented with 10% fetal bovine serum (FBS) and 1% penicillin/streptomycin (P/S) (Thermo Fischer Scientific) at 37°C in a humidified atmosphere containing 5% CO<sub>2</sub>. HeLa cervical adenocarcinoma, Human Embryonic Kidney 293T (HEK293T), hereafter called 293T cells and Hs766T pancreatic cancer cell lines were cultured in DMEM, whereas non-transformed HPDE and HPNE cell lines and the pancreatic cancer cell lines PDAC-1, PDAC-2, PDAC-3, PDAC-4, PDAC-5, BxPC-3, PANC-1, SU8686, CEPAC-1, HPAC, CAPAN-1, ASPC-1, MIAPaCa-2, HAF-II, PL45, SUIT 2.028, SUIT 2.027 and PP161 were cultured in RPMI 1640.

Cells growing in culture flasks were harvested when they reached confluency (twice or thrice a week). Briefly, old media was removed and cells were washed once with phosphate buffered saline (PBS). Cells were detached by incubation with trypsin-EDTA solution (Thermo Fischer Scientific) for about 2 minutes at 37°C, and resuspended in culture medium containing serum to inhibit further trypsin activity. The volume of cell suspension required to obtain the desired confluency was transferred to a new culture flask containing fresh medium.

#### **3.3.2. Cell seeding**

Prior to each experiment, cells were harvested (as described above) and depending on the cell line and type of experiment, a different number of cells was seeded onto different culture plates **Table 1**.



**Table 1: Number of cells seeded per well or plate for the different types of experiment.**

Experiment	Duration	Cell line	Type of plate	Nr of cells (per well /plate)
Immunofluorescence Live cells	3 /4days	HeLa, HEK293T,	12-well(with coverslip) 35mm	60-80% confluent
Western blot	3 days	HEK293T	6-well	$0.8 \times 10^6$
Western blot	4 days	HEK293T	6-well	$0.5 \times 10^6$
Western blot/qRT-PCR	3 days	Pancreatic cancer cells	10 cm dish	$1.5 \times 10^6$
Co-IP (GFP-Trap)	3 days	HEK293T	10 cm dish	$6.5 \times 10^6$
<sup>bio</sup> Ub pulldown	4 days	HEK293T	15 cm dish	$13.5 \times 10^6$
SRB assay	5 days	Pancreatic cancer cells	96-well	$0.04 \times 10^6$

For immunofluorescence or live cell microscopy experiments cells were seeded at 60-80% confluency onto sterile glass coverslips in 12-well culture plates (Costar) or in 35 mm ibiTreat  $\mu$ -dish slides (Ibidi), respectively.

For the rest of experiments the cell number was determined using a cell counting chamber. Briefly, the counting chamber was filled with an aliquot of cell suspension diluted in trypan blue solution. Only viable cells (non-stained with trypan blue) were counted. A total of four squares were counted, and cells touching only the upper and left lines of each square were considered to avoid counting the same cell twice. An average of the counts was multiplied by  $10^4$  and by the trypan blue dilution to give the number of cells/ml in the suspension.

### 3.3.3. Transfection

#### 3.3.3.1. DNA transfection

Twenty four hours after cell seeding, DNA transfection was performed using *XtremeGENE 9 (XTG9)* reagent (Roche). The transfection reagent was mixed with antibiotic- and serum-free DMEM, added drop by drop into a tube containing the plasmid DNA(1:2 DNA/*XTG9* ratio). The DMEM/transfection reagent/DNA tube was gently mixed, incubated for 25 minutes at room temperature and added drop by drop to

the cells whilst gently rocking the plate. Depending on the surface area (type of plate), different amounts of DNA, DMEM, transfection reagent and growth medium were used (Table 2).

**Table 2: Conditions for DNA transfection using *XtremeGENE9 (XTG9)* depending on the type of plate.**

Type of plate	ng DNA	$\mu\text{l}$ DMEM/XTG9	$\mu\text{l}$ growth medium
12-well	600	37.5	750
6-well	1200	75	1500
10cm	7200	450	9000
15cm	14400	900	19000

### 3.3.3.2. siRNA transfection

Transfection of small interfering RNAs (siRNAs) was performed using Lipofectamine RNAiMAX transfection reagent (Thermo Fisher Scientific) following manufacturer's recommendations. Briefly, transfection reagent was mixed with Opti-MEM Reduced Serum Medium (Thermo Fisher Scientific) and incubated for 2 minutes at room temperature. The transfection reagent/Opti-MEM mix was added dropwise into a tube containing siRNA diluted in Opti-MEM. The mixture was incubated for 20 minutes at room temperature and added to the cells whilst rocking the plate. For USP1 knockdown we used a pool of three commercial siRNAs from Ambion (Thermo Fisher Scientific) (s14723, s14724, and s14725) (10  $\mu\text{M}$ ). As a control, a siRNA oligonucleotide with no sequence specificity for any human RNA (siCTRL) was used (Thermo Fisher Scientific) (4390843) (10  $\mu\text{M}$ ). Depending on the type of plate, different amounts of siRNA, Opti-MEM, transfection reagent and growth medium were used (Table 3).

**Table 3: Conditions for siRNA transfection using Lipofectamine RNAiMAX depending on the type of plate.**

Type of plate	$\mu\text{l}$ siRNA	$\mu\text{l}$ Opti-MEM/RNAimax	$\mu\text{l}$ growth medium
12-well	1.5	120	1000
15 cm dish	20.25	1500	19000

### 3.3.4. Drug treatments

The following drugs were used in this Thesis: hydroxyurea (HU), a drug that arrests DNA replication, was used to induce monoubiquitination of PCNA; neocarzinostatin (NCS), a DNA damaging agent that produces DNA double-strand breaks, was used to induce the recruitment of 53BP1 and conjugated ubiquitin to DNA damage foci; the USP1 inhibitor ML323, and a platinum-based drug oxaliplatin.

Cells were treated for the time periods indicated in each experiment by replacing the growth medium with medium containing the desired drug at the concentration shown in **Table 4**.

**Table 4: List of drugs used in this study.** The drug, company, reference, stock and final concentrations (conc.) are indicated. \*ML323 and oxaliplatin final concentrations varied depending on the experiment; see *sections 3.3.5* and *section 3.5.1* for details.

Drug	Company	Reference	Stock conc.	Final conc.
Hydroxyurea (HU)	Sigma	H8627	500 mM	4 mM
Neocarzinostatin (NCS)	Sigma	N9162	0.5 mg/ml	100 ng/ml
ML323	Calbiochem	53-113-10001	100mM	50 $\mu$ M, *See legend
Oxaliplatin	Sigma	O9512	12.6mM	*See legend

### 3.3.5. Sulforhodamine B (SRB) cell viability assay

Cell viability was measured using the Sulforhodamine B (SRB) assay (Vichai and Kirtikara, 2006). Exponentially growing pancreatic cancer cells were seeded in 96-well plates, and 24 hours later were treated with oxaliplatin (0.0048, 0.019, 0.039, 0.078, 0.15, 0.31, 0.62 and 1.25  $\mu$ M), the USP1 inhibitor ML323 dissolved (0.39, 0.78, 1.5, 3.1, 6.25, 12.5, 25 and 100  $\mu$ M) or a combination of both drugs. The corresponding controls were incubated with growth medium without drugs, and their viability was considered as 100%. After 72 hours of drug exposure, the SRB assay was performed. Cells were fixed with ice-cold 50% (w/v) trichloroacetic acid (TCA) for 1 hour at 4°C, washed five times with H<sub>2</sub>O, and dried at room temperature. Next, plates were stained with SRB solution (0.4% (w/v) Sulforhodamine B (Acros Organics, Geel, Belgium) in

1% acetic acid) for 15 minutes at room temperature. Excess dye was then removed by washing four times with 1% (v/v) acetic acid, and dried again at room temperature. Finally, the protein-bound dye was dissolved in 10 mM Tris base solution for optical density determination at 492 nm using a microplate reader (Tecan Spectrafluor, Salzburg, Austria).

Growth inhibition curves, expressing growth inhibition as the percentage of control absorbance, were generated for each drug alone and in combination.  $IC_{50}$  values, defined as the drug concentration that inhibits cell growth by 50%, were calculated by fitting the data to a sigmoid dose-response curve using GraphPad Prism software (San Diego, CA). The percentage of cell survival was converted to fraction affected (Fa), defined as  $[100 - \% \text{ growth inhibition}]/100$ , and these data were used to determine the nature of the interaction between oxaliplatin and ML323.

Calculusyn software (Biosoft, Cambridge, UK) was used for the study of the pharmacological interaction between oxaliplatin and ML323. This program uses the median drug effect principle of Chou and Talalay (Chou and Talalay, 1984) to determine the combination index (CI), which quantitatively describes if the interaction between two drugs is antagonistic ( $CI \geq 1.2$ ), additive ( $0.8 < CI < 1.2$ ) or synergistic ( $CI \leq 0.8$ ) (**Table 5**). An antagonistic effect is observed when the combination of two drugs is less effective than the single drugs. An additive effect results when the combination of two drugs is equivalent to the sum of treatment with those drugs individually. A synergistic effect occurs when the effect of two drugs in combination is greater than the sum of individual effects of those drugs (Bijnsdorp et al., 2011). Calculusyn software was used to determine the CI values at a range of  $0.01 < Fa < 0.99$ , and to produce median-drug effect plots (Fa vs CI) for each cell line. Since experimental conditions with a Fa lower than 0.5 are generally considered as less therapeutically relevant (Bijnsdorp et al., 2011), CI values at Fa of 0.5, 0.75, and 0.9 were averaged for each experiment, and this value was used to calculate the mean between experiments. The resulting CI was used to determine if the combination of both drugs resulted in an antagonistic, additive or synergistic effect.

**Table 5: Simplified CI values and their interpretation following the method of Chou-Talalay:** A CI value below 0.8 indicates a synergistic effect. A CI value between 0.8 and 1.2 represents an additive effect. A CI value higher than 1.2 indicates antagonism.

Simplified CI values and their interpretation (Chou-Talalay Method)	
<0.8	Synergistic
0.8-1.2	Additive
>1.2	Antagonistic

### 3.4. FLUORESCENCE MICROSCOPY TECHNIQUES

#### 3.4.1. Immunofluorescence

Cells expressing GFP- or YFP-tagged fluorescent proteins were fixed with 3.7% formaldehyde (Sigma) in PBS for 30 minutes and coverslips were mounted onto microscope slides (Zuzi) using Vectashield aqueous mounting medium containing 4',6-diamidino-2-phenylindole (DAPI) (Vector Laboratories) to visualize the nuclei. To detect biotinylated proteins by fluorescence microscopy we used streptavidin, a bacterial protein with strong affinity for biotin, fluorescently labeled with AlexaFluor 594.

Detection of endogenous or ectopic proteins with non-fluorescent tags (e.g. Myc or Xpress epitopes) was carried out by immunofluorescence (IF). Cells were fixed with 3.7% formaldehyde in PBS for 30 minutes and permeabilized with 0.2% Triton X-100 (TX-100, Sigma) for 10 minutes. Following a blocking step with 3% bovine serum albumin (BSA, Sigma) in PBS for 1 hour, the primary antibodies were diluted in blocking solution, and applied for 1 hour. After washing twice with PBS, and adding BSA 3% for 1 minute, cells were incubated for 1 hour with the corresponding fluorescently-labelled secondary antibody diluted in blocking solution. After washing, coverslips were mounted onto microscope slides (Zuzi) using Vectashield with DAPI (Vector Laboratories). Details about the antibodies used for immunofluorescence are provided in **Table 6**.

**Table 6: List of antibodies used for immunofluorescence.**

<b>Antibody</b>	<b>Company</b>	<b>Reference</b>	<b>Host</b>	<b>Dilution</b>
<b>Xpress</b>	Thermo Fisher Scientific	R910-25	Mouse	1:300
<b>53BP1</b>	Novus	NB100-304	Rabbit	1:300
<b>FK2</b>	Enzo Life Sciences	BML-PW8810-0100	Mouse	1:600
<b><math>\gamma</math>H2AX</b>	Merck Millipore	05-636	Mouse	1:500
<b>Streptavidin-AF594</b>	Jackson Immuno Research	016-580-084	-	1:200
<b>Myc-tag</b>	Cell signaling Technology	#2276S	Mouse	1:400
<b>USP1</b>	Cell signaling Technology	#8033S	Rabbit	1:200
<b>Mouse AF633</b>	Thermo Fisher Scientific	A21050	Goat	1:400
<b>Mouse AF594</b>	Thermo Fisher Scientific	A11005	Goat	1:400
<b>Rabbit AF594</b>	Thermo Fisher Scientific	A11012	Goat	1:400

### 3.4.2. Live cell microscopy

293T cells were grown in 35mm ibiTreat  $\mu$ -dish slides (Ibidi) were transfected, and 24 hours later cells images were collected using Zeiss Apotome 2 fluorescence microscope with 40X objective.

### 3.4.3. Microscopes

Slides were examined at the SGIKER Analytical and High-Resolution Microscopy in Biomedicine Facility (UPV/EHU) using different microscopes:

For standard visualization, a Zeiss Axioskop fluorescence microscope was used, and images were taken with a Nikon DS-Qi1Mc digital camera and the NIS-Elements F software. For confocal image acquisition, an Olympus Fluoview FV500 microscope was used, and images were taken with Olympus FV-Viewer software. For live cell analysis, Zeiss Apotome 2 fluorescence microscope was used, and images were taken with ZEN 2 software.

### **3.4.4. Image analysis for quantification of FK2 fluorescence and 53BP1 foci**

#### **3.4.4.1. Quantification of FK2 (conjugated ubiquitin) fluorescence**

5 or 10 microscopy fields per sample were captured with a 40X objective using a fluorescence Zeiss Axioskop microscope both for GFP (green channel) and FK2 (red channel). Fluorescence levels in the nuclei of at least 50 cells per sample were quantified using the “mean grey value” (MGV) measurement option of Fiji software (Schindelin et al., 2012). Background fluorescence was subtracted. FK2 intensity in GFP-positive cells was normalized to the intensity in nontransfected cells. To ensure unbiased results, the analysis was carried out in a “blind” manner, by masking the identity of the samples prior to image acquisition and quantification.

#### **3.4.4.2. Quantification of 53BP1 foci**

Between 5 and 10 microscopy fields were captured per sample with a 40X objective using a fluorescence Zeiss Axioskop microscope for GFP (green channel) and 53BP1 (red channel). At least 100 GFP-positive cells per sample were analysed and cells were classified as positive (more than 5 53BP1 foci) or negative (5 or less foci). Finally, the percentage of positive cells was calculated. As above the analysis was carried out in a “blind” manner.

## **3.5. TECHNIQUES FOR RNA ANALYSIS**

### **3.5.1. RNA isolation**

To isolate total RNA, cells were lysed by pipeting up and down with 500 µl Trizol (Thermo Fisher Scientific), and incubated for 5 minutes at room temperature. Next, 100 µl chloroform were added, and tubes were vigorously shaken and incubated for 2-3 minutes at room temperature. Samples were centrifuged at 12000 g for 10 minutes at 4°C. The aqueous phase was transferred to a clean microcentrifuge tube before adding 250 µl isopropanol, mixed and incubated for 10-15 minutes at room temperature. The interphase containing genomic DNA was subsequently used for the analysis of DNA adducts (*section 3.5.4*). Samples were centrifuged at 12000 g for 10 minutes at 4°C, and

the supernatant was carefully removed. The RNA pellet was washed twice with 70% ethanol. Finally, the RNA pellet was air dried and resuspended in 20  $\mu$ l RNase free H<sub>2</sub>O, and immediately put on ice. The RNA quantity and quality were determined using a NanoDrop, and the A260/A280 ratio > 1.8 was used as a purity criterion for all samples. RNA samples were stored at -80°C until use.

### **3.5.2. cDNA synthesis**

Complementary DNA (cDNA) was synthesized using the Dynamo cDNA Synthesis Kit for qRT-PCR (Thermo Fisher Scientific). The total reaction volume for reverse transcription was 20  $\mu$ l and contained 10  $\mu$ l of 2x RT buffer, 300 ng of random hexamers, 800 ng of RNA, and 2  $\mu$ l of M-MuLV RNaseH + reverse transcriptase. The reactions were incubated at 25°C for 10 min for primer extension, at 37°C for 30 min for cDNA synthesis, and at 85°C for 5 min for reaction termination. The cDNA solutions were diluted 10-fold and stored at -20°C.

### **3.5.3. qRT-PCR**

Primers and probes to specifically amplify USP1 (Hs00163427\_m1), UAF1 (Hs00368247\_m1) and Human GAPDH Endogenous Control (4326317E) were obtained from Applied Biosystems Assay-on-Demand Gene expression products. The qRT-PCR reaction was performed in a 25- $\mu$ l volume containing TaqMan Universal master mix (Applied Biosystems). All reactions were performed in duplicate using an ABI PRISM 7500 Sequence Detection System instrument (Applied Biosystems). Samples were amplified using the following thermal profile: 50°C for 2 minutes, 95°C for 10 minutes, 40 cycles of denaturation at 95°C for 15 seconds followed by annealing and extension at 60°C for 1 minute. Amplifications were normalized to GAPDH. The fold change was calculated by the  $\Delta\Delta$ CT method (Livak and Schmittgen, 2001) and results were plotted as  $2^{-\Delta\Delta CT}$ .

### **3.5.4. Analysis of DNA adducts using quantitative extra-long PCR (XL-PCR) and Taqman assays**

Genomic DNA samples were then analyzed using an extra-long PCR (XL-PCR) assay, followed by quantification with Taqman assays. The XL-PCR assay is based on the fact



that DNA adducts can block DNA polymerases, thus interfering with the DNA replication and decreasing the yield of PCR product. Using long PCR amplicons improves the sensitivity of the assay. The amplified target sequence used in our assay is part of the  $\beta$ -globin locus. XL-PCR was performed using the specific GeneAmp XL-PCR Kit (Applied Biosystems), starting from 100 ng of template DNA. The amplification of a 17.7-kb region of the  $\beta$ -globin gene was performed using the specific primers listed in **Table 7**. XL-PCR was initiated at 70°C by the addition of the rTth DNA polymerase, followed by 25 cycles of 94°C for 15 seconds, 68°C for 12 minutes. There was a final extension for 10 minutes at 72°C. All the PCR reactions were performed in a GeneAmp-PCR-9700 machine (Applied Biosystems). Following XL-PCR, the reaction products were diluted ten-fold and quantified using TaqMan assays in the ABI PRISM-7500 instrument, using specific primers and probes listed in **Table 7** and the same program than in *section 3.5.3*. A standard curve was generated by serial dilution of XL-PCR-amplified products from genomic DNA extracted from untreated samples to calculate the amount of amplification of each sample.

**Table 7: Primers and probes for XL-PCR and TaqMan reactions.**

Primers for XL-PCR	Sequence (5'-3')
$\beta$ -globin Forward	TTG AGA CGC ATG AGA CGT GCAG
$\beta$ -globin Reverse	TCAG GTT GAG GAT TCG GTC ACG
Primers and probe for Taqman-PCR	Sequence (5'-3')
$\beta$ -globin Forward	GAC CAG CCT GAC CAA CAT GGT GAA AC
$\beta$ -globin Probe	CAG CCG GGC GTG TGG TGC AT
$\beta$ -globin Reverse	TCAGGGTCGATAAGTCCACCGA

### 3.6. TECHNIQUES FOR PROTEIN ANALYSIS

#### 3.6.1. Protein extraction

HeLa or 293T cells from 6-well plates were washed once with ice-cold PBS, lysed by scrapping in 100  $\mu$ l lysis buffer (supplemented with  $\text{Na}_3\text{VO}_4$ , PMSF, a protease inhibitor cocktail (PIC) (Roche) and N-ethylmaleimide (NEM)). Samples were incubated for 30 minutes in a rotating platform at 4°C, centrifuged at 13000 rpm for 10

minutes at 4°C, and the supernatant was transferred to a clean microcentrifuge tube. Protein concentration was determined using the *Lowry* method.

Protein extraction from pancreatic cancer cell was carried out by resuspending the cells in 60 µl RIPA lysis buffer (supplemented with Na<sub>3</sub>VO<sub>4</sub>, PMSF and a PIC (Roche)). Lysates were centrifuged at 13000 g for 10 minutes at 4°C. Supernatants were transferred to a clean microcentrifuge tube, and protein concentration was determined using the *Bradford* method.

### **3.6.2. Protein quantification**

#### **3.6.2.1. Lowry method**

Protein concentration was determined using the modified *Lowry* method with a Bio-Rad Protein Assay kit. Bovine serum albumin (BSA) was used as a standard. Briefly, Reagent A + Reagent S were mixed at 50:1 a ratio and 25 µl were added to the diluted protein or BSA. Subsequently, 200 µl of Reagent B were added on top, and the mix was incubated 15 minutes at room temperature. Absorbance was measured at 750 nm in a microplate reader (PowerWave340).

#### **3.6.2.2. Bradford method**

Protein concentration of pancreatic cancer cells was determined using the *Bradford* method with the Bio-Rad Protein Assay Dye Reagent Concentrate. BSA was used to prepare the standard curve. 200 µl of BioRad dye reagent were added to diluted protein samples or BSA and incubated for 5 minutes at room temperature. Absorbance was measured at 600 nm in a microplate reader (Tecan Spectrafluor, Salzburg, Austria).

Following quantification, the concentration of protein samples was adjusted with lysis buffer to ensure identical loading. Finally, 6X Protein Loading Buffer or 4X Sample Buffer (Thermo Fisher Scientific) were added and samples were heated at 95°C for 5 minutes.

### 3.6.3. Immunoprecipitation using GFP-trap magnetic beads

Magnetic GFP-Trap (GFP-Trap®\_M, Chromotek) beads were used for the immunoprecipitation of GFP-fusion proteins from cellular extracts. GFP-Trap®\_M contains a GFP-binding protein (GBP) covalently coupled to the surface of magnetic beads, which enables an efficient isolation of any protein of interest fused to GFP or its derivatives, including YFP (Rothbauer et al., 2008) using a magnet. GFP or YFP-transfected cells grown in 10 cm plates were washed with PBS, scrapped in 1 ml IP Lysis Buffer (Pierce) containing PMSF and protease inhibitors (Pierce), and incubated for 30 minutes on ice with extensive pipeting every 5-10 minutes. Cell lysates were centrifuged at 13000 rpm for 10 minutes at 4°C, and the supernatant was transferred to a clean tube. A 100 µl aliquot was mixed with 6X Protein Loading Buffer, boiled at 95°C for 5 minutes and stored to use it as whole cell extract (WCE). The remaining lysate was mixed with equilibrated GFP-Trap®\_M beads and incubated for 3 hours in a rotating platform at 4°C. Magnetic beads were washed twice with 500 µl ice-cold lysis buffer. Finally, the beads were resuspended in 60 µl 1X protein loading buffer, boiled at 95°C for 5 minutes, and stored at -20°C.

### 3.6.4. Immunoblot

#### 3.6.4.1. SDS-PAGE (Sodium Dodecyl Sulfate-Polyacrylamide Gel Electrophoresis)

Polyacrylamide gels were polymerized between two glass plates in a gel caster, with a comb inserted at the top to create the sample wells (10 or 15). Gels were divided into:

- An upper **stacking gel** of low polyacrylamide percentage, where the proteins are concentrated at a narrow line migrating towards the anode.
- A **resolving gel** of higher polyacrylamide percentage (between 8 and 15%) with smaller pores where the proteins were separated according to their molecular weight.

Protein samples (20-40 µg per well) were resolved in a Bio-Rad MiniPROTEAN Tetra Cell vertical electrophoresis system at constant amperage in 1x Running buffer for approximately 1 hour and 30 minutes. BenchMark Pre-Stained Protein Ladder (Thermo

Fisher Scientific) or Precision Plus Protein All Blue Standard (Bio-Rad) were loaded as protein standards to determine the size of the proteins under analysis.

#### **3.6.4.2. Transfer and blocking**

Following electrophoresis, proteins were transferred from the gel to either a nitrocellulose (Bio-Rad) or a polyvinylidene difluoride (PVDF) (Bio-Rad) membrane. Transference was performed using the Bio-Rad Mini Trans-Blot® Cell transfer system in 1x transfer buffer for 1-2 hours at 100 V and 4°C. Membranes were stained with Ponceau S (Sigma) to check the successful transfer of the proteins. Following protein transfer, membranes were blocked with 5% (w/v) non-fat dry milk powder in TBS-T for 1 hour at room temperature with gentle shaking.

#### **3.6.4.3. Antibody incubation and detection**

Membranes were then incubated with the primary antibody (**Table 8**) diluted in blocking solution for either 1 hour at room temperature or overnight at 4°C with gentle shaking. Membranes were washed thrice for 5 minutes with TBS-T or PBS-T and subsequently incubated with the corresponding horseradish peroxidase (HRP)-labeled (**Table 8**) in blocking solution for 1 hour at room temperature with gentle shaking. Membranes were washed again as described above.

**Table 8: List of antibodies used for immunoblotting.** The  $\beta$ -actin or  $\alpha$ -tubulin antibodies are used as protein loading controls.

Antibody	Company	Reference	Host	Dilution	Incubation
GFP	Chromotek	3H9	Rat	1:1000	1 h, RT
Xpress	Thermo Fisher Scientific	R910-25	Mouse	1:5000	1 h, RT
$\beta$ -actin	Sigma	A5441	Mouse	1:3000	1 h, RT
PCNA	Santa Cruz	16D10	Mouse	1:400	O/N, 4°C
Biotin-HRP	Cell Signaling Technology	#7075S	Goat	1:1000	1 h, RT
PAF15	Abnova	H00009768-M01	Mouse	1:250	O/N, 4°C
$\alpha$ -tubulin	Sigma	T9026	Mouse	1:5000	1h, RT
Mouse HRP	Santa Cruz	sc-3697	Goat	1:3000	1 h, RT
Rabbit HRP	Santa Cruz	sc-2030	Goat	1:3000	1 h, RT
Rat HRP	Santa Cruz	sc-3823	Goat	1:3000	1 h, RT
RIF1	Bethyl Laboratories	A300-5697-T	Rabbit	1:500	O/N, 4°C
RIF1	Bethyl Laboratories	A300-5698-T	Rabbit	1:500	O/N, 4°C
RIF1	Bethyl Laboratories	A300-5699-T	Rabbit	1:500	O/N, 4°C

Membranes were developed with Pierce ECL Plus Western Blotting Substrate or SuperSignal West Femto Chemiluminescent Substrate (Thermo Fisher Scientific) using the Bio-Rad Chemi-Doc imaging software.

### 3.7. PULLDOWN OF ENDOGENOUS UBIQUITINATED PROTEINS USING <sup>bio</sup>Ub

#### 3.7.1. The bioUb strategy

Mass spectrometry (MS)-based proteomics is one of the most commonly used approaches for the large-scale identification of ubiquitin modified proteins. However, the low levels at which endogenous ubiquitinated proteins are usually present within the cell, makes identification of ubiquitinated proteins under physiological conditions a challenging task (Mayor and Peng, 2012). A key step is to sufficiently enrich the ubiquitin-conjugated material prior to the MS analysis. In this regard, the laboratory of

Dr. Ugo Mayor (Department of Biochemistry, UPV/EHU) has developed a new strategy, based on biotin tagging, for the efficient *in vivo* isolation of ubiquitin conjugates (Franco et al., 2011). This approach, termed <sup>bio</sup>Ub, has so far allowed the purification and enrichment of ubiquitinated proteins from *Drosophila* (Franco et al., 2011) and mice (Lectez et al., 2014), as well as from human cell lines (Min et al., 2014).

The <sup>bio</sup>Ub approach relies on the *in vivo* expression of the *E. coli* BirA biotin ligase fused to a synthetic linear polyubiquitin construct (Ub<sub>6</sub>-BirA). Each ubiquitin moiety in the construct bears a 16 amino acid long BirA recognition sequence, and can therefore be biotinylated by BirA. In the transfected cells, a precursor polypeptide with six ubiquitin molecules fused to BirA is produced. This precursor can be digested by the endogenous DUBs, allowing the release of BirA and the individual ubiquitin moieties fused to the BirA recognition sequence. Then, BirA biotinylates the ubiquitin molecules, thus generating a pool of biotinylated ubiquitin (<sup>bio</sup>Ub) within the cell. The <sup>bio</sup>Ub can then be incorporated into endogenous protein substrates by the action of the cellular ubiquitination machinery. <sup>bio</sup>Ub-conjugated proteins can be isolated and enriched using avidin-beads (**Figure 21**). The strong interaction between avidin and biotin (Marttila et al., 2000) allows the use of very stringent washes (Franco et al., 2011), resulting in the removal of interacting proteins and purifying only the ubiquitinated material and a few endogenously biotinylated carboxylases. The biotinylated material can then be subjected to MS or immunoblot analysis (Franco et al., 2011; Lectez et al., 2014; Min et al., 2014; Ramirez et al., 2015).

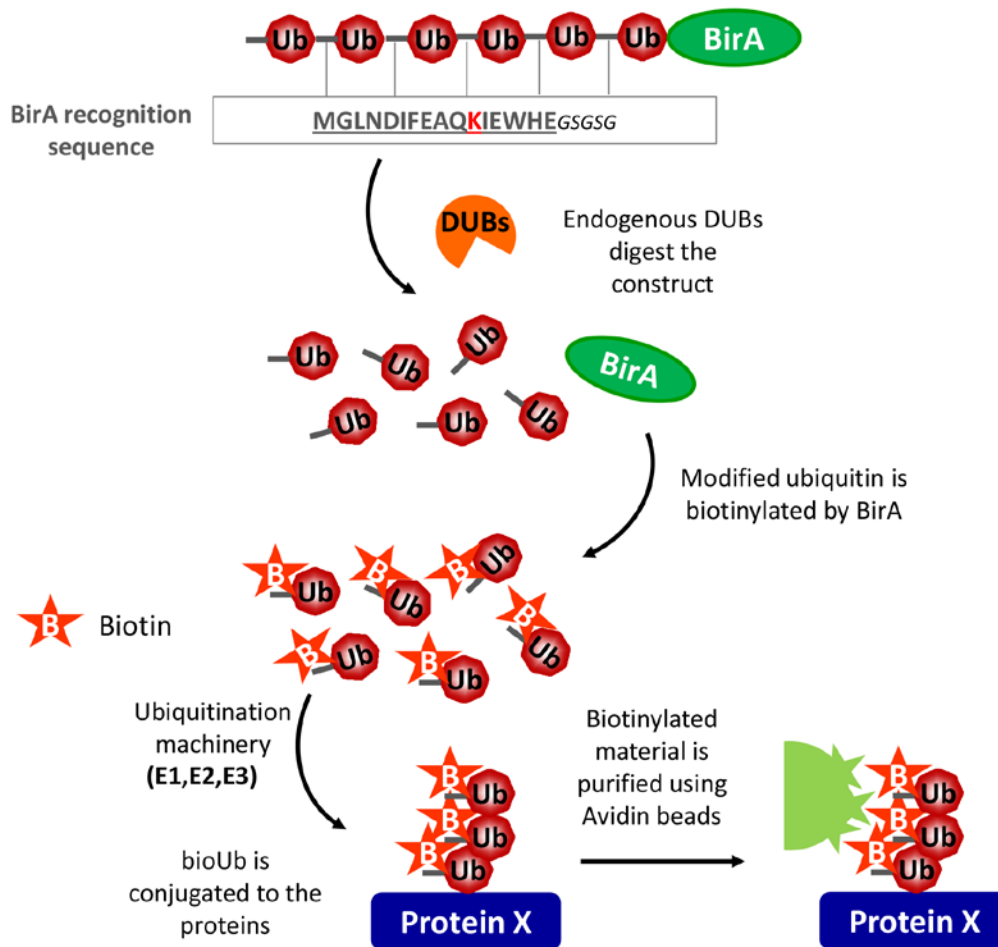


**Figure 21: The  $\text{bioUb}$  approach.** A chain of six ubiquitin moieties containing the BirA recognition sequence (underlined) fused to BirA is produced as a precursor polypeptide. The target sequence for biotinylation is underlined, with the lysine where the biotin is attached highlighted in red. Endogenous DUB enzymes process the precursor polypeptide releasing the free biotinylatable ubiquitin moieties and the BirA enzyme. BirA recognizes the target sequence and conjugates a biotin molecule to it generating a pool of biotinylated ubiquitin ( $\text{bioUb}$ ). The biotinylated ubiquitin is then conjugated to protein substrates by the cellular ubiquitination machinery. Biotinylated material (essentially ubiquitinated proteins) is purified using avidin beads. *Modified from (Franco et al., 2011).*

### 3.7.2. $\text{bioUb}$ protocol: preparation of cell extracts and purification of biotinylated proteins

$13.5 \times 10^6$  293T cells were plated in 15 cm dishes. 24 hours after plating, cells were transfected with siRNA against USP1 or siCTRL (as detailed in *section 3.3.3.2.*). Next day, cells were transfected (as described in *section 3.3.3.1*) with the pCAG- $\text{bioUb}$ -BirA plasmid encoding  $\text{bioUb}$ -BirA or, as a negative control of biotinylation, with the pCAG-

BirA plasmid, which encodes BirA. Immediately after transfection, growth medium was supplemented with 50  $\mu$ M biotin (Sigma). Next day, cells were collected in 7 ml of PBS, 1 ml was separated for immunoblot and the remaining cells were pelleted at 1500 rpm for 5 minutes at 4°C.

For pulldown, cell pellets were resuspended in 2,9 ml lysis buffer (8 M urea, 1% SDS, 50 mM NEM and protease inhibitor mixture) and then left in a rotator at 4°C for 20 minutes. Lysates were centrifuged for 5 minutes at 16100g at 4°C. Supernatants were applied to PD10 desalting columns (GE Healthcare), which were previously equilibrated with 25 ml of binding buffer containing 3 M urea (Sigma), 1 M NaCl (Sigma), 0,25% SDS (Sigma) and 50 mM NEM (Sigma) diluted in PBS. Afterwards, PD10-eluates (except 50  $\mu$ l that were kept for monitoring the inputs by SDS-PAGE), were incubated in a roller with 150  $\mu$ l of NeutrAvidin agarose beads suspension (Thermo Fisher Scientific), respectively for 1 hour at room temperature and 2 additional hours at 4°C. Unbound material (flow through, FT) was recovered by spinning down beads at 233 g (1000 rpm) for 2 minutes. Beads were then subjected to stringent washes with six different washing buffers (WB) for 5 minutes at room temperature. The number and order of washes were as follows: two times with WB1 (8 M Urea, 0.25 % SDS), three times with WB2 (6 M Guanidine-HCl), 1 time with WB3 (6.4 M Urea, 1 M NaCl, 0.2 % SDS), three times with WB4 (4 M Urea, 1 M NaCl, 10 % Isopropanol, 10 % Ethanol, 0.2 % SDS), 1 time with WB1, 1 time with WB5 (8 M Urea, 1 % SDS) and three times with WB6 (2 % SDS). All buffers were prepared in PBS (Thermo Fisher Scientific). Guanidine-HCl, isopropanol and ethanol were provided by Sigma, Panreac and Merck, respectively. Elution of the material bound to the beads was performed by heating the beads in a dry bath at 95 °C in 4X Laemmli buffer (250 mM Tris-HCl pH 7.5, 40 % Glycerol, 4 % SDS, 0.2 % Bromophenol blue) and 100 mM Dithiothreitol (DTT). The volume of elution buffer employed was half the volume of the NeutrAvidin agarose beads suspension used. Samples were centrifuged for 2 minutes at 16160 g to separate beads from the eluted material. Samples were then analyzed by electrophoresis, immunoblot or subjected to MS analysis.



### 3.7.3. Silver staining

In order to check the amount of purified material, 10 % of the eluted material was analysed by silver staining. Stainings were performed using the SilverQuest kit (Thermo Fisher Scientific) according to manufacturer's instructions. Briefly, gels were fixed in a 40 % Ethanol/10 % Acetic acid solution for 1 hour at room temperature. Then, they were incubated with a sensitizing solution (30% ethanol and 10% SilverQuest kit sensitizer) to improve protein reactivity toward silver ions, and thus enhance the protein staining. After removing excess of sensitizing solution with H<sub>2</sub>O, gels were incubated with a staining solution containing 1% SilverQuest kit stainer and subsequently washed with H<sub>2</sub>O to remove silver excess. Silver ions were then reduced to metallic silver using developing solution (10% SilverQuest kit developer and 1 drop SilverQuest kit developer enhancer) until proteins were detected.

## 3.8. IDENTIFICATION OF <sup>bio</sup>Ub-ENRICHED ENDOGENOUS UBIQUITINATED PROTEINS USING MASS SPECTROMETRY

The identification of ubiquitinated proteins was performed at the General Proteomics Service (SGIker) of the University of the Basque Country (UPV/EHU) using mass spectrometry based on a label-free quantification (LFQ) strategy. Eluted fractions from biotin pulldown experiments were trypsin-digested and extracted peptides run into a mass spectrometer as described in *section 3.8.2*. Mass spectra were then analysed using the MaxQuant software (Cox and Mann, 2008), with which protein identification and quantification of protein abundance were obtained.

### 3.8.1. General aspects of mass spectrometry

For MS-based proteomics (**Figure 22**), proteins extracted from cells or tissues are loaded into a gel and digested with specific proteases, such as trypsin. Next, peptides derived from proteins are separated by chromatography and analysed in a mass spectrometer, where they are ionized and separated according to their mass-to-charge ratio (m/z) (Steen and Mann, 2004). After assessing the m/z of the peptides, these ion precursors can be subjected to a second stage of fragmentation in the fragmentation chamber in

order to obtain additional information about the amino acid sequence (Steen and Mann, 2004). This is known as a tandem MS (MS/MS). The ion precursor and corresponding fragment ions are then analyzed using software that compares the experimental MS data with the theoretical mass of the proteins in a database. As the amino acid sequence of each protein is unique, so are the peptide fragments obtained by its proteolytic cleavage. Thereby, calculating the mass of each peptide, their sequence and the proteins they come from can be identified.

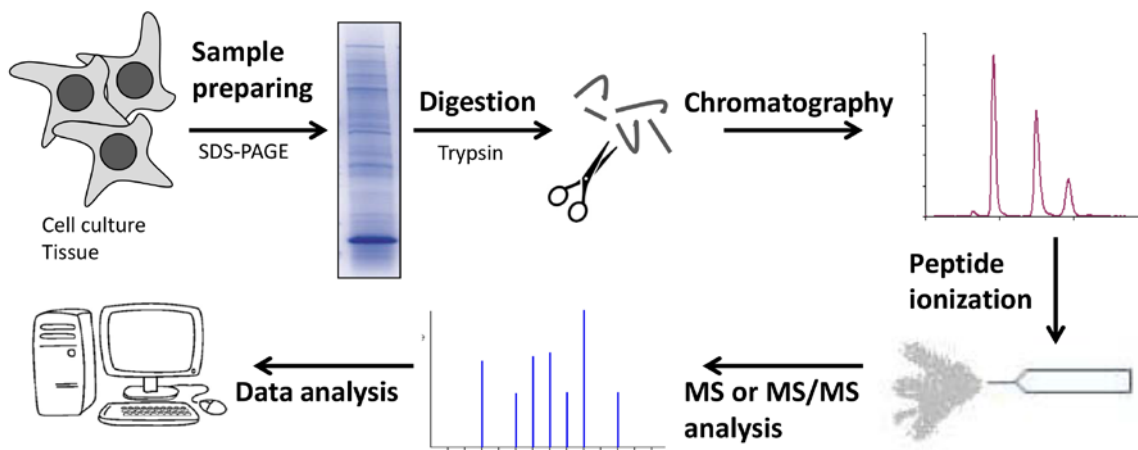


**Figure 22: Flow chart of a typical proteomics experiment.** Cells or tissues are loaded in a gel and digested with specific proteases (trypsin). Next, peptides are separated by chromatography and loaded into the mass spectrometer. Peptides are there ionized and separated according to their  $m/z$  and finally, real peptide mass is compared with the information from databases in order to identify the proteins.

### 3.8.2. In-gel trypsin digestion and peptide extraction

Proteins eluted from the biotin pull-down were fractionated in a precast gradient NuPAGE 4-12% Bis-Tris Gel (Thermo Fisher Scientific) and visualized with Colloidal Blue (Thermo Fisher Scientific). Each gel lane was cut into 4 slices (**Figure 23**), the avidin band was removed and proteins were subsequently subjected to in-gel trypsin digestion as previously described (Osinalde et al., 2015). Briefly, proteins were reduced and alkylated by incubating with 10 mM DTT for 45 minutes at 56 °C, and with 55 mM chloroacetamide (CAA) for 30 minutes at room temperature in darkness. Proteins were digested by incubating with trypsin overnight at 37 °C and finally, resulting peptides were extracted from the gel, dried down in a vacuum centrifuge and stored at -20 °C.

Peptide mixture was resuspended in 0.1 % formic acid previous to the LC-MS/MS analysis.

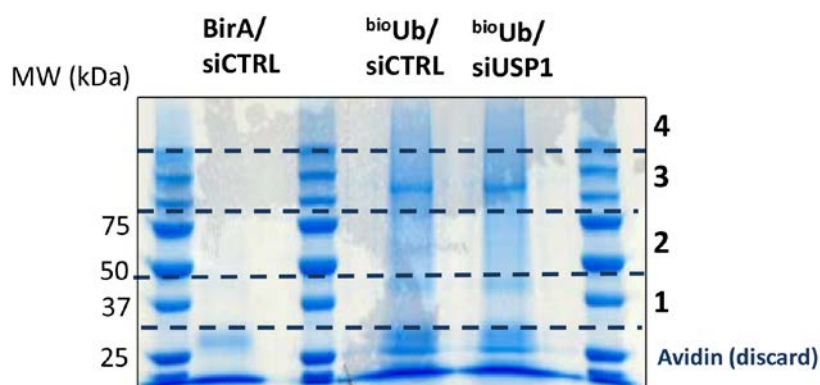


**Figure 23: Gel cutting for trypsin digestion and (LC)-MS/MS analysis.** Eluted proteins from biotin pull-down were loaded in a gel and stained with Colloidal Blue. Then, each lane was cut into 4 slices and the avidin bad was discarded.

### 3.8.3. Liquid chromatography (LC)-MS/MS analysis

Proteomic analyses were carried out using an EASY nLC-100 liquid chromatography system interfaced with a Q Exactive mass spectrometer (Thermo Fischer Scientific) via a Nanospray Flex ion source. Acidified peptides were loaded onto an Acclaim PepMap100 pre-column (75  $\mu\text{m}$  x 2 cm, Thermo Fisher Scientific) connected to an Acclaim PepMap RSLC (50  $\mu\text{m}$  x 15 cm, Thermo Fisher Scientific) analytical column. Peptides were eluted using a 45 minutes linear gradient of 2% - 40% acetonitrile in 0.1% formic acid at a flow rate of 300  $\text{nL min}^{-1}$  onto the nanoES Emitter (Thermo Fisher Scientific). Q Exactive was operated in a top-10 data-dependent mode. Survey scans were acquired at a resolution of 70 000 ( $m/z$  200) and fragmentation spectra at 17 500 ( $m/z$  200). Precursors were fragmented by higher energy C-trap dissociation (HCD) with normalized collision energy of 28 -. The maximum ion injection time was 120 ms for both survey and MS/MS scans, whereas AGC target values of  $3 \times 10^6$  and  $5 \times 10^5$  were used for survey and MS/MS scans, respectively. Repeated sequencing of peptide was minimized by excluding the selected peptide candidates for 45 seconds.

### **3.8.4. Data processing and bioinformatics analysis**

Acquired raw data files were searched against the UniProt human database version 2015\_09 (with 42129 sequence entries) using the Andromeda search engine from the MaxQuant software (version 1.5.3.17) (Cox and Mann, 2008; Cox et al., 2011) in which the spectra originated from the different samples corresponding to the same biological replica were combined. Mass tolerance of precursor and MS/MS spectra were set to 8 and 20 ppm, respectively. Enzyme specificity was set to trypsin, allowing for cleavage N-terminal to P and between D and P with a maximum of 2 missed cleavages. Carbamidomethylation of C was set as fixed modification whereas oxidation of M, protein N-terminal acetylation, and K GlyGly (not C-term) were selected as variable modifications for database searching. Match between runs option was enabled with 1.5 minutes match time window and 20 minutes alignment window to match identification across samples. The minimum peptide length was set to 7 amino acids. The maximum FDR at peptide and protein levels were specified as 0.01. Normalized spectral protein intensities (LFQ intensity) were calculated using the MaxLFQ algorithm.

MaxQuant output data was analyzed with the Perseus module (version 1.5.6.0) (Tyanova et al., 2016). Initially, all contaminants, reverse hits and proteins with no unique peptides or intensity were removed. Only proteins that were quantified in two or three biological replicates of at least one of the conditions were kept for further analysis included in the LFQ analysis. Subsequently, missing values were replaced with values from a normal distribution (width 0.3 and down shift 1.8). Two-sided t test was performed to identify statistically significant changing proteins. The statistical tests were corrected for multiple hypotheses testing using permutation-based FDR, and the parameters were chosen to provide sufficient input in the subsequent analysis (FDR = 0.05 and 250 randomizations).

### 3.9. SUPPLEMENTARY MATERIALS AND METHODS

#### 3.9.1. PCR reactions and programs

##### PCR reaction A

Component	Volume( $\mu$ l)
H <sub>2</sub> O	40.50
10 $\times$ PfuUltra II reaction buffer	5.00
dNTPs (10 mM)	1.00
DNA template ( $\approx$ 80 ng/ $\mu$ l)	1.00
Forward primer (10 $\mu$ M)	1.00
Reverse primer (10 $\mu$ M)	1.00
PfuUltra II fusion HS DNA polymerase	0.50
<b>TOTAL</b>	<b>50.00</b>

##### PCR program A

Temperature	Time	N <sup>o</sup> Cycles
95°C	2 min	1
95°C	20 sec	
55°C	20 sec	30
72°C	15 sec/kb	
72°C	3 min	1
4°C	$\infty$	

**PCR reaction B**

Component	Volume ( $\mu$ l)
H <sub>2</sub> O	38.00
10× QuikChange Lightning Buffer	5.00
QuikSolution reagent	1.50
dNTP mix	1.00
DNA template ( $\approx$ 50 ng/ $\mu$ l)	1.00
Forward primer (100 ng/ $\mu$ l)	1.25
Reverse primer (100 ng/ $\mu$ l)	1.25
QuikChange Lightning Enzyme	1.00
<b>TOTAL</b>	<b>50.00</b>

**PCR program B**

Temperature	Time	N° Cycles
95°C	2 min	1
95°C	20 sec	
55°C	10 sec	18
72°C	30 sec/kb	
72°C	5 min	1
4°C	$\infty$	

**PCR reaction C**

Component	Volume ( $\mu$ l)
H <sub>2</sub> O	17.24
10× QuikChange Multi reaction Buffer	2.5
QuikSolution reagent	0.5
dNTP mix	1.00
DNA template ( $\approx$ 50 ng/ $\mu$ l)	1.26
Forward primer (100 ng/ $\mu$ l)	0.75
Reverse primer (100 ng/ $\mu$ l)	0.75
QuikChange Multi Enzyme	1.00
<b>TOTAL</b>	<b>25.00</b>

**PCR program C**

Temperature	Time	N° Cycles
95°C	2 min	1
95°C	20 sec	30
55°C	30 sec	
65°C	4 min	
65°C	5 min	1
4°C	$\infty$	

### 3.9.2. Solutions

#### Tris-Acetic-EDTA (TAE) 50X

2 M Tris base

0.05 M EDTA

0.05% Acetic acid (v/v)

#### Agarose gel

1.5 % Agarose (w/v)

0.01% Ethidium bromide (v/v)

1X TAE

#### DNA loading buffer

0.2% Orange G (w/v)

40% sucrose (v/v)

#### 1X PBS (pH 7.6)

137 mM NaCl

2.7 mM KCl

1.8 mM  $\text{KH}_2\text{PO}_4$

8.1 mM  $\text{Na}_2\text{HPO}_4$

#### 6X Protein Loading Buffer

350 mM Tris-HCl pH 6.8

34.4% Glycerol (v/v)

10% SDS (w/v)

10%  $\beta$ -mercaptoethanol (v/v)

0.06% Bromophenol blue (w/v)

#### Tris Buffered Saline-Tween 20 (TBS-T) (pH 7.6)

20 mM Tris base

137 mM NaCl

0.1% Tween 20

#### RIPA protein lysis buffer

25mM Tris-HCl (pH 7.6)

150mM NaCl

1% NP-40

1% sodium deoxycholate

0.1% SDS

Protein lysis buffer

10 mM NaH<sub>2</sub>PO<sub>4</sub> (pH7.2)

1 mM EDTA

1 mM EGTA

150 mM NaCl

1% NP-40 (v/v)

10 mM β-glycerophosphate

10 mM PMSF

10 mM Na<sub>3</sub>VO<sub>4</sub>

PIC (Roche)

50 mM NEM

Running buffer

0.25 mM Tris base

1.92 mM Glycine

1% SDS

Transfer buffer

120 mM Tris base

40 mM Glycine

20% Methanol

Stacking gel for SDS-PAGE

63 mM Tris HCl pH6.8

0.1% SDS (v/v)

5% Acrylamide

0.1% TEMED

0.1% APS



Resolving gel for SDS-PAGE

376 mM Tris HCl pH8.8

0.1% SDS (v/v)

Acrylamide (variable %)

0.04% TEMED

0.1% APS



# Results

4



---

## 4. Results

### 4.1. INSIGHTS INTO THE REGULATION OF USP1 BY PHOSPHORYLATION AND AUTOCLEAVAGE

Phosphorylation and autocleavage are two key regulatory mechanisms for USP1. However, several aspects of this regulation are either controversial or not completely understood. Therefore, in this section we aim to gain further insight into these aspects.

#### 4.1.1. Phosphorylation of USP1 at serine 313 is dispensable for the formation and activity of USP1/UAF1 complex

The serine 313 (S313) residue is well established as a USP1 phosphorylation site (Cotto-Rios et al., 2011b). At the time this Thesis was initiated, several controversial findings regarding the identity of UAF1-binding motif in USP1 (Garcia-Santisteban et al., 2012; Villamil et al., 2012b) had raised the question of how relevant S313 phosphorylation might be for the formation and activity of the USP1/UAF1 complex in a cellular context.

To address this question, we generated non-phosphorylatable (S313A) and phosphomimetic (S313D) mutant versions of USP1, and tested their ability to interact with UAF1 using a previously described relocation assay (Garcia-Santisteban et al., 2012) based on the nuclear accumulation of UAF1 induced by USP1 co-expression. By using fluorescently-tagged proteins, the results of the assay can be observed both in live and in fixed cells.

**Figure 24A** shows the results of the relocation assay in live cells. Different versions of GFP-tagged USP1 (WT, S313A and S313D) or the YFP-empty vector were co-transfected together with mRFP-tagged UAF1 into 293T cells. As expected, UAF1-mRFP was predominantly located in the cytoplasm when co-expressed with YFP (negative control), and relocated to the nucleus when co-expressed with GFP-USP1 (Garcia-Santisteban et al., 2012), as a result of their interaction. Importantly, both GFP-USP1<sup>S313A</sup> and GFP-USP1<sup>S313D</sup> were able to relocate UAF1-mRFP to the nucleus, suggesting that both mutants are still able to interact with UAF1 (**Figure 24A**). Similar

results were obtained after cell fixation (**Figure 24B**). In line with these results, co-immunoprecipitation (co-IP) analysis showed that both GFP-USP1<sup>S313A</sup> and GFP-USP1<sup>S313D</sup> co-immunoprecipitated with Xpress-tagged UAF1 as efficiently as wild type GFP-USP1 (**Figure 24C**), confirming the result of the relocation assay.

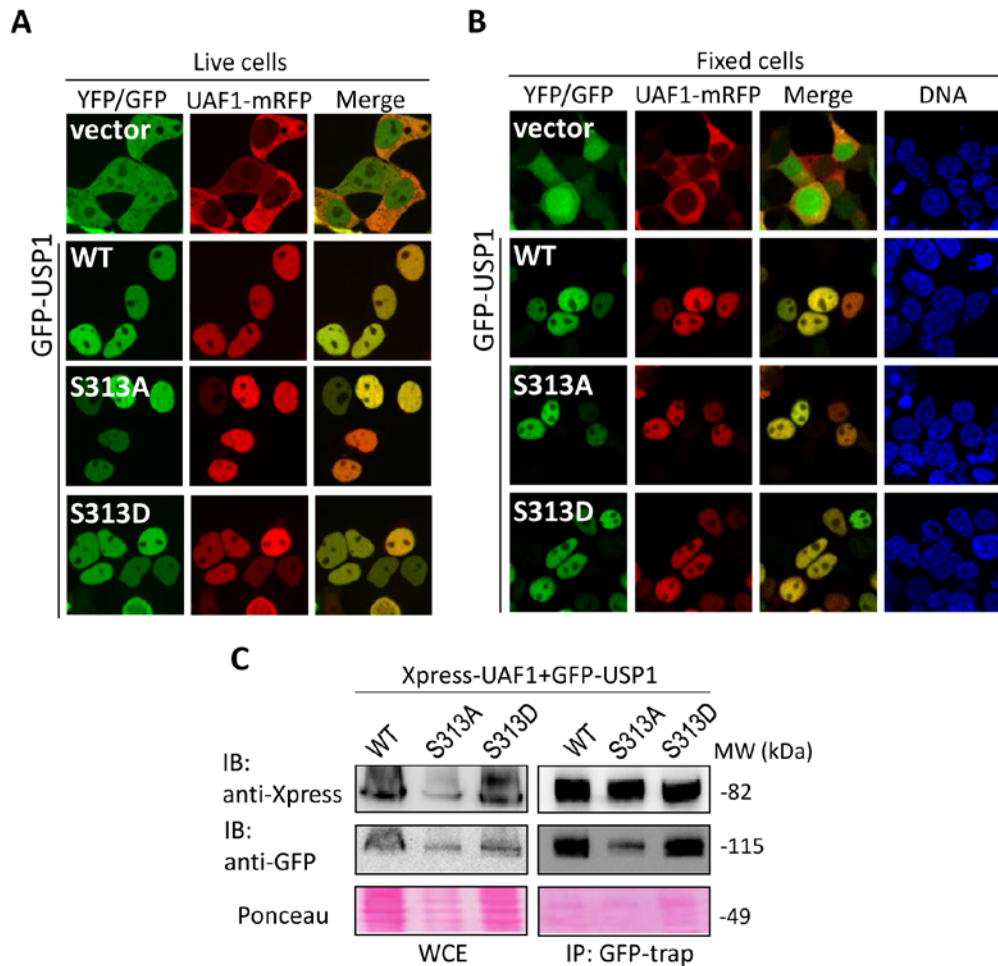


**Figure 24: UAF1 binds the non-phosphorylatable S313A mutant version of USP1 in cell-based assays.** **A** Images of live 293T cells co-expressing UAF1-mRFP with YFP (vector), GFP-USP1<sup>WT</sup>, GFP-USP1<sup>S313A</sup> or GFP-USP1<sup>S313D</sup>. UAF1-mRFP is cytoplasmic when co-expressed with YFP, but relocates to the nucleus when co-expressed with GFP-USP1<sup>WT</sup>, GFP-USP1<sup>S313A</sup> and GFP-USP1<sup>S313D</sup>. **B**. Images of fixed 293T cells co-transfected as in A. DAPI was used to counterstain the nucleus (DNA panels). **C**. Results of GFP-trap co-IP analysis in 293T cells. Xpress-UAF1 readily co-immunoprecipitates with GFP-USP1<sup>wt</sup>, GFP-USP1<sup>S313A</sup> and GFP-USP1<sup>S313D</sup>. A section of the membrane stained with Ponceau is shown to gauge protein loading. WCE, whole cell extract.

UAF1 binding promotes USP1 stability (Cohn et al., 2007). Thus, we next compared the effect of UAF1 co-expression on the levels of the different USP1 S313 mutants. As

shown in **Figure 25**, a dramatic increase in the level of all the GFP-USP1 variants tested was observed upon co-transfection with Xpress-UAF1. Of note, the increase in USP1 levels was accompanied by the appearance of a lower molecular weight band that most likely corresponds to the amino-terminal fragment of USP1 resulting from its autocleavage at the G670/G671 site (Huang et al., 2006). The appearance of this autocleavage product reflects the catalytic activation of USP1 induced by UAF1 binding. These results indicate that the S313A or S313D USP1 mutants are not impaired in their ability to undergo UAF1-induced stabilization or catalytic activation.

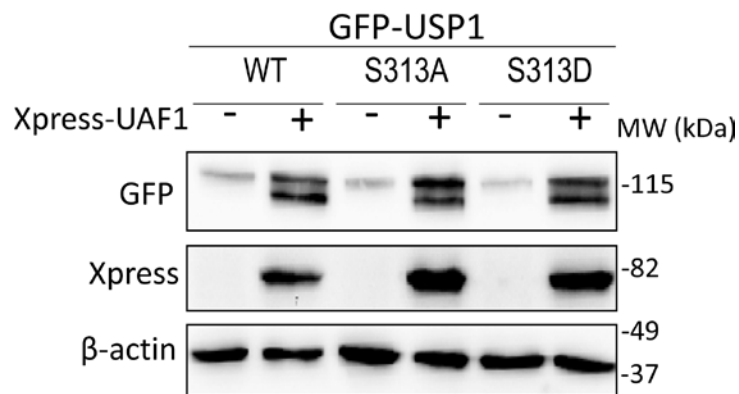


**Figure 25: UAF1 stabilizes and activates a non-phosphorylatable S313A mutant version of USP1.** Immunoblot analysis of 293T cells transfected with GFP-USP1<sup>WT</sup>, GFP-USP1<sup>S313A</sup> and GFP-USP1<sup>S313D</sup>, alone (-) or in combination with Xpress-UAF1 (+). The lower molecular weight band in (+) samples corresponds to the well-characterized N-terminal fragment that results from USP1 autocleavage and reflects catalytic activation of USP1 by UAF1. The shorter C-terminal fragment is not detected because it does not have GFP. UAF1 co-expression stabilized and activated GFP-USP1 wild type, GFP-USP1<sup>S313A</sup> and GFP-USP1<sup>S313D</sup> to a similar extent.

These findings indicate that phosphorylation at S313 is not critical for USP1/UAF1 complex formation and activity in a cellular context.

The S313A mutation has been reported to drastically reduce the activity of USP1 on an artificial fluorogenic substrate in *in vitro* assays (Villamil et al., 2012b). We tested the effect of this mutation on the ability of the USP1/UAF1 complex to deubiquitinate one of its physiological substrates: monoubiquitinated PCNA (UbPCNA).

To this end, 293T cells were co-transfected with plasmids encoding Xpress-UAF1 and either GFP-USP1 wild type, GFP-USP1<sup>S313A</sup> or GFP-USP1<sup>S313D</sup>. As a negative control,

we included a catalytically inactive mutant (C90S) version of USP1, which bears a mutation in one of the residues of the catalytic triad. Co-transfected cells were treated with hydroxyurea (HU), a drug that induces PCNA monoubiquitination (Huang et al., 2006) (**Figure 26A**). As expected, (**Figure 26B**), wild type USP1, but not USP1<sup>C90S</sup>, decreased the levels of HU-induced PCNA monoubiquitination. Importantly, both S313 mutants were able to reduce PCNA monoubiquitination. Nevertheless, the ratio of ubiquitinated to non-ubiquitinated PCNA (UbPCNA/PCNA ratio) was repeatedly observed in several independent experiments to be slightly higher in cells expressing GFP-USP1<sup>S313A</sup> and slightly lower in cells expressing GFP-USP1<sup>S313D</sup> in comparison to cells expressing wild type GFP-USP1. From these results, we conclude that phosphorylation at S313 is not necessary for USP1-mediated PCNA deubiquitination in HU-treated cells, although it might contribute to modulate this activity.

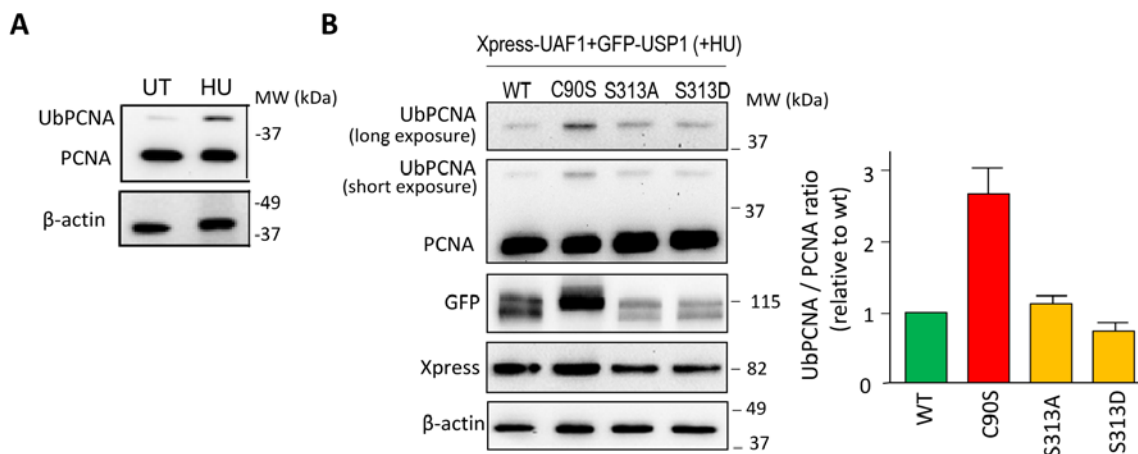


**Figure 26: USP1-mediated PCNA deubiquitination is not abrogated by the S313A mutation.** **A.** Immunoblot of 293T cells left untreated (UT) or treated with 4 mM hydroxyurea (HU) for 24 h to induce PCNA monoubiquitination. Using an anti-PCNA antibody, monoubiquitinated PCNA (UbPCNA) was detected as a band migrating around 10 kDa above the non-ubiquitinated form (PCNA). **B.** On the left, a representative example of immunoblot analysis of HU-treated 293T cells co-expressing Xpress-UAF1 with different GFP-USP1 variants. A short-exposure image showing both PCNA and UbPCNA, as well as a cropped image showing only UbPCNA with longer exposure time are shown. The ratio of ubiquitinated to non-ubiquitinated PCNA (UbPCNA/PCNA ratio) was determined by densitometry analysis of the immunoblot bands. The graph on the right shows the results (mean and SEM) of 7 independent experiments. The UbPCNA/PCNA ratio was similar in cells expressing Xpress-UAF1 with GFP-USP1<sup>WT</sup>, GFP-USP1<sup>S313A</sup> and GFP-USP1<sup>S313D</sup>, but higher in cells expressing the catalytically inactive GFP-USP1<sup>C90S</sup>.



#### 4.1.2. USP1 autocleavage at the G670/G671 diglycine motif occurs most likely in *cis*

Autocleavage of USP1 at G670/G671, a diglycine motif that resembles a ubiquitin linkage, was originally described as a mechanism that inactivates USP1 to allow for robust PCNA ubiquitination after UV-induced DNA damage (Huang et al., 2006). This autocleavage event can also occur in the absence of UV treatment (Cohn et al., 2007; Huang et al., 2006). In line with these reports, we have consistently observed that GFP-USP1<sup>WT</sup>, but not the catalytically inactive GFP-USP1<sup>C90S</sup>, readily undergoes cleavage when co-expressed with Xpress-UAF1 in 293T cells (see e.g. immunoblot in **Figure 26B**). This observation provides a convenient experimental system to further investigate USP1 autocleavage.

One aspect about USP1 autocleavage that remains to be elucidated is whether this cleavage event occurs intramolecularly (in *cis*) or intermolecularly (in *trans*) (**Figure 27A**). The three-dimensional structure of USP1 has not been solved, and the autocleavage motif lies within a non-conserved inserted domain whose structure cannot be reliably modeled using other USPs as template. Thus, it remains unknown if the cleavage site of a USP1 molecule can reach the catalytic site of the same molecule for the cleavage to occur in *cis*.

In an attempt to shed some light on this issue, we devised the experiment illustrated in **Figure 27B**. We generated a mutant with alanine substitutions at the G670/G671 cleavage site (USP1<sup>GG/AA</sup>). It has been shown that USP1<sup>GG/AA</sup> maintains its catalytic activity (Huang et al., 2006; Oestergaard et al., 2007) and, in fact, we found that it efficiently deubiquitinates UbPCNA when co-transfected with Xpress-UAF1 in 293T cells (not shown). However, USP1<sup>GG/AA</sup> cannot undergo autocleavage in *cis*. On the other hand, the catalytically inactive mutant (USP1<sup>C90S</sup>) does not undergo autocleavage. We reasoned that, if USP1 autocleavage occurs in *trans*, USP1<sup>GG/AA</sup> molecules could cleave USP1<sup>C90S</sup> molecules when expressed together.

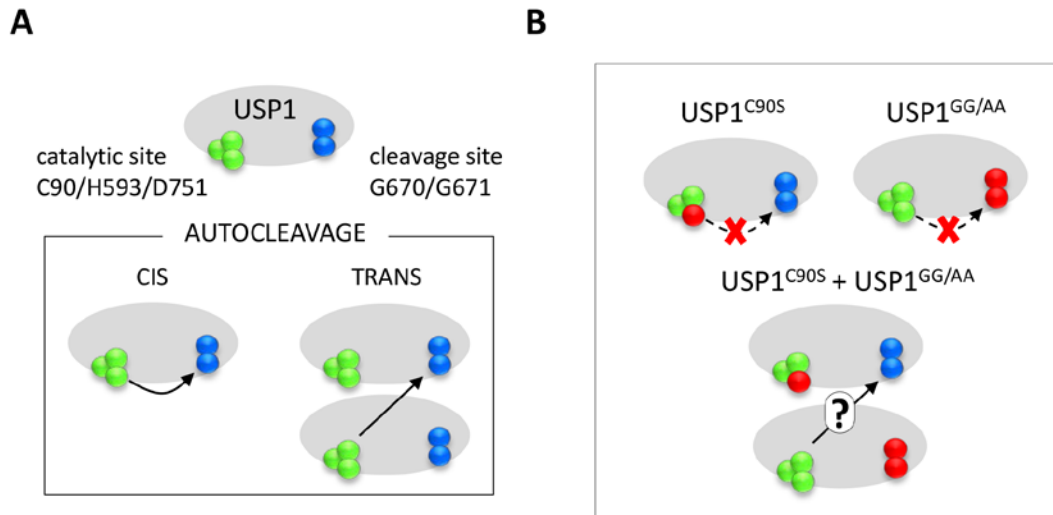


**Figure 27: Experimental design to test if USP1 autocleavage at the G670/G671 motif occurs in *cis* or in *trans*** **A.** Representation of USP1 showing the catalytic triad (C90/H593/D751, green spheres) and the autocleavage site (G670/G671, blue spheres). Below, potential *cis/trans* autocleavage modes. **B.** Experiment used to assess the cleavage mode. The C90S and GG/AA mutants (mutated residues in red) are unable to undergo *cis* autocleavage. If autocleavage occurs in *trans*, co-expression of both mutants could lead to cleavage of GFP-USP1<sup>C90S</sup> by GFP-USP1<sup>GG/AA</sup>.

To test this hypothesis, GFP-USP1<sup>GG/AA</sup> and GFP-USP1<sup>C90S</sup> were either individually or simultaneously co-expressed with Xpress-UAF1 in 293T cells. GFP-USP1<sup>WT</sup> was used as a positive control. As shown in **Figure 28**, simultaneous co-expression of GFP-USP1<sup>GG/AA</sup> and GFP-USP1<sup>C90S</sup> did not result in cleavage. It remains certainly possible that, in this experimental setting, GFP-USP1<sup>GG/AA</sup> and GFP-USP1<sup>C90S</sup> molecules did not come into close enough proximity for cleavage to occur in *trans* and, therefore, our results do not completely exclude the possibility of USP1 *trans* cleavage. Nevertheless, our findings support the view that the regulation of the USP1/UAF1 complex by USP1 autocleavage involves a *cis* cleavage event.

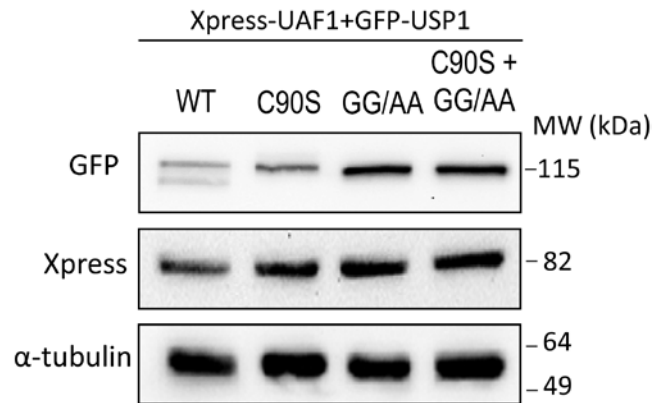


**Figure 28: USP1 autocleavage does not appear to occur in *trans*.** Immunoblot analysis of 293T cells co-expressing Xpress-UAF1 with the indicated GFP-USP1 constructs. No cleavage was observed upon co-expression of GFP-USP1<sup>C90S</sup> and GFP-USP1<sup>GG/AA</sup>, suggesting that *trans* cleavage does not occur.

In summary, in this section, we provide further insight into the two major regulatory mechanisms of USP1/UAF1 complex: we show that phosphorylation at USP1 serine 313 is not necessary for USP1/UAF1 complex formation or activity, and that USP1 autocleavage occurs most likely in *cis*.

## 4.2. CONFIRMATION AND FINE MAPPING OF THE USP1/UAF1 INTERACTION INTERFACE

As mentioned above, the identity of the UAF1 binding region(s) in USP1 has been a matter of some controversy (see **Figure 13**). Our group mapped the UAF1-binding site to a motif comprising USP1 residues 420-520 (Garcia-Santisteban et al., 2012), whereas, another research group latter mapped the UAF1-binding site to USP1 amino acid segment 235-408 (Villamil et al., 2012b).

In this section, we aim to solve the controversy about the UAF1-binding sites in USP1. Furthermore, we also made an effort to fine-map the specific residues that contribute to USP1/UAF1 interaction. It is important, in our opinion, to obtain as much detailed information as possible on the USP1/UAF1 binding interface, because disrupting the USP1/UAF1 complex might represent a future therapeutic strategy in cancer treatment.

### 4.2.1. Side-by-side comparison of the two reported UAF1-binding sites in USP1

In an attempt to gauge the contribution of the two proposed UAF1-binding regions of USP1 in a cellular context, we carried out a side-by-side test to compare the USP1(420–520) and USP1(235–408) segments using the UAF1 nuclear relocation assay. The 235–408 segment contains the USP1 nuclear localization signals (NLSs) and the S313 phosphorylation site. It must be noted that only a phosphomimetic S313D mutant version of this was reported by Villamil et al, to interact with UAF1 *in vitro* (Villamil et al., 2012b).

We used the constructs schematically represented in **Figure 29**: (i) full-length wild type USP1, (ii) the previously described USP1(420-520) fused to one of USP1 NLSs to ensure its nuclear accumulation (Garcia-Santisteban et al., 2012), (iii) S313 wild type and S313D versions of USP1(235–408) and (iv) S313 wild type and S313D versions of a USP1 fragment lacking the 420–520 motif (USP1(del420-520)).

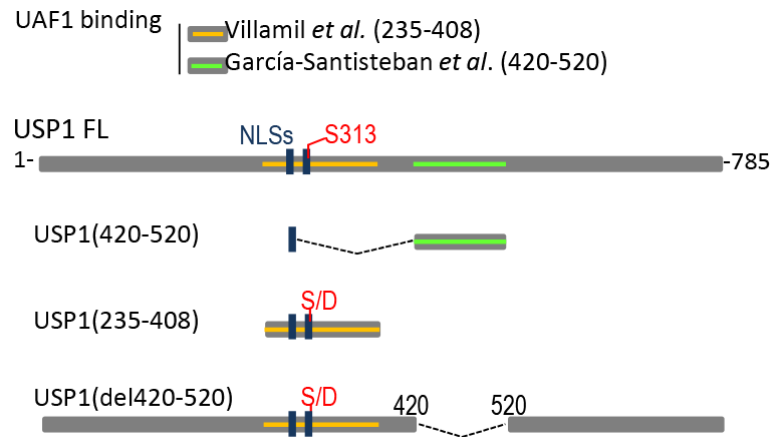


**Figure 29: Schematic representation of the USP1 constructs used for the UAF1-relocation assay.** The two UAF1 binding sites reported, the NLSs, and the S313 phosphorylation site are indicated. S/D indicates that both wild type (S) and phosphomimetic (D) variants of the 313 residue were tested.

YFP- or GFP-tagged versions of these USP1 variants were co-expressed with UAF1-mRFP in 293T cells and the percentage of cells showing nuclear (N), nuclear/cytoplasmic (N/C) or cytoplasmic (C) localization of UAF1-mRFP was determined. **Figure 30A** shows representative examples and the results of three independent assays are represented in **Figure 30B**. In line with our previous findings (García-Santisteban *et al.*, 2012), full-length USP1 and the USP1(420–520) fragment induced a complete relocation of UAF1-mRFP to the nucleus. In contrast, UAF1-mRFP remained largely cytoplasmic when co-expressed with the other USP1 variants tested, including USP1(235–408)<sup>S313D</sup> and USP1(del420-520)<sup>S313D</sup>. These results indicate that USP1 amino acid motif 420–520 is both necessary and sufficient for UAF1 binding in a cellular environment.

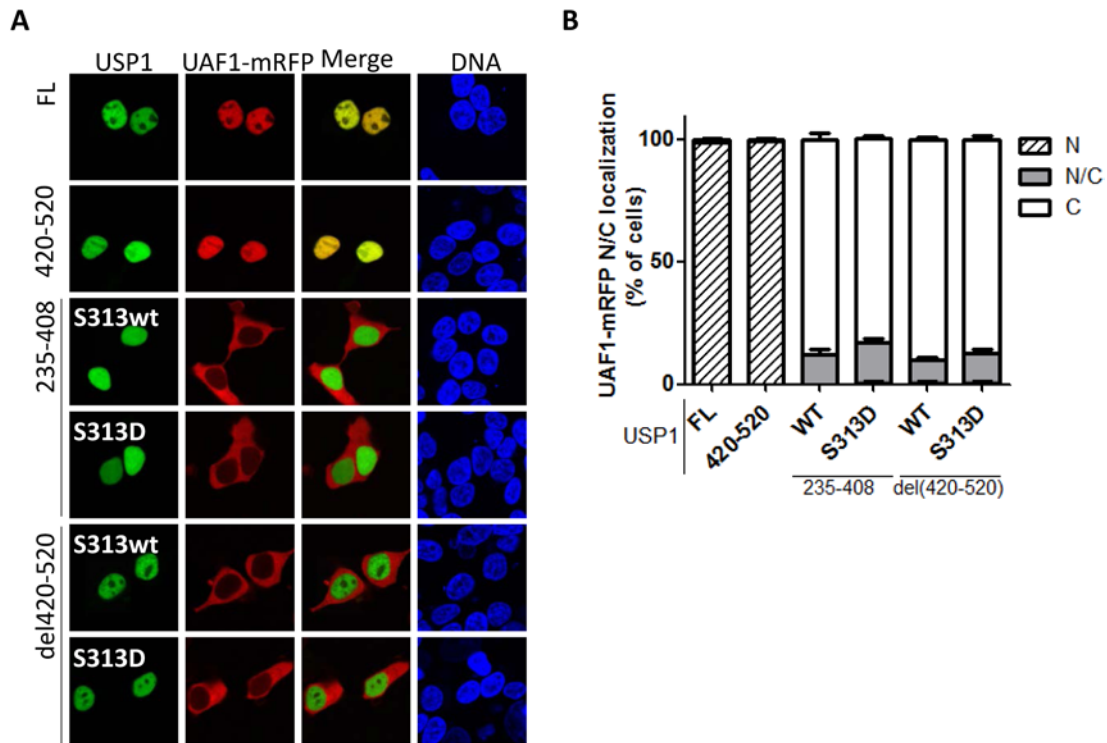


**Figure 30: Side-by-side comparison of two reported UAF1-binding sites in USP1 using a nuclear relocation assay.** **A.** Confocal images showing representative examples of the results using the UAF1 nuclear relocation assay. 293T cells were co-transfected with UAF1-mRFP and the different GFP or YFP-tagged-USP1 constructs. UAF1-mRFP clearly relocates to the nucleus when co-expressed with GFP-tagged USP1 full length and USP1(420–520), but not with the remaining deletion mutants. **B.** Graph showing the results of a semiquantitative analysis of the nuclear relocation assay. Slides were coded and the nuclear (N), nuclear/cytoplasmic (N/C) or cytoplasmic (C) localization of UAF1-mRFP was determined in at least 100 cells per slide. The results (mean and SEM) of three independent experiments are shown in the graph.

The failure of USP1(235–408)<sup>S313D</sup> to induce UAF1-mRFP nuclear relocation contrasts with the reported ability of this fragment to interact with UAF1 *in vitro* (Villamil et al., 2012b). We thought that these contrasting findings might result from competition between UAF1 and other proteins for binding to this USP1 fragment, an event that may occur in a cellular environment, but not in *in vitro* assays with purified proteins. Since the 235–408 motif overlaps with USP1 NLSs, we hypothesized that competition with the nuclear import machinery might prevent UAF1 binding to this motif (**Figure 31A**). To test this possibility, we generated a variant of the USP1(235–408) fragment, termed USP1(235-408)<sup>NLSm+NLS</sup>. As illustrated in **Figure 31A**, this variant bears inactivating mutations in USP1 NLSs (Garcia-Santisteban et al., 2012) that would prevent importin

binding. To induce nuclear localization of this fragment, we used a heterologous NLS from the SV40 large T antigen (SV40NLS) fused to its amino terminus. USP1(235-408)<sup>NLSm+NLS</sup> and the phosphomimetic USP1(235-408)<sup>NLSm+NLS/S313D</sup> remained unable to induce UAF1-mRFP relocation to the nucleus (**Figure 31B**). Although the possibility that the NLS-inactivating mutations might also interfere with UAF1 binding cannot be formally ruled out, these results suggest that the inability of USP1(235–408) fragment to promote UAF1 relocation cannot be ascribed to competition with the nuclear import machinery.

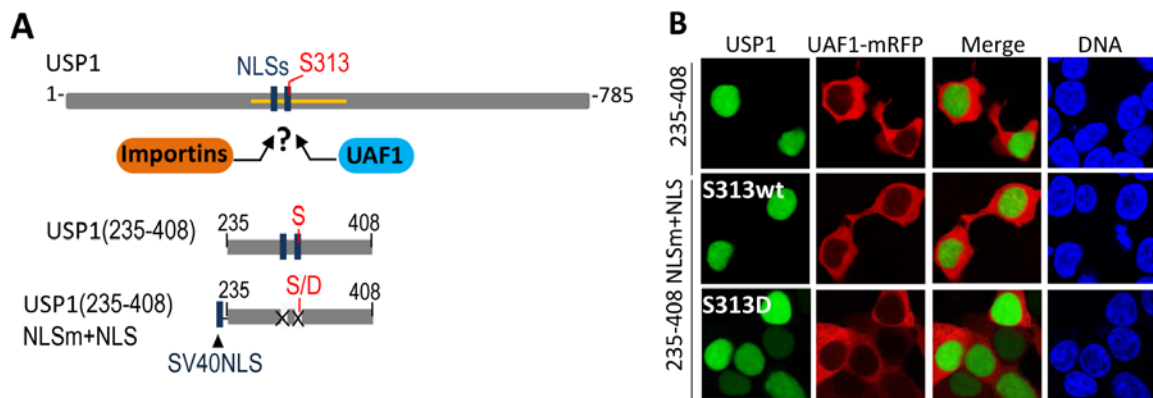


**Figure 31: Lack of UAF1 binding by the USP1(235-408) fragment is not due to competition with the nuclear import machinery.** **A.** Cartoon illustrating the hypothesis that UAF1 and importins might compete for binding to the USP1(235–408) segment. Below, schematic representation of the constructs used to test this hypothesis. USP1(235-408)<sup>NLSm+NLS</sup> bears NLSs mutations, and its nuclear localization is mediated by an SV40 NLS fused to its amino terminus. S313 wild type and S313D phosphomimetic mutants of this construct were tested in the UAF1 nuclear relocation. **B.** Confocal images showing representative examples of the assay. Mutation of USP1 NLSs does not facilitate in UAF1 binding to the 235–408 segment.

#### **4.2.2. The “Fingers” subdomain is the UAF1-binding site in USP1**

Considering the crucial role of UAF1 as activating cofactor, not only for USP1, but also for USP12 and USP46 (Cohn et al., 2009; Faesen et al., 2011), we reasoned that the critical UAF1-binding sequences would be conserved among these different DUBs. In order to test this possibility, we used CLUSTALW2 to align USP1, USP46 and USP12 amino acid sequences (**Figure 32**). The USP1 420–520 segment was found to be homologous to a central amino acid segment in USP12 and USP46. Therefore, we decided to carry out a deletion analysis followed by cell-based interaction assays to determine if this central motif mediates the binding of these other DUBs to UAF1. Taking into account the high sequence similarity between USP12 and USP46, here we limited our analysis to USP46.





As shown in **Figure 33A**, three deletion mutants of USP46 tagged with GFP were generated: an amino-terminal fragment (1–164), a central fragment (165–259), homologous to USP1(420–520), and a carboxy-terminal fragment (243–366). In agreement with a previous report (Urbé et al., 2012), we found that USP46-GFP is a cytoplasmic protein (**Figure 33B**). Thus, the SV40 NLS was fused to its amino terminus in order to force its nuclear import and carry out the UAF1-mRFP relocation assay (**Figure 33B**). This assay, (**Figure 33C**) as well as a subsequent co-IP analysis (**Figure 33D**), revealed that the UAF1-binding motif of USP46 lies within the 165–259 fragment. Thus, homologous amino acid sequences in USP1 and USP46 mediate binding to UAF1.

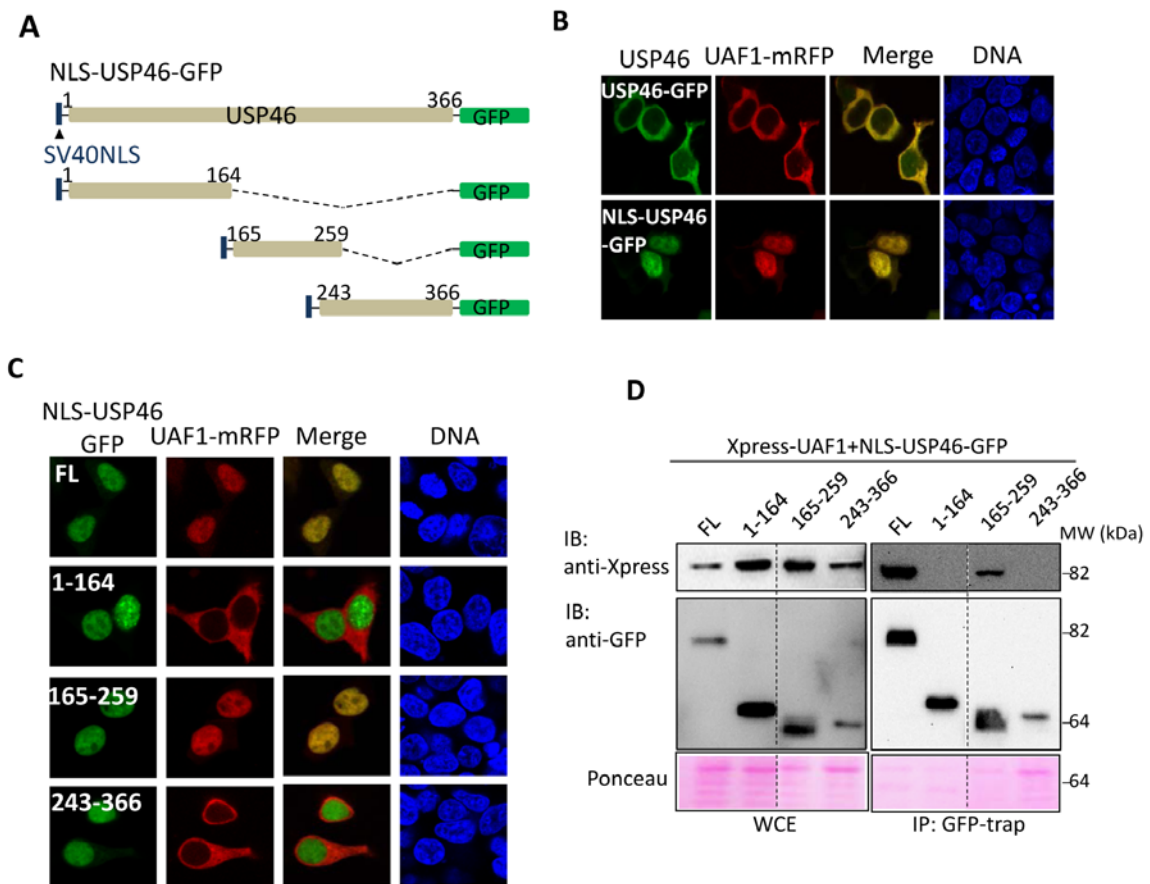


**Figure 33: Homologous amino acid motifs mediate binding of USP1 and USP46 to UAF1.** **A.** Schematic representation of GFP-tagged USP46 deletion mutants. A heterologous NLS (SV40 NLS) was fused to the amino terminal end of each fragment. **B.** Confocal images of 293T cells showing that USP46-GFP is cytoplasmic, but relocates to the nucleus when fused to the SV40 NLS. The localization of co-expressed UAF1-mRFP parallels that of the DUB. **C.** Confocal microscopy images show that nuclear relocation of UAF1-mRFP is induced by full

length (FL) and the 165–259 fragment, but not by the 1–164 or the 243–366 fragments. **D.** GFP-trap co-IP analysis of 293T cells, showing that Xpress-UAF1 co-immunoprecipitates with full-length USP46 and with the 165–259 fragment but not with the other two fragments tested. The dotted line indicates that the panel is a composite of two images from a single exposure of the same gel. WCE, whole cell extract. A section of the membrane stained with Ponceau is shown to gauge protein loading.

At the time we carried out these experiments, no data about the three-dimensional structure of USP1, USP12 or USP46 were available. Therefore, we used the SWISS-MODEL web tool (<http://swissmodel.expasy.org/>) to model the structure of the catalytic domains of these DUBs using the structure of USP7 catalytic domain (Hu et al., 2002) as a template. This model revealed that the UAF1 binding motifs of USP1 and USP46 map to their “Fingers” subdomains (**Figure 34**).

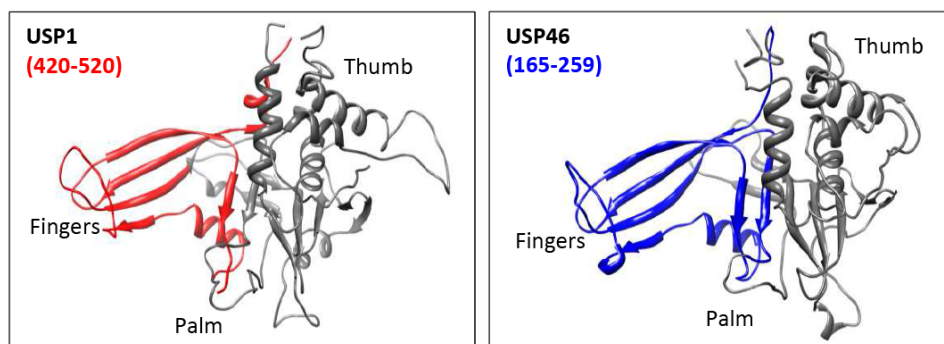


**Figure 34: The UAF1 binding domain in USP1 and USP46 corresponds to the “Fingers” subdomains of these DUBs.** Modeled structure of USP1 (left) and USP46 (right) catalytic domains using SWISS-MODEL and the USP7 structure 1NB8 (<http://swissmodel.expasy.org/>) as a template. The “Thumb”, “Palm” and “Fingers” subdomains are indicated. The UAF1-binding sites are highlighted in red (USP1 residues 420–520) or blue (USP46 residues 165–259).

#### 4.2.3. Fine-mapping of the UAF1/USP1 interaction

Our next goal was to identify the specific USP1 and UAF1 residues that contribute to their binding. This detailed characterization of the USP1/UAF1 interaction represents a necessary first step for future attempts to disrupt this interaction as a therapeutic strategy in cancer.

#### 4.2.3.1. Identification of USP1 residues that contribute to UAF1 binding

We hypothesized that critical residues for UAF1 interaction would be conserved in the “Fingers” subdomain of UAF1-binding DUBs, but not in the “Fingers” subdomain of other DUBs, such as USP7, that have not been reported to bind UAF1. We also reasoned that, since the front of the “Fingers” subdomain represents the primary site for ubiquitin binding (Hu et al., 2002, 2005), residues at the back of the “Fingers” would be more likely to be involved in the USP1/UAF1 interaction.

First, we used a relocation assay to confirm that USP7 “Fingers” subdomains (residues 314-411) does not bind UAF1. The USP7(Fingers)-GFP fragment was found to be predominantly cytoplasmic (not shown), and, thus, the SV40 NLS was added to its amino terminus in order to force its nuclear localization. As shown in (Figure 35), UAF1-mRFP remained in the cytoplasm when co-expressed with [NLS]-USP7(Fingers)-GFP, confirming the lack of interaction.

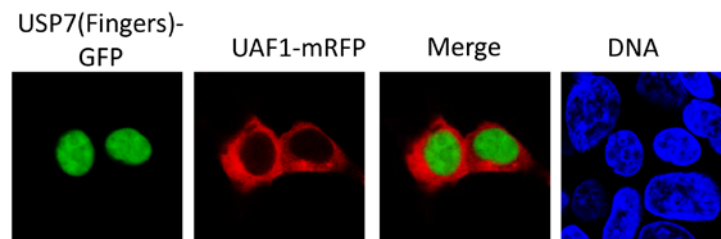


**Figure 35: USP7 “Fingers” subdomain does not bind UAF1.** UAF1 relocation assay in 293T showing that a [NLS]-USP7(Fingers)-GFP fragment does not induce nuclear relocation of UAF1-mRFP, indicating lack of interaction.

We applied CLUSTALW2-based alignment to compare the sequence of the “Fingers” subdomains of USP1, USP46 and USP7. In addition, a hypothetical three-dimensional model of the USP1 catalytic domain based on homology with USP7 structure 1NB8 (Hu et al., 2002) was used to deduce amino acid position. As illustrated in Figure 36, we selected four USP1 residues (Arg439, Leu441, Leu446, and Ser494) that are relatively well conserved in USP46, but not in USP7, and would be exposed at the back of the “Fingers” subdomain. We generated a mutant, termed GFP-USP1<sup>4m</sup>, in which these four residues were replaced with the corresponding USP7 residues (R439Q/L441K/L446R/S494A).

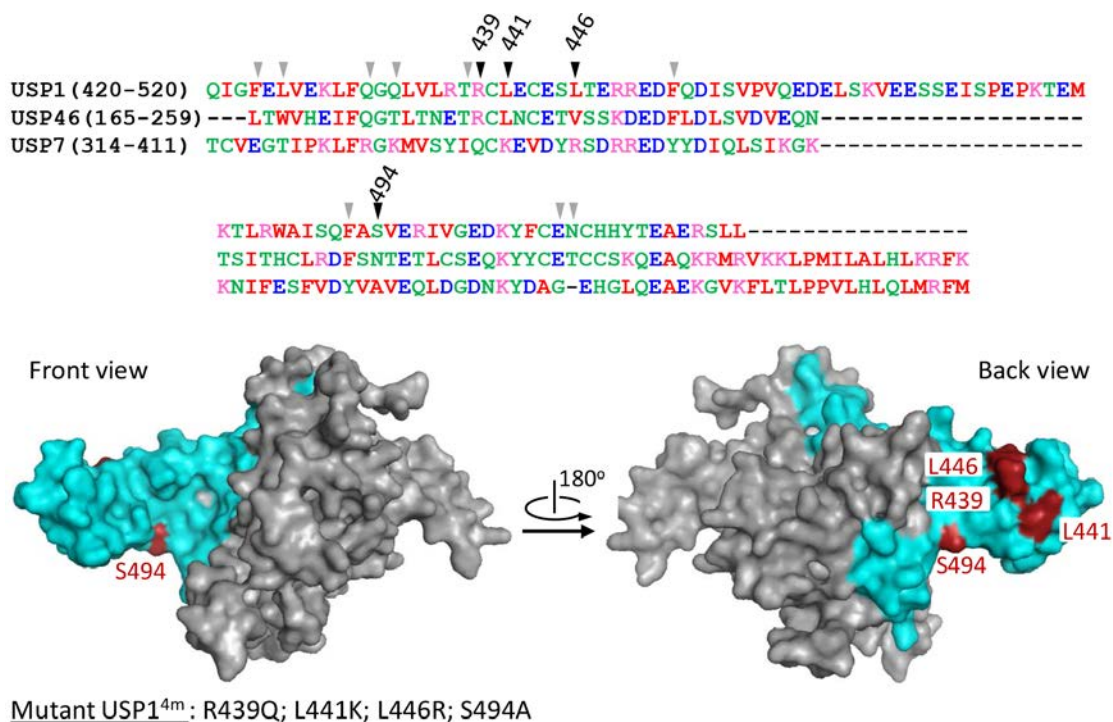


**Figure 36: Description of the experimental mutations introduced into the USP1 “Fingers” subdomain.** CLUSTALW2-based sequence alignment of the “Fingers” subdomains of USP1, USP46 and USP7. Letters are colored according to the physicochemical properties of the represented residue (<http://www.ebi.ac.uk/Tools/msa/clustalw2/help/faq.html>). Grey arrowheads indicate residues whose properties are similar in USP1 and USP46, but different in USP7. Below, a model of the USP1 catalytic domain based on homology with USP7 structure 1NB8 (Hu et al., 2002) is shown as a surface representation. The “Fingers” subdomain is colored cyan and both front and back views of the “open right hand” are shown. As explained in the text, we hypothesized that USP1 residues conserved in USP46 but not in USP7, and located on the “back” side of the “Fingers” subdomain, might be particularly relevant for UAF1 binding. Four USP1 residues that fulfill these requirements (R439, L441, L446 and S494) are indicated by black arrowheads in the alignment and highlighted in dark red in the model.

Somewhat disappointingly, using the nuclear relocation assay we found that GFP-USP1<sup>4m</sup> was still able to bind UAF1 (Figure 37).

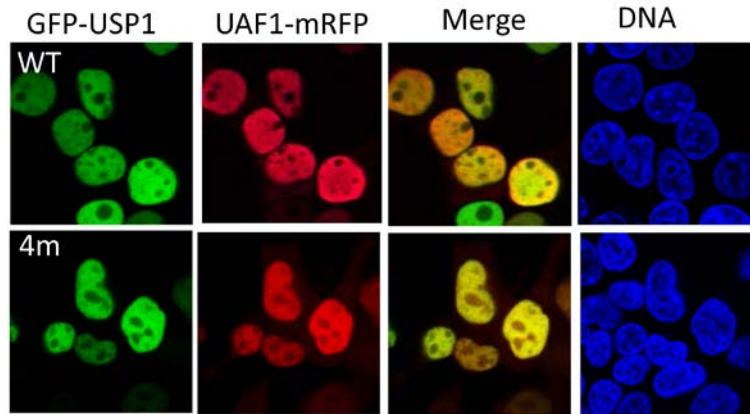


**Figure 37: The USP1<sup>4m</sup> mutant binds UAF1.** Confocal microscopy images of 293T cells showing that GFP-USP1<sup>WT</sup> and GFP-USP1<sup>4m</sup> are equally able to promote nuclear relocation of UAF1-Mrpf.

While our manuscript describing these findings (Olazabal-Herrero et al., 2016) was under review, the three-dimensional structure of the UAF1/USP46 complex bound to ubiquitin was published (Yin et al., 2015) (**Figure 38**). In line with our results, their structural data independently revealed that the UAF1 binding site in USP46 corresponds to the “Fingers” subdomain of the DUB. Other groups have later confirmed these results (Dharadhar et al., 2016; Li et al., 2016).

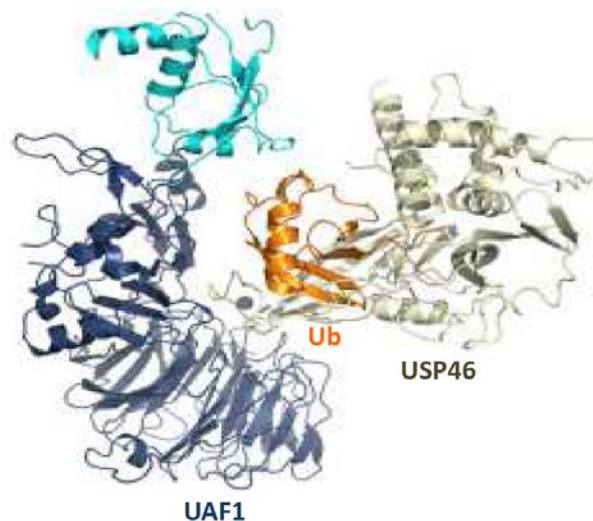


**Figure 38: UAF1/USP46/ubiquitin complex.** UAF1 is coloured blue (the β-propeller and ancillary domains in dark blue, and the Sumo-like domain in light blue), USP46 is coloured ivory and ubiquitin is coloured orange. The model reveals that USP46 “fingertips” directly bind to the top center of the β-propeller of UAF1. *Adapted from* (Yin et al., 2015).

Taking advantage of their structure data, Yin et al identified four amino acid residues on the tips of the “Fingers” subdomain of USP46 (E186, R181, L183 and E237) engaged in the interaction with UAF1. They called this group of residues the “ERLE” motif. The ERLE motif is conserved in USP12 (E190, R185, L187 and E241) and USP1 (E444, R439, L441 and E516) (**Figure 39**).

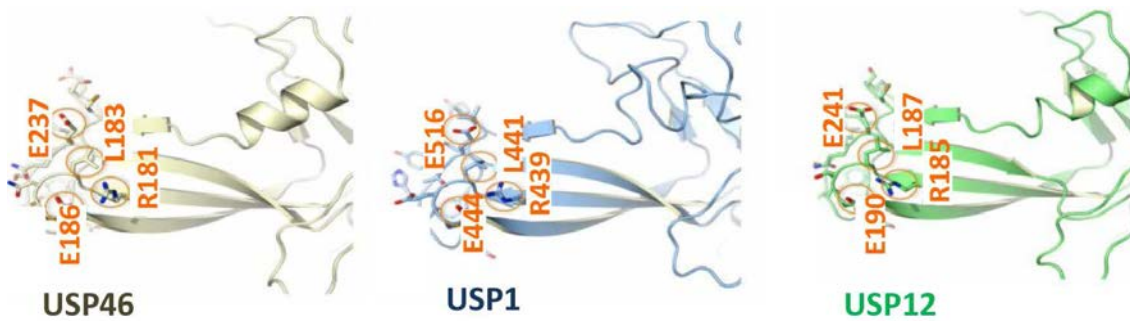


**Figure 39: The ERLE pattern that contributes to UAF1 binding in USP46, USP12 and USP1.** Homology models of USP12 and USP1 compared to USP46 structure illustrate conservation of key amino acid residues involved in UAF1 interaction. The pattern of four amino acid residues is circled including E186, R181, L183 and E237 in USP46; E190, R185, L187 and E241 in USP12 and E444 and R439, L441 and E516 in USP1. Adapted from (Yin et al., 2015).

As illustrated in **Figure 40**, the ERLE motif of USP1 includes two of the residues (R439 and L441) that we introduced in the USP1<sup>4m</sup> mutant. The most critical residue in the ERLE motif, however, turned out to be E444. In fact, Yin et al found that a USP1<sup>E444K</sup>, mutant or the equivalent USP46<sup>E186K</sup> mutant are unable to bind UAF1, and have their deubiquitinase activity abrogated (Yin et al., 2015). The equivalent mutation in USP12 (E190K) was not tested.

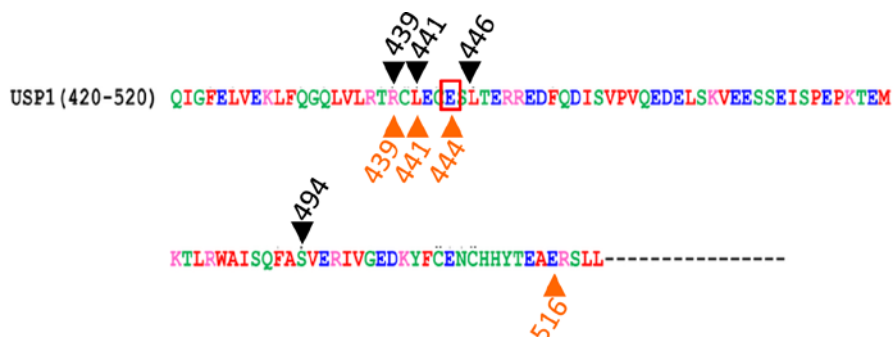


**Figure 40: Comparison of the amino acids in USP1 “Fingers” subdomain mutated by our group (black arrowheads) and Yin et al (orange arrowheads).** The most critical amino acid for the interaction with UAF1 (E444) is highlighted in red.

To independently confirm and extend their results, we generated plasmids encoding GFP-USP1<sup>E444K</sup>, YFP-[NLS]-USP46<sup>E186K</sup> and YFP-[NLS]-USP12<sup>E190K</sup>. Using the nuclear relocation assay, we found that the three mutants were unable to relocate UAF1 to the nucleus (**Figure 41**), thus confirming that these single point mutations efficiently disrupt the interaction of the three DUBs with UAF1.

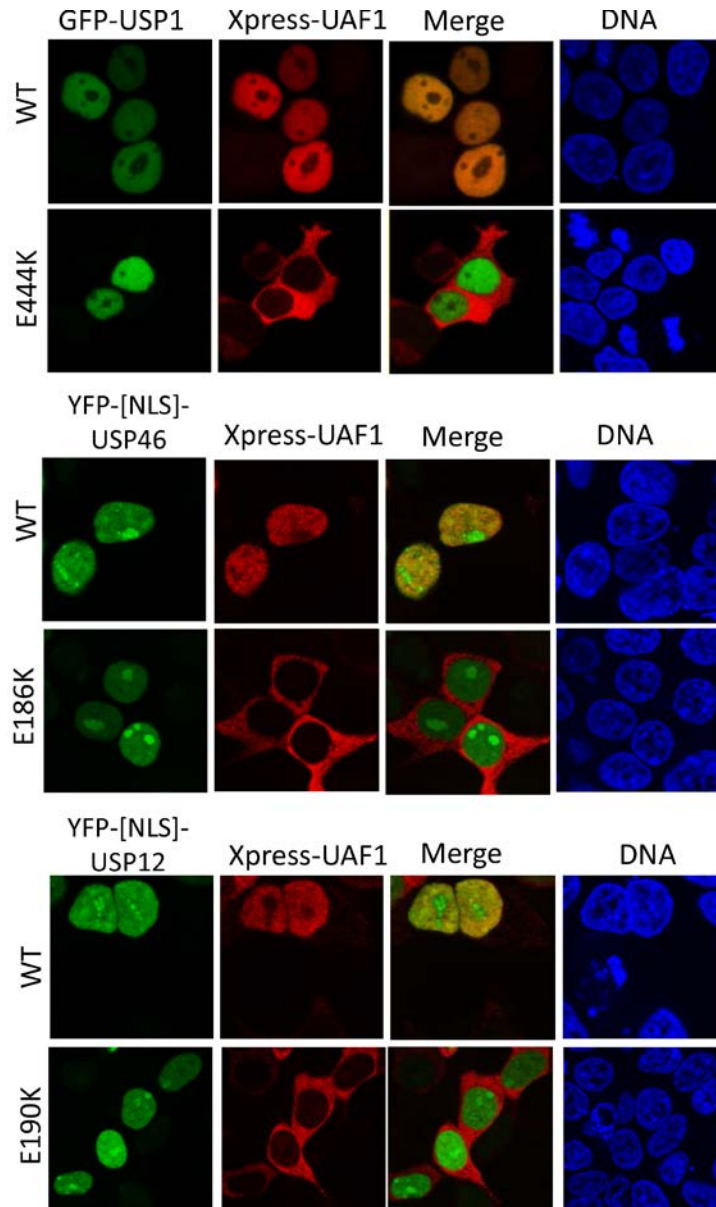


**Figure 41: The USP1<sup>E444K</sup>, USP46<sup>E186K</sup> and USP12<sup>E190K</sup> mutants do not interact with UAF1.** Representative examples of 293T cells showing that the USP1<sup>E444K</sup>, USP46<sup>E186K</sup> and USP12<sup>E190K</sup> mutants have lost their ability to induce nuclear relocation of Xpress-UAF1.



#### 4.2.3.2. UAF1 residues that contribute to DUB binding

Guided by the structural information, Yin et al also generated a triple UAF1 mutant, (UAF1<sup>3M</sup>) bearing three mutations in the  $\beta$ -propeller domain (K214E/W256A/R272D) that was unable to bind USP1 and USP46 (Yin et al., 2015). In order to independently validate and further refine their findings, we generated three different Xpress-tagged UAF1 mutants: UAF1<sup>3M</sup>, UAF1<sup>2M</sup> (K214E/W256A), and UAF1<sup>K214E</sup> (Figure 42A). We confirmed that these mutations did not alter the cytoplasmic localization of UAF1 (Figure 42B).

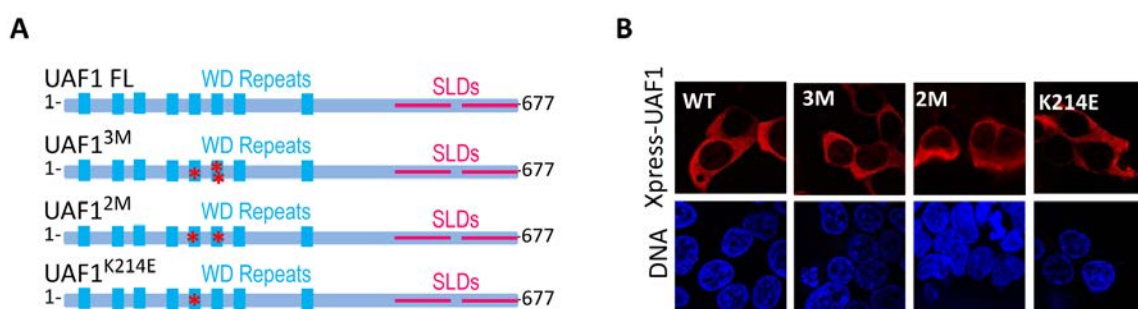


**Figure 42: Schematic representation of UAF1 mutants and their localization. A.** The WD-repeats of UAF1 are highlighted in blue and the Sumo-like domains 1 and 2 (SLDs) are depicted in pink. The mutations are indicated with a red asterisks. **B.** Confocal microscope images of 293T cells showing cytoplasmic localization of Xpress-tagged UAF1 mutants.

Using the nuclear relocation assay (Figure 43), we found that all the tested mutants, including the single point mutant UAF1<sup>K214E</sup> were unable to bind USP1, USP46, and USP12.

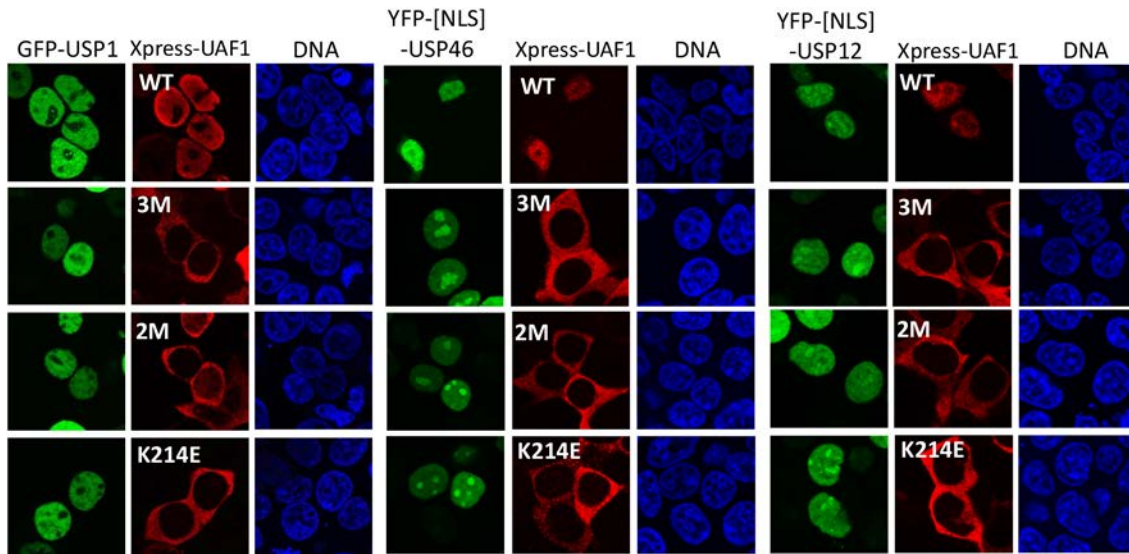


**Figure 43: A single point mutation (K214E) in UAF1 is enough to disrupt interaction with USP1, USP46 and USP12.** Confocal microscopy images of 293T cells showing that Xpress-tagged UAF1<sup>3M</sup>, UAF1<sup>2M</sup> and UAF1<sup>K214E</sup> do not relocate to the nucleus when coexpressed with GFP-USP1, or YFP-[NLS]-USP46 YFP-[NLS]-USP12.

In summary, we conclude that the E444 residue in USP1, and the K214 residue in UAF1 are crucial in the formation of the USP1/UAF1.

#### 4.2.4. Assessing the functional effect of the mutations that disrupt USP1/UAF1 interaction

Using mostly *in vitro* experiments, Yin et al showed that mutations that disrupt UAF1 binding prevented the catalytic activation of USP46 and USP1 (Yin et al., 2015). To further extend these findings in a cellular setting, we investigated how the single mutations USP1<sup>E444K</sup> and UAF1<sup>K214E</sup> affect the activity of the USP1/UAF1 complex in cells using two different readouts: (i) USP1 autocleavage and (ii) the ability to counteract HU-induced PCNA ubiquitination.

As shown in **Figure 44A**, USP1<sup>E444K</sup> did not undergo autocleavage when co-expressed with UAF1<sup>WT</sup> and, conversely, USP1<sup>WT</sup> did not undergo autocleavage when co-expressed with UAF1<sup>K214E</sup> (**Figure 44B**). Thus, consistent with the previous *in vitro* data, our findings indicate that these mutations abrogate catalytic activation of USP1 by UAF1 in cells.

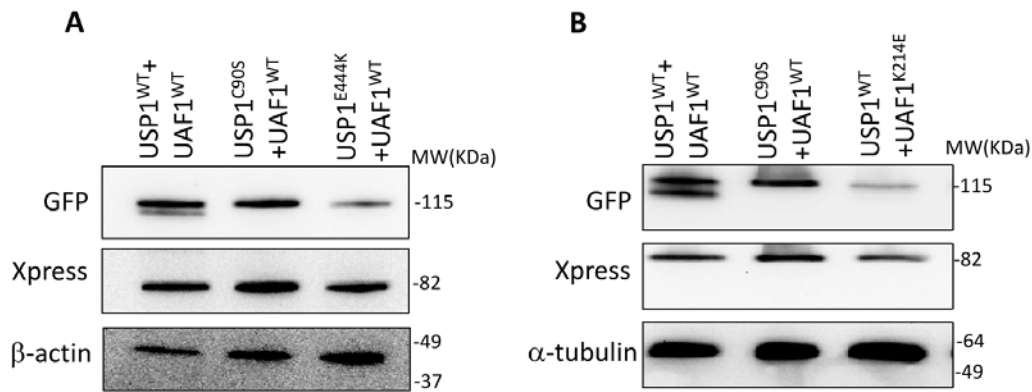


**Figure 44: Autocleavage analysis of USP1<sup>E444K</sup> and UAF1<sup>K214E</sup> mutants.** **A.** Immunoblot analysis showing that USP1<sup>E444K</sup> mutant does not undergo UAF1-induced autocleavage. **B.** Immunoblot analysis showing that UAF1<sup>K214E</sup> mutant does not induce USP1 autocleavage. In these experiments GFP-tagged USP1 constructs and Xpress-tagged UAF1 constructs were used. USP1<sup>C90S</sup> was included as a negative control.

On the other hand, UbPCNA levels were not decreased in cells co-expressing USP1<sup>E444K</sup> with UAF1<sup>WT</sup> (**Figure 45A**) as expected. Surprisingly, very low levels of UbPCNA were repeatedly observed in cells co-expressing USP1<sup>WT</sup> with UAF1<sup>K214E</sup> (**Figure 45B**). This was a puzzling observation, as we have shown above that UAF1<sup>K214E</sup> is unable to bind and catalytically activate USP1.

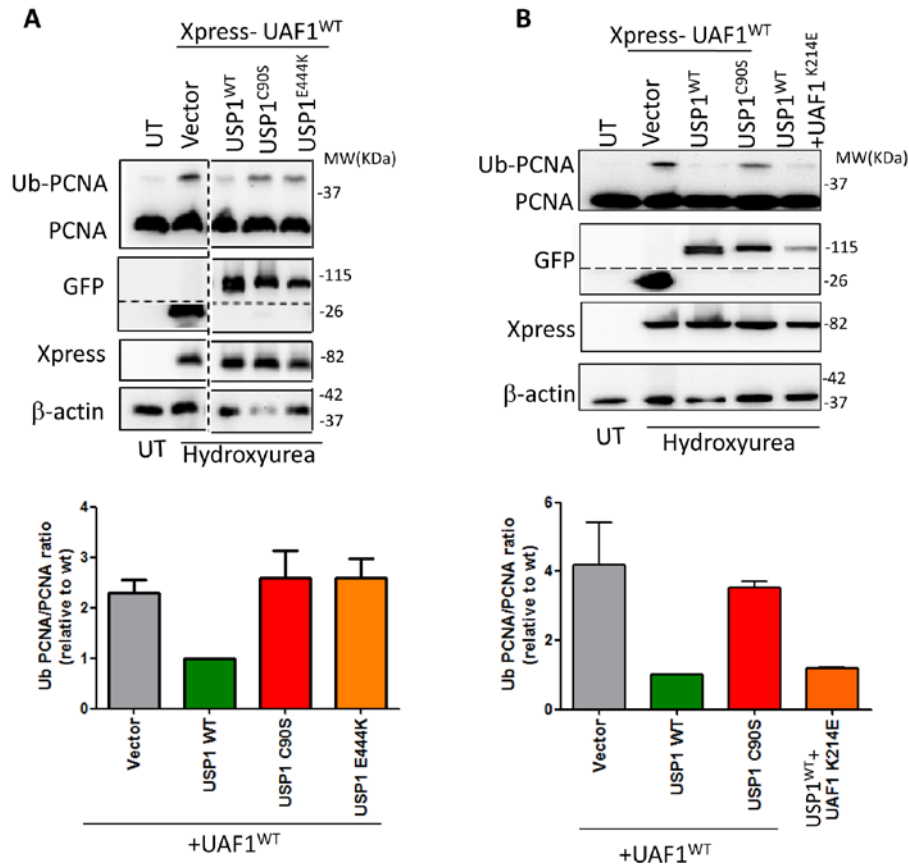


**Figure 45: Analysis of PCNA ubiquitination in cells expressing USP1<sup>E444K</sup> and UAF1<sup>K214E</sup> mutants.** Top, representative examples of immunoblot analysis of 293T cells co-transfected with the indicated plasmids and treated with 4 mM HU for 24 h. The dotted line indicates that the panel is a composite of two images from a single exposure of the same gel. The UbPCNA/PCNA ratio was determined by densitometry analysis of the immunoblot bands, and the graphs below show the results (mean and SEM) of 3 independent experiments. **A.** Co-expression of GFP-USP1<sup>E444K</sup> with Xpress-UAF1<sup>WT</sup> did not reduce HU-induced ubPCNA. **B.** Co-expression of GFP-USP1<sup>WT</sup> with Xpress-UAF1<sup>K214E</sup> reduced HU-induced UbPCNA.

Our unexpected findings with the UAF1<sup>K214E</sup> mutant raised the following question: does overexpressed “free” USP1 counteract PCNA monoubiquitination in a manner that does not require UAF1 binding and that is independent of its deubiquitinase activity?

To answer this question, we expressed GFP-USP1<sup>WT</sup> and the catalytically inactive mutant GFP-USP1<sup>C90S</sup> either alone or with wild type UAF1 in 293T cells. We found that, indeed, the levels of monoubiquitinated PCNA were clearly reduced in cells expressing GFP-USP1<sup>WT</sup> and, more surprisingly, also in cells expressing GFP-USP1<sup>C90S</sup> alone (red square) (**Figure 46**). Of note, when co-expressed with UAF1, only wild type USP1 reduced UbPCNA level.

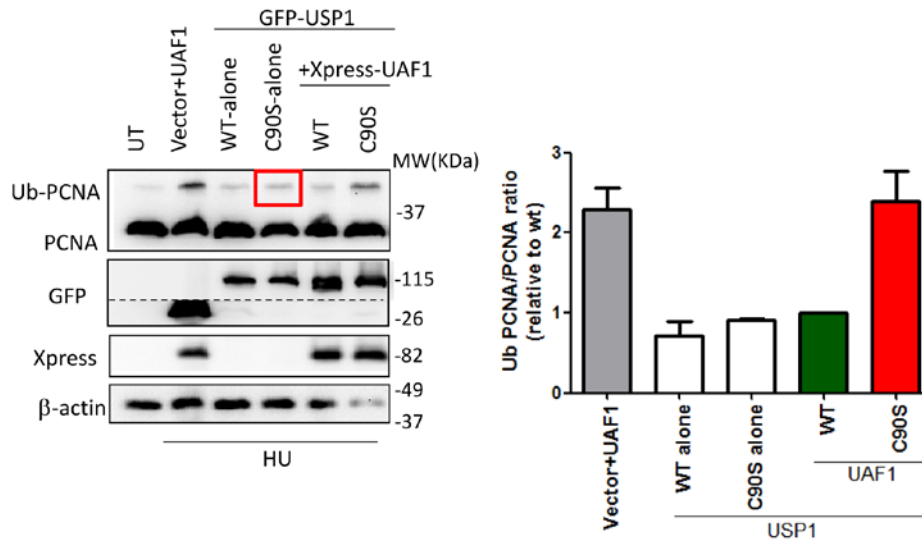


**Figure 46: Overexpression of GFP-USP1<sup>WT</sup> or GFP-USP1<sup>C90S</sup> alone decreases PCNA monoubiquitination.** Left, immunoblot analysis of 293T cells co-transfected with the indicated plasmids and treated with 4 mM hydroxyurea (HU) for 24 h. When expressed alone, both GFP-USP1<sup>WT</sup> and the catalytically inactive GFP-USP1<sup>C90S</sup> decrease HU-induced PCNA monoubiquitination (red square). In contrast, when co-expressed with Xpress-UAF1, only GFP-USP1<sup>WT</sup> decreases UbPCNA. The UbPCNA/PCNA ratio was determined by densitometry analysis of the immunoblot bands, and the graph on the right show the results (mean and SEM) of 3 independent experiments.

In summary, mutations that interfere with USP1/UAF1 binding prevent UAF1-mediated enzymatic activation of USP1 (as indicated by the lack of autocleavage). However, “free” USP1 may decrease PCNA monoubiquitination independently of its deubiquitinase activity, suggesting a previously undescribed “non-catalytic” effect of USP1 on the ubiquitination of PCNA.

### **4.3. USP1/UAF1 IN CANCER**

Although USP1 is not a frequently mutated gene in human tumors, the cancer mutation database *COSMIC* includes a number of USP1 mutations whose biological effect has not yet been tested. On the other hand, the USP1/UAF1 complex is emerging as a potential target in cancer therapy (García-Santisteban et al., 2013), but USP1 inhibitors have only been tested in a very limited set of tumor models.

In this section, we first identify two novel readouts to evaluate USP1/UAF1 cellular activity. Then we apply these readouts, as well as previously-established assays to investigate the functional consequences of several cancer-related USP1 mutations. Finally, we evaluate the effect of the USP1 inhibitor ML323, alone or in combination with the chemotherapeutic agent oxaliplatin, in a preclinical model of pancreatic cancer-derived cells.

#### **4.3.1. Novel functional readouts to study USP1 activity in cells: general ubiquitin deconjugation and blockade of 53BP1 foci formation**

A few physiological targets of USP1, such as PCNA, FANCD2 and ID2, have been identified (Huang et al., 2006; Nijman et al., 2005b; Williams et al., 2011). The ability to reverse the monoubiquitination of these three targets is frequently used as readout to study USP1 deubiquitinating activity in cells. Using commercially available reagents, we were unable to unambiguously detect FANCD2 and ID2 monoubiquitination by immunoblot. In contrast, UbPCNA was clearly and reproducibly detected and thus, the ability to reverse PCNA monoubiquitination is used throughout this Thesis as a readout for USP1 activity. However, our data (*section 4.2.4.*) suggest that overexpression of “free” USP1 can also decrease UbPCNA levels through a mechanism independent from its enzymatic activity.

We thought that this “non-catalytic” effect might complicate the functional characterization of some cancer-related USP1 mutants. Thus, we set out to discover novel cellular readouts for monitoring USP1 activity to complement the analysis of PCNA ubiquitination.

We focused on two events that occur in cells that suffer DNA double-strand breaks (DSBs). On one hand, we studied the formation of nuclear ubiquitin-containing foci that reflect the recruitment of ubiquitinated proteins to the sites of DNA damage (Messick and Greenberg, 2009). To this end, we used the FK2 antibody, a well-validated reagent that specifically recognizes conjugated, but not free, ubiquitin (Fujimuro et al., 1994). On the other hand, we studied the ubiquitination-dependent recruitment of 53BP1 to foci (Huyen et al., 2004). As a negative control, we studied the phosphorylation-dependent recruitment of  $\gamma$ H2AX to foci, an ubiquitin independent event (Fernandez-Capetillo et al., 2004; Rogakou et al., 1998).

We used the radiomimetic drug neocarzinostatin (NCS) as a genotoxic agent to induce DSBs. As shown in **Figure 47**, and consistent with previous reports (Bencokova et al., 2009; Morris et al., 2012; van Wijk et al., 2012), NCS (100ng/ml for 4 h) induced a dramatic increase in the number of FK2, 53BP1 and  $\gamma$ H2AX nuclear foci.

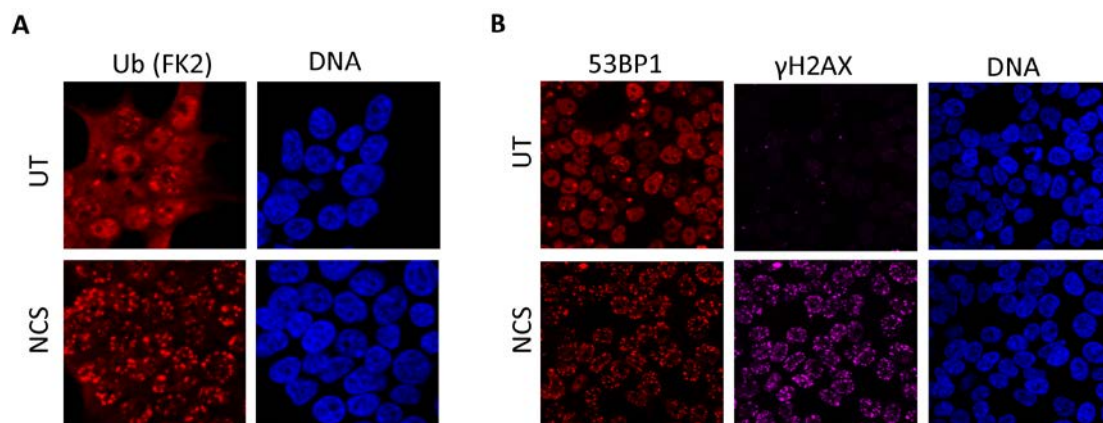


**Figure 47: Ubiquitinated proteins, 53BP1 and  $\gamma$ H2AX accumulate in nuclear damage foci after NCS treatment.** Immunofluorescence analysis of untreated (UT) or neocarzinostatin (NCS)-treated 293T cells. **A.** Staining with the FK2 antibody that recognizes conjugated ubiquitin. **B.** Double staining with anti-53BP1 (red) and anti- $\gamma$ H2AX (purple).

Next, 293T cells were transfected with GFP-USP1<sup>WT</sup> alone or co-transfected with Xpress-UAF1 plus GFP-USP1<sup>WT</sup> or GFP-USP1<sup>C90S</sup>. As a negative control, GFP fused to the SV40 NLS ([NLS]-GFP) was included. Transfected cells were either left untreated or treated with NCS and anti-FK2 immunofluorescence was performed. Strikingly, co-expression of GFP-USP1<sup>WT</sup> and Xpress-UAF1 resulted in a drastic reduction in the FK2 signal in the nucleus of untreated cells (**Figure 48A**), and

completely prevented the formation of FK2-positive foci in NCS-treated cells (**Figure 48B**). Importantly, none of these effects were noted in cells expressing the NLS-GFP control, GFP-USP1<sup>WT</sup> alone, or in cells co-expressing GFP-USP1<sup>C90S</sup> with Xpress-UAF1.

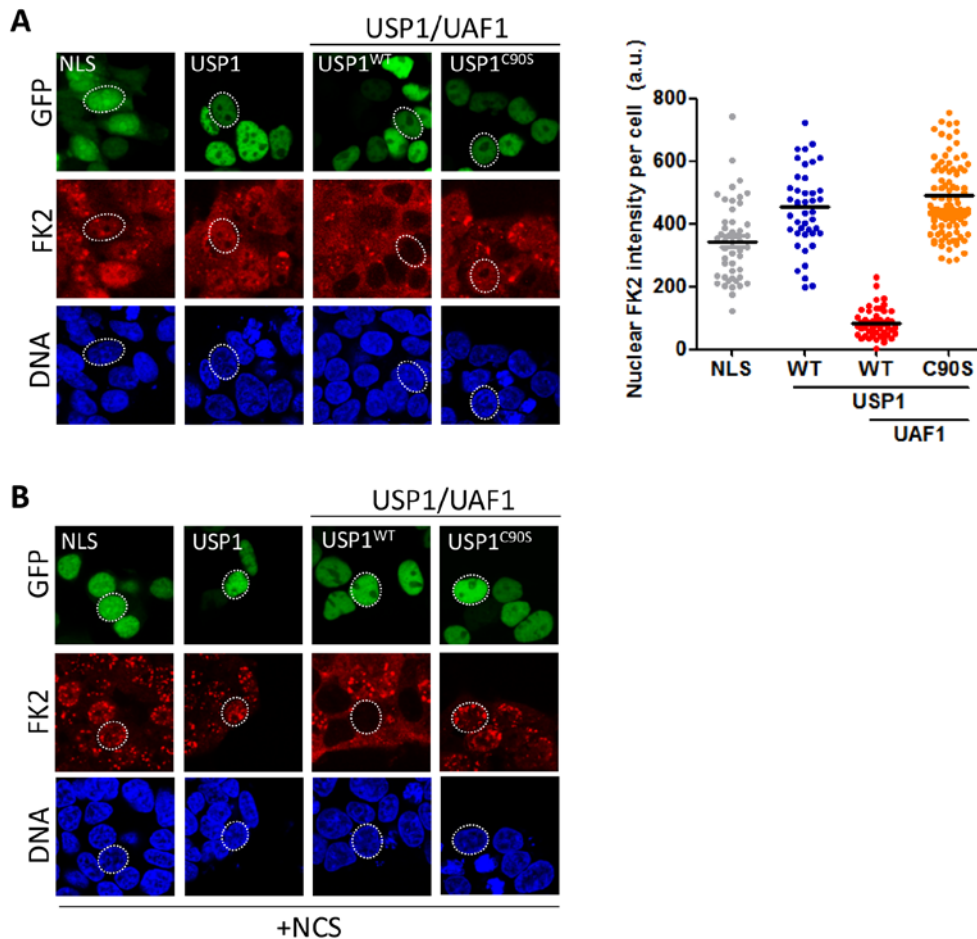


**Figure 48: Overexpression of the USP1/UAF1 complex decreases general ubiquitin conjugation in the nucleus. A.** Left, confocal microscopy images of FK2 immunostaining in 293T cells transfected with the indicated expression plasmids. The nucleus of a representative transfected cell per sample is circled by a dotted line. Using ImageJ, the intensity of the FK2 signal in the nucleus of at least 50 transfected cells with similar GFP expression levels was quantified per sample. Each dot in the graph (right) represents the intensity of the FK2 signal in the nucleus of a single cell, and the bar indicates the median. The data shown correspond to one experiment. Two independent experiments were performed, with similar results. Overexpression of USP1/UAF1 induces a drastic decrease in FK2 staining. **B.** Confocal microscopy images show FK2 immunostaining in 293T cells transfected as in A., and treated with 100 ng/mL neocarzinostatin (+ NCS) for 4 h. Almost not nuclear FK2 staining is detected in NCS-treated cells overexpressing USP1/UAF1.



On the other hand, overexpression GFP-USP1<sup>WT</sup> and Xpress-UAF1 completely blocked the recruitment of 53BP1 into NCS-induced foci (**Figure 49**). YFP-USP3, a DUB previously shown to interfere with 53BP1 recruitment (Sharma et al., 2014), was included as positive control in this experiment. 53BP1 recruitment was not reduced in cells expressing the [NLS]-GFP control, GFP-USP1<sup>WT</sup> alone, or in cells co-expressing GFP-USP1<sup>C90S</sup> and Xpress-UAF1.

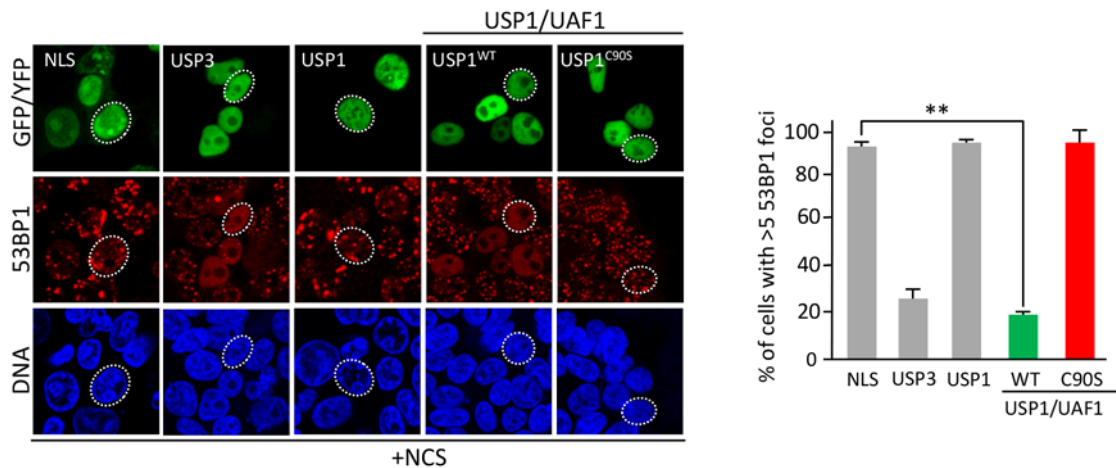


**Figure 49: Effect of USP1/UAF1 overexpression on the recruitment of 53BP1 to DNA damage foci.** Left, confocal microscopy images showing representative examples of 53BP1 immunostaining in 293T cells transfected with the indicated expression plasmids. Cells were treated with NCS (100 ng/mL) for 4 h before fixation. The graph (right) represents the percentage of cells showing more than five 53BP1 nuclear foci in each sample. The data shown correspond to the mean of three independent experiments, and error bars indicate the SEM. One hundred cells per condition were examined in each experiment. \*\* $p < 0.01$  (Student's t-test).

As expected, overexpression of GFP-USP1 and Xpress-UAF1 did not interfere with the phosphorylation-dependent recruitment of  $\gamma$ H2AX into NCS-induced nuclear foci.

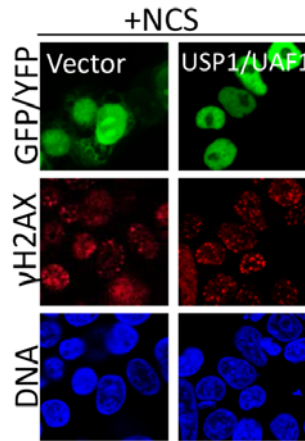


**Figure 50: Effect of USP1/UAF1 complex overexpression on  $\gamma$ H2AX.** Confocal microscopy images showing examples of  $\gamma$ H2AX immunostaining in 293T cells transfected with the indicated expression plasmids and treated with NCS. USP1/UAF1 overexpression does not interfere with recruitment of  $\gamma$ H2AX to DNA damage foci.

In summary, these results indicate that co-expression of USP1<sup>WT</sup> and UAF1 promotes general ubiquitin deconjugation and blocks the recruitment of 53BP1 to DNA damage-induced foci. Of note, unlike the “non-enzymatic” effect on PCNA described above, both effects are dependent on the expression of a catalytically active USP1/UAF1 complex.

The dramatic effect of USP1/UAF1 complex overexpression on nuclear ubiquitin conjugation prompted us to test the possibility that overexpression of other nuclear DUBs of the USP family might have a similar effect. *In vitro* analyses have shown that USP members are generally promiscuous in terms of the type of the ubiquitin linkage that they can process (Faesen et al., 2011; Komander et al., 2009), but little is known about their substrate promiscuity in a cellular context. We reasoned that depletion of conjugated ubiquitin, as detected by FK2 immunofluorescence, could be useful to gauge the relative substrate promiscuity of DUBs. In this regard, although FK2 immunostaining has been previously performed in cells overexpressing specific USPs, such as USP36 (Endo et al., 2009), USP29 and USP44 (Mosbech et al., 2013), USP16 (Zhang et al., 2014), or USP26 and USP37 (Typas et al., 2015), a systematic comparison of how overexpression of several different USP family DUBs affects the FK2 signal has not yet been attempted, to the best of our knowledge.

---

To address this issue, we directly compared the levels of FK2 immunofluorescence signal in the nucleus of 293T cells overexpressing four different GFP-tagged or YFP-tagged USPs (**Figure 51A**). Besides USP1, three nuclear USPs (USP3, USP7, and USP22) were tested. In these experiments, GFP-USP1 was co-expressed with Xpress-UAF1 and [NLS]-GFP was used as a negative control. The intensity of FK2 immunofluorescence in the nuclei of cells expressing the different USPs was normalized using the FK2 intensity in the nuclei of nontransfected cells from the same sample as a reference. The relative FK2 intensity was then plotted against the intensity of the nuclear GFP/YFP fluorescence (**Figure 51B**). Overexpression of the [NLS]-GFP control, YFP-USP3 or YFP-USP22 did not affect FK2 immunostaining, even at high expression levels, whereas a partial decrease in the intensity of the FK2 signal was noted in cells expressing moderate to high levels of YFP-USP7. In the case of USP1/UAF1, a drastic reduction in the FK2 signal was clearly evident even in cells expressing very low levels of GFP-USP1. FK2 immunofluorescence was also investigated in NCS-treated cells overexpressing these four different USPs. As shown in **Figure 51C**, FK2-positive foci were readily detected in cells expressing [NLS]-GFP, YFP-USP7, or YFP-USP22. In line with a previous report (Sharma et al., 2014), diffuse FK2 staining was observed, but no NCS-induced foci were observed, in cells expressing YFP-USP3. As described above, the FK2 signal was almost undetectable in cells expressing USP1/UAF1. These findings suggest that, when expressed at similar levels, the USP1/UAF1 complex shows higher substrate promiscuity than other nuclear DUBs in a cellular context.

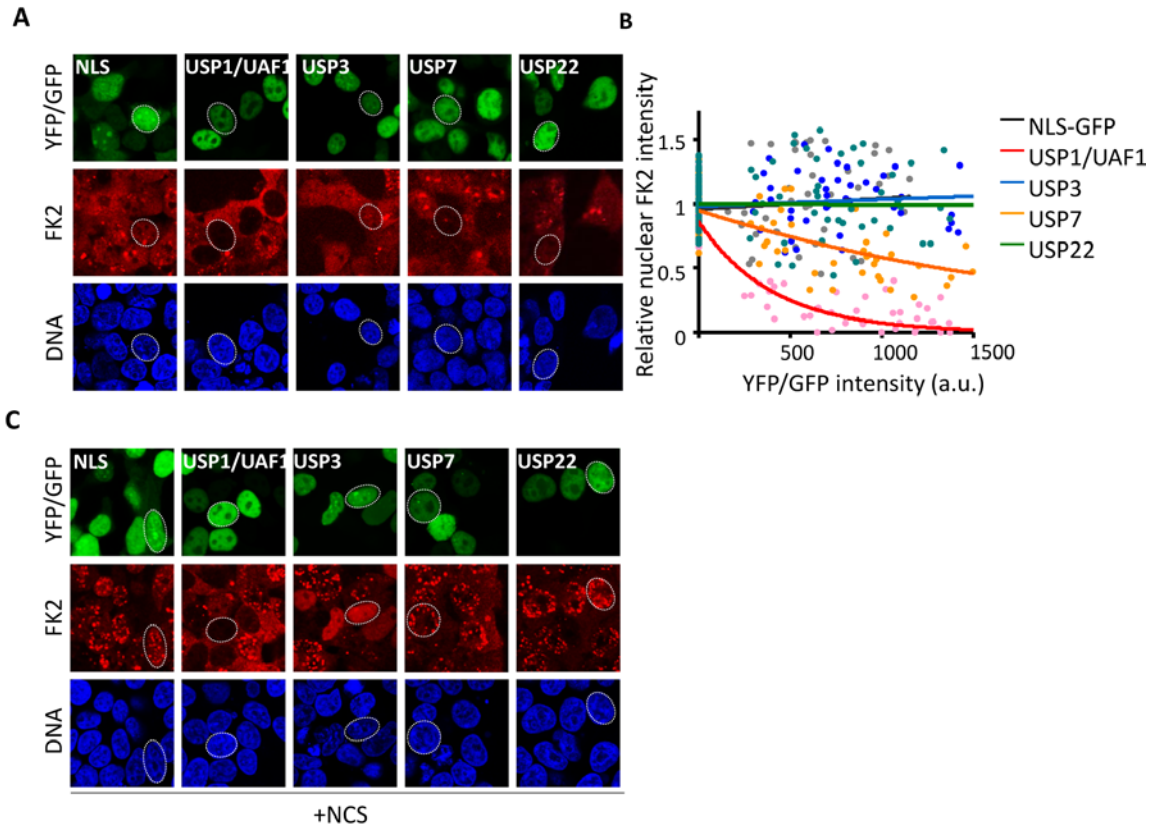


**Figure 51: Using depletion of conjugated ubiquitin as readout to compare USP1/UAF1 with other nuclear USPs.** **A.** Confocal microscopy images show examples of FK2 immunostaining in 293T cells transfected with the indicated expression plasmids. **B.** Graph showing the intensity of FK2 signal in the nuclei of 50 transfected cells per sample. Each dot in the graph represents a single cell. The FK2 fluorescence intensity was normalized to the intensity of the signal in the nuclei of nontransfected cells, and plotted against the YFP/GFP intensity. Trend lines were added with Excel. The data shown correspond to one experiment. Three individual experiments were carried out, with similar results. **C.** Confocal microscopy images show examples of FK2 immunostaining in 293T cells transfected as in A., and treated with 100 ng/mL NCS for 4 h.

In summary, these results identify general ubiquitin deconjugation and blockade of 53BP1 recruitment to foci as two novel readouts that can be used to investigate the functional effects of cancer-related USP1 mutations.

### 4.3.2. Functional effects of cancer-related USP1 mutations

Some USP1 mutations detected in tumors (S475Y, D502N, and S575R) affect residues in/near the “Fingers” subdomain, and several others (G667A, L669P, K673T and A676T) cluster around the G670/G671 autocleavage site (**Figure 52**).

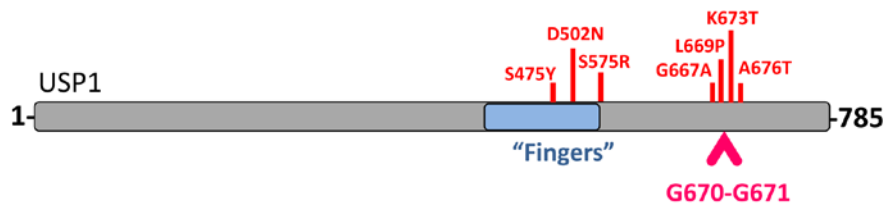


**Figure 52: Cancer-associated USP1 mutations in or near the “Fingers” subdomain or the G670/G671 autocleavage site.** Schematic representation of USP1 domain structure showing “Fingers” subdomain in light blue and the dyglycine autocleavage site highlighted in pink. The position of seven cancer-associated USP1 mutations reported in the *COSMIC* mutation database is indicated in red.

We investigated the effect of these seven mutations, using a battery of tests that included (i) ability to interact with UAF1 using the relocation assay, (ii) ability to undergo UAF1-induced autocleavage, (iii) ability to reverse HU-induced PCNA ubiquitination when co-expressed with UAF1, (iv) ability to promote general ubiquitin deconjugation, and (v) ability to prevent NCS-induced recruitment of 53BP1 to DNA damage foci.

#### 4.3.2.1. Functional characterization of cancer-related mutations in the USP1 “Fingers” subdomain

We selected two missense mutations in the “Fingers” subdomain residues (S475Y and D502N), which have been detected in endometrial carcinoma and melanoma samples, respectively (<http://cancer.sanger.ac.uk/cancergenome/projects/cosmic/>), and a third mutation, S575R, which is located just outside the “Fingers” subdomain but affects the most commonly mutated USP1 residue in tumors (**Figure 52**). We generated GFP-USP1<sup>S475Y</sup>, GFP-USP1D<sup>502N</sup> and GFP-USP1<sup>S575R</sup> mutants. The results of the nuclear relocation assay showed that the three mutants are able to interact with UAF1 (**Figure 53**).

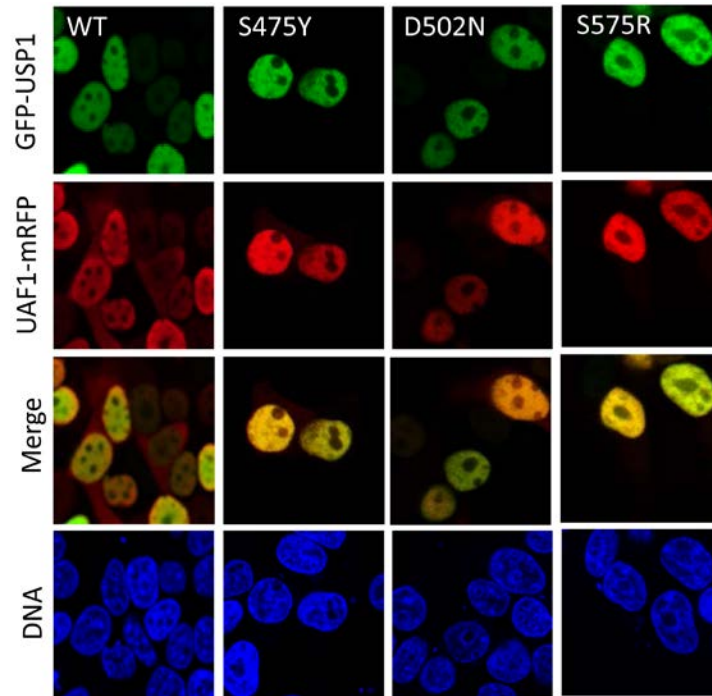


**Figure 53: UAF1 nuclear relocation assay of USP1 cancer-related mutations in/near the “Fingers” subdomain.** Confocal images showing examples of 293T cells co-expressing the indicated plasmids. All the mutants tested are able to relocate UAF1 to the nucleus.

These three “Fingers” mutants were also able to undergo UAF1-promoted autocleavage (**Figure 54**).

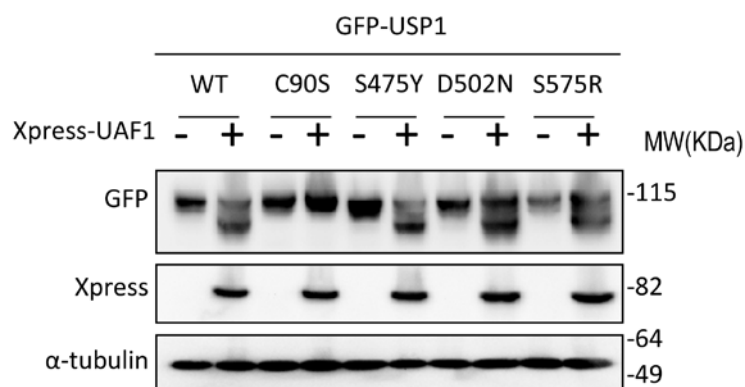


**Figure 54: Autocleavage analysis of USP1 cancer-related mutations in/near the “Fingers” subdomain.** Immunoblot analysis of 293T cells transfected with the indicated GFP-USP1 variants, either alone (-) or in combination with Xpress-UAF1 (+).-All the mutants tested are able to undergo autocleavage when coexpressed with UAF1.

Interestingly, one of the tested mutations, S475Y, but not the other two mutations tested, abrogated the ability of USP1 to deplete conjugated ubiquitin (**Figure 55A**), prevent 53BP1 recruitment to DNA damage foci (**Figure 55B**) and reduce ubPCNA levels (**Figure 55C**). Thus, the USP1<sup>S475Y</sup> mutant seems to be unable to catalyze substrate deubiquitination despite being capable to bind to and become activated by UAF1.

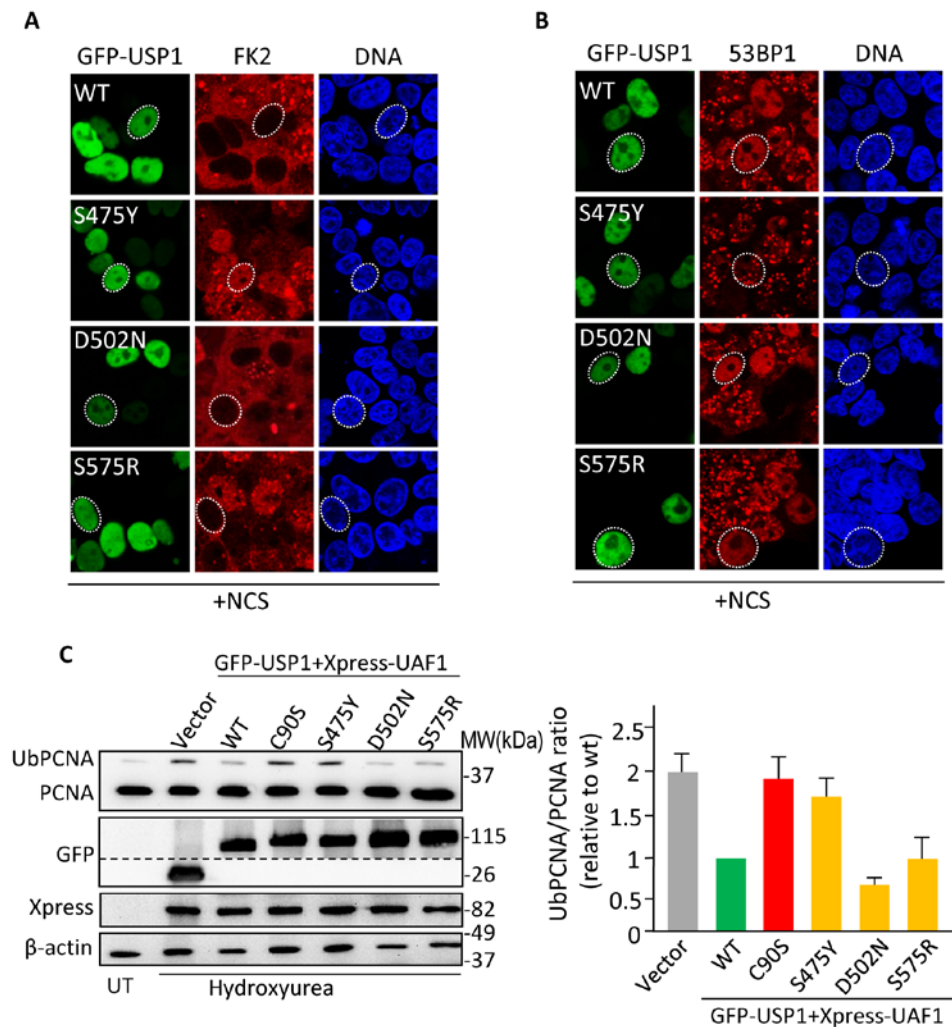


**Figure 55: Cellular activity assays to characterize the effect of USP1 cancer-related mutations in/near the “Fingers” subdomain. A, B.** Confocal microscopy images showing examples of FK2 and 53BP1 immunostaining in 293T cells co-transfected with the indicated expression plasmids and treated with NCS (100 ng/mL) 4 h before fixation. The nucleus of a representative cell in each sample is circled by a dotted line. GFP-USP1<sup>S475Y</sup> mutant was not able to deplete nuclear FK2 staining (A) or block 53BP1 foci recruitment (B). **C.** Immunoblot analysis of 293T cells co-transfected with the indicated expression plasmids and either left

untreated (UT) or treated with 4 mM hydroxyurea for 24 h. The UbPCNA/PCNA ratio was determined by densitometry analysis of the immunoblot bands. The graph on the right shows the results (mean and SEM of three independent experiments). GFP-USP1<sup>S475Y</sup> mutant was not able to deubiquitinate PCNA.

#### 4.3.2.2. Functional characterization of cancer-related mutations near USP1 autocleavage site

We also analysed four mutations (G667A, L669P, K673T and A676T) that cluster within a ten amino acid segment encompassing the G670/G671 autocleavage site. We used site-directed mutagenesis to introduce each of these amino acid changes into GFP-USP1, and we co-expressed these proteins with Xpress-UAF1 in 293T cells. None of these mutations disrupted USP1/UAF1 interaction, according to the results of the nuclear relocation assay (**Figure 56**).

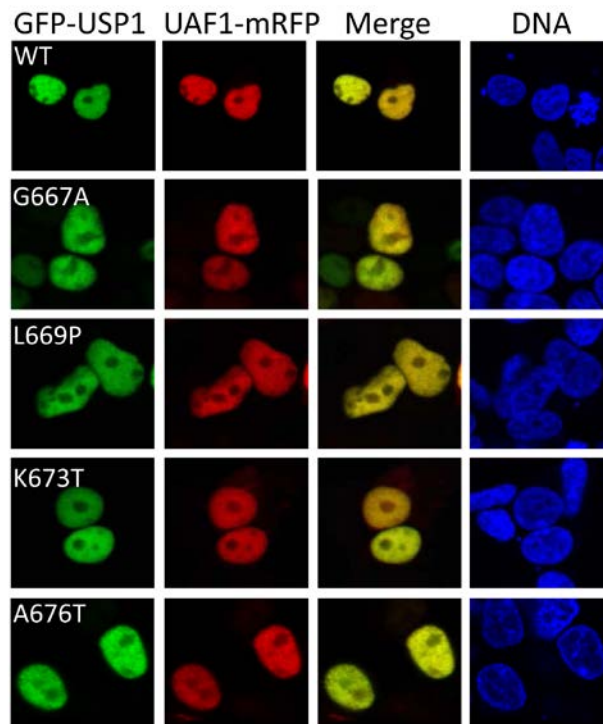


**Figure 56: UAF1 nuclear relocation assay of USP1 cancer-related mutations near the autocleavage site.** Confocal images showing examples of 293T cells co-expressing the indicated plasmids. All the mutants tested are able to relocate UAF1 to the nucleus.

Next, we evaluated the ability of these mutants to undergo UAF1-induced autocleavage. Immunoblot analysis (**Figure 57**) revealed that GFP-USP1<sup>G667A</sup>, GFP-USP1<sup>K673T</sup> and



GFP-USP1<sup>A676T</sup> were cleaved to a similar extent as wild type GFP-USP1. However, cleavage of the GFP-USP1<sup>L669P</sup> mutant was much less efficient.

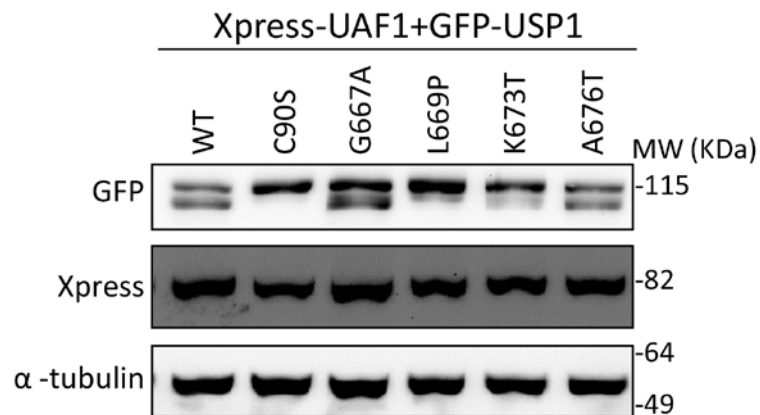


**Figure 57: Autocleavage analysis of USP1 cancer-related mutations near the autocleavage site.** Immunoblot analysis of 293T cells transfected with the indicated GFP-USP1 variants in combination with Xpress-UAF1. GFP-USP1<sup>G667A</sup>, GFP-USP1<sup>K673T</sup> and GFP-USP1<sup>A676T</sup> are cleaved as efficiently as wild type USP1, whereas GFP-USP1<sup>L669P</sup> is less efficiently cleaved.

Remarkably, the four tested mutants, including USP1<sup>L669P</sup>, were able to deplete FK2 signal (**Figure 58A**), block 53BP1 recruitment (**Figure 58B**) and decrease HU-induced PCNA ubiquitination (**Figure 58C**).

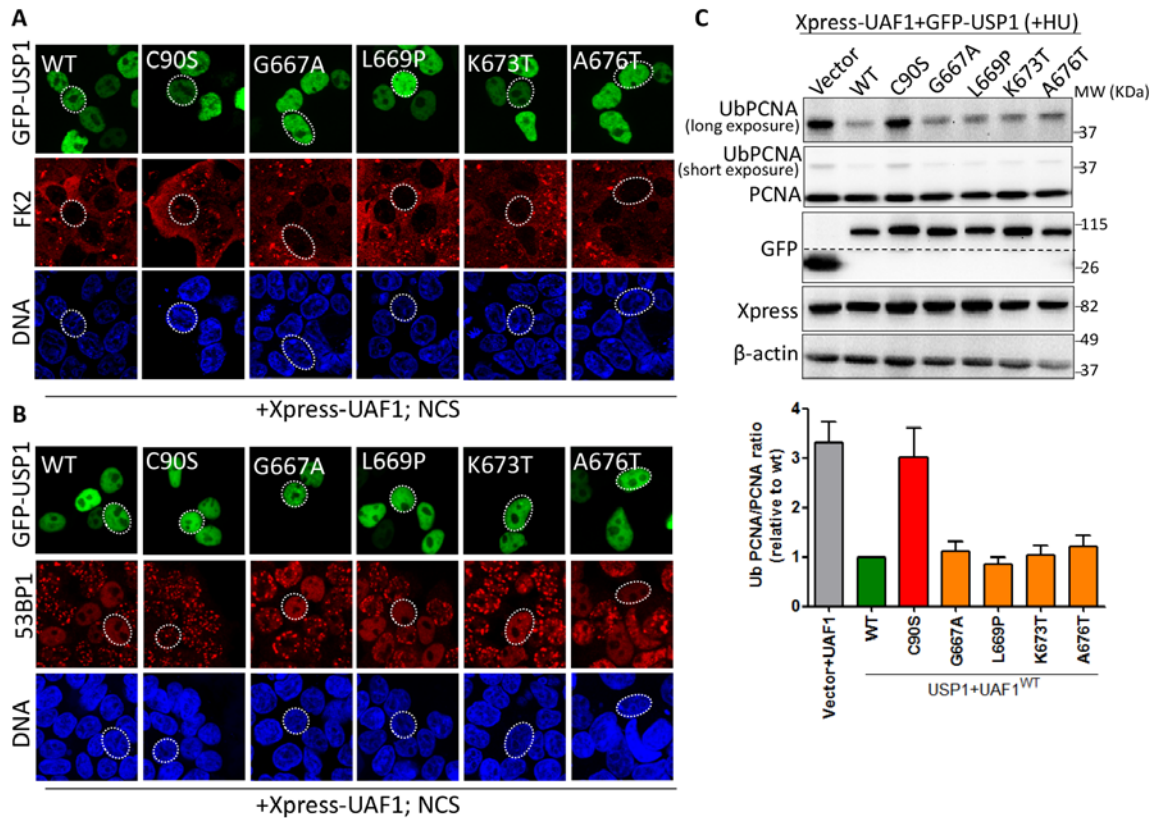


**Figure 58: Cellular activity assays to characterize the effect of USP1 cancer-related mutations near the autocleavage site. A, B.** Confocal microscopy images showing examples of FK2 and 53BP1 immunostaining in 293T cells co-transfected with the indicated expression plasmids and treated with NCS (100 ng/mL) 4 h before fixation. The nucleus of a representative cell in each sample is circled by a dotted line. All the mutants tested were able to deplete nuclear FK2 staining (A) or block 53BP1 foci recruitment (B). **C.** Immunoblot analysis of 293T cells co-transfected with the indicated expression plasmids and either left untreated (UT) or treated with 4 mM hydroxyurea for 24 h. The UbPCNA/PCNA ratio was determined by densitometry analysis of the immunoblot bands. The graph below shows the results (mean and SEM) of three independent experiments. All the mutants tested were able to deubiquitinate PCNA.

In summary, we have identified two cancer-related mutations that affect USP1 function (S475Y) or regulation by autocleavage (L669P).

#### 4.3.3. Activity of the USP1/UAF1 inhibitor ML323 in pancreatic cancer cells

Pancreatic cancer is a type of tumor with poor prognosis and limited therapeutic options (Vaccaro et al., 2011). Oxaliplatin, a platinum-based chemotherapeutic drug, is used to

---

treat pancreatic cancer patients, but resistance to this drug frequently arises (Chand et al., 2016). The USP1 inhibitor ML323 (Dexheimer et al., 2014), has been shown to reverse the resistance of non-small cell lung cancer (NSCLC) cell lines to the platinum-based drug cisplatin (Liang et al., 2014). Thus, we decided to explore the possibility that inhibiting the USP1/UAF1 complex with ML323 could increase the sensitivity of pancreatic cancer cells to oxaliplatin. Most of the experiments described in this section were carried out at the Pharmacology laboratory of VUmc (Amsterdam), under the supervision of Drs. Elisa Giovannetti and Godefridus J. Peters.

#### 4.3.3.1. Confirmation of ML323-mediated inhibition of the USP1/UAF1 in cells

ML323 has been reported to be a specific and potent inhibitor of the USP1/UAF1 complex. Although the original report (Liang et al., 2014) included some data obtained in cells, most of the validation of ML323 was done using *in vitro* biochemical assays. Thus, we decided to further evaluate the cellular effects of ML323.

First, we compared side by side the effect of ML323 with the effect of knocking down USP1 expression using small interfering RNA (siRNA) in 293T cells. We used a pool of three siRNA oligonucleotides that consistently reduces USP1 protein levels (**Figure 59A**). USP1 knockdown led to an increase in the percentage of cells having more than five FK2-positive foci in the nucleus, and a similar effect was noted in ML323-treated cells (**Figure 59B**). On the other hand, both USP1 silencing and ML323 treatment induced the recruitment of 53BP1 into nuclear foci (**Figure 59C**).

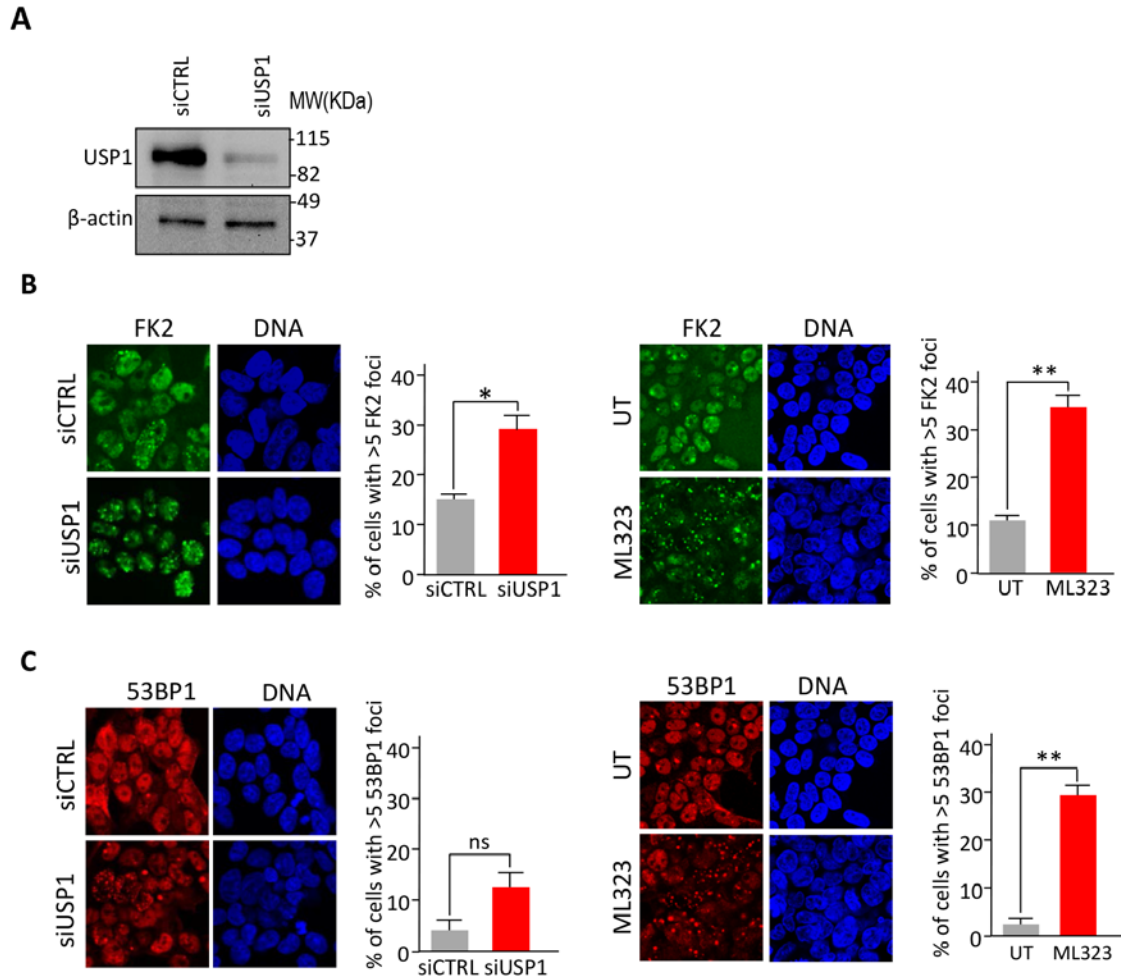


**Figure 59: Side by side comparison of the effect of ML323 with the effect of siRNA-mediated USP1 knockdown.** **A.** Efficacy of siRNA-mediated USP1 knockdown. 293T cells were transfected with a pool of three siRNAs targeting USP1 (siUSP1) or with scramble siRNA as a negative control (siCTRL). 48 h after transfection, immunoblot analysis of total protein extracts was carried out using anti-USP1 antibody. **B.** Confocal microscopy images show representative examples of FK2 immunostaining in 293T cells transfected with siCTRL or siUSP1 (left) or 293T cells untreated (UT) or treated with the USP1/UAF1 inhibitor ML323 (50 $\mu$ M) for 16h (right). The graphs represent the percentage of cells showing more than five FK2-positive nuclear foci in each condition. USP1 knockdown or ML323 treatment lead to a significant increase of FK2 foci. **C.** Confocal microscopy images show representative examples of 53BP1 immunostaining in 293T cells transfected or treated as in B. The graphs represent the percentage of cells showing more than five 53BP1-positive nuclear foci in each condition. USP1 knockdown or ML323 treatment lead to an increase of 53BP1 foci. In **A** and **B**, the graphs represent the data (mean and SEM) of four independent experiments. One hundred cells per condition were examined in each experiment. ns=non significant; \* $p < 0.05$ ; \*\* $p < 0.01$  (Student's t-test).

On the other hand, in order to gauge the potency of ML323 in a cellular context, we tested its capability to inhibit overexpressed USP1/UAF1. As shown above, co-expression of GFP-USP1 and Xpress-UAF1 depleted conjugated ubiquitin (**Figure 60A**) and blocked NCS-induced recruitment of 53BP1 into nuclear foci (**Figure 60B**). Both effects were clearly reversed by ML323, demonstrating the inhibition of overexpressed USP1/UAF1. These observations strongly suggest that the endogenous USP1/UAF1 complex would be effectively inhibited in cells treated with this compound.

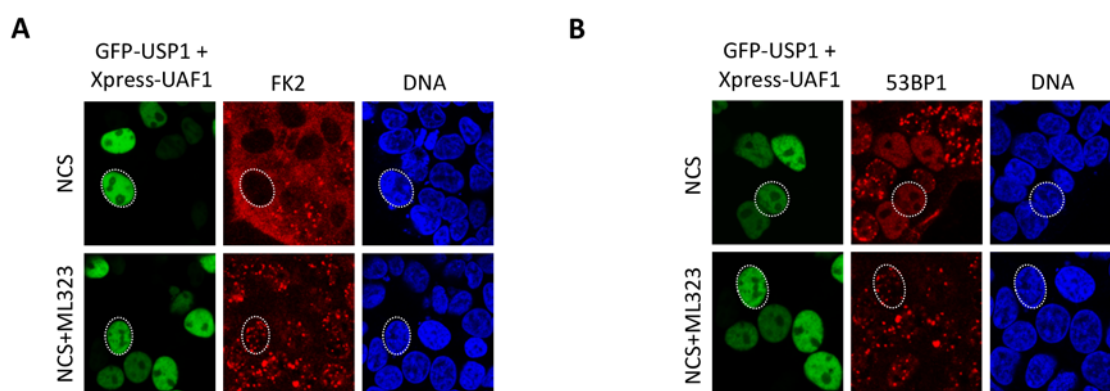


**Figure 60: ML323 reverses the effect of USP1/UAF1 overexpression on nuclear ubiquitin conjugation and 53BP1 recruitment.** Confocal microscopy images showing examples of FK2 (A) or 53BP1 (B) immunostaining in 293T cells co-expressing GFP-USP1 and Xpress-UAF1. Twenty-four hours after transfection, cells were either left untreated or pre-treated with ML323 (50  $\mu$ M) for 2 h. NCS (100 ng/mL) was subsequently added to all samples for an additional 2 h. ML323 efficiently reversed the effects of USP1/UAF1 overexpression.

#### 4.3.3.2. Expression of USP1 and UAF1 mRNA in pancreatic cancer

The levels of USP1 mRNA have been reported to be significantly altered in different types of cancer (García-Santisteban et al., 2013). We used quantitative RT-PCR (qRT-PCR) to investigate whether the levels of USP1 and UAF1 mRNA are altered in pancreatic cancer. We compared USP1 and UAF1 mRNA levels in normal pancreatic tissue (n=3) and pancreatic cancer tissue (n=5). We also measured USP1 and UAF1 mRNA in two non-transformed human pancreatic ductal epithelial cell lines (HPDE and HPNE) and in 19 pancreatic cancer cell lines. As shown in (**Figure 61A** and **B**), USP1 and UAF1 mRNA expression was higher in tumor tissues or tumor-derived cells than in normal samples. Interestingly, a strong correlation between USP1 and UAF1 expression was observed in pancreatic cancer cell lines (**Figure 61C**). Even if the number of tissue

samples analyzed here is limited, these data suggest that overexpression of the USP1/UAF1 complex may be a common event in pancreatic cancer, and thus, USP1/UAF1 inhibitors, such a ML323, might be an appropriate therapeutic option in this tumor type.

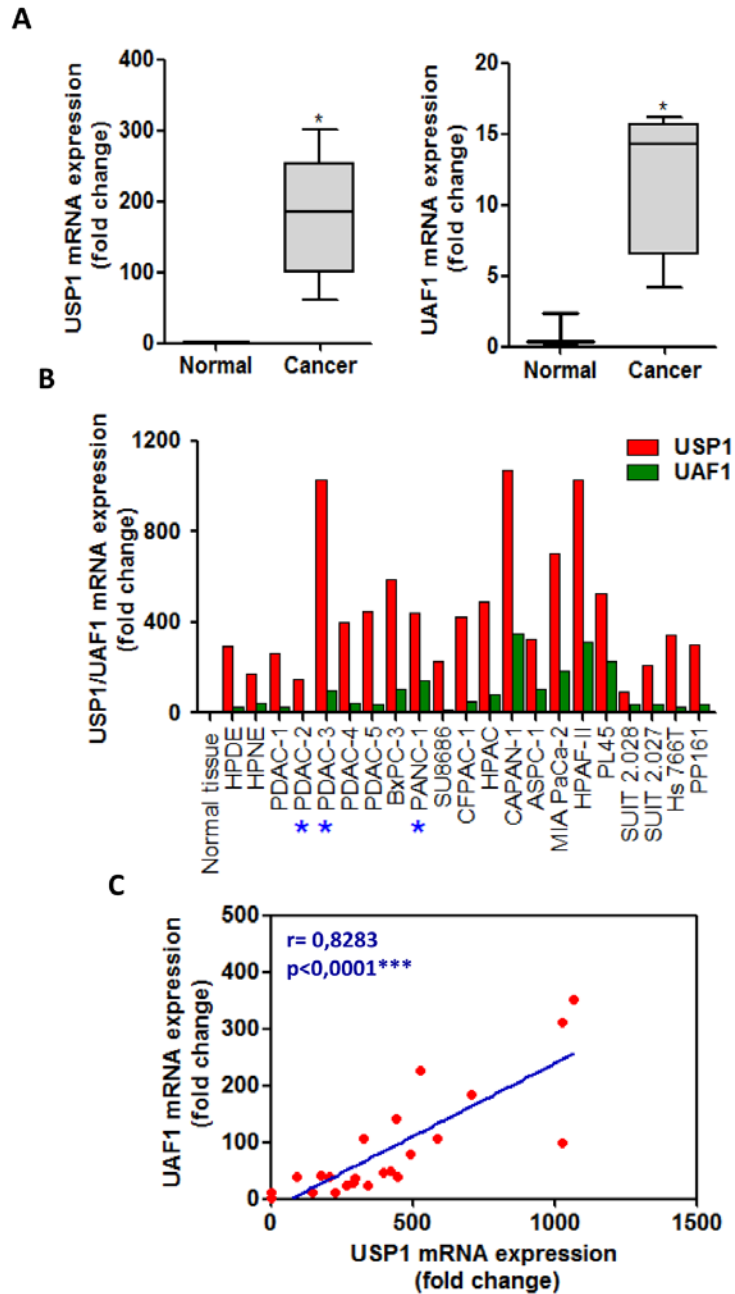


**Figure 61: USP1 and UAF1 mRNA expression is altered in pancreatic cancer. A.** Box plot graph showing the relative USP1 and UAF1 mRNA expression normalized to GAPDH in normal tissue (n=3) or pancreatic cancer tissue (n=5). Error bars indicate the SEM.\*p < 0.05.(Student’s t-test). **B.** Relative USP1 and UAF1 mRNA expression normalized to GAPDH in two non-transformed human pancreatic

ductal epithelial cell lines (HPDE and HPNE) and in 19 different pancreatic cancer cell lines compared to the average of three normal pancreas tissue samples. The relative mRNA levels were determined with the  $\Delta\Delta\text{Ct}$  method using the normal tissue value as a reference. USP1 is depicted in red and UAF1 in green. Blue asterisks indicate the cell lines selected for the following experiments **C**. Scatter-plot showing a strong co-relation between USP1 and UAF1 mRNA expression in pancreatic cancer. Pearson  $r=0.8283$  and  $***p<0.001$  (Student's t-test).

Based on the qRT-PCR results, we selected three cell lines (**Figure 61B**, blue asterisks) with different expression levels of USP1 and UAF1 mRNA: PDAC-2 (low), PANC-1 (intermediate) and PDAC-3 (high). The potential of ML323 as a therapeutic agent was evaluated in these three cell lines.

#### 4.3.3.3. ML323 acts synergistically with oxaliplatin in the pancreatic ductal adenocarcinoma PDAC-2 cell line

We first evaluated the effect of single-drug treatments with ML323 or oxaliplatin. Sulforhodamine B (SRB) assays were used to generate cell growth inhibition curves and to determine the  $\text{IC}_{50}$  (concentration of drug required for 50% cell growth inhibition) of oxaliplatin and ML323 (**Figure 62**).

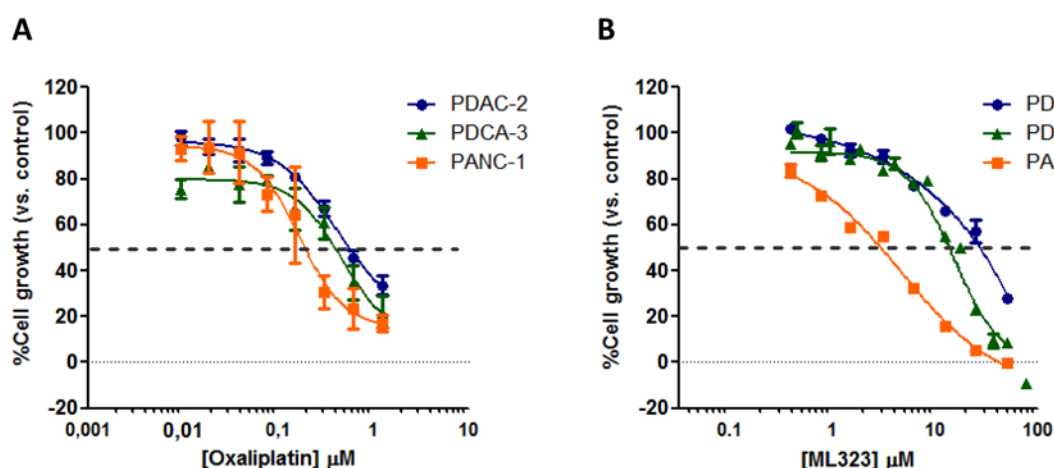


**Figure 62: Growth inhibition curves of PDAC-2, PDAC-3 and PANC-1 pancreatic cancer cell lines.** Exponentially growing cells seeded in 96 well plates were treated with different concentrations of oxaliplatin (**A**) or ML323 (**B**), and SRB assays were performed 72 hours after drug exposure. Growth inhibition curves were generated, where each point represents mean  $\pm$  SEM of at least 2 independent experiments. The dotted line represents the 50% of cell growth used to determine the  $\text{IC}_{50}$ .

**Table 9** summarizes the  $IC_{50}$  values obtained for oxaliplatin and ML323 (used as single drugs). In general terms, ML323 was less toxic than oxaliplatin, as indicated by higher  $IC_{50}$  values. In PDAC-2 cells, the  $IC_{50}$  for oxaliplatin was 0.55  $\mu$ M, and no substantial growth inhibition was observed with ML323 alone ( $IC_{50}=25$   $\mu$ M). In PDAC-3 cell, the  $IC_{50}$  values for oxaliplatin and ML323 were 0.43  $\mu$ M and 15  $\mu$ M respectively. Finally, in PANC-1 cells the  $IC_{50}$  values for oxaliplatin and ML323 were 0.17  $\mu$ M and 3.9  $\mu$ M respectively. In summary, PANC-1 cells exhibited the highest sensitivity to both oxaliplatin and ML323, whereas PDAC-2 was the most resistant cell line to these compounds.

**Table 9: Effect of the USP1/UAF1 inhibitor ML323 and the chemotherapy agent oxaliplatin as single-drugs in pancreatic cancer cell lines.** The  $IC_{50}$  value for oxaliplatin and ML323 was calculated for each cell line as described in *Figure 62*.

Cell line	Oxaliplatin ( $IC_{50}$ $\mu$ M)	ML323 ( $IC_{50}$ $\mu$ M)
PDAC-2	0.55	24.6
PDAC-3	0.43	15.16
PANC-1	0.17	3.9

Next, in order to evaluate the potential synergistic effects of the combination between oxaliplatin and ML323, SRB assays were performed in cells treated with both drugs using a fixed ratio based on the  $IC_{50}$  values of the single drugs (**Table 10**, Ratio O:M). **Figure 63** shows representative examples of growth inhibitory curves for oxaliplatin, ML323 or a combination of both drugs in each cell line. The combination  $IC_{50}$  values obtained in these experiments are presented in **Table 10** (O(+M)). In PDAC-2 cells, the  $IC_{50}$  value for oxaliplatin combined with ML323 was 0.24  $\mu$ M, substantially lower than the  $IC_{50}$  for oxaliplatin as single drug (0.55  $\mu$ M). In PDAC-3 cells, the  $IC_{50}$  value for the combination was 0.31  $\mu$ M, slightly lower than the  $IC_{50}$  for oxaliplatin as single drug (0.43  $\mu$ M). Finally, in PANC-1 cells, the  $IC_{50}$  value for the combination (0.15  $\mu$ M) was similar to the  $IC_{50}$  for oxaliplatin as single drug (0.17  $\mu$ M).



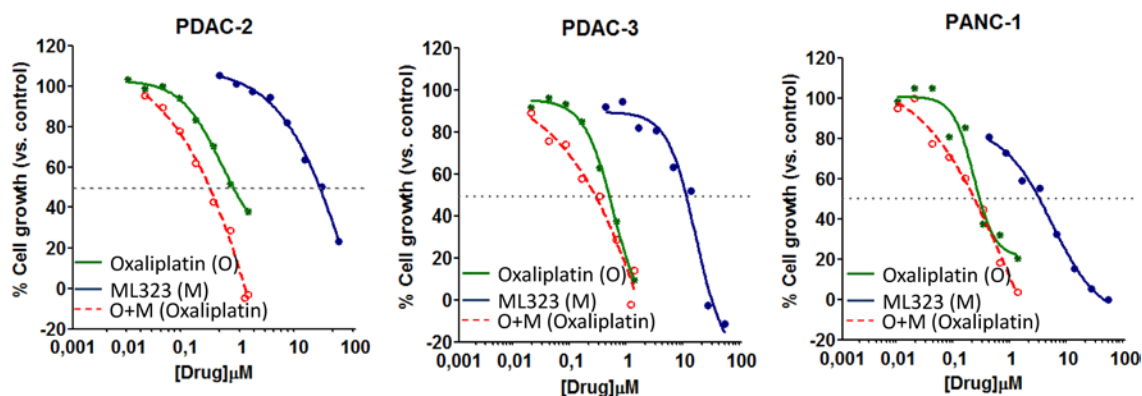


**Figure 63: Growth inhibition curves of PDAC-2, PDAC-3 and PANC-1 cell lines treated with oxaliplatin, ML323 or their simultaneous combination.** Exponentially growing cells seeded in 96 well plates were treated with oxaliplatin, ML323 or a combination of both drugs (O+M). The combination treatment was carried out using a constant oxaliplatin:ML323 ratio (see *Table 10*). After 72 hours of drug exposure, SRB assays were performed. Representative examples of the growth inhibition curves obtained in each cell line are shown. The drug concentration on the x-axis of the growth inhibition curves for the combination treatment indicates oxaliplatin concentration. The dotted line represents the 50% of cell growth used to determine the  $IC_{50}$ .

**Table 10: Effect of the combination between oxaliplatin and ML323 in pancreatic cancer cell lines.** Treatment with the two drugs in combination was carried out using a constant oxaliplatin:ML323 ratio (Ratio O:M) that was individually established for each cell line as the ratio of the  $IC_{50}$  values for each single drug. The  $IC_{50}$  values obtained in the combination treatments experiments are represented as O(+M)). At least three independent experiments per cell line were carried out.

Cell line	Oxaliplatin ( $IC_{50}$ $\mu$ M)	ML323 ( $IC_{50}$ $\mu$ M)	Ratio O:M	O(+M) ( $IC_{50}$ $\mu$ M)
PDAC-2	0.55	24.6	1:45	0.24
PDAC-3	0.43	15.16	1:35	0.31
PANC-1	0.17	3.9	1:25	0.15

To further analyse the interaction between oxaliplatin and ML323, the fraction affected ( $F_a$ ) and the combination index (CI) were calculated using CalcuSyn, and median-drug effect plots were generated (**Figure 64**).

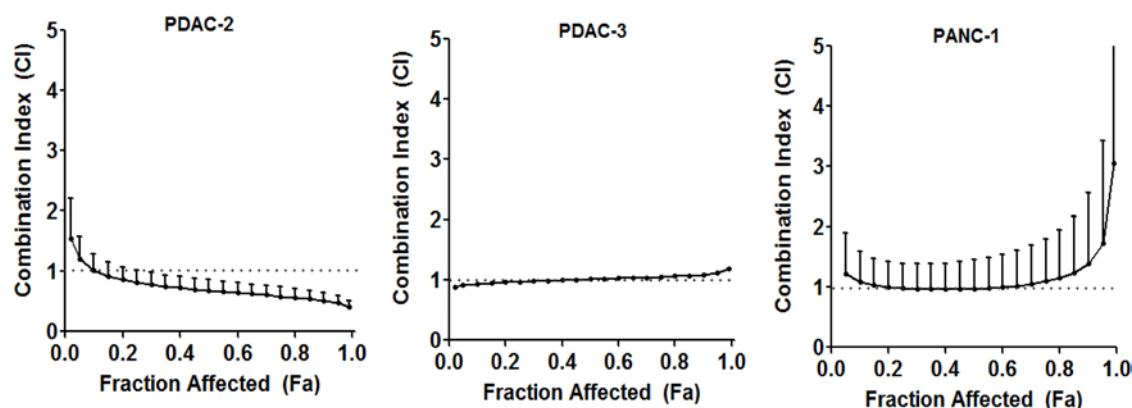


**Figure 64: Median-drug effect plots for PDAC-2, PDAC-3 and PANC-1 cell lines treated with oxaliplatin, ML323 or their combination.** Using Calcsyn, the effect of the combination of oxaliplatin and ML323 was compared to the effect of each drug to determine the combination index (CI) at a range of a Fa (Fraction-affected by the dose). The resulting CI values were plotted against the Fa to produce the median-drug effect plot for each cell line. The dashed horizontal line represents a CI=1.

Finally, CI values at Fa of 0.5, 0.75 and 0.9 were averaged for each experiment, and this value was used to calculate the mean CI between experiments (**Figure 65** and **Table 11**). A mean CI higher than 1.2 indicates an antagonistic effect of the drug combination, a mean CI value between 0.8 and 1.2 indicates an additive effect, and if the mean CI value is lower than 0.8 the effect is considered synergistic (Bijnsdorp et al., 2011) (**Table 5**). A strongly synergistic effect was observed for the combination of oxaliplatin and ML323 in PDAC-2 cell line whereas PDAC-3 presented an additive effect and PANC-1 an antagonistic effect (**Figure 65**). These findings indicate that, as previously noted in preclinical models of NSCLC, the USP1 inhibitor ML323 may synergize with platinum-based drugs, and increase the sensitivity of some pancreatic cancer-derived cells to these compounds.

**Table 11: The interaction between oxaliplatin and ML323.** The combination index (CI) value was calculated at a full range of Fa values using CalcuSyn. The final CI value for each experiment was determined as the average of the CI at Fa = 0.5, 0.75 and 0.9. At least three independent experiments per cell line were carried out, and the CI value indicated in the Table represents the mean of the final CI values of these experiments. According to the CI, the nature of the interaction between the drugs (Effect) was classified as synergistic (CI < 0.8), additive (0.8 < CI < 1.2) or antagonistic (CI > 1.2).

Cell line	Ratio O:M	O(+M) (IC <sub>50</sub> μM)	CI	Effect
PDAC-2	1:45	0.24	0.56	Synergistic
PDAC-3	1:35	0.31	1.06	Additive
PANC-1	1:25	0.15	1.27	Antagonistic

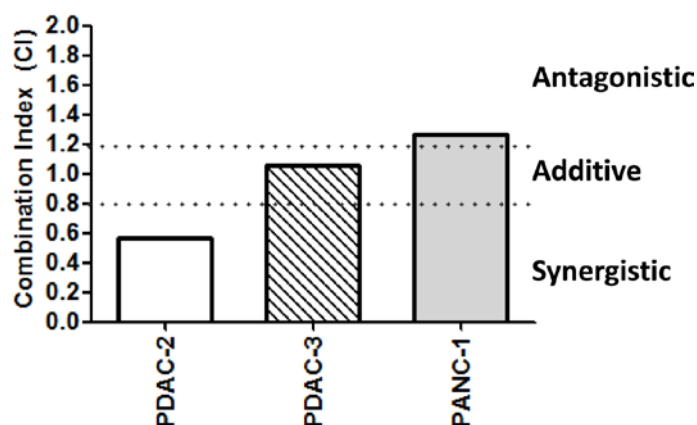


**Figure 65: Mean CI values of the oxaliplatin+ML323 combination in PDAC-2, PDAC-3 and PANC-1.** Dotted lines highlight the CI values (0.8 and 1.2) that establish the limits to identify each combination as synergistic (CI ≤ 0.8), additive (0.8 < CI < 1.2) or antagonistic (CI ≥ 1.2).

#### 4.3.3.4. Cellular changes associated to the treatment of pancreatic cancer cells with oxaliplatin and ML323

In an attempt to identify cellular changes associated to the effect of the oxaliplatin+ML323 combination, we treated PDAC-2 and PDAC-3 cells with oxaliplatin, ML323, or a combination of both drugs as indicated above. After 72h of treatment, we analysed three different cellular phenotypes that could be affected by the drugs: (i) USP1 and UAF1 mRNA levels, (ii) USP1 protein levels and (iii) formation of DNA adducts.

USP1 and UAF1 mRNA levels were analysed by qRT-PCR and normalized to the levels in the untreated (UT) control sample. The most obvious change was an increase in the mRNA levels of both USP1 and UAF1 in PDAC-2 cells treated with the oxaliplatin+ML323 combination (**Figure 66A**). Interestingly, in PDAC-3 cells only the levels of USP1 mRNA, but not UAF1 mRNA, were increased by the oxaliplatin+ML323 combination (**Figure 66B**).

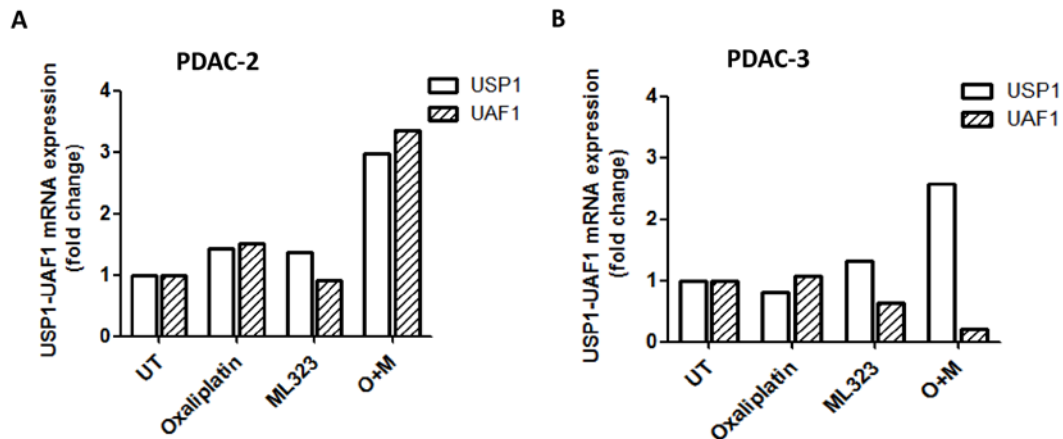


**Figure 66: Relative USP1 and UAF1 mRNA levels in PDAC-2 and PDAC-3 treated with oxaliplatin, ML323 or a combination of both drugs (O+M).** Graphs show USP1 and UAF1 mRNA expression levels in treated cells relative to untreated (UT) controls. USP1 and UAF1 levels determined with the  $\Delta\Delta C_t$  method and normalized with GAPDH.

USP1 protein levels were also analysed by immunoblot. In PDAC-2 cells (**Figure 67A**), oxaliplatin treatment increased USP1 protein. Conversely, ML323 treatment clearly decreased USP1 levels, and appeared to counteract the increase induced by oxaliplatin. In PDAC-3 cells (**Figure 67B**), oxaliplatin did not appear to increase USP1 protein levels. A decrease in USP1 was detected in cells treated with ML323 (either as single drug or in combination with oxaliplatin).

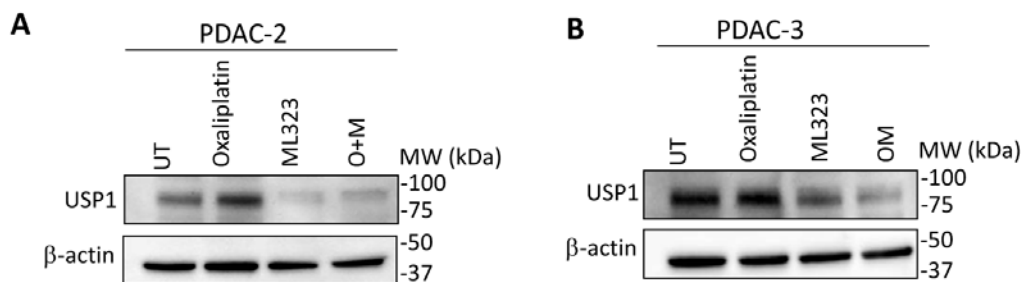


**Figure 67: Protein levels in PDAC-2 and PDAC-3 cell lines treated with oxaliplatin, ML323, a combination of both drugs (O+M).** Immunoblots showing the expression of USP1 protein and  $\beta$ -actin (loading control) in PDAC-2 and PDAC-3 upon 72 h of treatment.

Finally, we measured the formation of DNA adducts, a specific form of genetic lesions that consists on the covalent attachment of a chemical moiety to the DNA. In cells treated with platinum-based drugs, such as oxaliplatin, platinum-DNA adducts are formed, which interfere with replication and transcription, and eventually lead to cell death. Monitoring DNA adduct formation is frequently used as a method to assess the effectivity of platinum-based drugs (Stornetta et al., 2017).

The amount of adducts in a DNA sample can be estimated by using a technique based on the amplification of a long target sequence by PCR, coupled to Taqman quantification (see *section 3.5.4*). The presence of DNA adducts interferes with the PCR reaction and reduces target amplification (Laws et al., 2001). We used this technique to analyse DNA extracted from PDAC-2 and PDAC-3 cells either untreated, or treated with oxaliplatin, ML323, or a combination of both drugs.

As expected, oxaliplatin treatment consistently reduced target amplification compared to the UT sample (**Figure 68A and B**). ML323 as a single agent did not reduce target amplification indicating that this compound does not induce DNA adduct formation (**Figure 68A and B**). Cells treated with the oxaliplatin+ML323 combination had the lowest level of target amplification in PDAC-2 cell line, suggesting that the combination of oxaliplatin with ML323 induces more DNA adducts than oxaliplatin monotherapy (**Figure 68A**). In contrast, no significant differences between oxaliplatin and combination therapy were observed in PDAC-3 cell line (**Figure 68B**).

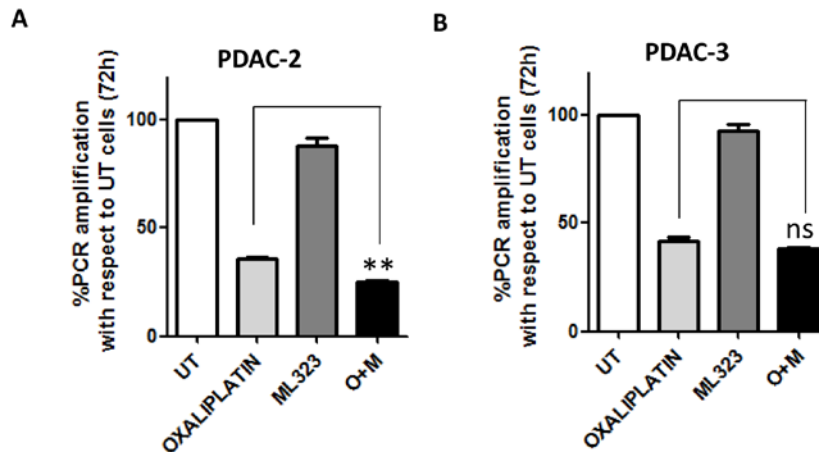


**Figure 68: Evaluation of DNA adducts by XL-PCR.** PDAC-2 (A) or PDAC-3 (B) cells were either left untreated (UT), or were treated with oxaliplatin, ML323 or a combination of both drugs (O+M) for 72h. XL-PCR was performed using primers specific for a target sequence in the  $\beta$ -globin gene. Then, TaqMan quantification of XL-PCR amplicons was performed using specific primers and probe. Graphs represent the percentage of amplification in treated samples relative to the untreated control of three different experiments (mean and SEM). ns=non significant; \* $p < 0.05$ ; \*\* $p < 0.01$  (Student's t-test).

#### 4.4. SEARCHING FOR NEW USP1 SUBSTRATES USING <sup>bio</sup>Ub

Most cellular proteins are regulated by ubiquitination and are thus likely substrates of specific DUBs. However, only around a hundred human DUBs exist (Nijman et al., 2005a). It is therefore reasonable to assume that each DUB may have a relatively wide repertoire of substrates. In the case of USP1, only a limited number of bona-fide targets (PCNA, FANCD2/FANCI and ID proteins) (Huang et al., 2006; Nijman et al., 2005b; Williams et al., 2011) have been identified. In order to gain a deeper understanding of USP1 biological function we decided to use the <sup>bio</sup>Ub system (Franco et al., 2011) to discover novel proteins that are deubiquitinated by USP1. The data presented in this section have been obtained in close collaboration with Drs. Juanma Ramírez, Ugo Mayor and Nerea Osinalde (Department of Biochemistry and Molecular Biology, UPV/EHU).

##### 4.4.1. The <sup>bio</sup>Ub system and mass spectrometry

Our strategy was to combine the <sup>bio</sup>Ub system together with USP1 silencing in 293T cells to identify proteins whose ubiquitination increases when USP1 is knocked down and thus, represent potential novel USP1 substrates (Figure 69).

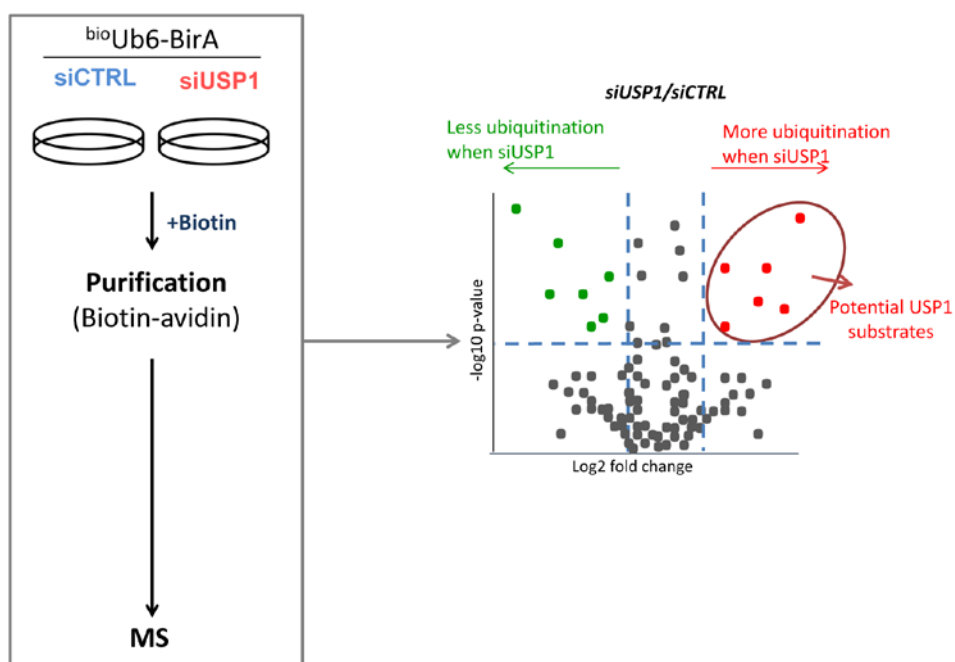


**Figure 69: Strategy for the identification of new USP1 substrates using <sup>bio</sup>Ub and MS.** The strategy was based on the combination of the <sup>bio</sup>Ub system with USP1

silencing. Biotinylated material was purified using biotin-avidin beads and analysed by MS. We used label-free-quantification (LFQ) to identify those hits that are more ubiquitinated when USP1 is silenced (circled by dark red in the volcano plot).

First, we followed the workflow illustrated in **Figure 70A** to ensure that the system worked properly in 293T cells. Using immunoblot (**Figure 70B**) and immunofluorescence (**Figure 70C**), we confirmed that the expression of  $^{bio}Ub_6$ -BirA plasmid was high enough to allow isolation of the ubiquitinated proteins in these cells for subsequent MS analysis. Importantly, USP1 was very efficiently silenced (**Figure 70B** and C). As expected, an FK2 smear was observed in all samples, suggesting that ubiquitin conjugation occurred to a similar extent in all conditions, whereas incorporation of biotinylated ubiquitin was only observed upon  $^{bio}Ub_6$ -BirA plasmid transfection (**Figure 70B**).

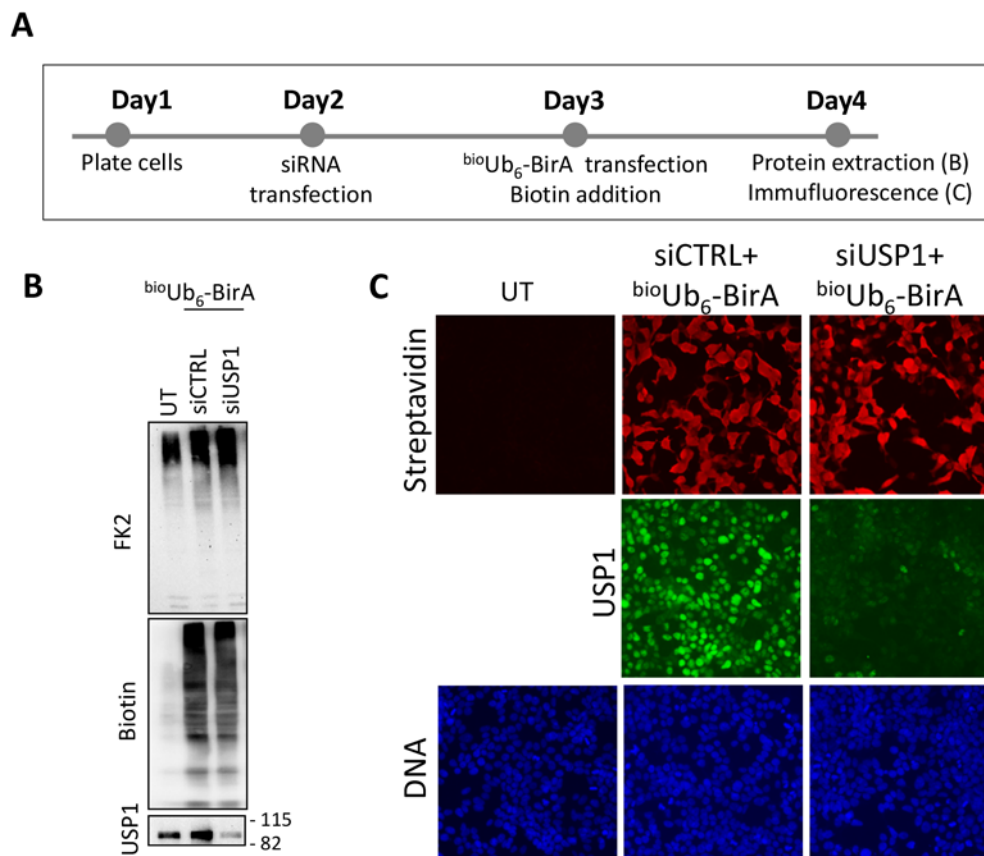


**Figure 70: Checking the efficiency of the  $^{bio}Ub$ /siUSP1 strategy in 293T cells. A. Workflow: on day 1, 293T cells were seeded. Next day, cells were left untransfected (UT) or transfected with siRNA scramble (siCTRL) or a pool of three**



siRNAs against USP1 (siUSP1). On day 3, cells were transfected with  $^{bio}Ub_6$ -BirA plasmid or left untransfected (UT) and biotin (50  $\mu$ M) was added. Finally, on day 4, cells were subjected to protein extraction (B) or immunofluorescence analysis (C). **B.** Immunoblot analysis using anti-USP1, anti-Biotin and anti-FK2 (conjugated ubiquitin) antibodies.  $^{bio}Ub$  conjugation was efficient and USP1 silencing competent. **C.** Immunofluorescence analysis using Streptavidin-AF594 (Streptavidin binds biotin) and anti-USP1 antibody.  $^{bio}Ub_6$ -BirA plasmid was highly expressed and USP1 efficiently silenced.

Once we ensured  $^{bio}Ub$  conjugation was efficient and USP1 silencing competent, we set up a larger-scale experiment, with three biological replicates, to carry out the purification of  $^{bio}Ub$ -tagged proteins following the workflow summarized in **Figure 71**. 293T plated in 15 cm dishes were transfected with pCAG-BirA together with siCTRL as a negative control or pCAG- $^{bio}Ub_6$ -BirA plasmid together with siCTRL or siUSP1, respectively. The pCAG-BirA negative control corresponds to the control plasmid expressing only BirA enzyme in order to ensure that protein biotinylation is not induced. Biotin was added to the culture medium. Cells were collected 24 hours after plasmid transfection.

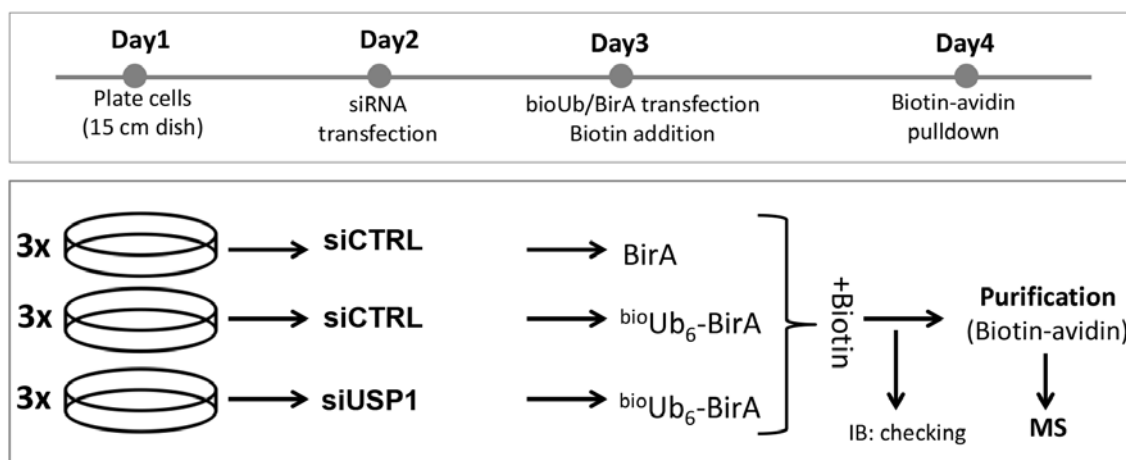


**Figure 71: The  $^{bio}Ub$ /siUSP1 experiment: from cells to biotin-avidin purification.**

*Workflow:* 293T cells were seeded in 15 cm dishes. Next day, cells were transfected with either siRNA scramble (siCTRL) or a pool of three siRNAs against USP1 (siUSP1). The third day cells were transfected with negative control BirA plasmid or  $^{bio}Ub_6$ -BirA plasmid and biotin (50  $\mu$ M) was added. Last day cells were collected. A small aliquot was used to check  $^{bio}Ub$  conjugation and USP1 silencing by immunoblot (IB) and the rest subjected to biotin-avidin purification and subsequent mass spectrometry (MS) analysis.

Immunoblot analysis demonstrated efficient protein biotinylation and USP1 silencing in the three replicates (**Figure 72**).

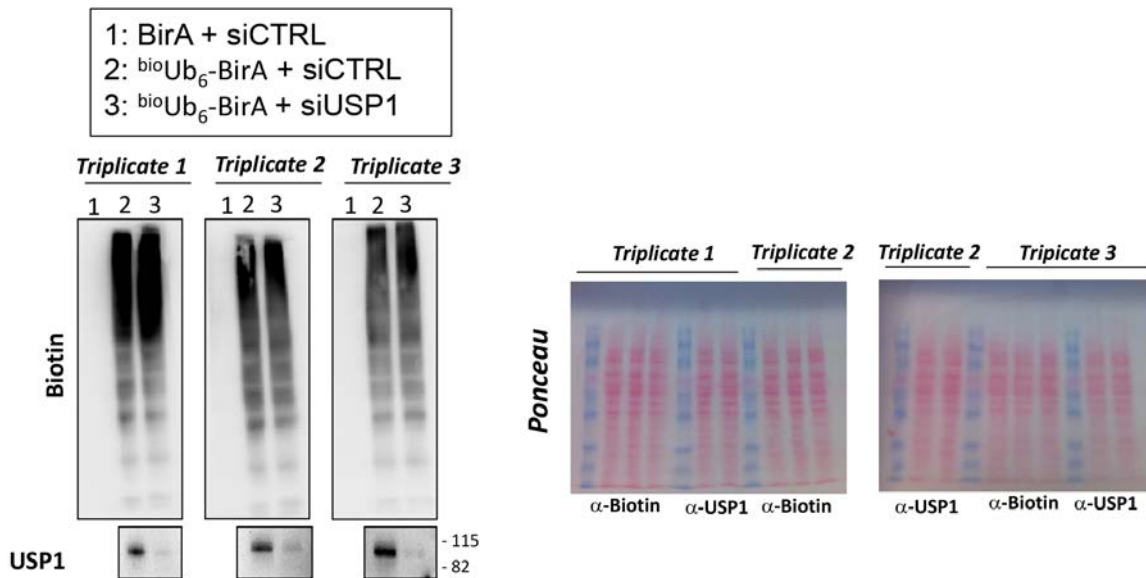


**Figure 72: Monitoring <sup>bio</sup>Ub conjugation and USP1 silencing in cells to be subjected to pulldown.** Immunoblot analysis with anti-biotin and anti-USP1 antibodies showing efficient conjugation of <sup>bio</sup>Ub and efficient silencing of USP1 in the three triplicate samples that were subsequently subjected to biotin pulldown. The membranes were stained with ponceau to check protein loading.

The remaining cells were processed under denaturing conditions, and subjected to biotin pulldown with NeutrAvidin agarose beads as described in *section 3.7.2*, in order to purify the ubiquitinated material. Analysis of the purified material by silver staining (**Figure 73, left**), and by anti-biotin immunoblot (**Figure 73, right**) indicated that the purification worked successfully.

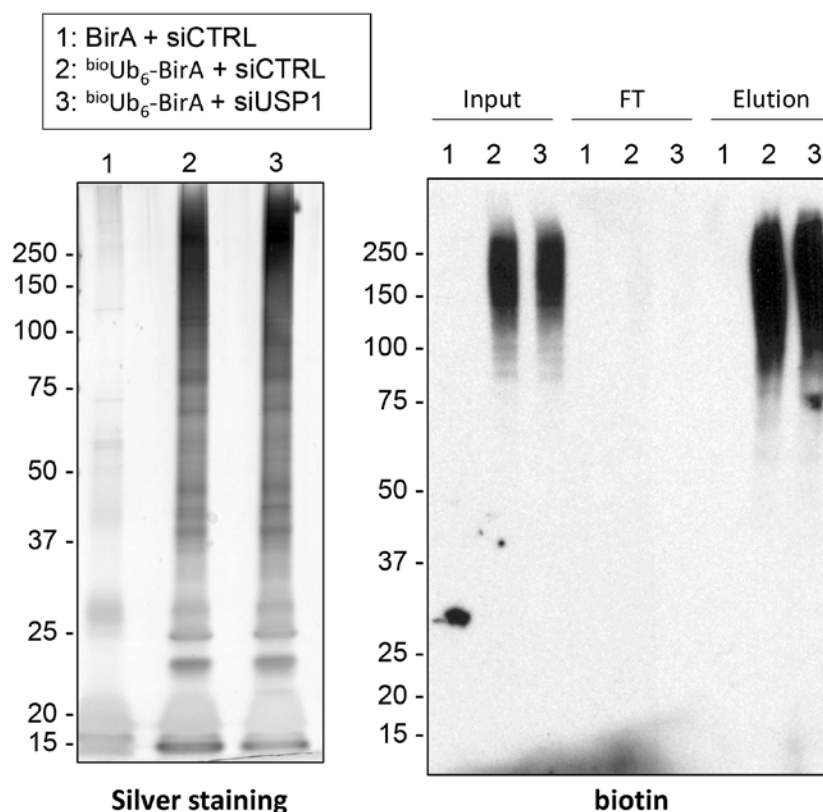


**Figure 73: Purification of biotinylated material.** Left panel: Representative silver staining of the purified material from one of the triplicates. Equal amounts of BirA and <sup>bio</sup>Ub<sub>6</sub>-BirA samples were analysed by SDS-PAGE, and stained with silver. Common bands between samples are expected to be composed mainly of endogenously biotinylated material, while the thick bands at around 40 kDa and below correspond to trimer, dimer and monomer forms of NeutrAvidin. The main high molecular weight smear observed in the experimental (<sup>bio</sup>Ub<sub>6</sub>-BirA) but not in the control (BirA) samples corresponds to the isolated ubiquitinated material. Right panel: Representative anti-biotin immunoblot. 1:60 dilution of the input and flow-through (FT) and 1:300 dilution of the elution, as indicated, were loaded.

Finally, the proteins eluted from the biotin-avidin pulldown were identified by using liquid chromatography-tandem mass spectrometry (LC-MS/MS) analysis. Proteins known to be common contaminants (Keller et al., 2008), reverse hits and proteins with no unique peptides or intensity were removed. Altogether, 1410 different proteins were identified in the <sup>bio</sup>Ub<sub>6</sub>-BirA+siCTRL (hereafter called siCTRL for the sake of simplicity) samples, and 1404 different proteins were identified in the <sup>bio</sup>Ub<sub>6</sub>-BirA+siUSP1 (hereafter siUSP1) samples. In total, 1449 different proteins were identified, and 1365 of those (95%) were present in both conditions (**Figure 74**). In principle, all these proteins have been modified by conjugation of biotinylated ubiquitin.

Our next goal was to estimate the relative abundance of these proteins in the siCTRL and the siUSP1 samples, to identify those that may be differentially ubiquitinated in the absence of USP1.

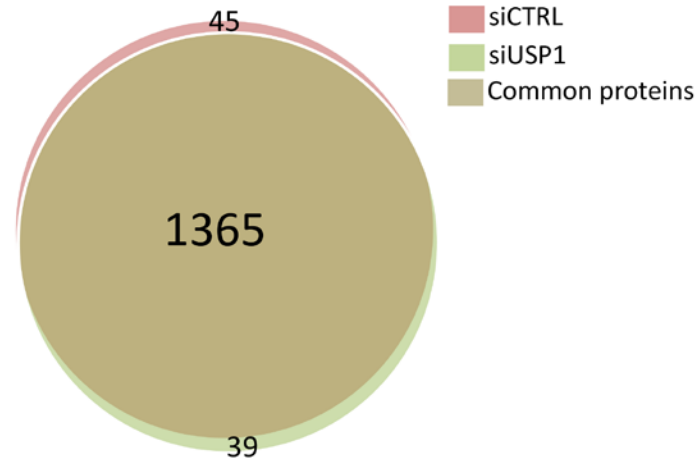


**Figure 74: Venn diagram indicating the overlap between the proteins identified in siCTRL and siUSP1 samples.** About 95 % of all the proteins identified were found in both samples (brown).

To this end, we used the Label Free Quantification (LFQ) method (Wong and Cagney, 2010). After confirming that each sample followed a normal distribution and that the correlation between samples was high, the siUSP1/siCTRL LFQ ratio (siUSP1(1+2+3 replicates)/siCTRL(1+2+3 replicates)) was calculated using the MaxLFQ algorithm. Of note only those proteins identified in two or three biological replicates of at least one of the conditions were included in the LFQ analysis.

Proteins whose siUSP1/siCTRL ratio was higher than 2, with a p-value (two-sided t-test) lower than 0.05, were considered to be significantly more ubiquitinated in the absence of USP1 (**Figure 75**). Reassuringly, the known USP1 substrate PCNA was identified as one of the proteins whose ubiquitination is significantly higher in the siUSP1 condition.

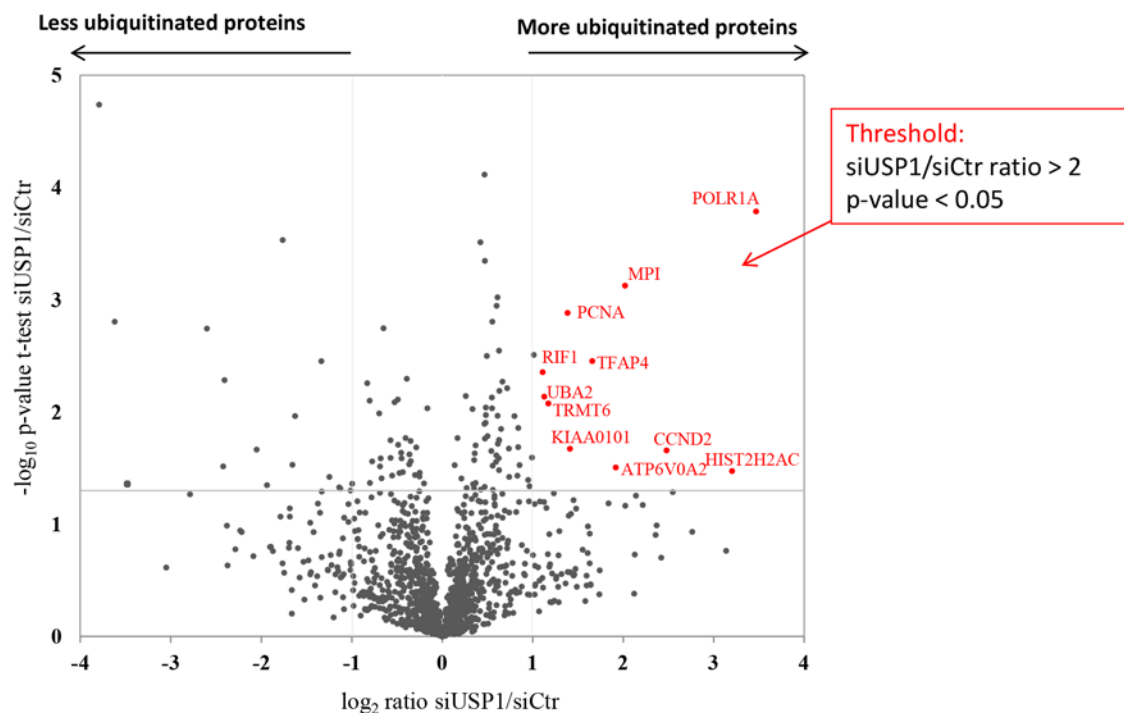


**Figure 75: Volcano plot showing the proteins that appeared differentially ubiquitinated upon USP1 silencing.** Proteins are ranked in a volcano plot. On the y axis, statistical p-value ( $-\log_{10}$  p-value siUSP1/siCTRL Lfq intensity ratio). On the x axis, siUSP1/siCTRL ratio ( $\log_2$  Lfq ratio siUSP1/siCTRL). Those proteins with a Lfq ratio higher than 2 (1 in  $\log_2$  scale) and p-value less than 0.05 (1.30 in  $-\log_{10}$  scale) were considered to be more ubiquitinated when USP1 is silenced (indicated in red).

In addition to PCNA, 10 proteins whose ubiquitination increases upon USP1 silencing were identified (Table 12). The list of potential novel USP1 substrates includes proteins involved in DNA repair (KIAA0101, RIF1), DNA transcription (POLR1A, TFAP4, HIST2H2AC), cell cycle regulation (CCND2, RIF1), Metabolism (MPI), ATP-related functions (ATP6V0A2), tRNA processing (TRMT6) and SUMOylation (UBA2).

**Table 12: List of potential USP1 substrates.** Gene names, Uniprot entry, the number of peptides including unique peptides identified for each protein, the siUSP1/siCTRL ratio and significance p-values are shown.

Gene names	Uniprot ID	Peptides (unique)	siUSP1/siCTRL	
			ratio	p-value
<b>POLR1A</b>	O95602	2(2)	11,06	1,64E-04
<b>CCND2</b>	P30279-2	1(1)	5,58	2,00E-02
<b>MPI</b>	P34949-2	1(1)	4,06	7,41E-04
<b>TFAP4</b>	Q01664	1(1)	3,16	3,55E-04
<b>HIST2H2AC</b>	Q16777	5(1)	9,22	3,30E-01
<b>ATP6V0A2</b>	Q9Y487	3(3)	3,78	2,80E-02
<b>KIAA0101</b>	Q15004-2	3(3)	2,66	2,10E-02
<b>PCNA</b>	P12004	10(10)	2,61	1,30E-03
<b>TRMT6</b>	Q9UJA5	2(2)	2,25	8,32E-03
<b>UBA2</b>	Q9UBT2	5(5)	2,19	7,24E-03
<b>RIF1</b>	Q5UIP0-2	6(6)	2,16	4,46E-03

#### 4.4.2. Validation of MS-detected potential novel USP1 substrates by immunoblot

Our next goal was to begin the validation of the potential novel USP1 substrates identified by MS. This validation can be carried out by direct immunoblot analysis using specific antibodies for the candidates.

We searched the published bibliography on the candidates, and decided to start with the DNA-repair related proteins RIF1 and KIAA0101. RIF1 plays a crucial role in the choice between DSB repair by NHEJ or HR (Daley and Sung, 2013). On the other hand, KIAA0101, known as PAF15 (PCNA-Associated Factor) is a small protein that interacts with PCNA and plays a key role in the exchange from DNA replicative polymerase to translesion synthesis polymerase in TLS (Xie et al., 2014)d. Thus, from a biological point of view, these two proteins seemed like interesting candidates to begin the validation.

We tested three commercially available anti RIF1 antibodies, but were unable to obtain consistent results.

A commercially available anti-PAF15 antibody reproducibly identified a single clear band in immunoblots, although with an apparent molecular weight slightly higher than the predicted for PAF15. We decide to use this antibody to confirm that an ubiquitinated

form of PAF15 protein accumulates upon USP1 silencing. As shown in **Figure 76**, a single band of similar intensity was detected with anti-PAF15 antibody in the three input samples. After biotin-streptavidin pull-down, no bands were observed in the BirA+siCTRL or the  $^{bio}Ub_6$ -BirA+siCTRL samples. In contrast, a single band (arrow) was detected in the  $^{bio}Ub_6$ -BirA+siUSP1 sample. This band migrated with an apparent molecular weight approximately 30 kD higher than the band in the input samples. Attachment of one ubiquitin molecule increases a protein molecular weight in about ~10 kDa, suggesting that more than one ubiquitin moieties have been attached in this case.

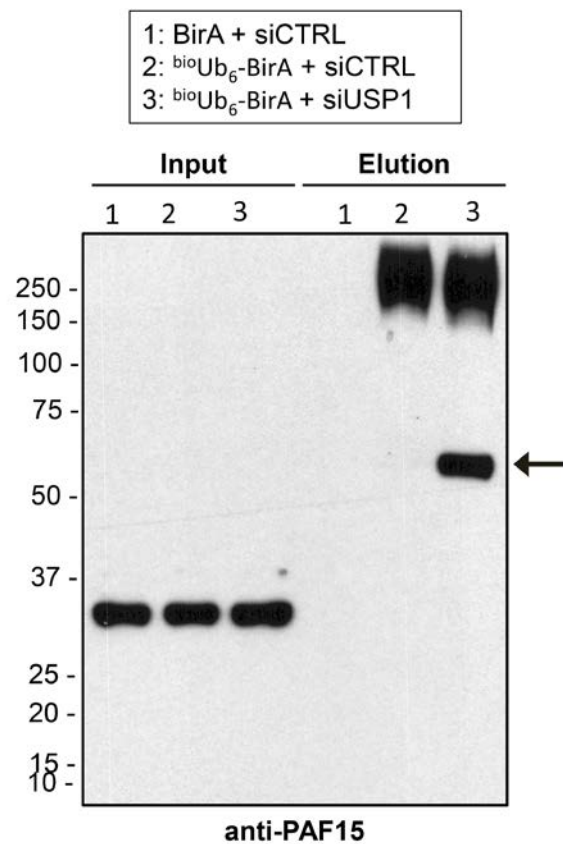


**Figure 76: Immunoblot validation of using anti-PAF15 antibody.** A single band of similar intensity is detected in input samples. In the elution of the  $^{bio}Ub$  pulldown, a higher molecular weight band is observed, only in the siUSP1 sample, indicating that the ubiquitination of the detected protein is increased after USP1 silencing. The difference in size with respect to the “input” band suggests conjugation of 3 ubiquitin moieties.

In summary, using  $^{bio}Ub$  strategy followed by MS analysis, 10 novel potential USP1 substrates have been identified, including the DNA damage-related proteins RIF1 and

PAF15. Although further experimental validation and analysis are required, our findings suggest potential novel roles of USP1 in the regulation of the DNA damage response.



#### 4.5. SEARCHING FOR MOLECULAR MECHANISMS THAT MAY UNDERLIE THE FUNCTIONAL DIFFERENCES BETWEEN USP12 AND USP46

Human deubiquitinases USP12 and USP46 are very similar proteins. As shown in **Figure 77**, the amino acid sequence identity between these proteins is 88%. The most prominent difference is the presence of 4 additional residues (MEIL) in the N-terminal of USP12 that are absent in USP46. Interestingly, USP12 and USP46 have been reported to share some cellular activities, but also to carry out unrelated functions. As a potential mechanism that might underlie the functional differences between these two DUBs, we hypothesized that USP12 and USP46 could display differences in binding to their cofactors or other proteins. In this section, we used subcellular relocation assays to characterize the interaction of these DUBs with their cofactors UAF1 and WDR20, as well as with DMWD, a poorly characterized interactor of these DUBs.



**Figure 77: USP12 and USP46 alignment using CLUSTAL-OMEGA.** USP12 and USP46 are almost equal in sequence with exception of 4 amino acids in the N-terminal of USP12 that are not present in USP46 (red square). Letters are colored according to the physicochemical properties of the represented residue. An “\*”

(asterisk) indicates fully conserved residues. A “:” (colon) indicates residues with strongly similar properties . A “.” (period) indicates residues with weakly similar properties as below.

#### **4.5.1. Analysis of USP12 and USP46 binding to UAF1 and WDR20 using relocation assays**

Whereas UAF1 binding appears to be sufficient to activate USP1 (Cohn et al., 2007, 2009), full enzymatic activation of USP12 and USP46 requires binding to both UAF1 and WDR20 (Dahlberg and Juo, 2014; Kee et al., 2010).

As shown in our previous work (Garcia-Santisteban et al., 2012; Olazabal-Herrero et al., 2015) and in *section 4.2.*, the nuclear relocation assay has proven to be a convenient and reliable approach to characterize the interaction of USP1, USP12 and USP46 with UAF1. Therefore, we decided to use a similar approach to characterize the interaction of USP12 and USP46 with WDR20. First, we confirmed that WDR20, like UAF1, is a cytoplasmic protein (**Figure 78A**). As previously detailed, unlike GFP-USP1, YFP-tagged USP12 and USP46 were located in the cytoplasm. Therefore, a NLS was fused to the N-terminal of the DUBs to force their entry into the nucleus and test their ability to relocate their cofactors (**Figure 78B**). 293T cells were co-transfected with GFP-USP1, YFP-[NLS]-USP12 or YFP-[NLS]-USP46 together with either UAF1-mRFP or Myc-tagged WDR20. As shown above (*section 4.2.3.*), GFP-USP1, YFP-[NLS]-USP46 and YFP-[NLS]-USP12 relocated UAF1 to the nucleus to a similar extent, suggesting that the three DUBs interact in a comparable manner with this cofactor (**Figure 78C**). On the other hand, GFP-USP1 did not induce relocation of Myc-WDR20, consistent with previous reports that these two proteins do not interact (Kee et al., 2010). Strikingly, the localization of YFP-[NLS]-USP12 and Myc-WDR20 drastically changed when these two proteins were co-expressed. As shown in **Figure 78D**, both proteins fully translocated to the plasma membrane where they co-localized. In marked contrast, a very limited relocalization of YFP-[NLS]-USP46 and Myc-WDR20 to the plasma membrane was noted. In fact, YFP-[NLS]-USP46 remained largely nuclear whereas Myc-WDR20 remained predominantly cytoplasmic in co-transfected cells. These observations, which have been confirmed in HeLa cells (not shown), suggest that WDR20 binds more strongly to USP12 than to USP46.

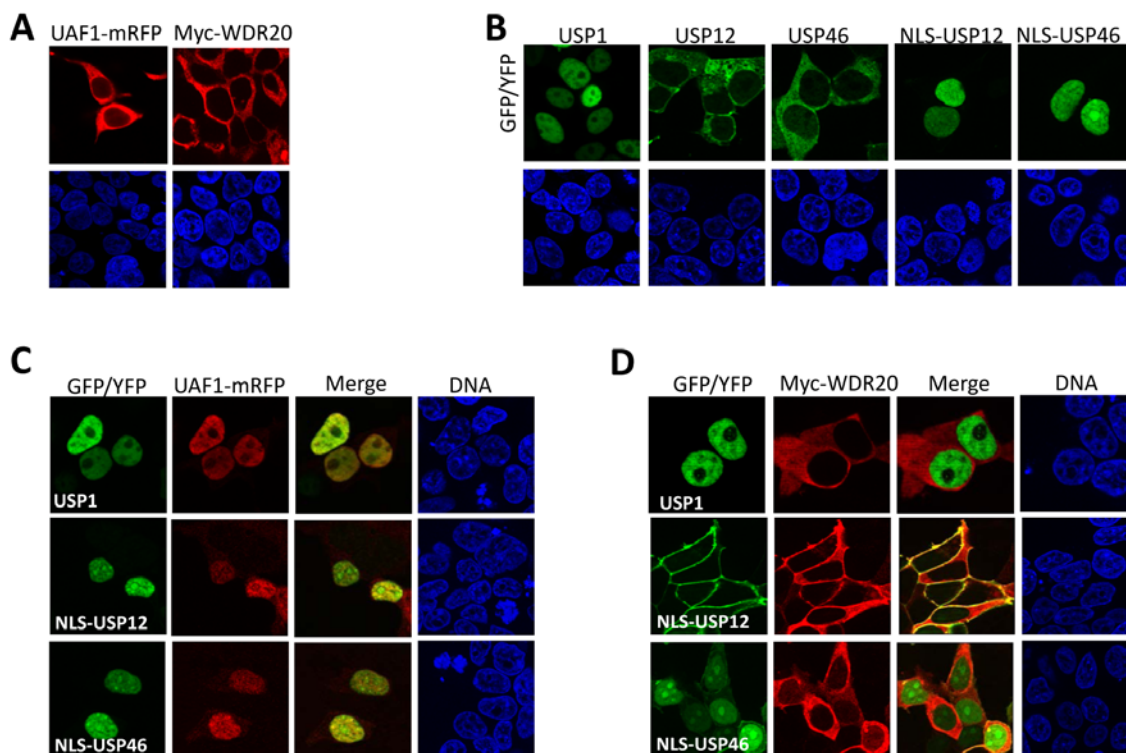


**Figure 78: Relocation assay to evaluate the interaction of USP1, USP12 and USP46 with the cofactors UAF1 and WDR20.** **A.** 293T cells co-transfected with UAF1-mRFP and Myc-WDR20, showing cytoplasmic localization of both proteins. **B.** 293T cells co-transfected with GFP-USP1, YFP-USP12, YFP-USP46, YFP-[NLS]-USP12 and YFP-[NLS]-USP46. **C and D.** Relocation assay in 293T cells co-transfected with UAF1-mRFP or Myc-WDR20 together with USP1 or NLS-fused USP12 and USP46.

#### 4.5.2. Analysis of the binding of DMWD, a WDR20 paralog, to USP12 and USP46

In 2009, Sowa and co-workers published the first global DUB interactome analysis by using a large-scale proteomic approach (Sowa et al., 2009). In this analysis, they reported thousands of DUB-binding proteins, including several interactors of USP12 and USP46. One of the USP12 or USP46 interactors reported by Sowa et al, a protein termed DMWD (dystrophia myotonica WD-repeat containing protein) called our attention, because we noted that this protein has a high sequence similarity (53% of identity) with WDR20 (Figure 79).



---

characterized by progressive muscle weakness (Ranum and Day, 2004). In the global proteomics analysis by Sowa et al., DMWD appeared as bound to USP12, USP46 and UAF1. These interactions, however, have not been validated in direct assays.

We decided to use the relocation assay to validate and characterize the binding of DMWD to USP12, USP46 and UAF1. First, we assessed the localization of Myc-tagged DMWD in 293T cells, and found it to be cytoplasmic (**Figure 80A**, left). As above, we used YFP-[NLS]-USP12 and YFP-[NLS]-USP46 to test their ability to relocate Myc-DMWD. As a negative control, we included USP1, which was not reported to interact with DMWD (Kee et al., 2010; Sowa et al., 2009). In addition, we generated a nuclear version of DMWD, termed YFP-[NLS]-DMWD (**Figure 80A**, right), in order to test its interaction with UAF1. Then, we co-expressed Myc-DMWD or YFP-[NLS]-DMWD with GFP-USP1, YFP-[NLS]-USP12, YFP-[NLS]-USP46 or Xpress-UAF1. As shown in **Figure 80B**, no apparent relocation of the proteins was noted in cells co-expressing Myc-DMWD with GFP-USP1 or YFP-[NLS]-USP46 neither in cells co-expressing YFP-[NLS]-DMWD with Xpress-UAF1. In contrast, a partial relocation of YFP-[NLS]-USP12 to the plasma membrane was observed when co-expressed with Myc-DMWD. Of note, this relocation was less pronounced than the one induced by Myc-WDR20.

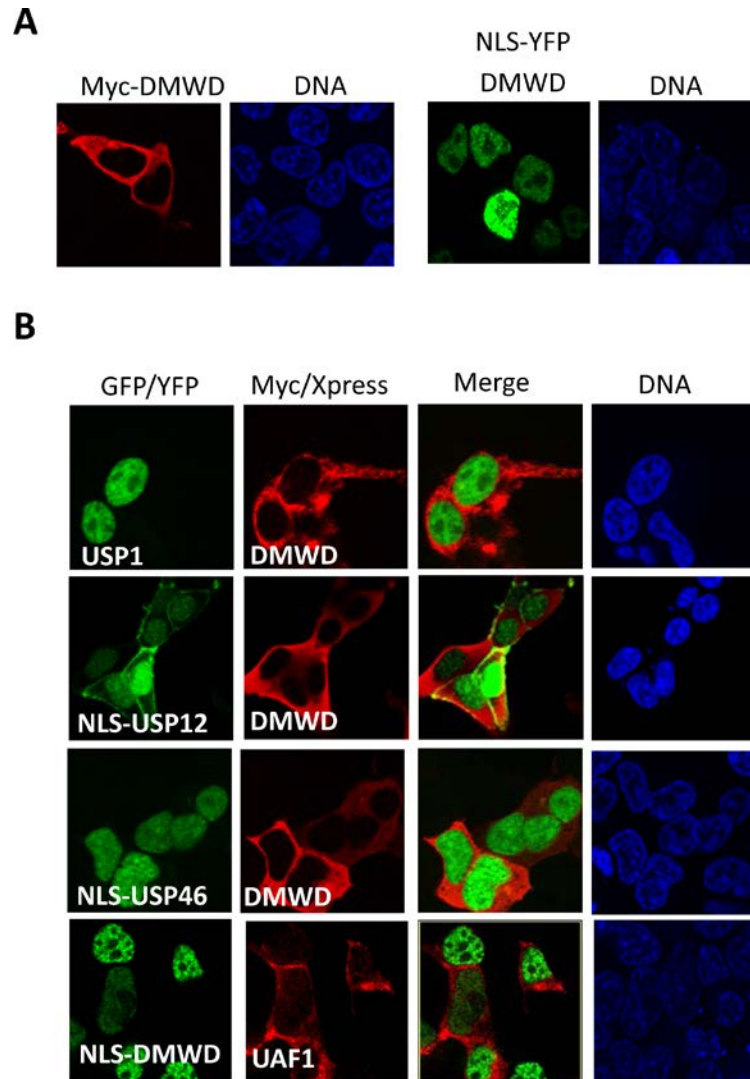


**Figure 80: Relocation assay to evaluate the interaction of USP1, USP12, USP46 and UAF1 with DMWD.** **A.** Confocal images of 293T cells expressing Myc-DMWD or YFP-[NLS]-DMWD. **B.** Confocal images of 293T cells expressing Myc-DMWD or YFP-[NLS]-DMWD together with YFP/GFP tagged USP1, NLS-USP12 and NLS-USP46 or Xpress-UAF1.

These results, therefore, validate the interaction between USP12 and DMWD previously reported by proteomics. However, we could not confirm the interaction of DMWD with USP46 or UAF1.

In summary, our findings unveil previously unknown differences in the binding of USP12 and USP46 to their cofactor WDR20 and to DMWD.

---

### 4.5.3. The amino terminal motif “MEIL” in USP12 contributes to binding to WDR20 and DMWD

We hypothesized that the different binding of USP12 and USP46 to WDR20 and DMWD could be related to differences in their amino acid sequence. The most evident difference is a 4 amino acid motif (MEIL) present in the extreme amino-terminal end of USP12, but absent in USP46 (**Figure 77**). We generated a version of YFP-[NLS]-USP12 lacking this short motif, termed YFP-[NLS]-USP12<sup>delMEIL</sup>. 293T cells were transfected with Myc-WDR20 together with YFP-[NLS]-USP12 or YFP-[NLS]-USP12<sup>delMEIL</sup>. As shown in **Figure 81A**, the USP12 mutant lacking the MEIL motif remained mostly in the nucleus when co-expressed with WDR20, suggesting that deletion of the MEIL motif virtually abrogated USP12/WDR20 interaction. Similar results were observed regarding the USP12/DMWD interaction (**Figure 81B**).

These observations suggest that the 4 amino acid motif MEIL at the amino-terminal end of USP12 significantly contributes to its interaction with WDR20 and DMWD, thus explaining why USP46, which lacks this motif, has a weaker or undetectable interaction with these proteins.

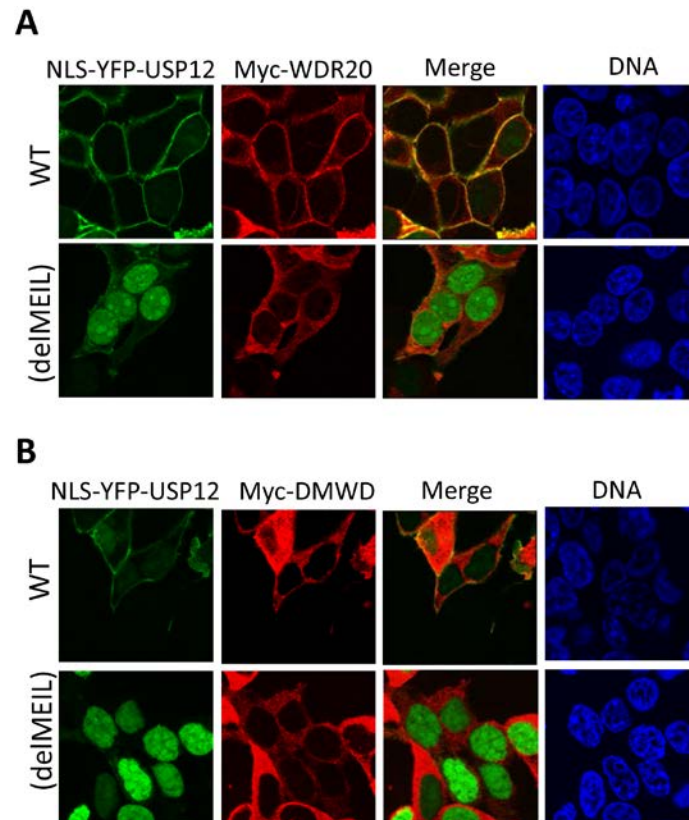


**Figure 81: The MEIL motif in the N-terminal of USP12 contributes to the interaction of USP12 with DMWD and WDR20.** Confocal images of 293T cells co-transfected with NLS-fused USP12 wild type or the mutant version lacking the N-terminus YFP-[NLS]-USP12<sup>deMEIL</sup> and Myc-WDR20 (A) or Myc-DMWD (B). Deletion of the MEIL motif drastically reduces the ability of USP12 to relocate to the plasma membrane when co-expressed with WDR20 or DWMD.



# Discussion

5



## 5. Discussion

Since the discovery of ubiquitin in 1975 (Goldstein et al., 1975), the field of protein ubiquitination has developed into a very active area of research. Over the last decades, most attention has been devoted to the enzymes that mediate the attachment of the ubiquitin to the target substrates, particularly to E3 ligases. More recently, the enzymes that reverse ubiquitination, the DUBs, have also attracted considerable research interest. It has been found that DUBs participate in essential cellular processes, and alterations in DUB function have been linked to various human diseases, including cancer (Fraile et al., 2012). However, our understanding of the function and regulation of DUBs lies behind that of E3 ligases.

The human genome encodes approximately 100 DUBs (Nijman et al., 2005a). In this Thesis, we have studied three human DUBs (USP1, USP12 and USP46) that share a common regulatory mechanism: its enzymatic activity requires binding to the cofactor UAF1 (Cohn et al., 2007, 2009).

Most of the work described here relates to USP1, which is emerging as a potential therapeutic target in cancer. First, focusing on the regulation of this DUB by phosphorylation, autocleavage and binding to UAF1, we clarify standing controversies and deepen into the details of these mechanisms. We also describe how cancer-related mutations in USP1 may affect its regulation and cellular activity. Next, we examine the effect of a novel USP1/UAF1 inhibitor, ML323, in cellular models of pancreatic cancer. Finally, we apply a novel approach, termed <sup>bio</sup>Ub, followed by quantitative proteomics and identify potential novel targets of USP1.

Regarding USP12 and USP46, two DUBs with a very high sequence similarity but some disparate functions, we identify a potential molecular basis for the observed functional differences between these enzymes.

## 5.1. DEEPENING INTO USP1 REGULATION: SERINE 313 PHOSPHORYLATION, AUTOCLEAVAGE AND UAF1-INTERACTION

Phosphorylation at Serine 313 (Cotto-Rios et al., 2011b; Villamil et al., 2012b), autocleavage at the G670/G671 diglycine motif (Huang et al., 2006) and interaction with UAF1 (Cohn et al., 2007) are critical events regulating USP1 function, but several aspects of these regulatory mechanisms are still controversial or remain to be elucidated.

Phosphorylation of USP1 at residue S313 regulates USP1 stability (Cotto-Rios et al., 2011b). It has also been reported to be necessary for UAF1 binding and activity in an *in vitro* experimental setting (Villamil et al., 2012b). In contrast to these *in vitro* data, our data using several cellular assays clearly indicate that phosphorylation of USP1 at S313 is not essential for UAF1 binding or activity. We have demonstrated interaction of a non-phosphorylatable mutant USP1<sup>S313A</sup> with UAF1 using a nuclear relocation assays in live and fixed cells, as well as with co-IP. Our findings have been later independently confirmed by another group (Yin et al., 2015). The experimental approach we used, with ectopically expressed proteins, has certainly limitations, but is, in our opinion, closer to a physiological setting than *in vitro* assays with purified recombinant proteins. Therefore, we conclude that S313 phosphorylation of USP1 is not required for UAF1 binding.

Importantly, USP1<sup>S313A</sup> forms a functional complex with UAF1 in transfected cells. This is shown by the clearly increased levels and autocleavage of the USP1<sup>S313A</sup> protein when co-expressed with UAF1, which indicate stabilization and catalytic activation of the mutant DUB. Furthermore the USP1<sup>S313A</sup>/UAF1 complex is able to reverse monoubiquitination of endogenous PCNA. It must be stressed that our data do not rule out the possibility that S313 phosphorylation plays a (non-essential) role regulating USP1 activity. In fact, we noted that a phosphomimetic mutant USP1<sup>S313D</sup> showed a slightly increased ability to reverse PCNA ubiquitination.

Autocleavage at the G670/G671 diglycine motif was originally reported to be induced by UV light (Huang et al., 2006). However, we noted that USP1 autocleavage is also

readily detected in untreated cells co-transfected with GFP-USP1 and Xpress-UAF1, probably as a result of the high levels of expression of the USP1/UAF1 complex. This observation provides a convenient experimental system to gain further mechanistic insight into this important regulatory mechanism. Our results, using a combination of USP1 mutants, suggest that USP1 autocleavage occurs intramolecularly (in *cis*) (**Figure 82**). The three-dimensional structure of the USP1/UAF1 complex has not yet been solved and, since the autocleavage site lies within a non-conserved inserted domain (Ye et al., 2009), it is impossible to model this area of USP1 using other USPs as template. Nevertheless, based on our findings, we predict that the diglycine motif of a USP1 molecule can reach its own catalytic site to undergo cleavage.

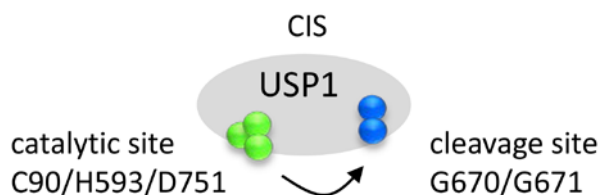


**Figure 82: Model representing the *cis* mode of autocleavage in USP1.**

The most important controversy at the beginning of this Thesis concerned the identity of the UAF1 binding motif in USP1. Using cell-based assays our group had initially mapped the UAF1-binding site to USP1(420-520) (Garcia-Santisteban et al., 2012). Later, Villamil et al, using *in vitro* assays with purified recombinant proteins, mapped the UAF1 binding site to USP1(235-408) (Villamil et al., 2012b), a region located within a non-conserved inserted domain (Ye et al., 2009) and containing the S313 phosphorylation site.

To address this controversy, we decided to compare side-to-side both potential UAF1 binding sites. The results of this direct comparison further support our initial findings that the critical UAF1 binding site is USP1 420-520 amino acid motif. The reasons for the discrepancy between the data obtained *in vitro* and in cell-based assays are not clear. Since USP1 NLSs (Garcia-Santisteban et al., 2012) overlap with the S313 phosphorylation site, we tested the possibility of competition between nuclear import receptors and UAF1 for binding to this region, but this does not appear to be the case.

It is important to note that the UAF1 binding region reported by Villamil et al. is not conserved in USP12 and USP46. In contrast, the 420-520 region is well conserved in the three UAF1-regulated DUBs. In fact, we demonstrate that the UAF1-binding motif of USP46 lies within the 165–259 fragment, a segment homologous to USP1(420-520). *In silico* modeling showed that USP1(420–520) and USP46(165–259) motifs lie within the “Fingers” subdomain of the DUBs. These data represented the first published report identifying the “Fingers” subdomains as the UAF1-binding site (Olazabal-Herrero et al., 2015), and have been subsequently validated by the three dimensional structures of USP12/UAF1 and USP46/UAF1 complexes (Dharadhar et al., 2016; Li et al., 2016; Yin et al., 2015).

## **5.2. FINE-MAPPING THE USP1/UAF1 INTERACTION**

In the context of the potential use of USP1 as a therapeutic target, it must be noted that, besides inhibiting its enzymatic activity with USP1 inhibitors, an alternative approach might involve interfering with the formation of USP1/UAF1 complex. To this end, knowing the molecular details of the USP1/UAF1 interaction is critical. Optimally, these details would be revealed by solving the three-dimensional structure of the USP1/UAF1 complex. However, this appears to be a challenging task that remains to be accomplished. As an alternative, we undertook a detailed mapping of the sequences involved in the USP1/UAF1 interaction.

We started this mapping effort before any structural information on the DUB/UAF1 complexes was available. Thus, we relied on two criteria to predict USP1 residues that might be important for UAF1 binding. On one hand, we reasoned that the critical residues would be conserved in USP12 and USP46, but not in other DUBs. On the other hand, since the front side of the “Fingers” subdomain of USPs usually engages in ubiquitin binding, we hypothesized that the critical residue(s) for binding to UAF1 would most likely be located at the back of USP1 “Fingers”. Using these criteria, we selected and mutated four amino acids R439, L441, L446, S494. Disappointingly, we found that a quadruple mutant (USP1<sup>4m</sup>) with mutations in these residues was still able to bind UAF1.

When our paper with these data was under review, Yin et al published the structure of the USP46/UAF1 complex (Yin et al., 2015). Making use of this structural information,

these authors identified a group of 4 residues on the tips of the “Fingers” (what they called the ERLE motif) that are important for UAF1 interaction in USP1, USP12 and USP46 (Yin et al., 2015). In the case of USP1, the ERLE motif is formed by E444, R439, L441 and E516. In our view, it is remarkable that, even without having the support of structural information, the changes we had decided to introduce into our USP1<sup>4m</sup> mutant included two residues in the ERLE motif (R439 and L441). Unfortunately we did not mutate E444, which turned out to be the most critical USP1 amino acid for UAF1 interaction (Yin et al., 2015).

Yin et al also identified three amino acid residues in the  $\beta$ -propeller domain of UAF1 (K214/W256/R272) that are important for interaction with the DUBs (Yin et al., 2015). Building on these data, we found that a single point mutation in UAF1 (K214E) is enough to disrupt the interaction with the three DUBs.

In summary, the data described in this Thesis (using cell-based assays) and data from other groups (using mostly *in vitro* assays) identify USP1 E444 and UAF1 K214 as critical residues for the USP1/UAF1 interaction. These findings provide information that may guide future attempts to disrupt the USP1/UAF1 complex as a therapeutic strategy.

Disruption of the USP/UAF1 complex is expected to abrogate USP1 activity. We decided to test this assumption, which is mostly based on *in vitro* data (Yin et al., 2015), using our cellular assays. As expected USP1<sup>E444K</sup> and UAF1<sup>K214E</sup> mutations abrogate autocleavage. Also as expected, USP1<sup>E444K</sup> was unable to decrease UbPCNA levels. However, co-expression of USP1<sup>WT</sup> with UAF1<sup>K214E</sup> led us to make an unexpected observation: UbPCNA levels were consistently reduced in these cells. This was puzzling because overexpressed USP1<sup>WT</sup> is expected to be “free” (co-expressed UAF1<sup>K214E</sup> cannot bind to USP1 and endogenous UAF1 molecules would be unable to bind all overexpressed USP1 molecules), and thus catalytically inactive. This observation suggested that “free” USP1 was still capable of counteracting PCNA ubiquitination in a manner that would not require its catalytic activity. This was subsequently confirmed by showing that UbPCNA levels are reduced in cells expressing USP1<sup>WT</sup> alone, as well as in cells expressing the catalytically inactive mutant USP1<sup>C90S</sup> alone.

As a possible explanation for these findings, we propose the model shown in **Figure 83**. In this model, when USP1<sup>WT</sup> and UAF1 are co-expressed in cells, they form USP1/UAF1 complexes that deubiquitinate PCNA. When USP1<sup>C90S</sup> and UAF1 are co-expressed they form catalytically inactive complexes that do not deubiquitinate PCNA **Figure 83A**. When either USP1<sup>WT</sup> or USP1<sup>C90S</sup> are expressed alone, they will be free and may prevent PCNA ubiquitination (rather than inducing its deubiquitination,) by a mechanism that does not require USP1 enzymatic activity. This mechanism requires the DUB to be “free” from UAF1, and might involve binding/sequestering a yet unknown protein (X) required for PCNA ubiquitination **Figure 83B**. Of note, this mechanism seems to be hampered in the case of the USP1<sup>E444K</sup> mutant, as cells overexpressing this mutant showed high levels of UbPCNA. If our model is correct, the E444K mutation, besides disrupting binding to UAF1, also disrupts binding to the “X” protein.

In normal cellular conditions, every USP1 molecule is thought to be in complex with UAF1 (Cohn et al., 2007) and thus, the physiological relevance of our observation is still unclear. However, it must be noted that other DUBs, such as yeast Ubp6 (an homolog of human USP14) have also been reported to present a “non-catalytic” effect (Hanna et al., 2006).

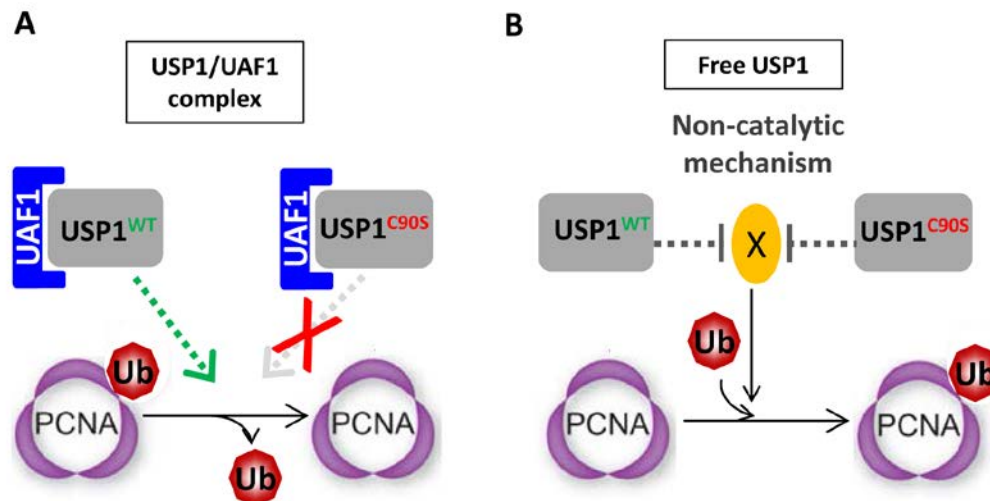


**Figure 83: A proposed model for the “non-catalytic” effect of USP1 in the regulation of PCNA ubiquitination.** In cells expressing a catalytically active USP1/UAF1 complex, UbPCNA undergoes deubiquitination. In cells overexpressing free USP1 (even the catalytically inactive C90S mutant), a “non-catalytic” mechanism counteracts PCNA ubiquitination.



---

### 5.3. FUNCTIONAL CONSEQUENCES OF CANCER-RELATED USP1 MUTATIONS

Around a hundred cancer-associated USP1 mutations are included in the *COSMIC* database. Some of these changes are non-sense or frameshift mutations that would most likely result in a non-functional allele, but most USP1 mutations lead to single amino acid substitutions whose effect is still unknown. Some of these missense mutations are located in/near the “Fingers” subdomain of USP1 (S475Y, D502N, and S575R), and several others are located in close proximity to USP1 autocleavage site (G667A, L669P, K673T and A676T).

We used a panel of cell-based assays to test the functional consequences of these cancer-related USP1 mutations. We evaluated their ability to bind UAF1, to undergo autocleavage and to decrease UbPCNA levels. In addition, prompted by the observation of the potential “non-catalytic” effect of USP1 on PCNA ubiquitination, we decided to search for novel functional readouts. We examined two well-characterized DNA damage-related phenomena: the recruitment of ubiquitinated proteins (Messick and Greenberg, 2009), and of 53BP1 (Huyen et al., 2004) into nuclear foci after cell treatment with the DSB-inducing agent NCS.

We found that USP1/UAF1 overexpression resulted in a striking depletion of conjugated ubiquitin from the nucleus, as determined by FK2 immunostaining. Such a general ubiquitin deconjugation was not observed in the nuclei of cells expressing other DUBs, such as USP3 or USP22, but was noted (although to a lesser extent) in cells expressing high levels of USP7. Of note, USP1/UAF1 and USP7 have been reported to have higher enzymatic activity than other USPs in biochemical analyses with artificial substrates (Cohn et al., 2007; Faesen et al., 2011; Villamil et al., 2012a). Our data suggest that this higher *in vitro* enzymatic activity translates into higher promiscuity of these USPs when they are ectopically expressed in cells. Importantly, such promiscuity limits the usefulness of USP1/UAF1 overexpression experiments to explore the role of the complex in specific cellular pathways and to identify its physiological substrates. More generally, although the number of DUBs compared in our study is certainly limited, our findings suggest that potential promiscuity should be taken into account when the results of DUB overexpression screens are interpreted.

On the other hand, we also found that USP1/UAF1 overexpression completely blocked the recruitment of 53BP1 into NCS-induced foci. A similar effect has been reported by overexpression of other DUBs, such as USP3 (Sharma et al., 2014). Admittedly, it is not possible to establish to what extent general ubiquitin deconjugation by USP1/UAF1 contributes to the observed blockade of 53BP1 recruitment. Thus, we cannot claim that the USP1/UAF1 complex plays a physiological role in regulating 53BP1 recruitment.

Regardless of their physiological relevance, the general ubiquitin deconjugation and the blockade of 53BP1 recruitment by USP1/UAF1 represent two novel clear-cut readouts expanding the battery of tests that can be used to investigate the phenotypical consequences of USP1 mutations. Using this battery of tests, we have identified two cancer-related mutations that affect USP1 function (S475Y) or regulation by autocleavage (L669P).

Cancer-related missense mutations that result in decrease deubiquitination activity have been identified in other DUBs, including USP7 (Huether et al., 2014). However, to the best of our knowledge, the S475Y substitution was the first cancer-related loss-of-function missense mutation identified in USP1 (Olazabal-Herrero et al., 2016). Interestingly, the S475Y mutation abrogates substrate deubiquitination without impairing UAF1 binding or autocleavage. In our view, a plausible explanation for this finding would be that this mutation interferes with the binding of the ubiquitin moiety in substrates to the complex. Thus, substrate deubiquitination would be impaired, but autocleavage would be preserved.

On the other hand, the L669P mutation severely reduces USP1 cleavage efficiency. This mutation is adjacent to the diglycine autocleavage motif. We hypothesize that this mutation might introduce a conformational change that hampers access of the cleavage site to the catalytic site. Importantly, USP1<sup>L669P</sup> is able to interact with UAF1 and clearly retains its ability to deubiquitinate substrates. This further demonstrates that autocleavage is not required for substrate deubiquitination, as already shown by the analysis of the experimental mutant USP1<sup>GG/AA</sup> (Huang et al., 2006, and our data not shown). It is tempting to speculate that, by disrupting the normal balance of USP1 cleavage, this L699P mutation may contribute to tumorigenesis, and further experiments should address this possibility.

---

## 5.4. EFFECT OF THE USP1 INHIBITOR ML323 IN PANCREATIC CANCER CELLS

The USP1/UAF1 complex is emerging as a potential therapeutic target in cancer (García-Santisteban et al., 2013). A major challenge in cancer therapy results from the development of drug resistance in tumor cells. Resistance may arise if cancer cells acquire an increased ability to repair or tolerate the DNA lesions induced by chemotherapeutic drugs, such as cisplatin or oxaliplatin, (Martin et al., 2008). It has been recently reported that the USP1 inhibitor ML323 (Dexheimer et al., 2014) may reverse cisplatin resistance in NSCLC cells (Liang et al., 2014). Here, we tested its effect in cellular models of pancreatic cancer.

Most of the validation of ML323 as an specific and potent inhibitor of the USP1/UAF1 complex has been done using *in vitro* assays (Liang et al., 2014). To further test the specificity of ML323, we compared the effect of the drug with siRNA-mediated USP1 knockdown. Both siUSP1 and ML323 treatment increased the number of 53BP1 and FK2-positive foci. We noted that ML323 treatment resulted in a more pronounced increase in the number of FK2 or 53BP1 foci than USP1 knockdown. This observation might indicate that the drug has additional effects besides inhibiting USP1/UAF1, but it might as well simply reflect a more complete blockade of USP1/UAF1 function by ML323. Additionally, we demonstrate that ML323 has the potency to inhibit overexpressed USP1/UAF1. Altogether, the results of these preliminary tests made us confident that the endogenous USP1/UAF1 complex would be competently inhibited in cells treated with ML323.

The effect of inhibiting USP1 has only been tested in NSCLC cells. We have further extended this analysis to pancreatic cancer, a cancer type with very poor prognosis and limited therapeutic alternatives.

Supporting the view that USP1 inhibition could represent a valid strategy in pancreatic cancer treatment, we found that USP1/UAF1 mRNA is commonly overexpressed in pancreatic cancer. Large scale analyses using microarray and RNAseq have shown that the mRNA levels of USP1 (García-Santisteban et al., 2013) and UAF1 (<https://www.oncomine.org/resource/login.html>) are frequently increased in different cancer types. Consistent with these observations, our qRT-PCR data in a limited

number of clinical samples as well as in a relatively large panel of pancreatic cancer derived cell lines indicate that overexpression of USP1 and UAF1 mRNA is also a common feature in this tumor type. Of note, expression of USP1 and UAF1 mRNA was higher in HPDE and HPNE non-transformed pancreatic cells than in normal pancreatic tissue (although lower than in most cancer-derived cell lines). This suggests that USP1/UAF1 mRNA levels may also increase during the establishment of cell cultures.

Interestingly, we found a strong correlation between the expression of USP1 and UAF1 in pancreatic cancer cell lines. The “non-catalytic” effect of free USP1 on PCNA ubiquitination described above raised the possibility that overexpression of the DUB alone might have phenotypical consequences. Nevertheless, these findings would suggest that overexpression of a catalytically active USP1/UAF1 complex (requiring co-overexpression of the DUB and its cofactor) might confer additional selective advantage for tumor development.

Three pancreatic cancer cell lines with different levels of USP1/UAF1 mRNA (PDAC-2 (low), PANC-1 (intermediate) and PDAC-3 (high)). were selected to analyze the effect of oxaliplatin and ML323 as single agents or in combination.

Our data suggest that higher levels of USP1 and UAF1 mRNA do not predict a more beneficial effect of ML323, as it might be expected. Rather, our results suggest that the effect of the oxaliplatin/ML323 combination is related to the degree of resistance to oxaliplatin as single agent. Thus, the oxaliplatin/ML323 combination had a synergistic effect in the cell line showing the highest resistance to oxaliplatin (PDAC-2), but an antagonistic effect in the most oxaliplatin-sensitive cell line (PANC-1). PDAC-3 cell line showed an additive drug interaction. A similar correlation was previously observed in a broad panel of NSCLC cell lines treated with the combination of cisplatin (another platinum-based drug) and pimozone (another USP1 inhibitor) (García-Santisteban et al., 2013).

In an attempt to elucidate some cellular factors that might determine the effect of the oxaliplatin/ML323 combination, we examined the levels of USP1/UAF1, as well as the presence of DNA adducts.

---

USP1 mRNA levels have been reported to change (decreasing after 4 h and increasing after 16 h) in cisplatin-treated NSCLC cells (Sourisseau et al., 2016). In contrast, we found no significant change in the levels of USP1 or UAF1 mRNA after 72 h treatment with oxaliplatin or ML323 as single agents. The oxaliplatin/ML323 combination increased USP1 levels in both cell lines, as well as UAF1 mRNA levels in PDAC-2 cells line. USP1 protein levels were increased by oxaliplatin treatment in PDAC-2 cell line, but not in PDAC-3. Interestingly, ML323 treatment (either as single drug or in combination with oxaliplatin) clearly decreased USP1 protein levels in both cell lines. In our view, the most firm conclusion that can be drawn from these results is that ML323, besides inhibiting USP1 activity, also decreases USP1 protein levels. Other USP1 inhibitors (SJB2-043 and pimozone), had been previously reported to decrease USP1 protein levels through proteasomal-mediated degradation (Mistry et al., 2013), but this effect had not been yet described for ML323.

On the other hand, we found that the synergistic effect of the oxaliplatin/ML323 combination observed in PDAC-2 cells correlates with a significant increase in the number of DNA adducts with respect to the oxaliplatin monotherapy. The relevance of this correlation needs to be further investigated using a larger panel of cell lines. Nevertheless, our findings are in line with previous data showing that synergistic effects of platinum-based drugs in combination with different agents are mainly dependent on an increase in platinum adduct formation (Avan et al., 2013; Xu et al., 2003). These findings in PDAC-2 cell line are illustrated in **Figure 84**.

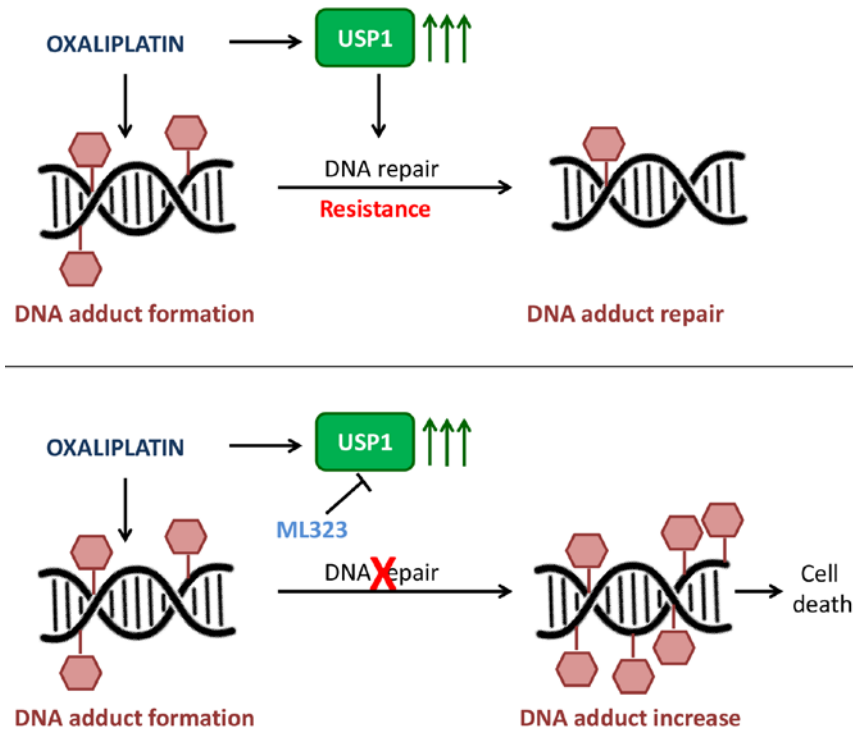


**Figure 84: The model proposed for explaining the synergistic effect observed in PDAC-2 cell line.**

In conclusion, although the number of cell lines analyzed is limited, our findings suggest that USP1 inhibition might contribute to reverse oxaliplatin resistance in pancreatic cancer by increasing the formation of platinum-DNA adducts.

## 5.5. NOVEL USP1 SUBSTRATES RELATED TO DNA DAMAGE

Given that only a few number of well-characterized USP1 substrates have been identified to date, we decided to search for novel targets. We used a recently-established system termed <sup>bio</sup>Ub (Franco et al., 2011) to pull down endogenous ubiquitinated proteins, followed by mass spectrometry. We combined this system with siRNA-mediated USP1 knockdown, and applied label-free quantification (LFQ) to identify endogenous proteins that are differentially ubiquitinated in USP1-silenced cells. Reassuringly, the known USP1 substrate PCNA turned out as one of the endogenous proteins showing increased ubiquitination after USP1 knockdown. Besides PCNA, we identified 10 novel potential USP1 substrates. We decided to begin the validation of these candidates, by focusing on RIF-1 and PAF15. These two proteins were

---

particularly interesting in our opinion because, like USP1, they have DNA damage-related functions (Daley and Sung, 2013; Xie et al., 2014).

Unfortunately, we have not yet been able to unambiguously validate these candidates due to technical difficulties with commercially available antibodies. On one hand, three different anti-RIF-1 antibodies did not provide convincing results in immunoblot analysis and no further validation of this protein has been yet attempted. On the other hand, using anti-PAF15 antibody, we have obtained encouraging, but not conclusive results. This antibody detected a clear single band. Interestingly, this band was detected in cell extracts from both control samples and siUSP1 samples, but only in the <sup>bio</sup>Ub pulldown eluates from siUSP1 samples. Moreover, the molecular weight of the band detected in the pulldown eluates was higher, suggesting an ubiquitinated form of the detected protein. Therefore, it seems reasonable to assume that we are detecting a protein that shows increased ubiquitination when USP1 is silenced, i.e. a USP1 substrate. However we cannot be absolutely confident that it is PAF15, since the size of the detected bands is higher than the predicted molecular weight of PAF15.

In summary, our study significantly expands the repertoire of USP1 targets and may provide novel insights into the role of USP1 in the DNA damage response. However, these candidates need to be validated before being considered bona-fide USP1 substrates. Our analysis serves as a pilot experiment to evaluate the possibility of applying a similar strategy to identify substrates for other DUBs in the context of the ProteoRed platform (Carlos III Networked Proteomics Platform).

## **5.6. USP12/USP46: SIMILAR PROTEINS, DIFFERENT FUNCTIONS**

USP12 and USP46 are nearly 90% identical at the amino acid level. Furthermore, they share UAF1 and WDR20 as activating cofactors (Cohn et al., 2009; Dahlberg and Juo, 2014; Kee et al., 2010), as well as some substrates and interactors (Sowa et al., 2009). One might assume that USP12 and USP46 would play largely overlapping roles in the cell. Indeed, these two DUBs have functions in common, but they also display disparate activities in unrelated cellular processes.

Here we show that the functional differences between USP12 and USP46 correlate with differences in their binding to the cofactor WDR20 and to the interactor DMWD. Using relocation assays, we found that co-expression of YFP-[NLS]-USP12 with WDR20 resulted in a striking relocation of both proteins to the plasma membrane. Such a relocation was also evident, although less pronounced, when YFP-[NLS]-USP12 was co-expressed with DMWD. In contrast, YFP-[NLS]-USP46 remained largely nuclear when co-expressed with WDR20 and no effect was observed when co-expressed with DMWD. In our view, the different extent of this relocation suggests that USP12 and USP46 bind differently to WDR20 and DMWD. Further experiments (e.g. co-IP or *in vitro* binding assays to determine the dissociation constants of each interacting pair) should be carried out to confirm our observations.

Interestingly, differential binding to these proteins may, in turn, be related to the presence (in USP12) or absence (in USP46) of a four amino acid motif (MEIL) at their extreme N-terminal end. Deleting this motif largely (although not completely) abrogates USP12/WDR20 and USP12/DMWD interaction, as detected using the relocation assay. The structure of a ternary USP12/UAF1/WDR20 complex has been recently solved (Li et al., 2016), showing that several residues in USP12 “Palm” subdomain contribute to WDR20 binding. However, it is important to note that the analysis by Li et al. does not provide structural information on the extreme N-terminal end of USP12, and thus, they cannot determine if this region (including the MEIL motif) engages in WDR20 binding. Based on our data and the data by Li et al., we propose the model illustrated in **Figure 85**. According to this model, two USP12 regions contribute to WDR20 binding: the “Palm” subdomain and the N-terminal MEIL motif. Although no structural information of USP46/WDR20 binding is available yet, we propose that USP46 (lacking the MEIL motif) binds WDR20 exclusively through the “Palm” subdomain. As a consequence, the USP46/WDR20 interaction would be weaker than the USP21/WDR20 interaction.



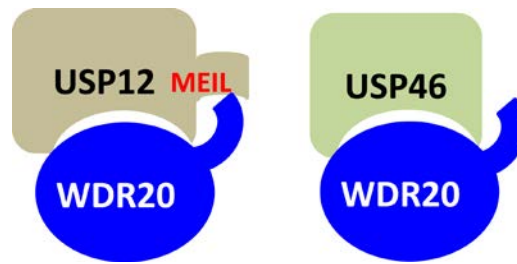


**Figure 85: A proposed model for the binding of USP12 and USP46 to WDR20.** WDR20 binds to the “Palm” subdomain and the MEIL motif of USP12. WDR20 only binds the “Palm” subdomain of USP46.

It is presently unknown why the interaction with WDR20 or DMWD induces DUB relocation to the plasma membrane. A likely explanation might be exposure of a previously masked plasma membrane recruitment motif in either the DUB or the interacting partner. This relocation might represent a novel mechanism to regulate DUB activity. In this regard, it has been reported that only a fraction of the USP12/UAF1 complexes associate with WDR20 (Kee et al., 2010). Thus, we propose that different USP12-containing complexes, with different level of enzymatic activity and different subcellular localization exist in the cells: USP12/UAF1 complexes with partial activity distributed in the cytoplasm or the nucleus, and USP12/UAF1/WDR20 complexes with full enzymatic activity located at the plasma membrane.



# Conclusions

6



## 6. Conclusions

1. In a cellular setting, USP1 phosphorylation at serine 313 is not necessary for UAF1 binding neither for its deubiquitinase activity.
2. Regulation of USP1 by autocleavage involves most likely an intramolecular (*cis*) cleavage event.
3. The “Fingers” subdomain is the critical UAF1-interacting region of UAF1-regulated DUBs. The USP1/UAF1 interaction can be disrupted by single point mutations of specific critical residues in the DUB (E444) or the cofactor (K214).
4. Besides the well-characterized deubiquitination of PCNA by the USP1/UAF1 complex, “free” USP1 might prevent PCNA ubiquitination independently of its deubiquitinase activity.
5. Ectopic overexpression of the USP1/UAF1 complex leads to a general ubiquitin deconjugation in the nucleus, and blocks 53BP1 foci recruitment to DNA damage.
6. Both the function and the regulation of USP1 can be altered by cancer-related missense mutations.
7. The USP1/UAF1 complex may represent a valid therapeutic target in pancreatic cancer: USP1 and UAF1 are overexpressed in this tumor type, and the USP1 inhibitor ML323 increases oxaliplatin sensitivity in a relatively resistant pancreatic cancer cell line.
8. Combining the <sup>bio</sup>Ub approach with siRNA-mediated DUB silencing and label-free quantification-based proteomics constitutes a useful strategy to search for novel DUB targets. We have identified 10 novel potential USP1 substrates, including the DNA damage-related proteins RIF1 and PAF15.
9. USP12 and USP46 bind differently to WDR20, and DMWD. This differential binding appears to be mediated by the presence/absence of a 4 amino acid motif

(MEIL) at their N-terminus, and may contribute to explain the previously observed functional differences between these two highly similar enzymes.

---

## 7. References

- Atkin, G., and Paulson, H. (2014). Ubiquitin pathways in neurodegenerative disease. *Front. Mol. Neurosci.* *7*.
- Avan, A., Pacetti, P., Reni, M., Milella, M., Vasile, E., Mambrini, A., Vaccaro, V., Caponi, S., Cereda, S., Peters, G.J., et al. (2013). Prognostic factors in gemcitabine-cisplatin polychemotherapy regimens in pancreatic cancer: XPD-Lys751Gln polymorphism strikes back. *Int. J. Cancer* *133*, 1016–1022.
- Avvakumov, G.V., Walker, J.R., Xue, S., Finerty, P.J., Mackenzie, F., Newman, E.M., and Dhe-Paganon, S. (2006). Amino-terminal dimerization, NRDP1-rhodanese interaction, and inhibited catalytic domain conformation of the ubiquitin-specific protease 8 (USP8). *J. Biol. Chem.* *281*, 38061–38070.
- Bencokova, Z., Kaufmann, M.R., Pires, I.M., Lecane, P.S., Giaccia, A.J., and Hammond, E.M. (2009). ATM activation and signaling under hypoxic conditions. *Mol. Cell. Biol.* *29*, 526–537.
- Bijnsdorp, I.V., Giovannetti, E., and Peters, G.J. (2011). Analysis of drug interactions. *Methods Mol. Biol. Clifton NJ* *731*, 421–434.
- Bouwman, P., Aly, A., Escandell, J.M., Pieterse, M., Bartkova, J., van der Gulden, H., Hiddingh, S., Thanasoula, M., Kulkarni, A., Yang, Q., et al. (2010). 53BP1 loss rescues BRCA1 deficiency and is associated with triple-negative and BRCA-mutated breast cancers. *Nat. Struct. Mol. Biol.* *17*, 688–695.
- Bremm, A., Freund, S.M.V., and Komander, D. (2010). Lys11-linked ubiquitin chains adopt compact conformations and are preferentially hydrolyzed by the deubiquitinase Cezanne. *Nat. Struct. Mol. Biol.* *17*, 939–947.
- Burska, U.L., Harle, V.J., Coffey, K., Darby, S., Ramsey, H., O'Neill, D., Logan, I.R., Gaughan, L., and Robson, C.N. (2013). Deubiquitinating enzyme Usp12 is a novel co-activator of the androgen receptor. *J. Biol. Chem.* *288*, 32641–32650.
- Cataldo, F., Peche, L.Y., Klaric, E., Brancolini, C., Myers, M.P., Demarchi, F., and Schneider, C. (2013). CAPNS1 regulates USP1 stability and maintenance of genome integrity. *Mol. Cell. Biol.* *33*, 2485–2496.
- Chand, S., O'Hayer, K., Blanco, F.F., Winter, J.M., and Brody, J.R. (2016). The Landscape of Pancreatic Cancer Therapeutic Resistance Mechanisms. *Int. J. Biol. Sci.* *12*, 273–282.
- Chapman, J.R., Taylor, M.R.G., and Boulton, S.J. (2012). Playing the End Game: DNA Double-Strand Break Repair Pathway Choice. *Mol. Cell* *47*, 497–510.
- Chau, V., Tobias, J.W., Bachmair, A., Marriott, D., Ecker, D.J., Gonda, D.K., and Varshavsky, A. (1989). A multiubiquitin chain is confined to specific lysine in a targeted short-lived protein. *Science* *243*, 1576–1583.
- Chen, J., Dexheimer, T.S., Ai, Y., Liang, Q., Villamil, M.A., Inglese, J., Maloney, D.J., Jadhav, A., Simeonov, A., and Zhuang, Z. (2011). Selective and cell-active inhibitors of the USP1/ UAF1

deubiquitinase complex reverse cisplatin resistance in non-small cell lung cancer cells. *Chem. Biol.* **18**, 1390–1400.

Chou, T.C., and Talalay, P. (1984). Quantitative analysis of dose-effect relationships: the combined effects of multiple drugs or enzyme inhibitors. *Adv. Enzyme Regul.* **22**, 27–55.

Cohn, M.A., Kowal, P., Yang, K., Haas, W., Huang, T.T., Gygi, S.P., and D'Andrea, A.D. (2007). A UAF1-containing multisubunit protein complex regulates the Fanconi anemia pathway. *Mol. Cell* **28**, 786–797.

Cohn, M.A., Kee, Y., Haas, W., Gygi, S.P., and D'Andrea, A.D. (2009). UAF1 is a subunit of multiple deubiquitinating enzyme complexes. *J. Biol. Chem.* **284**, 5343–5351.

Cooper, E.M., Cutcliffe, C., Kristiansen, T.Z., Pandey, A., Pickart, C.M., and Cohen, R.E. (2009). K63-specific deubiquitination by two JAMM/MPN+ complexes: BRISC-associated Brcc36 and proteasomal Poh1. *EMBO J.* **28**, 621–631.

Côté-Martin, A., Moody, C., Fradet-Turcotte, A., D'Abramo, C.M., Lehoux, M., Joubert, S., Poirier, G.G., Coulombe, B., Laimins, L.A., and Archambault, J. (2008). Human Papillomavirus E1 Helicase Interacts with the WD Repeat Protein p80 To Promote Maintenance of the Viral Genome in Keratinocytes. *J. Virol.* **82**, 1271–1283.

Cotto-Rios, X.M., Jones, M.J.K., Busino, L., Pagano, M., and Huang, T.T. (2011a). APC/CCdh1-dependent proteolysis of USP1 regulates the response to UV-mediated DNA damage. *J. Cell Biol.* **194**, 177–186.

Cotto-Rios, X.M., Jones, M.J., and Huang, T.T. (2011b). Insights into phosphorylation-dependent mechanisms regulating USP1 protein stability during the cell cycle. *Cell Cycle* **10**, 4009–4016.

Cox, J., and Mann, M. (2008). MaxQuant enables high peptide identification rates, individualized p.p.b.-range mass accuracies and proteome-wide protein quantification. *Nat. Biotechnol.* **26**, 1367–1372.

Cox, J., Neuhauser, N., Michalski, A., Scheltema, R.A., Olsen, J.V., and Mann, M. (2011). Andromeda: a peptide search engine integrated into the MaxQuant environment. *J. Proteome Res.* **10**, 1794–1805.

Cukras, S., Lee, E., Palumbo, E., Benavidez, P., Moldovan, G.-L., and Kee, Y. (2016). The USP1-UAF1 complex interacts with RAD51AP1 to promote homologous recombination repair. *Cell Cycle* **15**, 2636–2646.

Dahlberg, C.L., and Juo, P. (2014). The WD40-repeat proteins WDR-20 and WDR-48 bind and activate the deubiquitinating enzyme USP-46 to promote the abundance of the glutamate receptor GLR-1 in the ventral nerve cord of *Caenorhabditis elegans*. *J. Biol. Chem.* **289**, 3444–3456.

Daley, J.M., and Sung, P. (2013). RIF1 in DNA break repair pathway choice. *Mol. Cell* **49**, 840–841.

Das, D.S., Das, A., Ray, A., Song, Y., Samur, M.K., Munshi, N.C., Chauhan, D., and Anderson, K.C. (2017). Blockade of Deubiquitylating Enzyme USP1 Inhibits DNA Repair and Triggers Apoptosis in Multiple Myeloma Cells. *Clin. Cancer Res.* **23**, 2692–2701.



- Dexheimer, T.S., Rosenthal, A.S., Luci, D.K., Liang, Q., Villamil, M.A., Chen, J., Sun, H., Kerns, E.H., Simeonov, A., Jadhav, A., et al. (2014). Synthesis and structure-activity relationship studies of N-benzyl-2-phenylpyrimidin-4-amine derivatives as potent USP1/UAF1 deubiquitinase inhibitors with anticancer activity against nonsmall cell lung cancer. *J. Med. Chem.* *57*, 8099–8110.
- Dharadhar, S., Clerici, M., van Dijk, W.J., Fish, A., and Sixma, T.K. (2016). A conserved two-step binding for the UAF1 regulator to the USP12 deubiquitinating enzyme. *J. Struct. Biol.* *196*, 437–447.
- Endo, A., Matsumoto, M., Inada, T., Yamamoto, A., Nakayama, K.I., Kitamura, N., and Komada, M. (2009). Nucleolar structure and function are regulated by the deubiquitylating enzyme USP36. *J. Cell Sci.* *122*, 678–686.
- Faesen, A.C., Luna-Vargas, M.P.A., Geurink, P.P., Clerici, M., Merckx, R., van Dijk, W.J., Hameed, D.S., El Oualid, F., Ovaa, H., and Sixma, T.K. (2011). The Differential Modulation of USP Activity by Internal Regulatory Domains, Interactors and Eight Ubiquitin Chain Types. *Chem. Biol.* *18*, 1550–1561.
- Faesen, A.C., Luna-Vargas, M.P.A., and Sixma, T.K. (2012). The role of UBL domains in ubiquitin-specific proteases. *Biochem. Soc. Trans.* *40*, 539–545.
- Fernandez-Capetillo, O., Lee, A., Nussenzweig, M., and Nussenzweig, A. (2004). H2AX: the histone guardian of the genome. *DNA Repair* *3*, 959–967.
- Forbes, S.A., Bindal, N., Bamford, S., Cole, C., Kok, C.Y., Beare, D., Jia, M., Shepherd, R., Leung, K., Menzies, A., et al. (2011). COSMIC: mining complete cancer genomes in the Catalogue of Somatic Mutations in Cancer. *Nucleic Acids Res.* *39*, D945–D950.
- Fox, J.T., Lee, K., and Myung, K. (2011). Dynamic regulation of PCNA ubiquitylation/deubiquitylation. *FEBS Lett.* *585*, 2780–2785.
- Fraille, J.M., Quesada, V., Rodríguez, D., Freije, J.M.P., and López-Otín, C. (2012). Deubiquitinases in cancer: new functions and therapeutic options. *Oncogene* *31*, 2373–2388.
- Franco, M., Seyfried, N.T., Brand, A.H., Peng, J., and Mayor, U. (2011). A Novel Strategy to Isolate Ubiquitin Conjugates Reveals Wide Role for Ubiquitination during Neural Development. *Mol. Cell. Proteomics* *10*, M110.002188.
- Fujimuro, M., Sawada, H., and Yokosawa, H. (1994). Production and characterization of monoclonal antibodies specific to multi-ubiquitin chains of polyubiquitinated proteins. *FEBS Lett.* *349*, 173–180.
- Fujiwara, T., Saito, A., Suzuki, M., Shinomiya, H., Suzuki, T., Takahashi, E., Tanigami, A., Ichiyama, A., Chung, C.H., Nakamura, Y., et al. (1998). Identification and Chromosomal Assignment of USP1, a Novel Gene Encoding a Human Ubiquitin-Specific Protease. *Genomics* *54*, 155–158.
- Gangula, N.R., and Maddika, S. (2013). WD repeat protein WDR48 in complex with deubiquitinase USP12 suppresses Akt-dependent cell survival signaling by stabilizing PH domain leucine-rich repeat protein phosphatase 1 (PHLPP1). *J. Biol. Chem.* *288*, 34545–34554.

García-Santisteban, I., Zorroza, K., and Rodríguez, J.A. (2012). Two Nuclear Localization Signals in USP1 Mediate Nuclear Import of the USP1/UAF1 Complex. *PLOS ONE* 7, e38570.

García-Santisteban, I., Peters, G.J., Giovannetti, E., and Rodríguez, J.A. (2013). USP1 deubiquitinase: cellular functions, regulatory mechanisms and emerging potential as target in cancer therapy. *Mol. Cancer* 12, 91.

Geng, F., Wenzel, S., and Tansey, W.P. (2012). Ubiquitin and proteasomes in transcription. *Annu. Rev. Biochem.* 81, 177–201.

Gibson, D.G., Young, L., Chuang, R.-Y., Venter, J.C., Hutchison, C.A., and Smith, H.O. (2009). Enzymatic assembly of DNA molecules up to several hundred kilobases. *Nat. Methods* 6, 343–345.

Goldstein, G., Scheid, M., Hammerling, U., Schlesinger, D.H., Niall, H.D., and Boyse, E.A. (1975). Isolation of a polypeptide that has lymphocyte-differentiating properties and is probably represented universally in living cells. *Proc. Natl. Acad. Sci. U. S. A.* 72, 11–15.

Guzzo, C.M., and Matunis, M.J. (2013). Expanding SUMO and ubiquitin-mediated signaling through hybrid SUMO-ubiquitin chains and their receptors. *Cell Cycle* 12, 1015–1017.

Haglund, K., and Dikic, I. (2005). Ubiquitylation and cell signaling. *EMBO J.* 24, 3353–3359.

Haglund, K., Sigismund, S., Polo, S., Szymkiewicz, I., Di Fiore, P.P., and Dikic, I. (2003). Multiple monoubiquitination of RTKs is sufficient for their endocytosis and degradation. *Nat. Cell Biol.* 5, 461–466.

Hanna, J., Hathaway, N.A., Tone, Y., Crosas, B., Elsasser, S., Kirkpatrick, D.S., Leggett, D.S., Gygi, S.P., King, R.W., and Finley, D. (2006). Deubiquitinating Enzyme Ubp6 Functions Noncatalytically to Delay Proteasomal Degradation. *Cell* 127, 99–111.

Hershko, A. (1983). Ubiquitin: roles in protein modification and breakdown. *Cell* 34, 11–12.

Hershko, A., Heller, H., Elias, S., and Ciechanover, A. (1983). Components of ubiquitin-protein ligase system. Resolution, affinity purification, and role in protein breakdown. *J. Biol. Chem.* 258, 8206–8214.

Heyninck, K., and Beyaert, R. (2005). A20 inhibits NF-kappaB activation by dual ubiquitin-editing functions. *Trends Biochem. Sci.* 30, 1–4.

Hicke, L. (2001). Protein regulation by monoubiquitin. *Nat. Rev. Mol. Cell Biol.* 2, 195–201.

Hoege, C., Pfander, B., Moldovan, G.-L., Pyrowolakis, G., and Jentsch, S. (2002). RAD6-dependent DNA repair is linked to modification of PCNA by ubiquitin and SUMO. *Nature* 419, 135–141.

Hoeller, D., and Dikic, I. (2009). Targeting the ubiquitin system in cancer therapy. *Nature* 458, 438–444.

Housman, G., Byler, S., Heerboth, S., Lapinska, K., Longacre, M., Snyder, N., and Sarkar, S. (2014). Drug Resistance in Cancer: An Overview. *Cancers* 6, 1769–1792.

- Hu, M., Li, P., Li, M., Li, W., Yao, T., Wu, J.-W., Gu, W., Cohen, R.E., and Shi, Y. (2002). Crystal Structure of a UBP-Family Deubiquitinating Enzyme in Isolation and in Complex with Ubiquitin Aldehyde. *Cell* **111**, 1041–1054.
- Hu, M., Li, P., Song, L., Jeffrey, P.D., Chenova, T.A., Wilkinson, K.D., Cohen, R.E., and Shi, Y. (2005). Structure and mechanisms of the proteasome-associated deubiquitinating enzyme USP14. *EMBO J.* **24**, 3747–3756.
- Huang, T.T., Nijman, S.M.B., Mirchandani, K.D., Galardy, P.J., Cohn, M.A., Haas, W., Gygi, S.P., Ploegh, H.L., Bernards, R., and D’Andrea, A.D. (2006). Regulation of monoubiquitinated PCNA by DUB autocleavage. *Nat. Cell Biol.* **8**, 339–347.
- Huether, R., Dong, L., Chen, X., Wu, G., Parker, M., Wei, L., Ma, J., Edmonson, M.N., Hedlund, E.K., Rusch, M.C., et al. (2014). The landscape of somatic mutations in epigenetic regulators across 1,000 paediatric cancer genomes. *Nat. Commun.* **5**, 3630.
- Huo, Y., Khatri, N., Hou, Q., Gilbert, J., Wang, G., and Man, H.-Y. (2015). The deubiquitinating enzyme USP46 regulates AMPA receptor ubiquitination and trafficking. *J. Neurochem.* **134**, 1067–1080.
- Hurley, J.H., Lee, S., and Prag, G. (2006). Ubiquitin-binding domains. *Biochem. J.* **399**, 361–372.
- Huyen, Y., Zgheib, O., Ditullio, R.A., Gorgoulis, V.G., Zacharatos, P., Petty, T.J., Sheston, E.A., Mellert, H.S., Stavridi, E.S., and Halazonetis, T.D. (2004). Methylated lysine 79 of histone H3 targets 53BP1 to DNA double-strand breaks. *Nature* **432**, 406–411.
- Ikeda, F., and Dikic, I. (2008). Atypical ubiquitin chains: new molecular signals. “Protein Modifications: Beyond the Usual Suspects” review series. *EMBO Rep.* **9**, 536–542.
- Jackson, S.P., and Bartek, J. (2009). The DNA-damage response in human biology and disease. *Nature* **461**, 1071–1078.
- Jackson, S.P., and Durocher, D. (2013). Regulation of DNA damage responses by ubiquitin and SUMO. *Mol. Cell* **49**, 795–807.
- Jahan, A.S., Lestra, M., Swee, L.K., Fan, Y., Lamers, M.M., Tafesse, F.G., Theile, C.S., Spooner, E., Bruzzone, R., Ploegh, H.L., et al. (2016). Usp12 stabilizes the T-cell receptor complex at the cell surface during signaling. *Proc. Natl. Acad. Sci. U. S. A.* **113**, E705-714.
- Joo, H.-Y., Jones, A., Yang, C., Zhai, L., Smith, A.D., Zhang, Z., Chandrasekharan, M.B., Sun, Z., Renfrow, M.B., Wang, Y., et al. (2011). Regulation of Histone H2A and H2B Deubiquitination and Xenopus Development by USP12 and USP46. *J. Biol. Chem.* **286**, 7190–7201.
- Kee, Y., and D’Andrea, A.D. (2012). Molecular pathogenesis and clinical management of Fanconi anemia. *J. Clin. Invest.* **122**, 3799–3806.
- Kee, Y., Yang, K., Cohn, M.A., Haas, W., Gygi, S.P., and D’Andrea, A.D. (2010). WDR20 Regulates Activity of the USP12-UAF1 Deubiquitinating Enzyme Complex. *J. Biol. Chem.* **285**, 11252–11257.
- Keller, B.O., Sui, J., Young, A.B., and Whittall, R.M. (2008). Interferences and contaminants encountered in modern mass spectrometry. *Anal. Chim. Acta* **627**, 71–81.

- Kim, H., and D'Andrea, A.D. (2012). Regulation of DNA cross-link repair by the Fanconi anemia/BRCA pathway. *Genes Dev.* *26*, 1393–1408.
- Kim, J.M., Parmar, K., Huang, M., Weinstock, D.M., Ruit, C.A., Kutok, J.L., and D'Andrea, A.D. (2009). Inactivation of murine Usp1 results in genomic instability and a Fanconi anemia phenotype. *Dev. Cell* *16*, 314–320.
- Kirisako, T., Kamei, K., Murata, S., Kato, M., Fukumoto, H., Kanie, M., Sano, S., Tokunaga, F., Tanaka, K., and Iwai, K. (2006). A ubiquitin ligase complex assembles linear polyubiquitin chains. *EMBO J.* *25*, 4877–4887.
- Komander, D. (2010). Mechanism, specificity and structure of the deubiquitinases. *Subcell. Biochem.* *54*, 69–87.
- Komander, D., Clague, M.J., and Urbé, S. (2009). Breaking the chains: structure and function of the deubiquitinases. *Nat. Rev. Mol. Cell Biol.* *10*, 550–563.
- Kulathu, Y., and Komander, D. (2012). Atypical ubiquitylation - the unexplored world of polyubiquitin beyond Lys48 and Lys63 linkages. *Nat. Rev. Mol. Cell Biol.* *13*, 508–523.
- Larkin, M.A., Blackshields, G., Brown, N.P., Chenna, R., McGettigan, P.A., McWilliam, H., Valentin, F., Wallace, I.M., Wilm, A., Lopez, R., et al. (2007). Clustal W and Clustal X version 2.0. *Bioinforma. Oxf. Engl.* *23*, 2947–2948.
- Laws, G.M., Skopek, T.R., Reddy, M.V., Storer, R.D., and Glaab, W.E. (2001). Detection of DNA adducts using a quantitative long PCR technique and the fluorogenic 5' nuclease assay (TaqMan). *Mutat. Res.* *484*, 3–18.
- Lectez, B., Migotti, R., Lee, S.Y., Ramirez, J., Beraza, N., Mansfield, B., Sutherland, J.D., Martinez-Chantar, M.L., Dittmar, G., and Mayor, U. (2014). Ubiquitin profiling in liver using a transgenic mouse with biotinylated ubiquitin. *J. Proteome Res.* *13*, 3016–3026.
- Li, H., Lim, K.S., Kim, H., Hinds, T.R., Jo, U., Mao, H., Weller, C.E., Sun, J., Chatterjee, C., D'Andrea, A.D., et al. (2016). Allosteric Activation of Ubiquitin-Specific Proteases by  $\beta$ -Propeller Proteins UAF1 and WDR20. *Mol. Cell* *63*, 249–260.
- Li, X., Stevens, P.D., Yang, H., Gulhati, P., Wang, W., Evers, B.M., and Gao, T. (2013). The deubiquitination enzyme USP46 functions as a tumor suppressor by controlling PHLPP-dependent attenuation of Akt signaling in colon cancer. *Oncogene* *32*, 471–478.
- Liang, F., Longerich, S., Miller, A.S., Tang, C., Buzovetsky, O., Xiong, Y., Maranon, D.G., Wiese, C., Kupfer, G.M., and Sung, P. (2016). Promotion of RAD51-Mediated Homologous DNA Pairing by the RAD51AP1-UAF1 Complex. *Cell Rep.* *15*, 2118–2126.
- Liang, Q., Dexheimer, T.S., Zhang, P., Rosenthal, A.S., Villamil, M.A., You, C., Zhang, Q., Chen, J., Ott, C.A., Sun, H., et al. (2014). A selective USP1-UAF1 inhibitor links deubiquitination to DNA damage responses. *Nat. Chem. Biol.* *10*, 298–304.
- Livak, K.J., and Schmittgen, T.D. (2001). Analysis of relative gene expression data using real-time quantitative PCR and the 2<sup>(-Delta Delta C(T))</sup> Method. *Methods San Diego Calif* *25*, 402–408.

- Lukas, J., Lukas, C., and Bartek, J. (2004). Mammalian cell cycle checkpoints: signalling pathways and their organization in space and time. *DNA Repair* 3, 997–1007.
- Malakhov, M.P., Malakhova, O.A., Kim, K.I., Ritchie, K.J., and Zhang, D.-E. (2002). UBP43 (USP18) Specifically Removes ISG15 from Conjugated Proteins. *J. Biol. Chem.* 277, 9976–9981.
- Martin, L.P., Hamilton, T.C., and Schilder, R.J. (2008). Platinum resistance: the role of DNA repair pathways. *Clin. Cancer Res. Off. J. Am. Assoc. Cancer Res.* 14, 1291–1295.
- Marttila, A.T., Laitinen, O.H., Airene, K.J., Kulik, T., Bayer, E.A., Wilchek, M., and Kulomaa, M.S. (2000). Recombinant NeutraLite avidin: a non-glycosylated, acidic mutant of chicken avidin that exhibits high affinity for biotin and low non-specific binding properties. *FEBS Lett.* 467, 31–36.
- Mattern, M.R., Wu, J., and Nicholson, B. (2012). Ubiquitin-based anticancer therapy: carpet bombing with proteasome inhibitors vs surgical strikes with E1, E2, E3, or DUB inhibitors. *Biochim. Biophys. Acta* 1823, 2014–2021.
- Mayor, U., and Peng, J. (2012). Deciphering tissue-specific ubiquitylation by mass spectrometry. *Methods Mol. Biol. Clifton NJ* 832, 65–80.
- McClurg, U.L., Summerscales, E.E., Harle, V.J., Gaughan, L., and Robson, C.N. (2014). Deubiquitinating enzyme Usp12 regulates the interaction between the androgen receptor and the Akt pathway. *Oncotarget* 5, 7081–7092.
- Mendoza, H.M., Shen, L.-N., Botting, C., Lewis, A., Chen, J., Ink, B., and Hay, R.T. (2003). NEDP1, a highly conserved cysteine protease that deNEDDylates Cullins. *J. Biol. Chem.* 278, 25637–25643.
- Messick, T.E., and Greenberg, R.A. (2009). The ubiquitin landscape at DNA double-strand breaks. *J. Cell Biol.* 187, 319–326.
- Min, M., Mayor, U., Dittmar, G., and Lindon, C. (2014). Using in Vivo Biotinylated Ubiquitin to Describe a Mitotic Exit Ubiquitome from Human Cells. *Mol. Cell. Proteomics MCP* 13, 2411–2425.
- Mistry, H., Hsieh, G., Buhrlage, S.J., Huang, M., Park, E., Cuny, G.D., Galinsky, I., Stone, R.M., Gray, N.S., D'Andrea, A.D., et al. (2013). Small molecule inhibitors of USP1 target ID1 degradation in leukemic cells. *Mol. Cancer Ther.* 12, 2651–2662.
- Moretti, J., Chastagner, P., Liang, C.-C., Cohn, M.A., Israël, A., and Brou, C. (2012). The ubiquitin-specific protease 12 (USP12) is a negative regulator of notch signaling acting on notch receptor trafficking toward degradation. *J. Biol. Chem.* 287, 29429–29441.
- Morris, C., Tomimatsu, N., Richard, D.J., Cluet, D., Burma, S., Khanna, K.K., and Jalinot, P. (2012). INT6/EIF3E interacts with ATM and is required for proper execution of the DNA damage response in human cells. *Cancer Res.* 72, 2006–2016.
- Mosbech, A., Lukas, C., Bekker-Jensen, S., and Mailand, N. (2013). The Deubiquitylating Enzyme USP44 Counteracts the DNA Double-strand Break Response Mediated by the RNF8 and RNF168 Ubiquitin Ligases. *J. Biol. Chem.* 288, 16579–16587.

- Mukhopadhyay, D., and Dasso, M. (2007). Modification in reverse: the SUMO proteases. *Trends Biochem. Sci.* *32*, 286–295.
- Murai, J., Yang, K., Dejsuphong, D., Hirota, K., Takeda, S., and D’Andrea, A.D. (2011). The USP1/UAF1 complex promotes double-strand break repair through homologous recombination. *Mol. Cell. Biol.* *31*, 2462–2469.
- Nagase, T., Kikuno, R., Nakayama, M., Hirosawa, M., and Ohara, O. (2000). Prediction of the coding sequences of unidentified human genes. XVIII. The complete sequences of 100 new cDNA clones from brain which code for large proteins in vitro. *DNA Res. Int. J. Rapid Publ. Rep. Genes Genomes* *7*, 273–281.
- Nakayama, K.I., and Nakayama, K. (2006). Ubiquitin ligases: cell-cycle control and cancer. *Nat. Rev. Cancer* *6*, 369–381.
- Nijman, S.M.B., Luna-Vargas, M.P.A., Velds, A., Brummelkamp, T.R., Dirac, A.M.G., Sixma, T.K., and Bernards, R. (2005a). A Genomic and Functional Inventory of Deubiquitinating Enzymes. *Cell* *123*, 773–786.
- Nijman, S.M.B., Huang, T.T., Dirac, A.M.G., Brummelkamp, T.R., Kerkhoven, R.M., D’Andrea, A.D., and Bernards, R. (2005b). The deubiquitinating enzyme USP1 regulates the Fanconi anemia pathway. *Mol. Cell* *17*, 331–339.
- Oestergaard, V.H., Langevin, F., Kuiken, H.J., Pace, P., Niedzwiedz, W., Simpson, L.J., Ohzeki, M., Takata, M., Sale, J.E., and Patel, K.J. (2007). Deubiquitination of FANCD2 is required for DNA crosslink repair. *Mol. Cell* *28*, 798–809.
- Ohashi, M., Holthaus, A.M., Calderwood, M.A., Lai, C.-Y., Krastins, B., Sarracino, D., and Johannsen, E. (2015). The EBNA3 Family of Epstein-Barr Virus Nuclear Proteins Associates with the USP46/USP12 Deubiquitination Complexes to Regulate Lymphoblastoid Cell Line Growth. *PLOS Pathog.* *11*, e1004822.
- Olazabal-Herrero, A., García-Santisteban, I., and Rodríguez, J.A. (2015). Structure-function analysis of USP1: insights into the role of Ser313 phosphorylation site and the effect of cancer-associated mutations on autocleavage. *Mol. Cancer* *14*, 33.
- Olazabal-Herrero, A., García-Santisteban, I., and Rodríguez, J.A. (2016). Mutations in the “Fingers” subdomain of the deubiquitinase USP1 modulate its function and activity. *FEBS J.* *283*, 929–946.
- Osinalde, N., Sánchez-Quiles, V., Akimov, V., Blagoev, B., and Kratchmarova, I. (2015). SILAC-based quantification of changes in protein tyrosine phosphorylation induced by Interleukin-2 (IL-2) and IL-15 in T-lymphocytes. *Data Brief* *5*, 53–58.
- Park, E., Kim, J.M., Primack, B., Weinstock, D.M., Moreau, L.A., Parmar, K., and D’Andrea, A.D. (2013). Inactivation of Uaf1 causes defective homologous recombination and early embryonic lethality in mice. *Mol. Cell. Biol.* *33*, 4360–4370.
- Park, J., Lee, B.-S., Choi, J.-K., Means, R.E., Choe, J., and Jung, J.U. (2002). Herpesviral protein targets a cellular WD repeat endosomal protein to downregulate T lymphocyte receptor expression. *Immunity* *17*, 221–233.

- Petroski, M.D., and Deshaies, R.J. (2003). Context of multiubiquitin chain attachment influences the rate of Sic1 degradation. *Mol. Cell* *11*, 1435–1444.
- Petroski, M.D., and Deshaies, R.J. (2005). Function and regulation of cullin-RING ubiquitin ligases. *Nat. Rev. Mol. Cell Biol.* *6*, 9–20.
- Pickart, C.M., and Fushman, D. (2004). Polyubiquitin chains: polymeric protein signals. *Curr. Opin. Chem. Biol.* *8*, 610–616.
- Quesada, V., Díaz-Perales, A., Gutiérrez-Fernández, A., Garabaya, C., Cal, S., and López-Otín, C. (2004). Cloning and enzymatic analysis of 22 novel human ubiquitin-specific proteases. *Biochem. Biophys. Res. Commun.* *314*, 54–62.
- Ramirez, J., Martinez, A., Lectez, B., Lee, S.Y., Franco, M., Barrio, R., Dittmar, G., and Mayor, U. (2015). Proteomic Analysis of the Ubiquitin Landscape in the Drosophila Embryonic Nervous System and the Adult Photoreceptor Cells. *PLOS ONE* *10*, e0139083.
- Ranum, L.P.W., and Day, J.W. (2004). Myotonic dystrophy: RNA pathogenesis comes into focus. *Am. J. Hum. Genet.* *74*, 793–804.
- Rego, M.A., Harney, J.A., Mauro, M., Shen, M., and Howlett, N.G. (2012). Regulation of the activation of the Fanconi anemia pathway by the p21 cyclin-dependent kinase inhibitor. *Oncogene* *31*, 366–375.
- Renatus, M., Parrado, S.G., D’Arcy, A., Eidhoff, U., Gerhartz, B., Hassiepen, U., Pierrat, B., Riedl, R., Vinzenz, D., Worpenberg, S., et al. (2006). Structural Basis of Ubiquitin Recognition by the Deubiquitinating Protease USP2. *Structure* *14*, 1293–1302.
- Reyes-Turcu, F.E., Ventii, K.H., and Wilkinson, K.D. (2009). Regulation and cellular roles of ubiquitin-specific deubiquitinating enzymes. *Annu. Rev. Biochem.* *78*, 363–397.
- Richardson, P.G., Barlogie, B., Berenson, J., Singhal, S., Jagannath, S., Irwin, D., Rajkumar, S.V., Srkalovic, G., Alsina, M., Alexanian, R., et al. (2003). A Phase 2 Study of Bortezomib in Relapsed, Refractory Myeloma. *N. Engl. J. Med.* *348*, 2609–2617.
- Rogakou, E.P., Pilch, D.R., Orr, A.H., Ivanova, V.S., and Bonner, W.M. (1998). DNA double-stranded breaks induce histone H2AX phosphorylation on serine 139. *J. Biol. Chem.* *273*, 5858–5868.
- Rothbauer, U., Zolghadr, K., Muyldermans, S., Schepers, A., Cardoso, M.C., and Leonhardt, H. (2008). A versatile nanotrapp for biochemical and functional studies with fluorescent fusion proteins. *Mol. Cell. Proteomics MCP* *7*, 282–289.
- Satija, Y.K., Bhardwaj, A., and Das, S. (2013). A portrayal of E3 ubiquitin ligases and deubiquitylases in cancer. *Int. J. Cancer* *133*, 2759–2768.
- Schindelin, J., Arganda-Carreras, I., Frise, E., Kaynig, V., Longair, M., Pietzsch, T., Preibisch, S., Rueden, C., Saalfeld, S., Schmid, B., et al. (2012). Fiji: an open-source platform for biological-image analysis. *Nat. Methods* *9*, 676–682.
- Sharma, N., Zhu, Q., Wani, G., He, J., Wang, Q., and Wani, A.A. (2014). USP3 counteracts RNF168 via deubiquitinating H2A and  $\gamma$ H2AX at lysine 13 and 15. *Cell Cycle* *13*, 106–114.

- Sievers, F., and Higgins, D.G. (2014). Clustal Omega, accurate alignment of very large numbers of sequences. *Methods Mol. Biol.* Clifton NJ *1079*, 105–116.
- Sourisseau, T., Helissey, C., Lefebvre, C., Ponsonnailles, F., Malka-Mahieu, H., Olausson, K.A., André, F., Vagner, S., and Soria, J.-C. (2016). Translational regulation of the mRNA encoding the ubiquitin peptidase USP1 involved in the DNA damage response as a determinant of Cisplatin resistance. *Cell Cycle* *15*, 295–302.
- Sowa, M.E., Bennett, E.J., Gygi, S.P., and Harper, J.W. (2009). Defining the human deubiquitinating enzyme interaction landscape. *Cell* *138*, 389–403.
- Steen, H., and Mann, M. (2004). The ABC's (and XYZ's) of peptide sequencing. *Nat. Rev. Mol. Cell Biol.* *5*, 699–711.
- Stornetta, A., Zimmermann, M., Cimino, G.D., Henderson, P.T., and Sturla, S.J. (2017). DNA Adducts from Anticancer Drugs as Candidate Predictive Markers for Precision Medicine. *Chem. Res. Toxicol.* *30*, 388–409.
- Swaminathan, S., Amerik, A.Y., and Hochstrasser, M. (1999). The Doa4 deubiquitinating enzyme is required for ubiquitin homeostasis in yeast. *Mol. Biol. Cell* *10*, 2583–2594.
- Tyanova, S., Temu, T., Sinitcyn, P., Carlson, A., Hein, M.Y., Geiger, T., Mann, M., and Cox, J. (2016). The Perseus computational platform for comprehensive analysis of (prote)omics data. *Nat. Methods* *13*, 731–740.
- Typas, D., Luijsterburg, M.S., Wiegant, W.W., Diakatou, M., Helfricht, A., Thijssen, P.E., van den Broek, B., van de Broek, B., Mullenders, L.H., and van Attikum, H. (2015). The de-ubiquitylating enzymes USP26 and USP37 regulate homologous recombination by counteracting RAP80. *Nucleic Acids Res.* *43*, 6919–6933.
- Ulrich, H.D., and Walden, H. (2010). Ubiquitin signalling in DNA replication and repair. *Nat. Rev. Mol. Cell Biol.* *11*, 479–489.
- Urbé, S., Liu, H., Hayes, S.D., Heride, C., Rigden, D.J., and Clague, M.J. (2012). Systematic survey of deubiquitinase localization identifies USP21 as a regulator of centrosome- and microtubule-associated functions. *Mol. Biol. Cell* *23*, 1095–1103.
- Vaccaro, V., Melisi, D., Bria, E., Cuppone, F., Ciuffreda, L., Pino, M.S., Gelibter, A., Tortora, G., Cognetti, F., and Milella, M. (2011). Emerging pathways and future targets for the molecular therapy of pancreatic cancer. *Expert Opin. Ther. Targets* *15*, 1183–1196.
- Veen, A.G. van der, and Ploegh, H.L. (2012). Ubiquitin-Like Proteins. *Annu. Rev. Biochem.* *81*, 323–357.
- Verma, R., Aravind, L., Oania, R., McDonald, W.H., Yates, J.R., Koonin, E.V., and Deshaies, R.J. (2002). Role of Rpn11 metalloprotease in deubiquitination and degradation by the 26S proteasome. *Science* *298*, 611–615.
- Vichai, V., and Kirtikara, K. (2006). Sulforhodamine B colorimetric assay for cytotoxicity screening. *Nat. Protoc.* *1*, 1112–1116.



- Villamil, M.A., Chen, J., Liang, Q., and Zhuang, Z. (2012a). A noncanonical cysteine protease USP1 is activated through active site modulation by USP1-associated factor 1. *Biochemistry (Mosc.)* *51*, 2829–2839.
- Villamil, M.A., Liang, Q., Chen, J., Choi, Y.S., Hou, S., Lee, K.H., and Zhuang, Z. (2012b). Serine phosphorylation is critical for the activation of ubiquitin-specific protease 1 and its interaction with WD40-repeat protein UAF1. *Biochemistry (Mosc.)* *51*, 9112–9123.
- Vucic, D., Dixit, V.M., and Wertz, I.E. (2011). Ubiquitylation in apoptosis: a post-translational modification at the edge of life and death. *Nat. Rev. Mol. Cell Biol.* *12*, 439–452.
- Wang, T., Yin, L., Cooper, E.M., Lai, M.-Y., Dickey, S., Pickart, C.M., Fushman, D., Wilkinson, K.D., Cohen, R.E., and Wolberger, C. (2009). Evidence for Bidentate Substrate Binding as the Basis for the K48 Linkage Specificity of Otubain 1. *J. Mol. Biol.* *386*, 1011–1023.
- Waters, L.S., Minesinger, B.K., Wiltrout, M.E., D'Souza, S., Woodruff, R.V., and Walker, G.C. (2009). Eukaryotic translesion polymerases and their roles and regulation in DNA damage tolerance. *Microbiol. Mol. Biol. Rev. MMBR* *73*, 134–154.
- van Wijk, S.J.L., Fiskin, E., Putyrski, M., Pampaloni, F., Hou, J., Wild, P., Kensche, T., Grecco, H.E., Bastiaens, P., and Dikic, I. (2012). Fluorescence-based sensors to monitor localization and functions of linear and K63-linked ubiquitin chains in cells. *Mol. Cell* *47*, 797–809.
- Williams, S.A., Maecker, H.L., French, D.M., Liu, J., Gregg, A., Silverstein, L.B., Cao, T.C., Carano, R.A.D., and Dixit, V.M. (2011). USP1 deubiquitinates ID proteins to preserve a mesenchymal stem cell program in osteosarcoma. *Cell* *146*, 918–930.
- Wong, E., and Cuervo, A.M. (2010). Integration of Clearance Mechanisms: The Proteasome and Autophagy. *Cold Spring Harb. Perspect. Biol.* *2*, a006734.
- Wong, J.W.H., and Cagney, G. (2010). An overview of label-free quantitation methods in proteomics by mass spectrometry. *Methods Mol. Biol. Clifton NJ* *604*, 273–283.
- Xie, C., Yao, M., and Dong, Q. (2014). Proliferating cell unclear antigen-associated factor (PAF15): A novel oncogene. *Int. J. Biochem. Cell Biol.* *50*, 127–131.
- Xu, D., Shan, B., Lee, B.-H., Zhu, K., Zhang, T., Sun, H., Liu, M., Shi, L., Liang, W., Qian, L., et al. (2015). Phosphorylation and activation of ubiquitin-specific protease-14 by Akt regulates the ubiquitin-proteasome system. *eLife* *4*, e10510.
- Xu, J.-M., Azzariti, A., Severino, M., Lu, B., Colucci, G., and Paradiso, A. (2003). Characterization of sequence-dependent synergy between ZD1839 (“Iressa”) and oxaliplatin. *Biochem. Pharmacol.* *66*, 551–563.
- Yang, K., Moldovan, G.-L., Vinciguerra, P., Murai, J., Takeda, S., and D’Andrea, A.D. (2011). Regulation of the Fanconi anemia pathway by a SUMO-like delivery network. *Genes Dev.* *25*, 1847–1858.
- Ye, Y., Scheel, H., Hofmann, K., and Komander, D. (2009). Dissection of USP catalytic domains reveals five common insertion points. *Mol. Biosyst.* *5*, 1797–1808.

Yin, J., Schoeffler, A.J., Wickliffe, K., Newton, K., Starovasnik, M.A., Dueber, E.C., and Harris, S.F. (2015). Structural Insights into WD-Repeat 48 Activation of Ubiquitin-Specific Protease 46. *Struct. Lond. Engl.* 23, 2043–2054.

Zhang, Z., Yang, H., and Wang, H. (2014). The histone H2A deubiquitinase USP16 interacts with HERC2 and fine-tunes cellular response to DNA damage. *J. Biol. Chem.* 289, 32883–32894.

Zhao, Y., Brickner, J.R., Majid, M.C., and Mosammaparast, N. (2014). Crosstalk between ubiquitin and other post-translational modifications on chromatin during double-strand break repair. *Trends Cell Biol.* 24, 426–434.

Zheng, L., Baumann, U., and Reymond, J.-L. (2004). An efficient one-step site-directed and site-saturation mutagenesis protocol. *Nucleic Acids Res.* 32, e115.

Zhu, X., Ménard, R., and Sulea, T. (2007). High incidence of ubiquitin-like domains in human ubiquitin-specific proteases. *Proteins* 69, 1–7.

## 8. Supplementary tables

**Supplementary table 1: List of plasmids obtained from other researchers.** The name of the plasmid, the provider and their respective research centers are detailed.

<b>Plasmid</b>	<b>Provider</b>	<b>University /Institute</b>
<b>GFP-USP1</b>	Dr. René Bernards	Netherlands Cancer Institute, Amsterdam, The Netherlands
<b>Xpress-UAF1</b>	Dr. Jae U. Jung	Harvard University, Boston, MA
<b>GFP-USP3</b>	Dr. Pier Paolo di Fiore	University of Milan, Milan, Italy
<b>pC1 USP7</b>	Dr. Roger Everet	Univesity of Glasgow, Glasgow UK
<b>Flag-HA-USP46</b>	Dr. John W. Harper (Addgene)	Harvard Medical School, Boston, USA
<b>Flag-HA-USP22</b>	Dr. John W. Harper (Addgene)	Harvard Medical School, Boston, USA
<b>pCAG-BirA</b>	Dr. Ugo Mayor	University of the Basque Country (UPV/EHU), Leioa, Spain
<b>pCAG-bioUb<sub>6</sub>-BirA</b>	Dr. Ugo Mayor	University of the Basque Country (UPV/EHU), Leioa, Spain

**Supplementary table 2: Plasmids obtained by cloning.** Information about the generated plasmid, the name of the insert, the template used, the cloning method, forward (F) and reverse (R) primers, the ligated vector and the restriction enzymes.

Plasmid	Insert	Template	Cloning method	F primer	R primer	Vector	Restriction-sites
YFP-USP1(235-408)	USP1(235-408)	GFP-USP1	PCR	AOL12	AOL11	pEYFP C-1	KpnI/BamHI
NLS(SV40)-USP1(235-408)NLSm-GFP	USP1(235-408)	YFP-USP1(235-408)NLSm	PCR	AOL30	AOL31	NLS(SV40)-GFP	BamHI/AgeI
NLS(SV40)-USP1(235-408)NLS-GFP	USP1(235-408)NLSm	YFP-USP1(235-408)	PCR	AOL30	AOL31	NLS(SV40)-GFP	BamHI/AgeI
NLS(SV40)-USP46-GFP	USP46	Flag-HA-USP46	PCR	AOL32	AOL33	NLS(SV40)-GFP	BamHI/AgeI
NLS(SV40)-USP46(1-164)-GFP	USP46(1-164)	Flag-HA-USP46	PCR	AOL32	AOL34	NLS(SV40)-GFP	BamHI/AgeI
NLS(SV40)-USP46(165-259)-GFP	USP46(165-259)	Flag-HA-USP46	PCR	AOL35	AOL38	NLS(SV40)-GFP	BamHI/AgeI
NLS(SV40)-USP46(243-366)-GFP	USP46(243-366)	Flag-HA-USP46	PCR	AOL37	AOL33	NLS(SV40)-GFP	BamHI/AgeI
NLS(SV40)-USP7(314-411)-GFP	USP46(314-411)	YFP-USP7	PCR	AOL55	AOL56	NLS(SV40)-GFP	BamHI/AgeI
NLS(SV40)m-USP46-GFP	USP46	NLS(SV40)-USP46-GFP	PCR	AOL32	AOL33	NLS(SV40)m-NET22-GFP	BamHI/AgeI
NLS-YFP-NLS-USP46	USP46	NLS(SV40)-USP46-GFP	PCR	AOL92	AOL93	NLS-YFP-NLS	BamHI/HindIII
NLS-YFP-NLS-USP12	USP12	USP12 gBlock	gBlock	-	-	NLS-YFP-NLS	BamHI/HindIII
YFP-USP22	USP22	Flag-HA-USP422	PCR	AOL51	AOL52	pEYFP C-1	KpnI/BamHI
YFP-DMWD	DMWD	DMWD gBlock	Gibson cloning	-	-	pEYFP C-1	HindIII
Myc-DMWD	DMWD	YFP-DMWD	Subcloning	-	-	Myc-MCS	BamHI/HindIII
NLS-YFP-NLS-DMWD	DMWD	YFP-DMWD	Subcloning	-	-	NLS-YFP-NLS	BamHI/HindIII
Myc-WDR20	WDR20	WDR20 gBlock	gBlock	-	-	Myc-MCS	BamHI/HindIII
NLS-YFP-NLS-USP12(delMEIL)	USP12(5-370)	NLS-YFP-NLS-USP12	PCR	AOL101	UJAR18BIS	NLS-YFP-NLS	BamHI/HindIII

**Supplementary table 3: List of primers used for PCR cloning.** Primer names (Primer ID) and the corresponding nucleotide sequences in 5'→3' direction are indicated.

Primer ID	Sequence (5'→3')
AOL11	AGGTGAGGATCCTCAACCATTACAGGTGTAAC
AOL12	TCTGAGGGTACCGAAATACCTCATCCGAAAG
AOL30	TCTGAGGAGGATCCAGAAATACCTCATCCGAAAGAG
AOL31	AGGTGAGACCGGTGGAACATTTACAGGTGTAACAG
AOL32	TCTGAGGAGGATCCAATGACTGTCCGAAACATCGCC
AOL33	AGGTGAGACCGGTGGCTCTCTTGACTGATAGAATAAAAT
AOL34	AGGTGAGACCGGTGGTTCTGGTTATTATTTCCGCAGG
AOL35	TCTGAGGAGGATCCACTCACCTGGGTCCATGAGATTTTCAG
AOL37	TCTGAGGAGGATCCAAGGGTAAAAAGCTGCCCATGATC
AOL38	AGGTGAGACCGGTGGCTTGAACCGCTTTAGGTGCAG
AOL55	TCTGAGGAGGATCCAACCTGTGTAGAGGGCACCATAC
AOL56	AGGTGAGACCGGTGGATACATAAATTCATCAG
AOL92	TCTGAGCAAGCTTCGGCCACCATGACTGTCCGAAACATCGCC
AOL93	AGGTGAGGATCCTTACTCTCTTGACTGATAGAATAAAAT
AOL51	TCTGAGGGTACCGCCACCATGGTGTCCCGCCAGAGCCC
AOL52	AGGTGAGGATCCCTACTCGTATTCCAGGAACTG
AOL101	TCTGAGCAAGCTTCGATGACAGTCTCAAATTCGCCTC
UJAR18BIS	AAACAAGTTAACAACAAC

**Supplementary table 4: List of plasmids mutated by site-directed mutagenesis.** The name of the plasmid, the template used in the PCR, the amino acid substitution (Aa substitution) as well as the forward (F) and reverse (R) primers are indicated.

Plasmid	Template	Aa substitution	Primer F	Primer R
GFP-USP1 S313A	GFP-USP1	S313A	UJAR167	UJAR168
GFP-USP1 S313D	GFP-USP1	S313D	UJAR169	UJAR170
YFP-USP1(235-408)	YFP-USP1(235-408)	S313D	UJAR169	UJAR170
YFP-USP1(del420-520)S313D	YFP-USP1(del420-520)	S313D	UJAR169	UJAR170
NLS(SV40)-USP1(235-408)NLSm-GFP S313D*	NLS(SV40)-USP1(235-408)NLSm-GFP	S313D	UJAR169	AOL54
GFP-USP1 (R439Q/L441K/L446R/S494A)	GFP-USP1	(R439Q/L441K/L446R/S494A)	IGS188, AOL59	IGS189,AOL60
NLS-YFP-NLS-USP46 E186K	NLS-YFP-NLS-USP46	E186K	AOL97	AOL98
NLS-YFP-NLS-USP12 E190K	NLS-YFP-NLS-USP12	E190K	AOL95	AOL96
GFP-USP1 E444K	GFP-USP1	E444K	AOL73	AOL74
Xpress-UAF1 K214E	Xpress-UAF1	K214E	AOL77/AOL78	-
Xpress-UAF1 K214E/W256A	Xpress-UAF1	K214E/W256A	AOL77/AOL78	-
Xpress-UAF1 K214E/W256A/R272D	Xpress-UAF1	K214E/W256A/R272D	AOL89	AOL84
GFP-USP1 S475Y	GFP-USP1	S475Y	AOL69	AOL70
GFP-USP1 D502N	GFP-USP1	D502N	AOL71	AOL72
GFP-USP1 S575R	GFP-USP1	S575R	IGS115	IGS116
GFP-USP1 G667A	GFP-USP1	G667A	AOL41	AOL42
GFP-USP1 L669P	GFP-USP1	L669P	AOL43	AOL44
GFP-USP1 K673T	GFP-USP1	K673T	AOL45	AOL46
GFP-USP1 A676T	GFP-USP1	A676T	AOL47	AOL48
GFP-USP1 GG/AA	GFP-USP1	G670A/G671A	AOL49	AOL50

**Supplementary table 5: List of primers used for mutagenesis.** Primer names (Primer ID) and the corresponding nucleotide sequences in 5' → 3' direction are indicated.

Primer ID	Sequence (5' → 3')
UJAR167	GCTACAAGTGATACATTAGAGGCTCCTCTAAAATAATTCCCAAG
UJAR168	GGGAATTATTTTAGGAGGAGCCTCTAATGTATCACTTGATGCTTTTC
UJAR169	GCTACAAGTGATACATTAGAGGATCCTCTAAAATAATTCCCAAG
UJAR170	GGGAATTATTTTAGGAGGATCCTCTAATGTATCACTTGATGCTTTTC
AOL54	GGGAATTATTTTAGGAGGATCCTCTAATGTATCACTTGATGCTGC
IGS188	GGTATTAAGGACGACAGTCAAGGAATGTAAAGTCGAACAGAAAGAAGAGAAG
IGS189	CTTCTGTTTCGACTTTCACATTCCTGCACTGCGTCTTAATACCAGCTGACC
AOL59	CACAATTTGCTGCAGTAGAAAGGATTGTAGGAGAAGATAAATTTCTG
AOL60	CTTCTCTACAATCCTTTCTACTGCAGCAAATTGTAAATTGCC
AOL97	GAAACTCGATGCTTGAAGTAAACTGTTAGTAGCAAAGATGAAG
AOL98	CTACTAACAGTTTTACAGTTCAAGCATCGAGTTTCATTGGTAAG
AOL95	GAAACCAGATGTCTTACTTGTAAACTATAAGCAGCAAAGATGAAG
AOL96	CTTGCTGCTTATAGTTTTACAAGTAAGACATCTGGTTTCATTAGTTAATG
AOL73	GACGCGTTGCTTGAATGTAAAGTTTAAACAGAAAGAAGAGAAGATTTCAAG
AOL74	CTTCTCTCTTTCTGTTAACTTTTACATCCAAGCAACGCGTCTTAATACC
AOL77	CTTAAAGGGCACACGGATAATGTGGAGGCATTGCTATTAACAGAG
AOL78	GTCCATGATGAAGGTTGGCGGCTGCAAGTCAATGATGCCTTC
AOL89	GTATTCTGGTGAGACGACAGGAAGATTATTGTACAGACCTAAGAAACCC
AOL84	CAATAAATCTTCTGTCGCTCCACCAGAATACACATGTGTGAAGGCATC
AOL69	GAGGAGAGTTCTGAAATTTATCCAGAGCCAAAAACAGAAATGAAGACCCCTG
AOL70	CTTCATTCTGTTTTGGCTCTGGATAAATTCAGAACTCTCTACTTTG
AOL71	GAAAGGATTGTAGGAGAAAATAAATTTCTGTGAAAAGTCCATCATTATAC
AOL72	GATGGCAGTTTTACAGAAATATTATTTCTCCTACAATCCTTTCTACTGAAG
IGS115	GCACAAAGCCAACTAACGACAGATATGGATTATTGCGGTTGTG
IGS116	CGCAAATAATCCATATCTGTCGTTAGTTGGCTTTGTGCTCCATTC
AOL41	AAAAAAATGTAGAAGCTATTGCACTTCTGGAGGACAAAAGAGCAAAG
AOL42	GTCCTCAAGAAGTGAATAGCTTCTACATTTTTTTGTTCAAAC
AOL43	GTAGAAGCTATTGGACTTCTGGAGGACAAAAGAGCAAAGCAG
AOL44	GCTCTTTGCTCCAGGAAGTCCAATAGCTTCTACATTTTTTTG
AOL45	CTTCTGGAGGACAAACGAGCAAAGCAGATTATGAGCTATAC
AOL46	CTCATAATCTGCTTTGCTCGTTTGTCTCCAAGAAGTCCAATAG
AOL47	GGAGGACAAAAGAGCAAACAGATTATGAGCTATACAACAAAG
AOL48	GTATAGCTCATAATCTGTTTTGCTCTTTGTCTCCAAGAAGTCCAATAG
AOL49	GCTATTGGACTTCTTGACGACAAAAGAGCAAAGCAGATTATGAG
AOL50	CTGCTTTGCTTTTTGTGCTGCAAGAAGTCCAATAGCTTCTAC

**Supplementary table 6: List of primers used for sequencing.** Primer names (Primer ID), the corresponding nucleotide sequences, forward or reverse and the vector where they hybridize are indicated.

<b>Primer ID</b>	<b>Sequence (5' → 3')</b>	<b>Forward/Reverse</b>	<b>Hybridize</b>
UJAR17	AGTCCGCCCTGAGCAAAG	Forward	pEYFP C-1
UJAR18BIS	AAACAAGTTACAACAAC	Reverse	pEYFP C-1
UJAR49	GACGCAAATGGGCGGTAG	Forward	pEYFP C-1
AOL99	CTTTTCAATGAGGAAAGAC	Forward	DMWD
IGS3	AAATATACTGATGAACTT	Forward	USP1
IGS154	GATGTATAGCAACATACC	Forward	UAF1